Inaugural dissertation

for

obtaining the doctoral degree

of the

Combined Faculty of Mathematics, Engineering and Natural Sciences

of the

Ruprecht - Karls - University

Heidelberg

Presented by

Teng-Feng Li (M.Sc.)

born in: Changsha, China

Oral examination: 20/03/2024

Identification of RBM39 as a key regulator of innate immune response, governing basal expression of IRF3 and other critical pathway components

Referees: *1. Prof. Dr. Ralf Bartenschlager*

2. Prof. apl. Dr. Volker Lohmann

Contents:

Abstract:

The cell intrinsic innate immune response serves as the first line of defense of a host cell against microbial invasions. It initiates with the activation of pattern recognition receptors (PRRs) by various pathogen-associated molecular patterns (PAMPs), through complex signaling pathways, resulting in the expression of Interferons (IFNs) and numerous Interferon-stimulated genes (ISGs) to eliminate invading pathogens. The key players in this process are well-established, however, increasing numbers of regulatory factors have also been discovered in recent years, playing vital roles in tuning the innate immune response. Some of these factors are exclusively expressed in certain tissue or cell-types, shaping the specific responses there.

Toll-like receptor 3 (TLR3) is a PRR residing in the endosome of certain cell types, including endothelial cells and hepatocytes. To identify host factors involved in TLR3 pathway of hepatocytes, my colleagues initiated a CRISPR/Cas screening in two liver cell lines, Huh7-Lunet-TLR3 and PH5CH cells, and identified 55 candidate genes potentially affecting TLR3 responses. After a large-scale siRNA validation, they finally narrowed down the candidates to three genes, protein tyrosine phosphatase receptor type T (PTPRT), lysine demethylase 2A (KDM2A) and RNA binding motif protein 39 (RBM39). Since PTPRT and KDM2A showed off-target effects, my thesis mainly focused on the analysis of the innate immune function of RBM39.

RBM39 is an RNA binding protein involved in transcriptional regulation and splicing of many genes, mainly contributing to cell cycle control and metabolic pathways. In this study, I found that RBM39 furthermore plays a role in innate immunity signaling, including TLR3, RIG-I, MDA5 and IFN pathways. Upon poly(I:C) stimulation, loss of RBM39 significantly attenuated these pathways not only in liver-based cell lines but also in human alveolar epithelial cell, A549. This role was further confirmed during virus infections where RBM39 also affected virus-induced ISG expression. Furthermore, knockdown of RBM39 specifically inhibited the type III IFN but not type I IFN pathway, due to a down-regulation of the type III IFN receptor subunit IL10RB. In addition, I observed that RBM39 affected mainly IRF3-dependent ISG induction but not the production NF-κB-induced inflammatory cytokines, IL6 and TNFAIP3, pointing to an IRF3-related regulation by RBM39, at least upon TLR3 activation. Indeed, further investigation uncovered that deletion of RBM39 significantly reduced IRF3 expression, partly resulting from

its co-transcriptional function and highly associated with its role as alternative splicing factor. RNA sequencing (RNA-seq) analysis in PH5CH revealed that downregulation of RBM39 results in a switch from the functional IRF3 isoform to dysfunctional ones, leading to a reduction of IRF3 protein expression and thus a suppression of the IFN response. This analysis further identified other important innate immune factors regulated by RBM39 either at the transcription level or by alternative splicing, such as RIG-I, MDA5, IL10RB, STAT1 and STAT2. A proteomic analysis confirmed the reduction of RIG-I, STAT1 and STAT2, collectively highlighting the role of RBM39 in cell intrinsic innate immunity. In addition, Indisulam, a sulfonamide drug mediating RBM39 degradation and used for cancer treatment in clinical trials, was found to act as an innate immune inhibitor, reducing IRF3 expression and ISGinduction. This data suggests that targeting of RBM39 might be a strategy to tune down exaggerating innate immune responses, e.g. for the therapy of autoimmune disorders.

To comprehensively understand the role of TLR3 in liver-specific antiviral immunity, I also collected 14 TLR3 single nucleotide polymorphisms (SNPs), and investigated their functionality in Huh7.5 cells, an immune-incompetent liver hepatoma cell line lacking TLR expression. The function of TLR3 SNPs L360P, P680L, L742F, G743S were severely impaired while R811S, R867Q, M870V were partly reduced. However, further in-depth analysis going beyond the scope of this thesis are required to draw conclusions on the mechanisms underlying the functional defects.

Zusammenfassung:

Die zelleigene, angeborene Immunantwort dient als erste Verteidigungslinie einer Wirtszelle gegen mikrobielle Invasionen. Sie beginnt mit der Aktivierung von Mustererkennungsrezeptoren (Pattern Recognition Receptors, PRRs) durch verschiedene pathogen-assoziierte molekulare Muster (Pathogen-associated Molecular Patterns, PAMPs) über komplexe Signalwege, die zur Expression von Interferonen (IFNs) und zahlreichen Interferon-stimulierten Genen (ISGs) führen, um eindringende Krankheitserreger zu eliminieren. Die Hauptakteure dieses Prozesses sind gut bekannt, aber in den letzten Jahren wurde auch eine zunehmende Zahl von regulatorischen Faktoren entdeckt, die bei der Modulation der angeborenen Immunantwort eine entscheidende Rolle spielen. Einige dieser Faktoren werden ausschließlich in bestimmten Geweben oder Zelltypen exprimiert und prägen dort die spezifischen Immunantworten.

Der Toll-like-Rezeptor 3 (TLR3) ist ein PRR, der sich im Endosom bestimmter Zelltypen befindet, darunter Endothelzellen und Hepatozyten. Um Wirtsfaktoren zu identifizieren, die am TLR3-Signalweg von Hepatozyten beteiligt sind, wurde in Vorarbeiten ein CRISPR/Cas-Screening in zwei Leberzelllinien, Huh7-Lunet-TLR3 und PH5CH-Zellen, durchgeführt. Dabei wurden 55 Kandidatengene identifiziert, die potenziell die TLR3-Antwort beeinflussen. Nach siRNA-Validierung konnte die Kandidatenliste auf drei Gene eingegrenzt werden, die von mir näher charakterisiert wurden: Protein-Tyrosin-Phosphatase-Rezeptor Typ T (PTPRT), Lysin-Demethylase 2A (KDM2A) und RNA-Bindungsmotiv-Protein 39 (RBM39). Da PTPRT und KDM2A Off-Target-Effekte zeigten, konzentrierte sich meine Arbeit hauptsächlich auf die Analyse der angeborenen Immunfunktion von RBM39.

RBM39 ist ein RNA-bindendes Protein, das an der Transkriptionsregulierung und dem Spleißen vieler Gene beteiligt ist und hauptsächlich zur Kontrolle des Zellzyklus und verschiedener Stoffwechselwege beiträgt. In konnte ich darüber hinaus eine Rolle von RBM39 bei der Regulation der angeborenen Immunität identifizieren, einschließlich der TLR3-, RIG-I-, MDA5- und IFN-Signaltransduktionspfade. Nach Poly(I:C)-Stimulation führte der Verlust von RBM39 zu einer signifikanten Abschwächung dieser Signalwege nicht nur in leberbasierten Zelllinien, sondern auch in menschlichen Alveolarepithelzellen (A549). Diese Rolle wurde auch während Virusinfektionen bestätigt, bei denen RBM39 auch die virusinduzierte ISG-Expression beeinflusste. RBM39 beeinflusste außerdem spezifisch den Typ-III-IFN-, aber nicht den Typ-I-

IFN-Signalweg, was auf eine verminderte Expression der Typ-III-IFN-Rezeptoruntereinheit IL10RB zurückzuführen war. Darüber hinaus beobachtete ich, dass RBM39 hauptsächlich die IRF3-abhängige ISG-Induktion beeinflusste, nicht aber die Produktion der NF-κB-induzierten inflammatorischen Zytokine IL6 und TNFAIP3, zumindest bei TLR3-Aktivierung.

Weitere Untersuchungen ergaben, dass die Deletion von RBM39 die basale IRF3-Expression signifikant reduzierte, was einerseits auf seine kotranskriptionelle Funktion zurückzuführen war und andererseits mit seiner Rolle als alternativer Spleißfaktor zusammenhing. Eine RNA-Sequenzierungsanalyse (RNA-seq) in PH5CH ergab, dass die Herunterregulierung von RBM39 zu einem Wechsel von der funktionellen IRF3-Isoform zu dysfunktionellen Isoformen führte, was eine Verringerung der IRF3-Proteinexpression und damit eine Unterdrückung der IFN-Antwort zur Folge hatte. Bei dieser Analyse wurden auch andere wichtige Faktoren des angeborenen Immunsystems identifiziert, die von RBM39 entweder auf der Transkriptionsebene oder durch alternatives Spleißen reguliert wurden, wie z. B. RIG-I, MDA5, IL10RB, STAT1 und STAT2. Eine Proteomanalyse bestätigte die Verringerung von RIG-I, STAT1 und STAT2, was insgesamt die Rolle von RBM39 bei der zellinternen angeborenen Immunität unterstreicht. Darüber hinaus wurde festgestellt, dass Indisulam, ein Sulfonamid, das den Abbau von RBM39 vermittelt und in klinischen Studien zur Krebsbehandlung eingesetzt wird, als Hemmstoff des angeborenen Immunsystems wirkt und die IRF3-Expression und ISG-Induktion verringert. Diese Daten deuten darauf hin, dass die gezielte Beeinflussung von RBM39 eine Strategie sein könnte, um überschießende angeborene Immunreaktionen zu dämpfen, z. B. bei der Therapie von Autoimmunkrankheiten.

Um die Rolle von TLR3 bei der leberspezifischen antiviralen Immunität umfassend zu verstehen, habe ich außerdem die Funktionalität von 14 TLR3-Einzel-Nukleotid-Polymorphismen (SNPs) in Huh7.5-Zellen, einer immuninkompetenten Leber-Hepatom-Zelllinie ohne TLR-Expression, untersucht. Die Funktion der TLR3-SNPs L360P, P680L, L742F, G743S war stark beeinträchtigt, während die Aktivität von R811S, R867Q, M870V teilweise reduziert war. Weitere eingehende Analysen, die über den Rahmen dieser Arbeit hinausgehen, sind erforderlich, um die Mechanismen zu klären, die den Funktionsstörungen zugrunde liegen.

1 Introduction

1.1 General review of innate immune system

The immune system is an essential defense system to fight against microbial assault from the environment. In vertebrates, it comprises two main parts: the innate immune system and the adaptive immune system (1). The innate immune system is an ancient defense mechanism that has been evolutionarily conserved from primitive multicellular organisms, fungi, plants, and insects to vertebrates, serving as the host's first line of defense and reacts rapidly to invading pathogens through nonspecific mechanisms (*2*), while the adaptive immune system mainly relies on the collaboration of two types of cells, B cells and T cells, to provide a specific and long-lasting protection for the host (*3*).

Innate immunity consists of several components, including physical barriers, innate immune cells, cell receptors, cytokines, antimicrobial peptides and complement system (Figure 1).(*1*). Physical barriers, such as the skin and mucosa, separate the host's internal environment from the external environment, preventing the entry of pathogens (*4, 5*). However, this protection has limitations. Once pathogens breach the physical barrier, cellular receptors expressed in various cells play a crucial role in recognizing invasions, initiating signaling cascades to produce cytokines and antimicrobial peptides for eliminating infections (*6, 7*). In addition, the complement system can also be activated to directly lyse pathogens, enhance the abilities of phagocytic cells, such as macrophages, or facilitate the action of inflammatory mediators, all of which contribute to the collective defense against infections (Figure 1) (*8*).

Furthermore, the produced cytokines and chemokines activate effector cells of innate immunity, such as epithelial cells (*9*), natural killer cells (NK cells) (*10*), mast cells (*11*), macrophages (*12*), and dendritic cells (DCs) (*13*), to either directly destroy pathogens through phagocytosis and inflammation or to modulate the adaptive immune response if the innate immune system is unable to clear the threat.

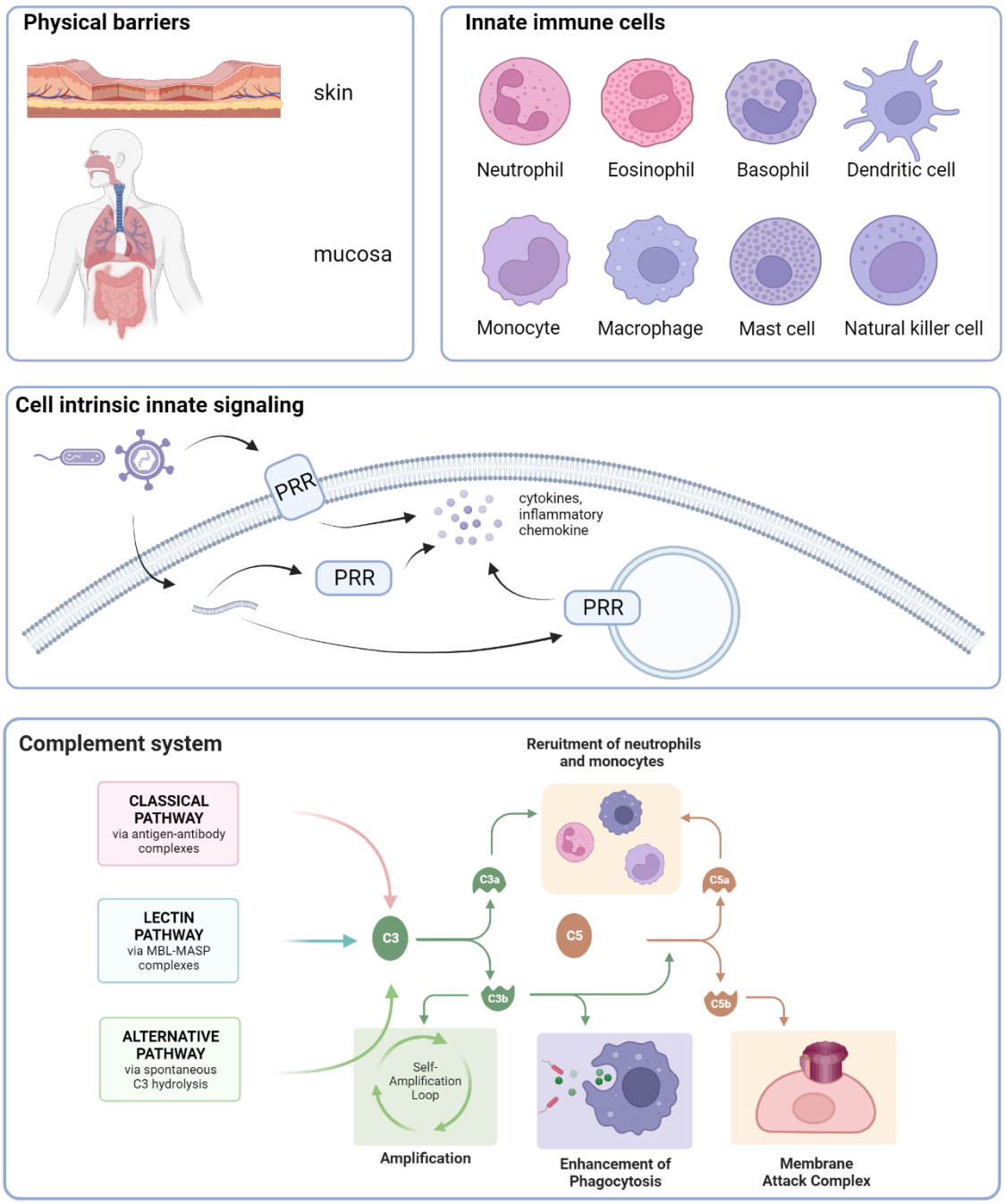

Figure 1. Overview of the innate immune system. The skin and mucous membranes in the respiratory, digestive, and reproductive tracts constitute physical barriers that effectively separate microbes from the external environment. When pathogens manage to breach this first line of defense, innate immune cells become activated through pattern recognition receptors (PRRs) located on the cell membrane or within the cells. These PRRs are responsible for recognizing pathogen-associated patterns (PAMPs) and initiating complex signaling cascades, leading to the production of antimicrobial proteins, cytokines, and pro-inflammatory chemokines. Besides, complement system was activated through three pathways, the classical, lectin and alternative pathways. Sequential cleavage and binding events on convertases, such as C3 and C5, ultimately lead to the recruitment of neutrophils and monocytes, the enhancement of phagocytosis, or the assembly of the membrane attack complex. All of these works together to combat and eliminate infections. Adapted from (*14, 15*) by Biorender.

1.2 Cell receptors and signal transduction

The detection of pathogens by germline-encoded pattern recognition receptors (PRRs) initiates cell intrinsic innate signaling to trigger rapid and immediate innate immune responses, which is the first and a crucial step for the activation of the whole immune system and also the focus of my study.

Various components of pathogens, such as bacteria-synthesized carbohydrates (lipopolysaccharide (LPS) from gram-negative bacteria (*16*), mannose (*17*)), bacterial flagellin (*18*), gram-positive bacterial lipoteichoic acids (*19*), nucleic acids (DNA (*20, 21*) or RNA (*22-24*) from bacteria and viruses), fungal glucans (*25*) , and chitin (*26*), can serve as pathogen-associated molecular patterns (PAMPs). These PAMPs enable the recognition of the innate immune system by a limited numbers of pattern recognition receptors (PRRs), thereby initiating complex innate immune signaling to protect the host from infections.

PRRs can be mainly classified into five families, which are membrane-bound PRRs, including Toll-like receptors (TLRs) and C-type lectin receptors (CLRs), as well as cytoplasmic PRRs, including NOD-like receptors (NLRs), absent in melanoma 2 (AIM2)-like receptors (ALRs), and retinoic acid-inducible gene (RIG)-I-like receptors (RLRs) (*27*). These receptors are expressed not only in innate immune cells, such as dendritic cells and macrophages, but also in other cell types, such as epithelial cells and endothelial cells (*28, 29*).

1.2.1 Toll-like receptors:

The TLR family comprises type I integral membrane glycoproteins localized at the plasma membrane or the endolysosomal membrane. They are characterized by variable N-terminal leucine-rich repeat (LRR) motifs, a transmembrane region, and a cytoplasmic Toll/interleukin 1 (IL-1) receptor (TIR) homology domain. Toll, originally known for its role in dorsoventral axis development (*30*), was later discovered to have anti-fungal functions in Drosophila (*31*). As a mammalian homolog of Toll receptor, TLR4 was also identified in 1997 for its role in inducing inflammatory genes (*32*). Following that, an increasing number of Toll-like receptors were discovered. So far, ten TLRs have been identified in humans (TLR1-10), and twelve in mice (TLR1-9 and TLR11-13). TLR1-10 exhibit conservation across both humans and mice, with the exception of TLR10, which is not functional in mice. TLR11-13, on the other hand, are unique to mice (*33*). In this discussion, we will focus on human TLRs.

TLR1, TLR2, TLR4, TLR5, and TLR6 are expressed on the cell surface and primarily recognize membrane components of microbes (Figure 2). TLR2 forms a heterodimer with TLR1 to recognize triacyl lipopeptides (*34*) or with TLR6 to sense diacyl lipopeptides (*35*). TLR4 is responsible for detecting lipopolysaccharides (LPS) (*36*), while TLR5 recognizes bacterial flagellin (*37*). In contrast, TLR3, TLR7, TLR8, and TLR9 are localized on the endosomal membrane and play a key role in recognizing nucleic acid components from microorganisms or damaged cells. Specifically, TLR3 is widely expressed in various cell types, including hepatocytes, detecting double-stranded (ds) viral RNA or self-RNAs from damaged cells (*23, 38, 39*). TLR7 and TLR8 are involved in recognizing single-stranded (ss) RNA (*22, 40*), and TLR9 recognizes ssRNA containing unmethylated cytidine-phosphate-guanosine (CpG) motifs (*20, 41*). Notably, TLR7 and TLR9 are primarily expressed in plasmacytoid dendritic cells (pDCs), suggesting a cell-type specific innate immune regulation (*6*). TLR10 has been reported to sense a protein originated from human immunodeficiency virus-1 (HIV-1), glycoprotein 41 (gp41) (*42*) and also serves as a negative regulator of the TLR2 pathway (*43*). However, due to the limited research available, its biological function in humans has not been fully determined yet.

1.2.1.1 TLR signaling pathways

The recognition of specific ligands by TLRs leads to the dimerization of the cytosolic TIR domain. This, in turn, recruits various adaptor proteins, including TIR domain-containing adaptor protein (TIRAP)/Mal, myeloid differentiation primary response protein 88 (MyD88), TIRAP-inducing IFN-β (TRIF), TRIF-related adaptor molecule (TRAM), and sterile-alpha and armadillo motif-containing protein (SARM) (*33*) (Figure 2). Based on the usage of these adaptors, TLR signaling can be categorized into MyD88-dependent pathways and TRIF-dependent pathways.

MyD88-dependent pathways

With the exception of TLR3, most TLRs rely on MyD88 for downstream signaling. Moreover, TLR2/TLR1, TLR2/TLR6, and TLR4 dimers require TIRAP/Mal to bridge the connection between TLRs and MyD88 (*44, 45*). Following their binding to TLRs, MyD88 recruits IL-1 receptor-associated kinase (IRAK) 4, which subsequently activates other IRAK family kinases, including IRAK1, IRAK2 and IRAKM, forming a complex known as Myddosome (*46-49*). The IRAKs are subsequently released from MyD88 and interact with an E3 ligase, tumor necrosis factor (TNF) receptor-associated factor 6 (TRAF6). In cooperation with E2 ubiquitin-conjugating enzymes Ubc13 and Uev1A, TRAF6 catalyzes the formation of lys63 (K63)-linked polyubiquitin chains

on TRAF6 itself and IRAK1 (*50, 51*). This process leads to the activation of transforming growth factor (TGF)-β-activated kinase 1 (TAK1), TAK1-binding protein (TAB) 1, TAB2, and TAB3, subsequently resulting in the phosphorylation of the IκB kinase (IKK) complex and mitogen-activated protein kinase (MAPKs) (*52, 53*).

Subsequently, the IKK complex, consisting of IKK-α, IKK-β, and nuclear factor k-light-chain-enhancer of activated B cells (NF-κB) essential modulator (NEMO), phosphorylates IκBα, an inhibitor of NF-κB, leading to its proteasomal degradation (*54, 55*). This allows NF-κB to translocate into the nucleus, where it induces the expression of proinflammatory cytokines. Meanwhile, MAPKs further phosphorylate kinase p38 and subsequently cyclic AMP-responsive element-binding protein (CREB), thus regulating the transcription of genes containing cAMP response elements (CRE). Additionally, MAPKs also phosphorylate c-Jun N-terminal kinases (JNKs) and extracellular signal-regulated protein kinase (ERK), activating activator protein 1 (AP-1) and, in turn, inducing an inflammatory response (*54, 56*). In plasmacytoid dendritic cells (pDCs), TLR7, TLR8 and TLR9 also interact with IRF5 and IRF7 through MyD88 and produce type I IFNs (*57-59*).

TRIF-dependent pathways

Specifically, TLR3 does not rely on MyD88 but instead is exclusively dependent on TRIF for downstream signaling activation. On the other hand, TLR4 utilizes both adaptors to initiate different signaling cascades. Upon activation, TRAM binds to TLR4 dimers, creating a platform referred to as the Triffosome (*60, 61*). This platform recruits TRIF as an adaptor protein (*62*). TLR3 also recruit TRIF as adaptor protein but does not require TRAM. Once activated, TRIF interacts with TRAF6, recruiting receptor-interacting protein 1(RIP1) and then initiating the NF-κB pathway to induce inflammation (*63*). It also further activates IKK-related kinase TANK-binding kinase 1 (TBK1) and inhibitor of NF-kB kinase (IKKi) through TRAF3 (*52, 64*). Subsequently, TBK1 and IKKi phosphorylate IRF3, resulting in its self-dimerization. The IRF3 dimer then translocates into the nucleus, where it produces interferons (IFNs) and various antimicrobial interferon-stimulated genes (ISGs) (Figure 2) (*52, 64, 65*).

In addition to the factors mentioned above, Unc-93 homolog B1 (UC93B1) plays a crucial role in controlling the trafficking of TLRs from the endoplasmic reticulum (ER) to the cell surface or intracellular compartments (*66*). Furthermore, for endosomal TLRs, including TLR3, TLR7, TLR8, and TLR9, efficient cleavage of their cytoplasmic domain by enzymes such as cathepsins B, S,

L, H, K, and asparaginyl endopeptidase is vital for conformational changes and proper functionality (*67-69*).

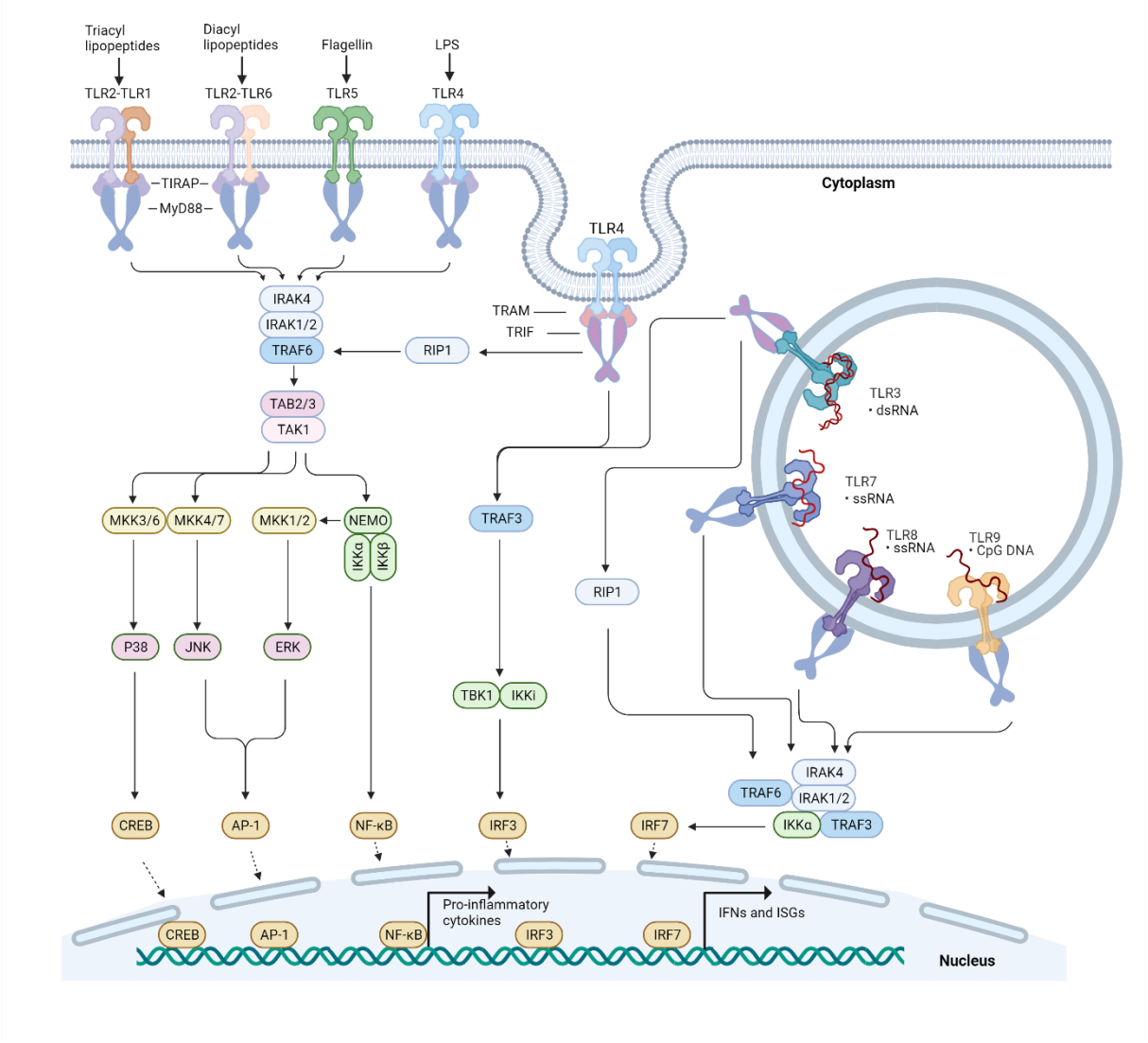

Figure 2. TLR signaling pathways. TLR2 forms heterodimers with either TLR1 or TLR6. Along with TLR4 and TLR5 homodimers, these receptors recognize ligands on the cell surface. TLR4 can also translocate into endosomes through endocytosis upon activation. TLR3, TLR7, TLR8, and TLR9 are localized on the endosomal membrane and are responsible for recognizing nucleic acids released from pathogens. Upon binding with their respective ligands, TLR signaling is initiated by the dimerization of receptors. This process recruits TIRAP and MyD88 or, specifically for TLR3 and TLR4, TRAM and TRIF, as adaptors through TIR domain interaction. This interaction activates downstream signaling molecules, leading to the formation of the Myddosome, which includes IRAK4, IRAK1, and IRAK2. IRAK1 further activates the E3 ubiquitin ligase TRAF6 to synthesize K63-linked polyubiquitin chains, resulting in the recruitment and activation of the TAK1 complex, eventually activates the NF-κB factor. TAK1 also binds and activates MAPKs, including MKK4/7 and MKK3/6, which further activate JNK and p38, respectively. The activation of IKKβ also leads to the activation of MKK1 and MKK2, which further activate ERK1/2. The activation of these MAPKs results in the activation of important transcription factors such as CREB and AP1. These transcription factors work in coordination with NF-κB to promote the induction of pro-inflammatory cytokines. For the TLR3 and TLR4 pathways, TRIF recruits TRAF6 and TRAF3, leading to the recruitment of the kinase RIP1 and activation of the TAK1 complex and IKK complex. This activation results in the activation of NF-κB and MAPKs. TRIF also promotes the TRAF3-dependent activation of

TBK1 and IKKε (originally IKKi), which further phosphorylate and activate IRF3. In the case of TLR7, TLR8, and TLR9 signaling in pDCs, IRF7 can bind to the Myddosome and is directly activated by IRAK1 and IKKε. Activation of IRF3 and IRF7 leads to the induction of type I and type III interferons (IFNs). Adapted from (*33*) using Biorender.

1.2.2 C-type lectin receptors

C-type lectin receptors (CLRs) form a family comprising over 1,000 proteins characterized by conserved C-type lectin-like domains (CTLDs). They are predominantly expressed in immune cells, such as dendritic cells and myeloid cells, and also in epithelial cells, mainly recognizing carbohydrates such as mannose and galactose (*70*). These CLRs include both soluble and transmembrane forms and play essential roles in various physiological processes, such as endocytosis, phagocytosis, cell adhesion, complement activation, tissue remodeling, antimicrobial defense, and inflammation (*71*). Their specific functions vary depending on the cell lineages.

While soluble CLRs serve as antimicrobial proteins, growth factors and opsonins, playing roles in multiple cellular process, such as cell development and inflammation (*70*), transmembrane CLRs initiate the intracellular signaling to regulate immunological responses. The signaling of CLRs with immunoreceptor tyrosine-based activation motifs (ITAMs) are most comprehensively investigated. The binding between ITAMs and adaptor proteins activates the downstream signaling. For instance, in myeloid cells, dectin 1 and dectin 2 recruit spleen tyrosine kinase (SYK), which initiates the formation of a complex containing caspase-recruitment domain protein 9 (CARD9), B cell lymphoma/leukaemia 10 (BCL-10) and mucosa-associated lymphoid tissue lymphoma translocation protein 1 (MALT1), resulting in the activation of the NF-κB pathway (*72, 73*). In contrast, CLRs like myeloid inhibitory C-type lectin (MICL), recruit tyrosine and inostitol phosphatases, such as Src homology 2 (SH2) domain containing inositol polyphosphate 5-phosphatase 1 (SHIP1), to restrain the inflammatory pathways initiated by other receptors (*74*). Some CLRs also function as regulators of other receptors, such as NKG2D in NK cells (*75*). Some examples of CLR pathways are shown in Figure 3.

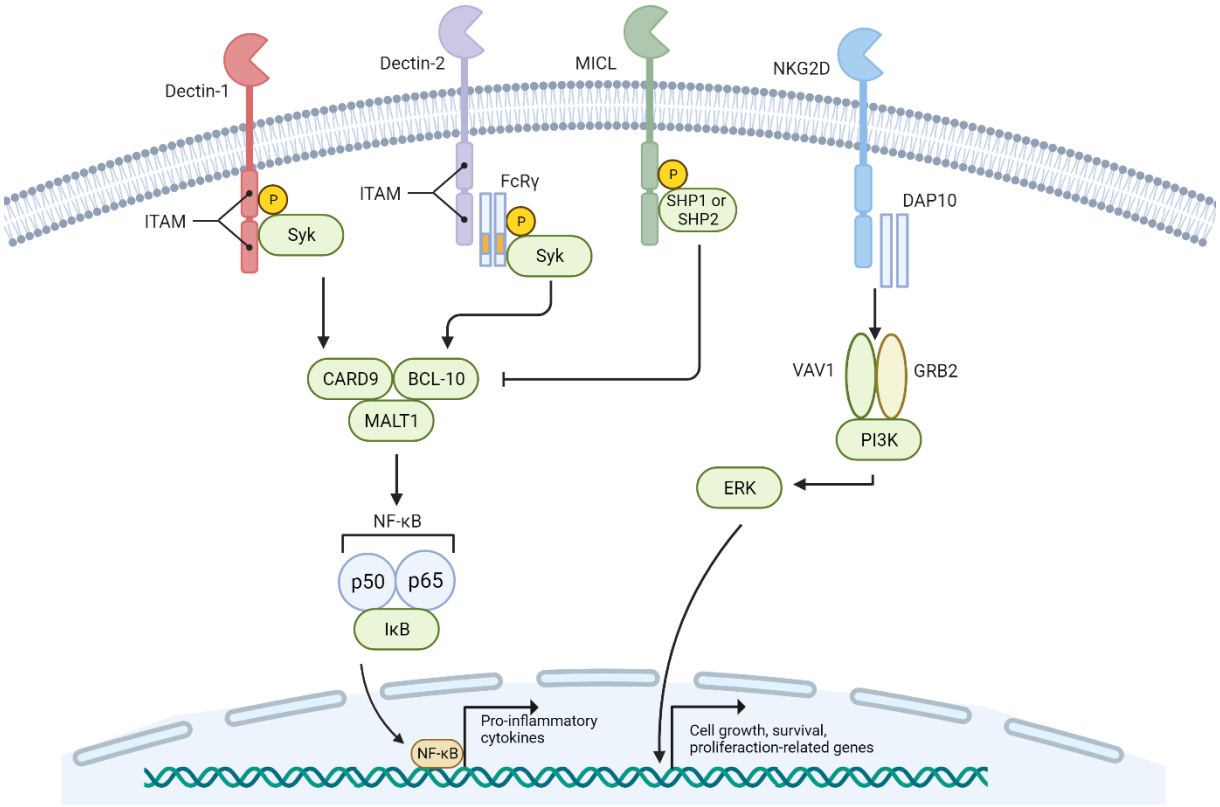

Figure 3. CLR signaling pathways. Transmembrane C-type lectins that can activate signaling pathways and regulate multiple cellular processes. For instance, receptors like Dectin1 and Dectin 2, which contain immunoreceptor tyrosine-based activation motifs (ITAMs), directly recruit Syk kinase or use an adaptor, Fc receptor γ-chain (FcRγ). This activation leads to the formation of a complex consisting of caspase-recruitment domain protein 9 (CARD9), B cell lymphoma/leukemia 10 (BCL-10), and mucosa-associated lymphoid tissue lymphoma translocation protein 1 (MALT1), ultimately resulting in the induction of NF-κB-dependent pro-inflammatory cytokines. On the other hand, MICL interacts with SHP1 or SHP2, effectively inhibiting the NF-κB pathway. In contrast, NKG2D interacts with the adaptor protein DAP10, which triggers signaling through the p85 subunit of phosphoinositide 3-kinase (PI3K) and a growth factor receptor-bound protein 2 (GRB2)–VAV1 signaling complex. This complex requires ubiquitin-dependent endocytosis for the activation of NK cell effector functions via extracellular signal-regulated kinase 1 (ERK1) and ERK2. It regulates signaling from other pathways and induces the transcription of genes associated with cell growth, survival, and proliferation. Adapted from (*70*) with Biorender.

1.2.3 NOD-like receptors

Nucleotide binding oligomerization domain (NOD)-like receptors form an evolutionarily conserved group of cytosolic receptors characterized by a common structure that contains a N-terminal protein-protein interaction domain, a central NOD domain with ATP/GTPase activity and a C-terminal leucin-rich repeat (LRR) (*76*).

Based on structural differences, Nucleotide binding oligomerization domain (NOD)-like receptors can be subclassified into four subfamilies: NLRA, NLRB, NLRC, and NLRP (*77, 78*). The NLRA subfamily has only one known member, MHC-II transactivator (CIITA), which contains an N-terminal transactivation domain. CIITA coactivates the transcription of MHC-II and is thus involved in adaptive immunity (*79, 80*). In the NLRB subfamily, the only member in humans is NLR family apoptosis inhibitory protein (NAIP), which features a baculoviral inhibition of apoptosis protein repeat (BIR) at the N-terminus and recognizes bacterial flagellin (*81, 82*). The NLRC family comprises six members: NOD1, NOD2, NLRC3, NOD3, NLRC4, NLRC5, and NLRX1. They all share the common feature of one or two N-terminal CARD domains, except for NLRC3 and NLRC5 that contain undefined N-terminus. Among them, NOD1 and NOD2 are the best-studied, as they are involved in bacterial sensing (*83, 84*). The NLRP subfamily is characterized by an N-terminal Pyrin domain and participates in the regulation of inflammation and cell homeostasis (*85*). NLRs play a role not only in innate immunity but also in various cellular processes, including adaptive immunity, cell metabolism, and development (*85*).

NOD1 and NOD2 are two NLRs that activate the NF-κB pathway. This activation requires an adaptor protein called Receptor Interacting Serine/Threonine Kinase 2 (RIP2), which is recruited to NLRs oligomers via CARD-CARD interactions. RIP2 is polyubiquitinated by E3 ubiquitin ligases, such as X-linked inhibitor of apoptosis (XIAP), and subsequently self-phosphorylated. This self-phosphorylation leads to an interaction with TRAF proteins, including TRAF1, TRAF2, and TRAF6, resulting in NF-κB activation (*86-89*). In addition, NOD1 has also been reported to activate type I IFN pathway via Interferon stimulated gene factor 3 (ISGF3) (*90*). In contrast, NLRP2 has been observed to function as negative regulators, inhibiting the NF-κB pathway (*91*).

Furthermore, NLRs also play a crucial role in the assembly of the inflammasome, a protein complex associated with inflammatory cell death. NLRP1, NLRP3, and NLRC4 are considered essential components of the inflammasome. Upon ligand recognition, NLRs undergo oligomerization and recruit apoptosis-associated speck-like protein containing A (ASC) through pyrin-pyrin interactions. This recruitment of ASC subsequently activates pro-caspase-1, leading to the cleavage of proinflammatory cytokines IL-1β and IL-18. The secretion of these

cytokines ultimately induces pyroptosis-mediated cell death (*5*). A simplified overview of NLR is shown (Figure 4).

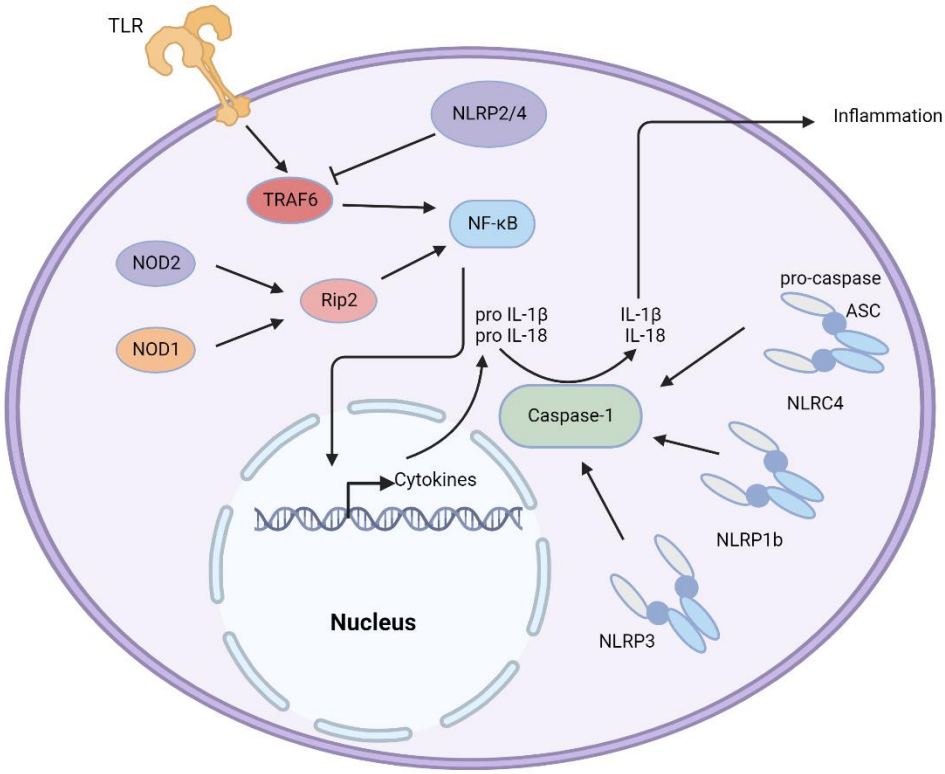

Figure 4. NLR signaling pathways. NOD1 and NOD2 are responsible for activating the NF-κB pathway via RIP2, inducing pro-IL-1β and pro IL-18. Other NLR receptors, such as NLRP2 and NLRP4, have been identified as negative regulators of this pathway. Inflammasomes can be assembled by NLRP1b, NLRP3, NLRC4. Upon triggering by multiple stimuli, inflammasomes activate caspase-1, producing mature IL-18 and IL-1β, inducing inflammation. Adapted from (*85*) with Biorender.

1.2.4 AIM2-like receptors

AIM2-like receptors are another group of human cytoplasmic DNA sensors, including AIM2 (*92*), interferon gamma inducible protein (IFI) 16 (*93*), IFIX (*94*), and myeloid cell nuclear differentiation antigen (MNDA) (*95*) characterized by a N-terminal pyrin domain for activation of downstream signals and a C-terminal hematopoietic interferon-inducible nuclear protein with 200-amino-acid repeats (HIN200) domain that recognizes DNA structure (*96*).

ALRs also play a pivotal role in the assembly of inflammasomes. Similar to NLRs, ALRs recruit apoptosis-associated speck-like protein containing a card (ASC) through pyrin-pyrin interactions, resulting in the activation of caspase-1 and the release of IL-1β in response to double-stranded DNA (dsDNA) (*97*). IFI16 has been shown to induce interferons (IFNs) and interferon-stimulated genes (ISGs) through the stimulator of interferon response Cyclic guanosine monophosphate–adenosine monophosphate (cGAMP) interactor (STING)-TBK-

IRF3 axis (*98*). However, it has also been reported that ALRs are dispensable for the interferon response (*99*). More investigation is still required to answer this question. Additionally, AIM2, but not IFIX, IFI16, and MNDA, can activate the NF-κB pathway and induce pro-inflammatory cytokines (*97*). As the investigation of ALR is limited, a brief overview of ALR pathways with IFIT16 and AIM2 is shown (Figure 5).

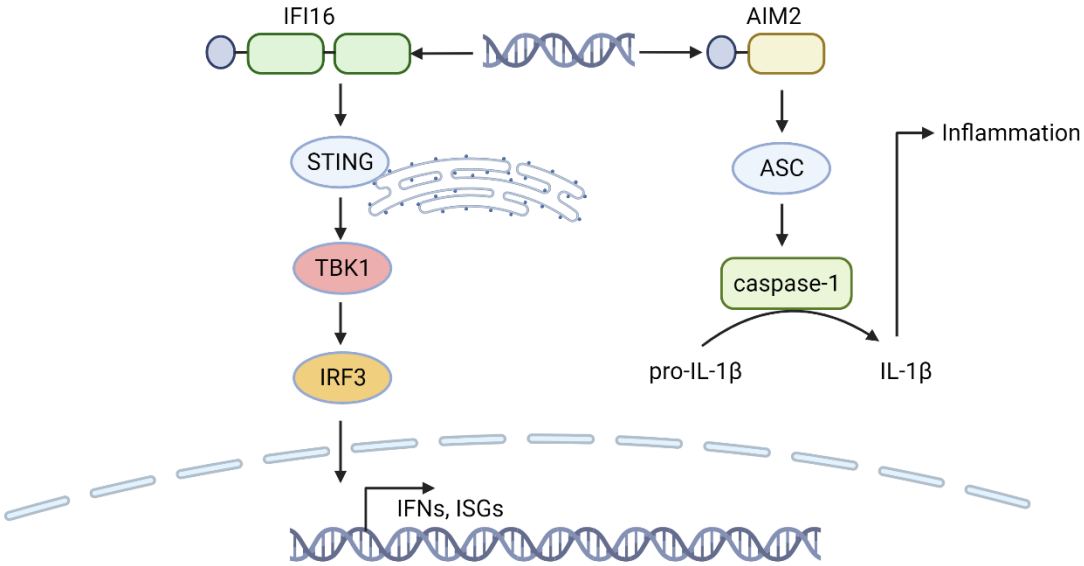

Figure 5. ALR signaling pathways. IFI16 recognizes double-stranded DNA (dsDNA) and activates TBK1 through the stimulator of interferon genes protein (STING). As a result, IRF3 is phosphorylated and translocated into the nucleus, inducing the production of interferons (IFNs) and interferon-stimulated genes (ISGs). AIM2 is involved in inflammasome formation, and upon activation, it activates caspase-1 via ASC, leading to the maturation of IL-1β and the induction of inflammation. Adapted from (*100*) using Biorender.

1.2.5 RIG-I-like receptors

RIG-I-like receptors consist of three members localized in the cytoplasm of all cell types (*101*), retinoic acid-inducible gene I (RIG-I), melanoma differentiation-associated protein 5 (MDA5) and laboratory of genetics and physiology 2 (LGP2). All RLRs share the structure of a central DExD/H box RNA helicase domain and a carboxy- terminal domain (CTD). Specially, RIG-I and MDA5 contain two additional N-terminal caspase activation and recruitment domains (CARD) that are essential for the downstream signaling (*102*). LGP2 lacks the CARDs, however, has the regulatory function to RIG-I and MDA5 pathways (*103*).

RIG-I specifically recognizes dsRNA structure with 5’ triphosphate (PPP) end (*104*), while MDA5 is primarily responsible for sensing long double-stranded RNA (dsRNA) (0.5-7kb) (*105, 106*).

RIG-I undergoes a conformational change and exposes the CARDs and helicase domain upon ligand binding, whereas MDA5 maintains an open conformation upon RNA binding (*27*). Several E3 ligases are also involved in RIG-I activation, such as tripartite motif-containing protein 25 (TRIM25), RING-finger protein leading to RIG-I activation (Riplet) and Mex-3 RNA binding family member C (MEX3C). These E3 ligases ubiquitinate RIG-I at different residues and leading to the formation of a ubiquitination complex (*107-109*). The complex further interacts with another regulatory factor, 14-3-3ε and is translocated to mitochondria for the binding with adaptor protein, mitochondrial antiviral signaling protein (MAVS) (*110*). MAVS, which localize at the mitochondrial membrane, also contains a CARD domain. It binds with the CARDs of RIG-I and MDA5, leading to the phosphorylation of TBK1 and inhibitor of nuclear factor kappa-B kinase subunit epsilon (IKKε). The activation subsequently triggers IRF3/IRF7 for the production of IFNs and interferon-stimulated genes (ISGs), as well as NF-κB, inducing pro-inflammatory cytokines and chemokines (*111*). However, LGP2 functions as a regulator of RIG-I and MDA5 pathways. In vitro studies have reported it a negative regulation of the RIG-I pathway through various mechanisms (*112-114*). In contrast, evidence has demonstrated that LGP2 facilitate the interaction between MDA5 and its stimulatory RNA, thereby enhancing MDA5 signaling (*115*). The overview of RLR pathways is shown in Figure 6.

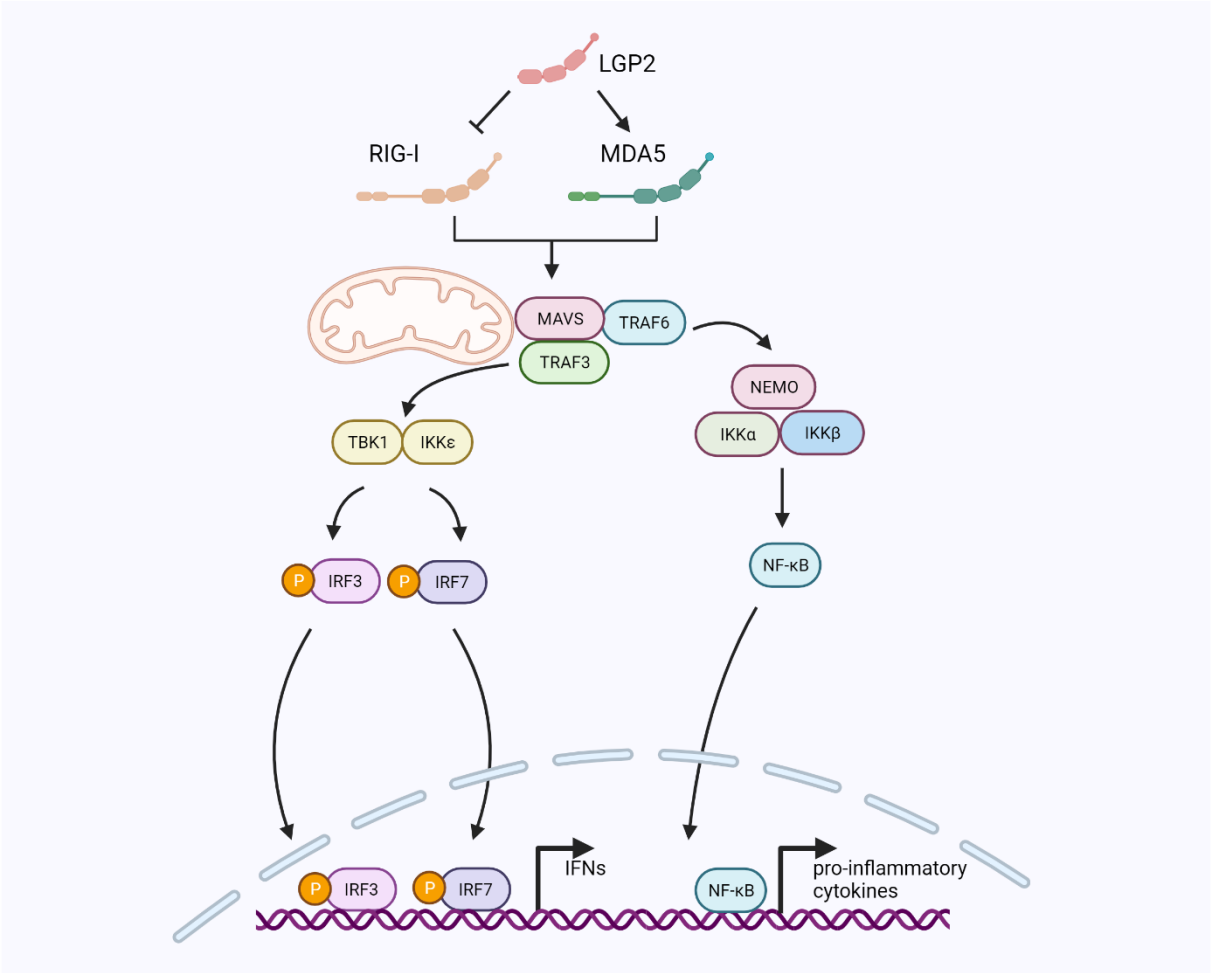

Figure 6. RLR signaling pathways. RIG-I and MDA5 can be triggered by short 5'ppp dsRNA and longer dsRNA, respectively. Upon activation, they both activate MAVS, which localizes at the mitochondria. This activation further leads to downstream TBK1 and IKKε via TRAF3, resulting in the phosphorylation and dimerization of IRF3 and IRF7. Additionally, MAVS also triggers the NEMO-IKKα-IKKβ complex via TRAF6, which leads to the release of NF-κB. These transcription factors subsequently translocate into the nucleus, where they induce the production of interferons (IFNs) and pro-inflammatory cytokines. LGP2 alone does not trigger innate immune response but positively regulates MDA5 and negatively modulates RIG-I signaling. The figure is made by biorender.

1.2.6 Other PRRs

In addition to the mentioned families, there are other Pattern Recognition Receptors (PRRs) that do not belong to these families. One such example is cyclic guanosine monophosphate (GMP)-adenosine monophosphate (AMP) (cGAMP) synthase (cGAS), a cytosolic DNA sensor that recognizes DNA from microbial pathogens. It recruits the stimulator of interferon genes (STING) and activates the TBK1-IRF3 axis to induce the production of interferons (IFNs) and interferon-stimulated genes (ISGs), or NF-κB, resulting in the production of pro-inflammatory cytokines (*116*). Another well-known PRR is protein kinase R (PKR), which senses double-stranded RNA (dsRNA) and phosphorylates α subunit of eukaryotic initiation factor 2 (eIF2).

This phosphorylation inhibits translation in host cells as a defense mechanism against infections (*117*). With intensive study of innate immune signaling, an increasing number of PRRs have emerged, collectively contributing to the intricate host defense mechanisms.

1.2.7 Interferon signaling

A wide variety of pathogen-associated molecular patterns (PAMPs) encoded by pathogens initiate divergent signaling pathways through distinct Pattern Recognition Receptors (PRRs) but converge at the TBK1-IRF3 axis, leading to the production and secretion of interferons. The secreted IFNs helps infected cells and surrounding non-infected cells establish antimicrobial defenses and induces a wide range of ISGs.

IFNs are a diverse group of cytokines named for their ability to interfere with viral infections. There are three types of IFNs in human cells. Type I IFN is the largest subgroup, including 13 subtypes such as IFNα, IFNβ, IFNω, IFNκ, and IFNε. Type III IFN comprises four members: IFNλ1, IFNλ2, IFNλ3, and IFNλ4, which share structural similarities with interleukin-10 (*118*). Notably, IFNλ4 is a pseudogene for most non-African humans (*119*). Type II IFN has only one member, IFNγ, and it is primarily expressed in immune cells. (*120*).

Various PRRs, such as RLRs and TLRs, initiate distinct cell-intrinsic innate immune pathways upon binding with their corresponding ligands and converge to phosphorylate IRF3, leading to IFN production and secretion. Both Type I and Type III IFNs, in turn, bind to their receptors, IFNAR and IFNLR, respectively, in an auto- and paracrine manner, recruiting Janus kinase 1 (JAK1) and tyrosine kinase 2 (TYK2). This results in self-phosphorylation on the endodomain of these receptors, which subsequently phosphorylates signal transducer and activator of transcription (STAT) 1 and STAT2. STAT1 and STAT2, along with interferon regulatory factor 9 (IRF9), form a ternary complex called Interferon-stimulated gene factor 3 (ISGF3), which binds to the IFN-stimulated response elements (ISREs) and leads to the expression of hundreds of ISGs with antimicrobial or immunoregulatory functions (Figure 7) (*118*).

Despite the identification of hundreds of ISGs since their initial discovery, only a limited number have been extensively studied in terms of functionality. Some ISGs exhibit antiviral functions, for example, interferon-induced protein with tetratricopeptide repeats 1 (IFIT1) has been reported to sequester viral PPP-RNA, inhibiting the replication of virus with this structure (*121*). Myxovirus resistance protein 1 (MxA) also demonstrates antiviral activity against various viruses, including influenza virus (*122*). Conversely, other ISGs may be detrimental to

the host, such as chemokine interferon-γ inducible protein 10 kDa (CXCL10), which induces inflammation and enhances lung injury (*123, 124*). Besides, some ISGs play dual role; for instance, ISG15 mediate a conjugation process called ISGylation that prolongs the activation of IRF3 and enhance the cell intrinsic innate signaling (*125*) but also inhibits key components like RIG-I and STAT2 to provide negative feedback to IFNs pathway (*126*). Despite these insights, the underlying mechanisms of most ISGs remain unclear.

The shared downstream signaling of type I and type III IFN pathways functions similarly. However, increasing evidence showed that type I and type III IFNs-induced ISGs profile exhibit temporal and spatial difference (*127, 128*). These differences could attribute to the distinct usage of receptors. IFNAR, composed of IFNAR1 and IFNAR2 subunits, is expressed in all cell types. In most cases, type I IFNs firstly bind IFNAR2 with high affinity and then recruit the lower-affinity IFNAR1 (*118*). In contrast, IFNβ bind IFNAR1 with higher affinity and induce ISGs more potently compared with IFNα (*129, 130*). On the other hand, IFNLR, mainly expressed on epithelial cells (*131*), is made of IFNL1 and IL10Rβ. The latter is shared with other IL-10 family members, such as IL-22, IL-10 (*132, 133*). IFNλ binds to IFNLR1 with high affinity and subsequently recruits IL-10Rβ to activate downstream signaling. This difference in binding affinity contributes to the distinct outcome of ISG transcription in magnitude and kinetics (*118*). Nevertheless, the mechanism underlying these fine-tune modulations in type I and type III IFNs are still elusive.

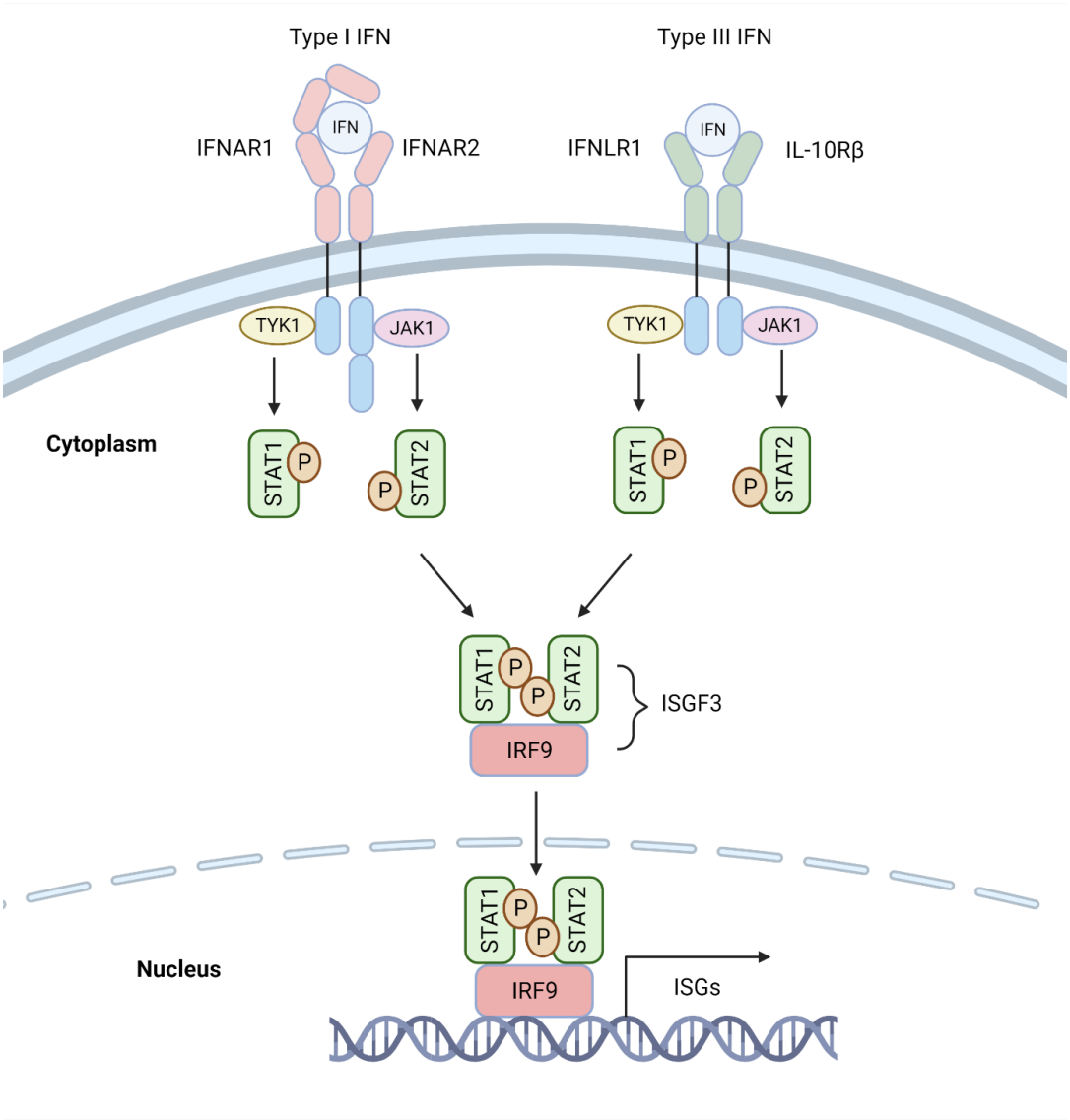

Figure 7. Type I and Type III IFN signaling pathways. Type I IFNs bind to a receptor comprised of the IFNAR1 and IFNAR2 subunits, while Type III IFNs interact with a receptor comprised of the IFNLR1 and IL-10Rβ subunits. These receptor subunits then form heterodimers, recruiting tyrosine kinase 1 (TYK1) and janus kinase 1 (JAK1) kinases, which further phosphorylate STAT1 and STAT2. Phosphorylated STAT1 and STAT2, along with IRF9, form a complex named ISGF3, which translocates into the nucleus and initiates the transcription of ISGs. Adapted from (*118*) via Biorender.

1.3 Antiviral innate immunity

Viruses are a group of extremely simple microorganisms. The typical components of a virus particle comprises only genome and proteins, some viruses, referred as enveloped viruses, also carry lipid and carbohydrates originated from the host (*134*). According to the genome types, viruses can be classified as double-stranded (ds) DNA viruses, single-stranded (ss) DNA viruses, dsRNA viruses, ssRNA viruses (positive strand or negative strand), retroviruses, and segmented viruses (*135*).

As viruses rapidly replicate and spread, they have emerged as the leading cause of infectious diseases in humans, posing a severe threat to human health. The recognition of viruses by pattern recognition receptors (PRRs) triggers immune responses to counteract infections. However, viruses have evolved intricate strategies to escape detection or disrupt the cascades of innate immune signaling. Therefore, studying this dynamic interplay offers valuable insights into the fundamental mechanisms of the innate immune system and the development of therapeutics against infections.

1.3.1 Overview of virus recognition by the cell intrinsic innate immune response

Viral genomic RNA or double-stranded RNA intermediates can trigger RIG-I and MDA5 in cytoplasm or TLR3 in the endosome, and initiate cell-intrinsic immune signaling to counteract virus infection.

It has been reported that the knockout of RIG-I in mouse embryonic fibroblasts (MEFs) severely impaired the production of IFN-β and the transcription of ISGs induced by Newcastle disease virus (NDV), vesicular stomatitis Virus (VSV), and sendai virus (SeV) (*136*). In an in vivo study involving Japanese encephalitis virus (JEV) infection, it was observed that IFNα production in RIG-I knockout mice, but not in MDA5 knockout mice, was markedly decreased. These mice also exhibited higher susceptibility compared to wild-type (WT) mice, suggesting the critical role of RIG-I-specific recognition in host immune defense against JEV (*137*). While hepatitis E virus (HEV) seems to be sensed by both RIG-I and TLR3 to induce high antiviral response (*138*)

On the other hand, MDA5 is responsible for the recognition of Picornaviridae viruses, such as encephalomyocarditis virus (EMCV) (*137*), hepatitis A virus (HAV) (*139*), hepatitis D virus (*140*), and Mengo virus (*137*). Norovirus, a gastroenteritis-causing virus belonging to the Caliciviridae family, was also reported to be sensed by MDA5 (*141*). Notably, recent studies have shown that LGP2 is also required for MDA5-dependent recognition of HAV (*139*) and HDV (*140*). Reovirus-induced IFN-β production was dramatically impaired in MDA5 knockout mice but completely abolished in RIG-I and MDA5 double knockout mice, demonstrating the participation of both RIG-I and MDA5 in virus sensing (*142*). Similarly, two members of the Flaviviridae family, Dengue virus (DENV) and West Nile virus (WNV), were also recognized by both RIG-I and MDA5 (*143*).

The role of RIG-I-like receptors (RLRs) in protecting host cells against virus invasion has been extensively investigated. However, the complex role of TLR3 during virus infection has not yet been fully elucidated. TLR3 has been reported to play an important role in specific viral infections. For example, during infection with encephalomyocarditis Virus (EMCV), TLR3-deficient mice exhibited a lower innate immune response and had a lower survival rate (*137*). In the case of coxsackievirus B subtype 3 (CVB3) infection, the TLR3-dependent type II IFN pathway was shown to be crucial for host defense, as TLR3-deficient mice were more vulnerable to infection (*144*). TLR3 is also required for the prevention of the dissemination of herpes simplex virus 1 (HSV-1) in the central nervous system (*145*). In various other viral infections, including West Nile virus (WNV) (*146*) and respiratory syncytial virus (*147*), TLR3 has also been shown to play essential roles in mounting antiviral cytokines and chemokines, ultimately improving host survival.

However, there have been paradoxical findings as well. For instance, a study on WNV suggested that TLR3-mediated inflammation might facilitate the entry of the virus into the brain, leading to encephalitis (*146*). In the context of influenza A virus (IAV) infection, TLR3-deficient mice had more efficient viral replication in the lung but surprisingly showed a higher survival rate (*148*). Detrimental roles of TLR3 have also been reported in liver infections. In the case of Punta Toro virus (PTV) infection, the loss of TLR3 in mice was associated with lower liver disease and reduced lethality (*149*). Furthermore, TLR3 has been implicated in the establishment of glomerulonephritis in hepatitis C virus (HCV)-infected renal cells (*150*) .

The role of TLR3 in antiviral immunity remains complex and context-dependent, and further investigations are needed to better understand its functions in different viral infections.

1.3.2 Viral evasion strategies

To establish infection in the host, viruses have evolved various strategies to counteract the innate immune sensing system. These strategies include:

Circumventing sensing mechanisms: Some viruses directly interfere with the host's ability to sense viral RNA. For example, poliovirus uses a non-structural protein called Vpg to cap its genomic RNA, preventing the activation of RIG-I (*151*). Ebola virus VP35 sequesters viral RNA and competes with RIG-I to avoid immune sensing (*152*). Influenza A virus NS1 has been reported to bind to dsRNA and antagonize RIG-I recognition (*153*). Other viruses, such as DENV, HCV, and Severe Acute Respiratory Syndrome Coronavirus Type 2 (SARS-CoV-2), reorganize

the endoplasmic reticulum (ER) membrane to create replication organelles that physically block the sensing of cytosolic PRRs (*154-156*).

Interfering with signaling Components: Some viruses interfere with key components of innate immune signaling pathways, thus preventing their activation. For instance, the vaccinia poxvirus protein A46R, containing a TIR domain, competes with the TIR adaptor TRIF and inhibits IRF3 activation (*157*). Zika virus NS3 sequesters 14-3-3ϵ and 14-3-3η, inhibiting their interaction with RIG-I (*158*). Sendai virus V protein selectively binds to and inhibits MDA5 (*159*), IAV NS1 suppresses tripartite motif containing 25 (TRIM25)-mediated RIG-I ubiquitination (*160*), while HCV NS3-4A targets the E3 ligase Riplet, abolishing ubiquitination (*161*).

Cleavage or degradation of proteins: Viruses can cleave or degrade essential proteins in innate immune pathways to disable them. For example, Coxsackievirus B3 (CVB3) 3Cpro cleaves RIG-I (*162*), while CVB3 and Enterovirus 71 (EV71) use 2Apro to cleave MDA5 and MAVS (*163*). HCV NS3-4A can cleave MAVS to abrogate the RIG-I pathway (*164*). Hepatitis B virus (HBV) HBx ubiquitinates MAVS at Lys136, leading to proteasome-mediated degradation (*165*). During Hepatitis A virus (HAV) infection, 3ABC degrades MAVS (*166*), and 3CD antagonizes TLR3 by cleaving TRIF (*167*). Besides, foot-and-mouth disease virus (FMDV) cleaves MDA5 using a viral leader protein (*168*).

These various strategies employed by viruses allow them to evade or disable the host's innate immune system and establish a successful infection.

As this study mainly focused on RNA sensors, including TLR3, RIG-I and MDA5, five RNA viruses were used as tools to stimulate corresponding pathways.

1.3.3 Sendai virus

Sendai virus (SeV) is a enveloped, negative-stranded RNA virus consisting of a 15 kb genome, which tightly binds with the nucleocapsid protein N (*169*). The genome of SeV encodes six structural proteins. Nucleocapsid protein N, phosphoprotein P, polymerase L, together with viral genomic RNA, forms the nucleocapsid (*170*). The nucleocapsid closely interacts with the matrix protein M at the inner face of a lipid membrane (*171*). Another two structural proteins anchored on the surface of the membrane, hemagglutinin neuraminidase (HN) and glycoprotein F, are responsible for the binding, fusion and entry of the virus (*172*). Once nucleocapsid is released into the cytoplasm, the viral polymerase firstly initiates transcription

to generate a positive strand, then, the positive strand is translated into viral proteins, switching the virus to a replication mode, initiating the synthesis of negative genomic RNA (*169*). Finally, the genomic RNA is assembled with major structural proteins into virions with the assistance of the accessory protein C (*173*) and is released from cells with the help of M, HN and F (*169*).

The genomic RNA of SeV contains a 5'PPP modification and thus can be recognized by RIG-I (*174*). Additionally, during the replication, SeV sometimes generates uncomplete replication products, referred as defective interfering (DI) RNAs, these RNAs have been reported as RIG-I agonists and induce strong IFN responses (*175*). To evade the innate immune responses, SeV V protein directly binds with IRF3 and interferes with its activation (*176*), and C protein has also been reported to counteract IFN signal transduction (*177*)

1.3.4 Rift Valley fever virus

Rift Valley fever virus (RVFV) is an enveloped, segmented RNA virus. The genome is composed of two negative segments, L (6404 nt) and M (3885 nt), and an ambisense segment, S (1690 nt) (*178*). The L segment encodes the viral RNA-dependent RNA polymerase (RdRp), L protein (200), whereas the M segment encodes a polyprotein that generates two glycoproteins, Gn and Gc, and two nonstructural protein NSm1 and NSm2, after cleavage (227). The S segment encode nucleoprotein N and nonstructural protein NSs. RVFV utilize Gn and Gc for attachment and fusion to cells, respectively (*179*). Similar to other RNA viruses, each segment of RVFV is transcribed into mRNA, translating into viral proteins, and then initiates replication using polymerase L. N protein and NSs are also essential in these processes (*180, 181*). In the end, Gn/Gc glycoproteins mediate the assembly of viral particles (*182*) and budding from the Golgi compartment (*183*).

The genomic RNA of RVFV has been reported to be recognized primarily by RIG-I (*184*). In addition, transmission of exosomes from RVFV-infected cells to recipient cells could activate RIG-I and induce IFN-dependent autophagy (*185*). To counteract it, NSs of RVFV interact with several host immune factors to inhibit the expression of type I IFNs (*186*). In addition, RVFV induces an alternative splicing of a significant factor in the RIG-I pathway, atypical RIO kinase 3 (RIOK3), reducing the type I IFN production (*187*).

1.3.5 Hepatitis D virus

Hepatitis D virus (HDV) is a defective, negative stranded RNA virus with a 1.7 kb circular RNA genome that encodes only one protein, HDAg (*188*). It relies on the Hepatitis B virus (HBV) surface antigen (HBSAg) for the dissemination (*189*). The coinfection of HDV and HBV causes severe viral hepatitis (*190*). HDV infection initiates from an interaction with sodium taurocholate co-transporting polypeptide (NTCP) and fusion with cell membrane using HBV envelope protein, L-HBsAg (*191*). Viral ribonucleoprotein (RNP) then is transported into the nucleus where the rod-structured RNA genome generates both positive and negative RNA, producing the Small (S)-HDAg. Subsequently, adenosine deaminase acting on RNA 1 (ADAR1) of the host introduces a mutation on the S-HDAg, leading to an open reading frame (ORF) extension. This mutated RNA then produces Large (L)-HDAg, forming RNPs together with the RNA genome and S-HDAg and being released with the help of HBsAg (*188*).

HDV RNA replication is required for the activation of innate immune responses via MDA5, with LGP2 also reported as essential for proper MDA5 sensing (*140, 192*). It has been reported that both type I and type III IFN treatment only moderately inhibit HDV replication (*192*), which suggests a potential innate immune evasion strategy; however, research in this area is still limited and the specific mechanisms are unknown.

1.3.6 Hepatitis E virus

Hepatitis E virus is a positive stranded RNA virus. Its 7.2 kb genome encodes three open reading frames (ORFs). ORF1 encodes a multifunctional protein that contains a methyltransferase domain, a guanyltransferase domain, a cysteine protease domain, a macrodomain, an RNA-helicase domain and an RNA-dependent RNA polymerase domain (*193*). ORF2 encodes the viral capsid protein, while ORF3 encodes a small protein that is involved in virus egress (*194*). The life cycle of HEV is still elusive (*195*). ORF2 has been reported to mediate the virus entry (*196*). After entry, the viral genome is released into the cytoplasm of the cell and directly translated into the ORF1-encoded protein. Then, a negative strand RNA intermediate is produced as template for the production of positive genomic RNA and subgenomic RNA. ORF2 and ORF3 are translated by subgenomic RNAs (*197*) and were reported to be responsible for assembly (*198*) and release of the virion (*199*), respectively.

HEV genomic RNA induces strong innate immune responses (*200*). Inhibition of the TLR3 pathway by suppressing TRIF has been reported to reduce HEV-induced IL-8 expression (*201*).

RIG-I and MDA5 have also been suggested as potential sensors (*138*). Controversially, TLR3, RIG-I and MDA5 have been shown to be dispensable for the recognition (*200*). However, the PRRs responsible for its sensing are still unclear. Various viral proteins of HEV exhibit inhibitory functions on innate immune signaling. For example, the protease domain of ORF1 has been shown to deubiquitinate RIG-I and TBK1 (*202*), the methyltransferase inhibits the MDA5-mediated IFNs activation (*203*), ORF2 suppresses factors of the RIG-I and TLR3 pathways (*204*) and ORF3 attenuates the TLR3-mediated NF-κB signaling (*205*). These studies are mostly in vitro using overexpression system, the real effect of viral proteins in in vivo studies still need to be determined.

1.3.7 Severe acute respiratory syndrome coronavirus 2 (SARS-CoV-2)

Severe acute respiratory syndrome coronavirus 2 (SARS-CoV-2), belonging to the Coronaviridae, is a large positive stranded, enveloped RNA virus and has caused severe human respiratory diseases since the 2019 pandemic (*218*). The genome of SARS-CoV-2 is approximately 30 kb in length and contains 14 ORFs, encoding 29 viral proteins. Two-third of the genome at the 5’ end encode only two large polyproteins, pp1a and pp1ab (*219*). These two proteins are cleaved into 16 non-structural proteins (NSPs) by two viral proteases, M^{pro} and PL^{pro}. These NSPs participate in viral transcription and replication. In addition, four ORFs at the 3’ end encode four structural proteins: nucleocapsid (N), spike (S) protein, membrane (M) protein and envelope (E) protein, which are responsible for viral entry and release. Other accessory proteins are encoded by the region between the four ORFs (*220*). In brief, SARS-CoV-2 attaches and enter cells via S protein, and start the translation of viral proteins with its positive genome. Then, a set of viral proteins is recruited to its genome to initiate replication. Eventually, the viral genome and structural proteins are assembled into virions and released by exocytosis (*221*).

While MDA5 and LGP2 may be the major RNA sensors recognizing genomic RNAs or replicative intermediate of SARS-CoV-2 (*222*), RIG-I also appear to play a role (*223*). However, large numbers of viral proteins of SARS-CoV-2 have inhibitory roles in innate immunity, aiding the virus in establishing infection. These viral proteins block innate immune signaling through cleavage (Nsp3, Nsp5), degradion (Nsp5, Nsp14) or phosphorylation inhibition (Nsp1, Nsp5, Nsp6, Nsp12, Nsp13) of several key innate immune factors and many other mechanisms (*224*).

1.4 TLR3 SNPs and infectious diseases

Even though the role of TLR3 in antiviral immunity is controversial, TLR3 single nucleotide polymorphisms (SNPs) were shown to be closely linked to infectious diseases. Statistical analysis identified the L199F mutation of TLR3 in herpes simplex encephalitis (HSE) patient and varicella-zoster virus encephalitis patient, it is strongly associated with high susceptibility of herpes simplex virus infection (*225*). L297V, L360P, G743D, R811I, R867Q were found in patients with HSE. In the peripheral blood mononuclear cells (PBMCs) with the L297V mutation, IFN response did not show impairment, however, L360P, G743D, R811I, R867Q in P2.1 cell lines were reported as loss-of-function (*226, 227*). F303S was identified in influenza-associated encephalopathy patients and also showed suppressed NF-κB and IFNβ production in HEK293 cells (*228*). L412F is highly associated with herpes labialis, Zika virus microcephaly, Japanese encephalitis, severe coronavirus disease 2019 (COVID-19), chronic hepatitis C infection and high susceptibility of cytomegalovirus (CMV) (*229-234*). It reduced IFNγ response in NK cells, even though the cytokines production was not affected in general. P554S and P680L were reported in HSE patients as well, fibroblasts from individuals carrying these mutations exhibited a significant impairment in the production of IFNβ, IFNλ and IL-6 upon poly(I:C) stimulation (*235*). In addition, F459L and M870V were also reported to be related to chronic HCV infection and life-threatening COVID-19, respectively (*236, 237*). These pieces of evidence hint at the pivotal role of TLR3 during virus infection; however, a comprehensive study of these SNPs on certain cell type, for instance, hepatocyte, has not been conducted and the specific role of TLR3 during hepatitis virus infection has not been clarified.

1.5 A CRISPR-Cas9 screen to identify cellular factors contributing to the TLR3 response in hepatocytes

To comprehensively understand the innate immune responses in hepatocytes on a broader scale, a genome-wide CRISPR/Cas9 screen in hepatocytes, with a specific focus on the TLR3 pathway in hepatocytes was conducted, followed by a large-scale siRNA validation.

1.5.1 The principle of CRISPR-Cas9 system.

Genome-wide clustered regulatory interspaced short palindromic repeats (CRISPR)/Cas9 screen is widely used for identifying host determinants in virus replication (*238, 239*) and innate immunity (*240, 241*).

CRISPR/Cas9 is the adaptive immune system of bacteria, which integrates exogenous DNA, such as that from virus, between short repeat sequences of their genome called CRISPR locus. (*242*). Subsequently, bacterial RNA polymerase transcribes these sequences into CRISPR RNAs (crRNAs) (*243*). Simultaneously, another transactivating CRISPR RNA (tracrRNA) is transcribed from upstream of the CRISPR locus (*244*). These two RNAs then hybridize and form a duplex, incorporating into CRISPR-associated nuclease 9 (Cas9) and forming an RNP (*245*). The foreign sequence in crRNA leads the RNP to target its complementary sequences and cleaves the DNA to generate a double strand break (DSB) (Figure 8) (*245*). This strategy provides bacteria with resistance to virus infection or plasmid conjugation (*246*). The DNA targets can be manipulated by replacing crRNA:tracrRNA with a designed guide RNA containing the interested sequence (*245*).

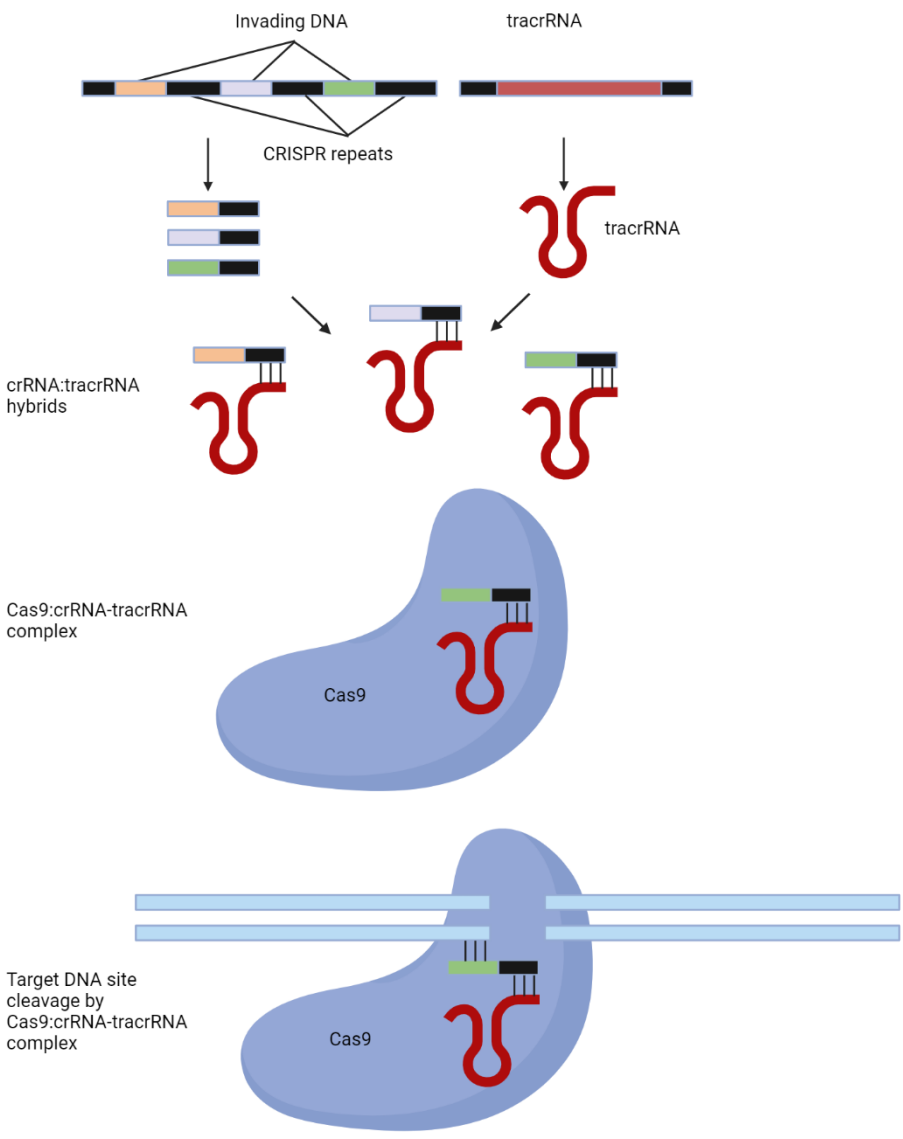

Figure 8. The mechanism of CRISPR/Cas9 system. The invading RNA are inserted into the genome of bacteria, separated by several CRISPR repeats. crRNA is produced from these regions, carrying the foreign sequences. A tracrRNA is transcribed from upstream of the CRISPR repeat region, hybridizing with crRNA through base-paring. The duplex then is then incorporated into a nuclease called Cas9 and cleaves the target sequence that matches with crRNA. Adapted from (*247*) and created by Biorender.

Next, two types of DNA repair mechanisms: nonhomologous end-joining (NHEJ) and homology-directed repair (HDR), are engaged in the DSB repair. NHEJ directly joint the two broken DNA parts and usually causes random insertions or deletions (Indels), which sometimes results in open reading frame shift, thereby disrupting the protein function (*248*), while HDR uses a homologous DNA template to reconstruct the broken DNA (Figure 9) (*249*). Indels mutation on target site can be achieved by NHEJ, and by providing a homologous DNA template into cells, insertion and replacement can also be obtained through HDR. Besides, more applications, such as rearrangement, gene activation and DNA modification, are also available (*247*).

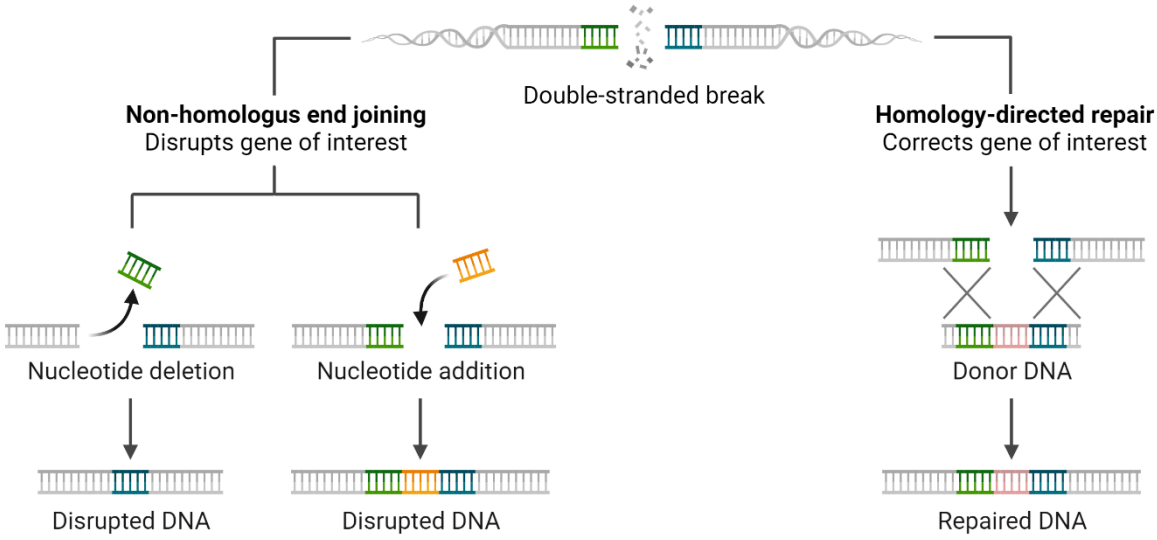

Figure 9. The mechanism of NHEJ and HDR. Double-stranded break (DSB) in eukaryotic cells can be repaired in two ways: NHEJ and HDR. NHEJ repair is a simple but error-prone, which directly ligates the DSB with random deletions or insertions as no temple is referred. In contrast, HDR repair the DSB using the information from a homologous DNA template, providing more accuracy. Adapted from (*250*) with Biorender.

CRISPR/Cas9 system has high specificity; however, the mismatches between guide RNA and target sequence are still possible, sometimes resulting in unwanted cleavage or off-target events. In general, the mismatches at 5' end of the targeting sequence are more tolerant to

the system than the mismatched at the 3' end (*251*). However, the exact numbers of mismatches and the position of nucleic acid substitutions required for the off-target event are not entirely predictable.

1.5.2 A Genome-wide CRISPR/Cas9 screen identified factors contributing to the TLR3 response in hepatocytes

The initial purpose of the screen was to identify innate immune factors involved in the TLR3 pathway in hepatocytes. It was performed by my previous colleagues, Jannik Traut and Dr. Oliver Grünvogel, and started from a CRISPR/Cas9 screen in two hepatic cell lines, PH5CH and Huh7-Lunet-TLR3.

PH5CH is a non-neoplastic, immortalized liver cell line (*252*). It constitutively expresses TLR3, RIG-I and MDA5 (Betz et al., unpublished data) and is considered as immune-competent. In contrast. Huh7-Lunet is an hepatocellular carcinoma-derived cell line (*253*) that lacks the expression of TLR3 (Betz et al., unpublished data) and was transduced with ectopic TLR3 via lentiviral particles to achieve TLR3 competence (Huh7-Lunet-TLR3).

1.5.3 tBID death reporter

To positively select cells with phenotypes of interest, a truncated BH3 interacting domain death agonist (tBID) death reporter was generated by Jannik Traut.

BID is a protein of the BCL-2 family, which comprises some major apoptosis regulators (*254*). In the apoptosis process, BID is cleaved by caspase 8, converting it into its active form, truncated BID. This active form then binds with BCL2 Associated X (BAX) and BCL2 Antagonist/Killer 1 (BAK), both located at mitochondria. The interaction triggers the release of cytochrome c from the mitochondria, forming a complex with apoptotic protease activating factor 1 (APAF-1) and Caspase 9. Ultimately, this cascade activates effector caspase-3, leading to numerous cleavage event of cellular protein and resulting in cell death (*255*).

In the death reporter, tBID is tightly regulated by an IFIT1 promoter. Upon TLR3 activation, the signaling is initiated, triggering the phosphorylation and translocation of IRF3 and further the production of IFNs. These factors then bind to IFIT1 promoter, inducing the expression of tBID and eventually leading to the apoptosis and cell death (Figure 10).

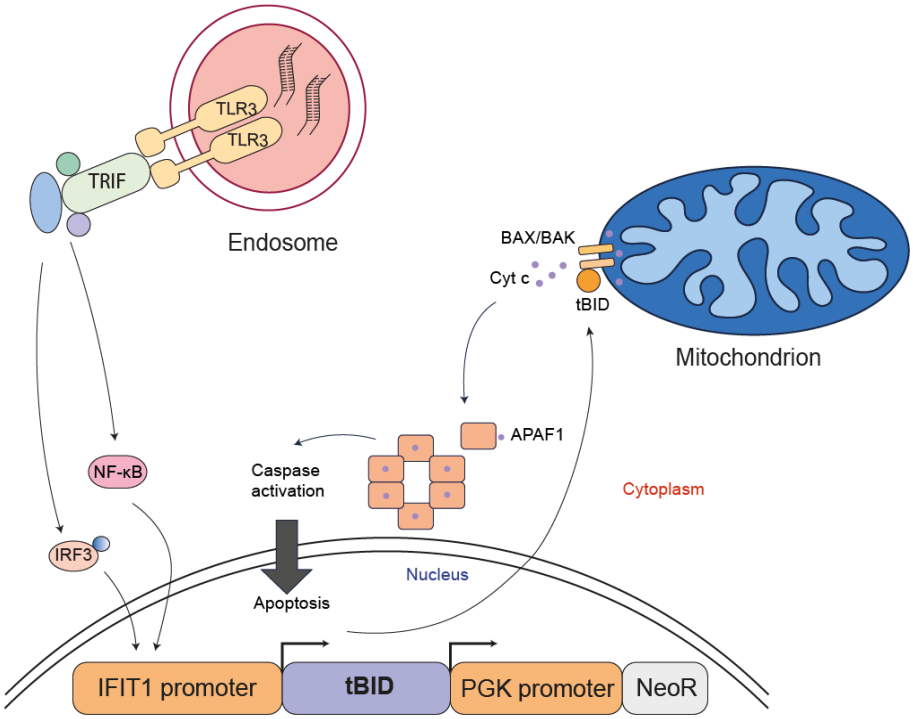

Figure 10. Schematic of tBID death reporter and its mechanism. The tBID expression is tightly controlled under the IFIT1 promoter, while PGK promoter control the neomycin resistance. Upon TLR3 triggering, IRF3 and NF-κB are activated and then bind to IFIT1 promoter, producing the toxic tBID. tBID subsequently binds to BAX and BAK, releasing cytochrome c from mitochondria to cytoplasm. This leads to the interaction between cytochrome c and APAF1, forming an oligomer that ultimately activates effector Caspase to induce apoptosis.

1.5.4 Work flow of the CRISPR-Cas9 screen

The tBID luciferase reporter, together with constructs containing the enzyme Cas9 (lentiCRISPRv2) were transduced into PH5CH and Huh7-Lunet-TLR3 cells via lentivirus. After antibiotic selection, stable cells were obtained and further transduced with lentiviral vectors encoding the GeCKOv2.0 human genome-wide single guide RNA (sgRNA) library, containing a total of 122,411 unique sgRNAs targeting 19,050 genes (with 6 sgRNAs per gene) and 1,864 miRNAs (with 4 sgRNAs per miRNA). A further antibiotic selection was performed. A synthetic analog of double-stranded RNA (dsRNA), polyinosinic:polycytidylic acid (Poly(I:C)) was used for stimulation. It is a strong agonist of TLR3, RIG-I and MDA5 (*256, 257*). By adding it to the cell culture supernatant, a specific activation of the TLR3 pathway was achieved. Stimulation of cells with an intact TLR3 signaling activated the IFIT1 promoter on the tBID death reporter, producing the tBID protein and inducing apoptosis, while TLR3-deficient cells generated by CRISPR/Cas9 knockout should survive (Figure 12).

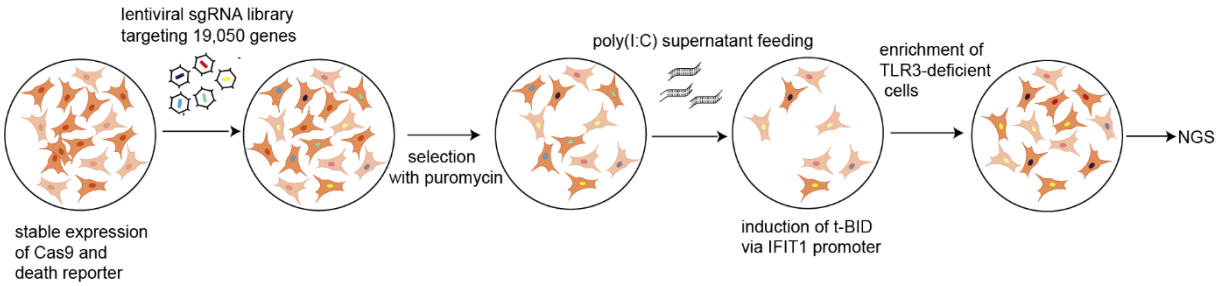

Figure 11. Workflow of the CRISPR/Cas9 screen. PH5CH cells and Huh7-Lunet-TLR3 cells were transduced with tBID death reporter, lentiviral sgRNA library, and Cas9. After selection, the cells were fed with poly(I:C) to specifically activate the TLR3 pathway. Cells with intact TLR3 pathway were supposed to be activated, producing tBID and finally eliminated. Surviving cells should be TLR3-deficient due to the inactivation of a factor contributing to the TLR3 response by a specific sgRNA. These cells were enriched, the sgRNA sequences amplified from genomic DNA were analyzed by next generation sequencing (NGS).

1.5.5 Potential innate immune factors identified in the screen and their validation

From the surviving cells, genomic DNA was extracted, sgRNA sequences amplified by PCR, using conserved linker sequences, and subjected to next generation sequencing (NGS) to identify the sequences corresponding to the employed sgRNAs (Figure 11). After intensive bioinformatic analysis, 50 protein coding genes and 5 miRNAs were defined as candidates (Table 1). Further information about the CRISPR/Cas9 screen procedure and details on the bioinformatic analysis can be found in Jannik Traut Master thesis and Dr. Oliver Grünvogel's PhD thesis.

Table 1. CRISPR/Cas9 screen Candidate gene list.

Gene Symbol	Name
ACTL8	Actin Like 8
ALG10B	ALG10B, Alpha-1,2-Glucosyltransferase
AMER3	APC Membrane Recruitment Protein 3
APEX2	Apurinic/Apyrimidinic Endodeoxyribonuclease 2
C12orf29	Chromosome 12 Open Reading Frame 29
C19orf43	Chromosome 19 Open Reading Frame 43
C1QB	Complement C1q B Chain
C22orf26	Chromosome 22 Open Reading Frame 26
CCT2	Chaperonin Containing TCP1 Subunit 2
COPA	Coatomer Protein Complex Subunit Alpha
FAM71B	Family With Sequence Similarity 71 Member B

GPT2	Glutamic-Pyruvic Transaminase 2
GPX8	Glutathione Peroxidase 8 (Putative)
HINFP	Histone H4 Transcription Factor
ISCU	Iron-Sulfur Cluster Assembly Enzyme
ITGA3	Integrin Subunit Alpha 3
KDM2A	Lysine Demethylase 2A
KLC4	Kinesin Light Chain 4
KLHL14	Kelch Like Family Member 14
KRTAP4-4	Keratin Associated Protein 4-4
MAD2L1	MAD2 Mitotic Arrest Deficient-Like 1 (Yeast)
MLST8	MTOR Associated Protein, LST8 Homolog
MRPL41	Mitochondrial Ribosomal Protein L41
NARS	Asparaginyl-TRNA Synthetase
NEUROD2	Neuronal Differentiation 2
PCF11	PCF11 Cleavage And Polyadenylation Factor Subunit
PHB2	Prohibitin 2
PIGW	Phosphatidylinositol Glycan Anchor Biosynthesis Class W
PNN	Pinin, Desmosome Associated Protein
PRPF19	Pre-MRNA Processing Factor 19
PRSS45	Protease, Serine 45
PSTPIP1	Proline serine threonine phosphatase-interacting protein-1
PTPRT	Protein Tyrosine Phosphatase, Receptor Type T
RALB	RAS Like Proto-Oncogene B
RAN	RAN, Member RAS Oncogene Family
RBM39	RNA Binding Motif Protein 39
RBM8A	RNA Binding Motif Protein 8A
RDM1	RAD52 Motif Containing 1
RIMBP2	RIMS Binding Protein 2
SLC45A2	Solute Carrier Family 45 Member 2
SPC24	SPC24, NDC80 Kinetochore Complex Component
TICAM1	Toll Like Receptor Adaptor Molecule 1
TLR3	Toll like receptor 3
TMEM230	Transmembrane Protein 230
TSC22D1	TSC22 Domain Family Member 1
TXNL4A	Thioredoxin Like 4A

UNC93B1	Unc-93 Homolog B1
VTN	Vitronectin
WTIP	Wilms Tumor 1 Interacting Protein
ZNF552	Zinc Finger Protein 552
hsa-mir-1273a	MicroRNA 1273a
hsa-mir-1299	MicroRNA 1299
hsa-mir-4732	MicroRNA 4732
hsa-mir-6870	MicroRNA 6870
hsa-mir-708	MicroRNA 708

To further confirm the knockdown phenotype of each candidate, two colleagues, Santa-Mariela Olivera-Ugarte and Dr. Arthur Lang, conducted a siRNA validation for individual genes, firstly in Huh7-Lunet-TLR3 cells and then in PH5CH cells. The knockdown of most genes either upregulated IFIT1 mRNA levels or did not show any effect upon poly(I:C) stimulation. Still, the silencing of some candidates showed reduced IFIT1 mRNA expression upon poly(I:C) supernatant feeding (Figure 12).

The four most promising candidates, Protein Tyrosine Phosphatase Receptor Type T (PTPRT), Lysine Demethylase 2A (KDM2A), cleavage and polyadenylation factor II subunit (PCF11) and RNA Binding Motif Protein 39 (RBM39) were further validated in PH5CH cells via siRNA. They exhibited pro-immune function there as well (Figure 12).

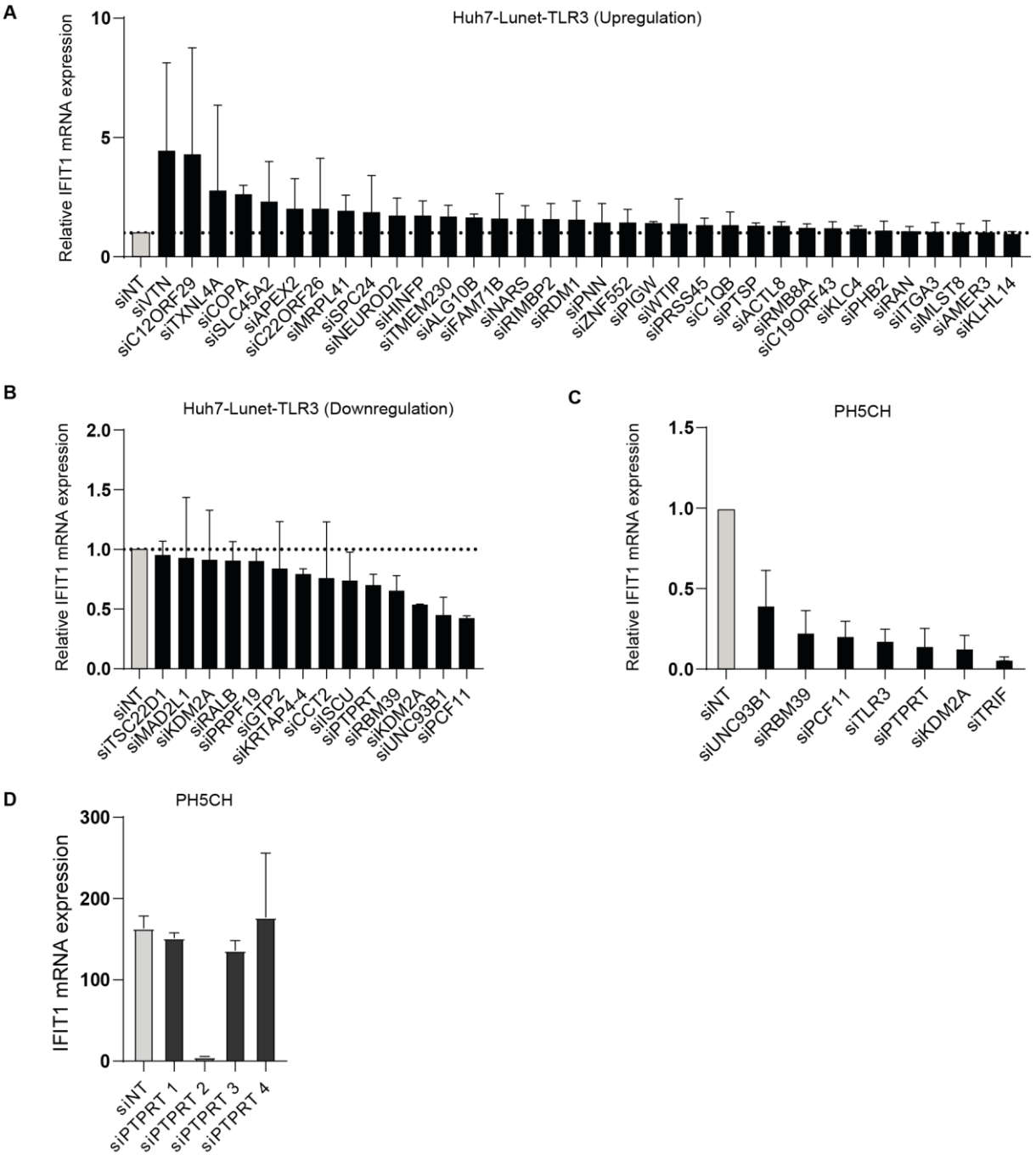

Figure 12. The siRNA validation of potential innate immune factors. (A-D) siRNA knockdown was conducted in Huh7-Lunet-TLR3 cells first, the four most significant candidates were further tested in PH5CH cells. Cells were treated with siRNA targeting each candidate for 48 h and fed with 50 µg/ml poly(I:C) in the supernatant for 8 h. IFIT1 mRNA was measured by qPCR to quantify the induction of the TLR3 pathway, data were normalized to siNT, thereby candidates were grouped into "upregulation" (A) or "downregulation" (B and C). IFIT1 mRNA expression upon 4 individual siPTPRT transfection and 50 µg/ml poly(I:C) supernatant feeding was measured (D). siNT: non-targeting siRNA. The designation of the 50 candidates follows the nomenclature of Table 1. siTRIF was used as a positive control.

1.5.5.1 The role of PCF11

PCF11, a key player in transcriptional processes, interacts with RNA polymerase II and is crucial for both transcription termination and 3' end processing of mRNA (*258*). Beyond these functions, PCF11 is also responsible for polyadenylation of the mRNA for numerous genes, indicating a multifaceted involvement in various cellular progresses. The downregulation of PCF11 is associated with regression of neuroblastoma and provided a target for therapeutic interventions (*259*). Interestingly, it has been reported as an immune-related factor a statistical analysis of lung adenocarcinoma (*260*), but its immune function has not been validated so far. Considering the complexity of the regulatory function of this protein, it was not investigated in depth in this study.

1.5.5.2 The role of PTPRT

PTPRT, a tyrosine phosphatase, plays a critical role in signaling transduction by dephosphorylating signal transducer and activator of transcription 3 (STAT3), consequently dampening the STAT3 signaling pathway (*261*). Beyond its role in regulating STAT3, PTPRT is implicated in deregulating paxillin phosphorylation, functioning as a tumor suppressor in colorectal cancer (*262*).

However, a literature reported that PTRPT is primarily expressed in brain and plays critical role in synapse formation (*263*). Additionally, a previous RNA-seq analysis confirmed that it is not expressed in liver cells (Betz et al., unpublished data), indicating an off-target event. Still, one siRNA targeting PTPRT was extremely efficient in blocking TLR3 responses (siPTPRT2, Figure 12D), suggesting that it might be worthwhile to identify the true target gene.

1.5.5.3 The role of KDM2A

KDM2A, a histone demethylase, plays a crucial role in the regulation of chromatin structure. With a specific affinity for CpG islands, it is involved in demethylating lysine 36 of histone 3 (H3K36) (*264*). This enzymatic activity positions KDM2A at the interface of epigenetic modifications, influencing gene expression patterns. Notably, KDM2A has been implicated in tumorigenesis, it has been reported to increase cell proliferation and invasiveness of lung cancer (*265*). Its regulatory effects on Wnt/β-catenin signaling also contributes to embryonic development and tissue homeostasis (*266*) highlighting its multifaceted involvement in biological processes.

Furthermore, KDM2A's impact extends to the immune system, where its inhibition has been shown to enhance adaptive immunity by promoting T-cell proliferation (*267*). This connects the chromatin dynamics with the modulation of key cellular components involved in immune function. However, its role in innate immunity is unknown so far.

1.5.5.4 The role of RBM39 in mRNA splicing and beyond

RBM39, also known as hepatocellular carcinoma 1 (HCC1), coactivator of activating protein-1 (AP-1) and estrogen receptors (ERs) (CAPERα), was firstly identified as an auto-antigen in a hepatocellular carcinoma patient in 1993 (*268*). It is upregulated in various cancers, such as breast cancer, lung cancer and colorectal cancer, and thus highly associated with the malignant progression (*269-271*).

RBM39, belonging to RNA binding protein (RBP) family, contains a serine/arginine-rich domain at the N-terminus, followed by three RNA recognition motifs (RRMs). The last RRM is also known as U2AF homology motif (UHM), which is homologous to the UHM-ligand motif (ULM) of the key splicing factor, U2AF65. It was believed that RBM39 participates in alternative splicing by binding with U2AF65 via UHM-ULM interaction (*272*).

Splicing is a unique RNA post-transcriptional regulation of eukaryotes. In eukaryotic cells, protein-coding segments (exons) of pre-mRNA are intervened by non-coding segments (introns) (*273*). Splicing removes these intervals, enabling the production of functional proteins and is thus an essential post-transcriptional step (*274*).

Alternative splicing, achieved by selectively including or excluding these exons or introns (Figure 13), significantly diversifies the proteome. In addition, abnormal splicing can sometimes produce premature termination codons (PTCs) on transcripts, resulting in translation termination and subsequent degradation of the transcript by nonsense-mediated mRNA decay (NMD) (*275*). These mechanisms collectively provide regulatory functions to many biological processes, such as brain development (*276*), DNA repair (*277*) and immune responses (*278*).

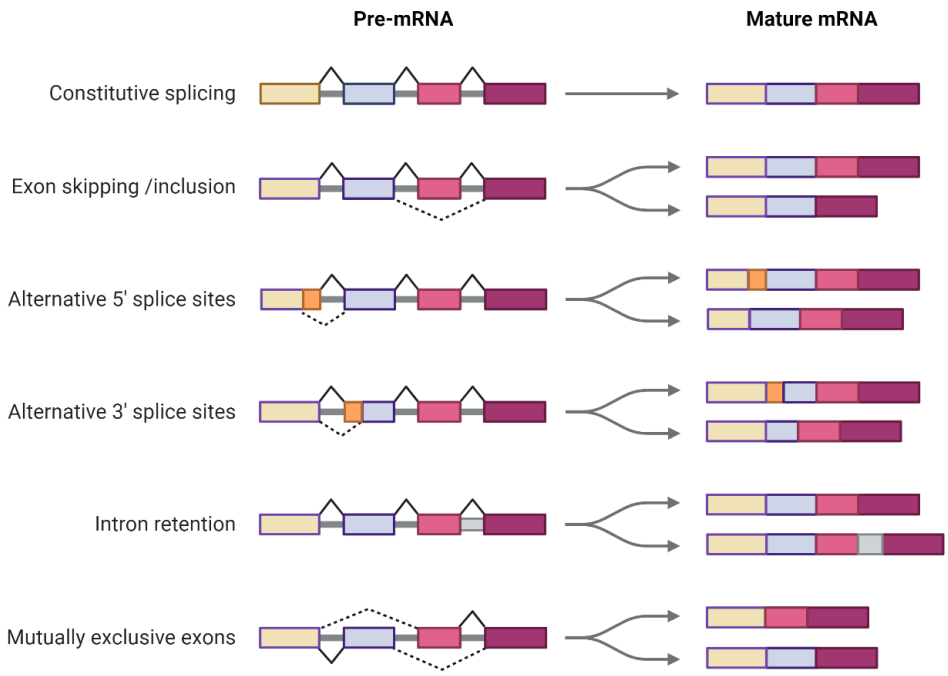

Figure 13. Distinct outcomes of alternative splicing. In alternative splicing, the selection of exons (exon skipping/inclusion), 5' splice sites and 3' splice sites, or the retention of introns results in the production of different mature mRNAs. Adapted from (*276*) and created by Biorender.

Beyond alternative splicing. In vivo studies have shown that the splicing mediated by RBM39 is essential for cancer cell survival (*279, 280*). A couple of sulfonamides, such as Indisulam, were found targeting RBM39 and thereby regarded as potential therapy for various cancers (*281, 282*). In this process, sulfonamides function as molecule glue that recruits RBM39 to an E3 ligase, DDB1 and CUL4 associated factor 15 (DCAF15), which ubiquitinates RBM39 and leads to proteasome-dependent degradation (*283, 284*).

More research has discovered the multifunction of RBM39. Except for the splicing function, it also characterized as a coactivator of AP-1, ERα, and ERβ (*285*). Furthermore, it was reported to inhibit lymphocytes transformation mediated by v-Rel, a viral NF-κB homolog (*286*). In addition, by regulating the transcription of c-Myc, RBM39 is involved in cell proliferation and metabolism as well (*287*). A clinical study has reported that degradation of RBM39 by sulfonamide drug enhanced anti-tumor immunity by producing more neo-epitopes (*288*). However, the function of RBM39 on innate immunity is still largely unknown.

2 Aims of the study

To comprehensively understand the innate immune responses in hepatocytes on a broader scale, a genome-wide CRISPR/Cas9 screen in hepatocytes, with a specific focus on TLR3, followed by a siRNA validation, were conducted by my previous colleagues. Four host factors emerged as potential innate immune factors. However, two of them showed off-target effects, while the specificity of RBM39's role was confirmed. Additionally, to obtain a nuanced understanding of the specific role of TLR3 in hepatocytes, a collection of TLR3 mutations was assembled and awaits validation. Therefore, my thesis followed several aims.

Identify off-targeted siRNA targets: A siRNA knockdown will be conducted using the siRNA showing off-target effect. An RNA sequencing will be followed to pinpoint the downregulated genes as candidates. The function of these candidates on TLR3 pathway will be evaluated in liver cell models.

Investigate the function of RBM39 in innate immunity: I aimed to access the functionality of RBM39 in various PRR-mediated pathways, focusing on TLR3 but also involving RIG-I and MDA5. These will be performed in hepatocytes but also other cell-types to compare the specificity of RBM39's role. I further aimed to understand the role of RBM39 on virus-induced immune response and virus replication. In addition, I aimed to understand the mechanism of RBM39-mediated regulation on innate immunity. I intend to identify innate immune factors that are regulated by RBM39. I will further investigate the biological processes related to RBM39's function in cell intrinsic innate immune response, including the RNA binding, co-transcription activity and splicing function.

Evaluate TLR3 SNPs in hepatocytes: I aim to compare the function of TLR3 SNPs associated with human diseases withTLR3 WT in activating TLR3-mediated cell intrinsic innate immune responses in hepatocytes.

By pursuing these aims, the goal is to achieve a more comprehensive understanding of the regulation of cell intrinsic innate immune responses in hepatocytes, especially confirming the specific role of TLR3 in the liver.

3 Materials and Methods:

3.1 Cloning:

3.1.1 PCR

Plasmids list:

Plasmid	Antibiotic resistance	Source
pWPI-RBM39.Esc	Neomycin	Provided by Arthur Lang
pWPI-RBM39.G268V	Neomycin	Generated in this study
pWPI-HA-RBM39.Esc	Neomycin	Generated in this study
pWPI-RBM39.Esc-HA	Neomycin	Generated in this study
pWPI-HA-RBM39. ∆ UHM	Neomycin	Generated in this study
pWPI-KDM2A	Neomycin	Generated by Arthur Lang
pWPI-SF-KDM2A	Neomycin	Generated in this study
pWPI-IRF3.sgRNA.Esc	Neomycin	Generated in this study
pWPI-TLR3	Puromycin	Provided by Ombretta Colasanti
pWPI-TLR3 L199F	Puromycin	Generated in this study
pWPI-TLR3 N284I	Puromycin	Provided by Jasper Hesebeck-Brinckmann
pWPI-TLR3 L297V	Puromycin	Provided by Jasper Hesebeck-Brinckmann
pWPI-TLR3 F303S	Puromycin	Generated in this study
pWPI-TLR3 L360P	Puromycin	Provided by Jasper Hesebeck-Brinckmann
pWPI-TLR3 L412F	Puromycin	Provided by Jasper Hesebeck-Brinckmann
pWPI-TLR3 F459L	Puromycin	Generated in this study

pWPI-TLR3 P554S	Puromycin	Provided by Jasper Hesebeck-Brinckmann
pWPI-TLR3 P680L	Puromycin	Generated in this study
pWPI-TLR3 L742F	Puromycin	Generated in this study
pWPI-TLR3 G743D	Puromycin	Generated in this study
pWPI-TLR3 R811I	Puromycin	Generated in this study
pWPI-TLR3 R867Q	Puromycin	Generated in this study
pWPI-TLR3 M870V	Puromycin	Generated in this study
pGL3-basic	Ampicillin	Promega, Madison, USA
pGL3-IRF3 982	Ampicillin	Generated in this study
pGL3-IRF3 149	Ampicillin	Generated in this study
PX459-backbone	Puromycin	Purchased (Addgene)
PX459-RBM39 KO1	Puromycin	Generated in this study
PX459-RBM39 KO2	Puromycin	Generated in this study
PX459-RBM39 KO3	Puromycin	Generated in this study
PX459-RBM39 KO4	Puromycin	Generated in this study
pAPM-backbone	Puromycin	Purchased (Addgene)
pAPM-shRBM39 1	Puromycin	Generated in this study
pAPM-shRBM39 2	Puromycin	Generated in this study
pAPM-shRBM39 3	Puromycin	Generated in this study

All polymerase chain reactions (PCRs) were conducted using PhusionFlash High-Fidelity Master Mix (ThermoFisher Scientific, Waltham, MA, USA) in a PCR Thermocycler (Analytik Jena, Jena, Germany). The reaction mixture for a 20 µl volume was set up as follows:

Components	Amount

DNA template	10 ng plasmid or 100 ng genomic DNA/PCR products
10 µM Primers	1 µl
PhusionMaster Mix (2x)	10 µl
miliQ water	Up to 20µl

The PCR program was set up as below:

Steps	Temperature	Time	Program
1	95°C	10s	Go to step 2
2	95°C	5s	Go to step 3
3	Primer melting temperature (Tm) of primers (shown in PCR amplification strategies)	30s	Go to step 4
4	72°C	1kb/15s	Go to step 2 (30 cycles)
5	72°C	5min	Go to step 6
6	4°C	∞	End

The RBM39.G268V, IRF3.sgRNA.Esc, and TLR3 SNPs sequences were amplified from plasmids pWPI-RBM39.Esc, pWPI-IRF3, and pWPI-TLR3, respectively, through overlap PCR. For segment 1, a forward primer without mutation and a reverse primer containing the mutation were used, while for segment 2, a forward primer with the mutation and a reverse primer without mutation were employed. Segments 1 and 2 were designed to have an approximately 15 bp overlap. Subsequently, these two segments were used as templates, using primers for a full-length PCR product to generate the mutated full-length sequence. Genomic DNA from PH5CH cells was extracted using the NucleoSpin Tissue Mini kit (Macherey Nagel, Düren, Germany). IRF3 promoter sequences, IRF3-982 and IRF3-149, were amplified from the genomic DNA of PH5CH cells. Details about PCR amplification are shown below:

PCR amplification strategies:

Product name	Template	Forward primer	Reverse primer	Tm
RBM39.G268V segment 1	pWPI-RBM39.Esc	#1	#4	62°C
RBM39.G268V segment 2	pWPI-RBM39.Esc	#3	#2	62°C
RBM39.G268V	RBM39.G268V segment 1 and 2	#1	#2	62°C
HA-RBM39.Esc	pWPI-RBM39.Esc	#5	#6	57°C
RBM39.Esc-HA	pWPI-RBM39.Esc	#7	#8	69°C
HA-RBM39. Δ UHM	pWPI-RBM39.Esc	#6	#9	68°C
SF-KDM2A	pWPI-KDM2A	#10	#11	65°C
IRF3.sgRNA.Esc Segment 1	pWPI-IRF3	#12	#15	62°C
IRF3.sgRNA.Esc Segment 2	pWPI-IRF3	#14	#13	62°C
IRF3.sgRNA.Esc	IRF3.sgRNA.Esc Segment 1 and 2	#12	#13	62°C
TLR3 L199F segment 1	pWPI-TLR3	#16	#19	63°C
TLR3 L199F segment 2	pWPI-TLR3	#18	#17	63°C
TLR3 L199F	TLR3 L199F segment 1 and 2	#16	#17	65°C
TLR3 F303S segment 1	pWPI-TLR3	#16	#21	64°C

TLR3 F303S segment 2	pWPI-TLR3	#20	#17	64°C
TLR3 F303S	TLR3 F303S segment 1 and 2	#16	#17	65°C
TLR3 F459L segment 1	pWPI-TLR3	#16	#23	63°C
TLR3 F459L segment 2	pWPI-TLR3	#22	#17	63°C
TLR3 F459L	TLR3 F459L segment 1 and 2	#16	#17	65°C
TLR3 P680L segment 1	pWPI-TLR3	#16	#25	63°C
TLR3 P680L segment 2	pWPI-TLR3	#24	#17	63°C
TLR3 P680L	TLR3 P680L segment 1 and 2	#16	#17	65°C
TLR3 L742F segment 1	pWPI-TLR3	#16	#27	63°C
TLR3 L742F segment 2	pWPI-TLR3	#26	#17	63°C
TLR3 L742F	TLR3 L742F segment 1 and 2	#16	#17	65°C
TLR3 R867Q segment 1	pWPI-TLR3	#16	#29	65°C
TLR3 R867Q segment 2	pWPI-TLR3	#28	#17	65°C
TLR3 R867Q	TLR3 R867Q segment 1 and 2	#16	#17	65°C

TLR3 M870V segment 1	pWPI-TLR3	#16	#31	65°C
TLR3 M870V segment 2	pWPI-TLR3	#30	#17	65°C
TLR3 M870V	TLR3 M870V segment 1 and 2	#16	#17	65°C
IRF3-982	Genomic DNA of PH5CH	#32	#33	60°C
IRF3-149	Genomic DNA of PH5CH	#34	#33	60°C

Primers for cloning:

Number	Sequence
#1	GCAGGCGCGCCATGGCAGACGATATTGATATTG
#2	TTTACTAGTTCATCGTCTACTTGGAACCAG
#3	CATAACTGAAGATATGCTTCGTGTGATCTTTGAG
#4	CTCAAAGATCACACGAAGCATATCTTCAGTTATG
#5	AGCTATGGCGCGCCATGGCCTACCCATACGACGTACCAGATTACGCTATGGCAGACGATATTGAT
#6	TAGTTTACTAGTTCATCGTCTACT
#7	ATTATAGGCGCGCCATGGCAGACG
#8	TTAGGCACTAGTTCAAGCGTAATCTGGTACGTCGTATGGGTAGGCCATTCGTCTACTTGGAACCAGTA GCTGTG
#9	TTAGGCACTAGTTCAAGAGGCAGCTGCAGCTAAAGC
#10	ATCTTGGGCGCGCCATGTGCTCTGGGAGATTCCAGAATATT
#11	CTTAGTACTAGTTTAGCTGATCTTCTGTATCAGCTTCTC
#12	CAAGCCTCAGACAGTGGTTC
#13	CGTAGTTTACTAGTTCAGCTCTCC
#14	TCCGAGATCCAATTGACTGACTAACCAGGGCAGGATCCGTGGC
#15	GTTAGTCAGTCAATTGGATCTCGGACAACTGGAGGGCGTGGCC
#16	CAGGTGTCGTGAGGAATTTCGAC
#17	GAATTCCTGCAGCCCGTAGTTTACTAG
#18	GAACTGGATATCTTTGCCAATTCATCTTTTAA
#19	TTAAAAGATGAATTGGCAAAGATATCCAGTTC
#20	GGCTTCCACAACTAGAATATTCCTTCCTAG
#21	CTAGGAAGGAATATTCTAGTTGTGGAAGCC
#22	CAGGAATGGAGAGGTCTAGAAAATATTTTAGAAATC
#23	GATTTCTAAAATATTTTCTAGACCTCTCCATTCCTG
#24	CTTTGCAACACTCTACCTCACTATCATG
#25	CATGATAGTGAGGTAGAGTGTTGCAAAG
#26	CAGTACATCGAGTTTTTGGTTTCAAAGAAATAG

#27	CTATTTCTTTGAAACCAAAAACTCGATGTACTG
#28	CATGCACTCTGTTTGCAAAGAGGAATG
#29	CATTCCTCTTTGCAAACAGAGTGCATG
#30	GCACTCTGTTTGCGAAGAGGAGTG
#31	CACTCCTCTTCGCAAACAGAGTGC
#32	CGGGGTACCAGAGTTAGGAGGGAGCCTC
#33	GGAAGATCTGCCCTTTTTTGGGTTTCC
#34	CGGGGTACCGTCTCCTCCACTGAACTCGTAC
#35	CACCGCTACGTTCTTCATGGCCGT
#36	AAACACGGCCATGAAGAACGTAGC
#37	CACCGTAGAAGCAAAGAGAGGCGA
#38	AAACTCGCCTCTCTTTGCTTCTAC
#39	CACCGTGCCATCCGAGGAAAGATT
#40	AAACAATCTTTCCTCGGATGGCAC
#41	CACC GAGGCAACCCAATCTTTCCT
#42	AAAC AGGAAAGATTGGGTTGCCTC
#43	TCGAGAAGGTATATTGCTGTTGACAGTGAGCGAAGACTGAAGCTTCAGCTTTAGTAGTGAAGCCACAG ATGTACTAAAGCTGAAGCTTCAGTCTGTGCCTACTGCCTCGG
#44	AATTCCGAGGCAGTAGGCACAGACTGAAGCTTCAGCTTTAGTACATCTGTGGCTTCACTACTAAAGCT GAAGCTTCAGTCTTCGCTCACTGTCAACAGCAATATACCTTC
#45	TCGAGAAGGTATATTGCTGTTGACAGTGAGCGCGCTCAGTGCCTCTAGCAATAGTAGTGAAGCCACAG ATGTACTATTGCTAGAGGCACTGAGCTTGCCTACTGCCTCGG
#46	AATTCCGAGGCAGTAGGCAAGCTCAGTGCCTCTAGCAATAGTACATCTGTGGCTTCACTACTATTGCT AGAGGCACTGAGCGCGCTCACTGTCAACAGCAATATACCTTC
#47	TCGAGAAGGTATATTGCTGTTGACAGTGAGCGAATAATTTAACTCCTGAGGAAATAGTGAAGCCACAG ATGTATTTCCTCAGGAGTTAAATTATCTGCCTACTGCCTCGG
#48	AATTCCGAGGCAGTAGGCAGATAATTTAACTCCTGAGGAAATACATCTGTGGCTTCACTATTTCCTCA GGAGTTAAATTATTCGCTCACTGTCAACAGCAATATACCTTC
#49	CCAGACACCTCTCCGGACAC
#50	TAATACGACTCACTATAGGGCAGCTCAGCACATGCCTCAC

3.1.2 Agarose Gel Electrophoresis:

A 0.8%-2% agarose gel was prepared based on the size of PCR products (see below) in TAE buffer (40mM TRIS, 40 mM acetic acid, 1 mM EDTA). GelRed Nucleic Acid Gel Stain (Biotium, Fremont, USA) was added to the melted gel at a 1:10000 dilution. PCR products were mixed with 6x DNA loading dye (ThermoFisher scientific, Waltham, USA) and loaded into lanes. GeneRuler 1kb DNA ladder (ThermoFisher scientific, Waltham, USA) was loaded separately to indicate the size of bands. The gel was run at 100 V for 30 min to 1 h until the desired bands were fully separated Imaging was performed using the Intas UV system (Intas science imaging, Göttingen, Germany).

PCR product size	**Agarose concentration**
500 bp-7 kb	0.8%

400 bp-6 kb	1%
200 bp-3 kb	1.5%

3.1.3 Gel purification

Following agarose gel electrophoresis, the desired bands were excised and extracted using the Gel and PCR cleanup kit (Macherey Nagel, Düren, Germany) according to the manufacturer's instructions. The DNA concentration of PCR products was measured using Nano Drop Lite (ThermoFisher scientific, Waltham, USA).

3.1.4 Restriction digestion

PCR products, primers or plasmids were digested with restriction enzymes at 37°C for 2.5 h or overnight and then inactivated by incubating at 80 °C for 20 min. The reaction was set up as follows:

Components	**Volume (50 µl reaction mixture)**
DNA	1 µg
10X CutSmart Buffer (New England Biolabs, Ipswich, USA)	5 µl
Enzyme 1	10 units
Enzyme 2	10 units
Nuclease-free water	Up to 50 µl

3.1.5 Ligation

Digested DNA fragments were purified by Gel and PCR clean-up kit (Macherey Nagel, Düren, Germany) as mentioned above. The ligation mixture was set up as below and incubated at 16 °C for 2 h or overnight.

Components	**Volume (20 µl reactions)**
Linear vector DNA	100 ng
Insert DNA	5:1 molar ratio over vector
10X T4 DNA Ligase buffer	2 µl

(ThermoFisher scientific, Waltham, USA)	
T4 DNA Ligase (ThermoFisher scientific, Waltham, USA)	1 µl (1U)
Nuclease-free water	Up to 20 µl

3.1.6 Transformation

DH10α bacteria competent cells were thaw on ice for 10 min, 20 µl ligation products or 10 ng plasmid were aliquoted and then mixed gently with 50 µl competent cells. After 30 min incubation on ice, the competent cells were heat-shocked at 42 °C for 90 s and then transferred on ice for 2 min. 900 µl Lysogeny Broth (LB) medium were added, the competent cells were cultivated at 37 °C, 180 rpm for 45 min in a shaker incubator. Subsequently, competent cells with ligation products were centrifuged at 4000 rpm for 5 min and resuspended in 50 µl LB medium, and then spread evenly in an ampicillin LB-dish using a sterilized spreader. The dishes were cultivated at 37 °C overnight, colonies were collected and cultivated in ampicillin LB medium for 12 h. Plasmids were extracted by NucleoSpin plasmid kit (Macherey Nagel, Düren, Germany) according to manufacturer's instruction and were sent for sequencing (GATC Biotech, Konstanz, Germany).

3.2 Cell culture:

Cell lines	Antibiotic resistance	Sources
PH5CH	None	A gift from K. Shimotohno
PH5CH RBM39.Esc	Neomycin	Generated by lentiviral transduction
PH5CH KDM2A	Neomycin	Generated by lentiviral transduction
PH5CH SF-KDM2A	Neomycin	Generated by lentiviral transduction
PH5CH RBM39 G268V	Neomycin	Generated by lentiviral transduction
PH5CH IRF3 KO	None	From Andreas Betz

PH5CH eIRF3	Neomycin	Generated by lentiviral transduction
PH5CH RBM39 KO pool 1-4	Puromycin	Generated by lentiviral transduction
new PH5CH RBM39 KO pool 1 and 2	Puromycin	Generated by EPO
PH5CH shRBM39 1-3	Puromycin	Generated by lentiviral transduction
Huh7-Lunet	None	A gift from Charles M. Rice
Huh7-Lunet-TLR3	Puromycin	From Oliver Grünvogel
Huh 7.5	None	A gift from Charles M. Rice
Huh 7.5-TLR3	Puromycin	From Ombretta Colasanti
Huh 7.5-RIG-I	Puromycin	From Ombretta Colasanti
Huh 7.5-MDA5	Blasticidin	From Ombretta Colasanti
A549	None	ATCC
A549-IFNAR/IFNLR KO	None	A gift from Marco Binder
HepG2-NTCP	Puromycin	A gift from Stephan Urban
HepG2/C3A	None	A gift from Loan Viet Dao Thi
Primary mouse hepatocytes	None	A gift from Martina Muckenthaler
Primary human hepatocytes	None	Purchased from BioIVT

Unless mentioned specifically, all cells were cultivated in DMEM (Dulbecco's Modified Eagle Medium,Life Technologies, Darmstadt, Germany) supplemented with 10% fetal bovine serum, nonessential amino acids (Life Technologies), 100 U/mL penicillin, and 100 ng/mL streptomycin (Life Technologies). Primary human hepatocytes (PHH) were cultured in William E media containing 1% (v/v) Glutamax, 1% (v/v) Non-Essential Amino Acids, 1% (v/v) penicillin/streptomycin (all from Gibco, Waltham, USA), 0.2% (v/v) neomycin (Invivogen, USA),

2% (v/v) B27 (Gibco, Waltham, USA), 1% (v/v) N2 supplement (Gibco, Waltham, USA), 100 mM nicotinamide (Sigma-Aldrich, USA), 1.25 mM N-acetylcysteine (Sigma-Aldrich, USA), 10 µM Y27632 (Peprotech, USA), 1 µM A83-01 (Tocris, UK). All cells were cultivated in an incubator at 37°C and 5% CO2.

3.3 Lentivirus preparation and transduction

5 x 10^6 HEK293T cells were seeded in a 10 cm dish with 8 ml complete DMEM (Gibco, Waltham, USA) one day before transfection. The next day, the medium was replaced with serum-free DMEM 30 minutes before transfection. A mixture containing 5.14 µg of the target plasmid, 5.14 µg of pCMV-Gag-Pol plasmid, and 1.71 µg of pMD2-VSVG plasmid was prepared in 400 µl Opti-MEM (Gibco, Waltham, USA) and then mixed with 400 µl Opti-MEM containing 0.9 mM Polyethylenimine (PEI) (Polyplus Transfection SA, Illkirch-Graffenstaden, France). The mixture was incubated at room temperature for 20 minutes and then added evenly to HEK293T cells with drops. Cells were cultivated at 37°C and 5% CO2 in an incubator for two days. The supernatant was filtered with a 0.45 µm filter (Cytiva, Marlborough, USA) to remove cell debris and stored at -80 °C or directly used for transduction.

2 x 10^5 PH5CH cells or 1.8 x 10^5 Huh7.5 cells were seeded in a well of a 6-well plate, and the lentivirus-containing supernatant was added to the well. After 2 days, cells were selected with corresponding antibiotics, and survived cells were expanded for further experiments.

3.4 CRISPR/Cas9 knockout

3.4.1 Genome-wide CRISPR/Cas9 screen

PH5CH and Huh7.5-Lunet-TLR3 cells stably expressing the tBID death reporter and Cas9 were generated through lentivirus transduction and selected under neomycin and puromycin pressure, respectively, using the method mentioned above. Subsequently, lentivirus containing the GeCKOv2.0 human genome-wide sgRNA library (Addgene, USA) was transduced into these cells at MOI=0.3 to ensure each cell contains less than one sgRNA. The sgRNA library targeted a total of 19,050 genes and 1,864 miRNAs, with 6 and 4 sgRNAs designed for each gene and miRNA, respectively. Additionally, 1,000 non-targeting genes served as controls. After a second round of antibiotic selection with puromycin, cells were stimulated with 50 µg/ml poly (I:C) or PBS as a control to activate the TLR3 pathway. In TLR3-

competent cells, tBID induction led to cell death upon stimulation, while surviving cells with a knockout phenotype were collected and enriched.

Subsequently, genomic DNA from these cells was extracted using the NucleoSpin Blood L kit (Macherey-Nagel, Germany) following the manufacturer's instructions, and barcodes were added to the sequences through PCR. After agarose electrophoresis and gel purification, DNA sequences were sent to GATC Biotech (Konstanz, Germany) for next-generation sequencing (NGS) using Illumina Hiseq (50 bp single reads, 240 million reads total, 20% PhiX DNA). NGS data was analyzed by Oliver Grünvogel. Fold changes in poly(I:C)-treated samples compared with PBS controls were calculated based on mRNA read counts from four biological replicates. The top 2,000 sgRNAs showing up-regulation in each cell line were analyzed, and genes targeted by at least 5 sgRNAs in at least 3 replicates were chosen as candidates.

3.4.2 RBM39 knockout by lentiviral transduction

4 pairs of sgRNA sequences were designed (Sigma-Aldrich, Burlington, Massachusetts, USA) to target the first 1-3 exons of the coding sequence of RBM39, each pair contains a forward sequence and a reverse sequence (primers #35-#42). Restriction sites CACC and AAAC were added to 5’ end of the forward and reverse sequences, respectively. Two sequences were annealed in PCR Thermocycler (Analytik jena, Jena, Germany) with the setting as below:

Components	**Volume**
Forward sequence (100 µM)	1 µl
Reverse sequence (100 µM)	1 µl
10 X T4 DNA Ligase buffer (ThermoFisher scientific, Waltham, USA)	1 µl
T4 PNK (ThermoFisher scientific, Waltham, USA)	1 µl
Nuclease-free water	Up to 10 µl

The mixture was heated to 95 °C for 5 min and gradually cooled down to 25 °C at 5 °C/min. The PX459-backbone was digested with BsmBI restriction enzyme at 55 °C for 1 h and treated

with 10 units of Calf-intestinal alkaline phosphatase (CIP) at 37°C for 1 h. The digested PX459-backbone and sgRNA dimers were purified by Gel and PCR clean-up kit (Macherey Nagel, Düren, Germany) following manufacturer's instruction. Afterwards, sgRNA dimers was diluted 1:200 and ligated with the PX459-backbone to produce plasmids PX459-RBM39 KO 1, 2, 3, 4. Lentivirus preparation and transduction was shown before. After that, cells were selected with puromycin and validated by qPCR and western blot. For single knockout clones screening, cells were diluted to 10 cells/ml in DMEM, 50 µl of suspended cells were seeded into each well of a 96-well plate. Cells were expanded for further validation.

3.4.3 RBM39 knockout by electroporation

All materials for Alt-R® CRISPR-Cas9 system were purchased from IDT (Newark, USA). Guide RNA in Alt-R® CRISPR-Cas9 system consists of two parts: crRNA and tracrRNA. crRNA contains a targeting region and a tracrRNA-binding region, while tracrRNA is a 67 nt RNA sequence with a complementary sequence of crRNA. crRNA: tracrRNA duplex, together with Cas9 nuclease, form a ribonucleoprotein RNP to edit target genomic DNA. Alt-R® crRNA and tracrRNA was resuspended in 1 X TE buffer (10Mm Tris, 0.1 mM EDTA, pH 7.5-8.0) to final concentration of 200 µM, Alt-R® Cas9 Electroporation Enhancer was resuspended in 1 X TE buffer to concentration of 100 µM. The crRNA ID and targeting sequence was shown below:

ID	Targeting sequence
Hs.Cas9.RBM39.1.AK	GGCGGCAAGAATTCGACCAA
Hs.Cas9.RBM39.1.AB	AGGCGTGCCAATCATAGTAC
Hs.Cas9.RBM39.1.AE	CCAGTTAATCCTATTGCTAG

For each reaction, 2 µl crRNA and 2 µl tracrRNA were annealed at 95 °C for 5 min, and then gradually cooled down to room temperature. Subsequently, crRNA:tracrRNA duplex was diluted to 100 µM in PBS and mixed with Alt-R® Cas9 enzyme as follows:

Components	Volume
1 X PBS	2.1 µl
crRNA:tracrRNA duplex (100 µM)	1.2 µl
Alt-R® Cas9 enzyme (10 µg/ul)	1.7 µl

Total	5 µl

The reaction was performed at room temperature for 20 min. 8^10^6 PH5CH cells were seeded into a 15 cm dish one day before the electroporation. The next day, cells were washed with 1^PBS once, trypsinized with 3 ml trypsin-EDTA and resuspended with pre-warmed conditioned media (The filtered DMEM medium harvested from cell dishes with 2-3 days growing cells). 2^10^6 cells were resuspended in 90 µl supplemented nucleofection solution (Lonza, Basel, Switzerland) in an Eppendorff tube (Eppendorff, Humburg, Germany) 5 µl RNP complex and 4 µl Electroporation enhancer was added. The mixture was then transferred into an electroporation cuvette and inserted into Amaxa 2b nucleofection device (Lonza, Basel, Switzerland) for electroporation. Eventually, cells were further transferred to 6-well-plate for expansion and validation. For single knockout clone screening, cells were diluted to 10 cells/ml and 50 µl cell suspension was seeded into each well of a 96-well plate. Cells are cultivated and expanded for further experiments.

3.5 Stable RBM39 knockdown by shRNA

Primers containing the shRNA (#43-#48), XhoI and EcoRI restriction site at 5' and 3' end, respectively, were designed and purchased from Sigma-Aldrich (St.Louis, USA). Primers were dissolved into nuclease-free water to a concentration of 100 µM, 10 µl of each primer and 20 µl nuclease-free water was mixed, and annealed at 95 °C for 5 min and slowly cooled down to room temperature. Subsequently, 1 µl annealed primers, 1 µl ligase buffer, 1 µl T4 PNK enzyme was added into 7.5 c nuclease-free water, and were incubate at 37 °C for 1 h. Afterwards, the mixture was diluted 1:10. 3 µg Vector pAPM_Rab18 was digested by XhoI and EcoRI at 37 °C for 1 h, further treated with 10 units CIP at 37 °C for 30 min, and purified by Gel and PCR clean-up kit (Macherey Nagel, Düren, Germany). The digested vector was eluted in 20 µl nuclease-free water. The ligation was set up as below:

Components	**Volume**
Primer duplex	2 µl
Digested vector	2 µl
10 X T4 ligase buffer (ThermoFisher scientific, Waltham, USA)	1 µl

T4 ligase (ThermoFisher scientific, Waltham, USA)	1 µl
Nuclease-free water	Up to 10 µl

After 1h incubation at room temperature, the ligation product was transformed into DH10α as previously mentioned. Plasmid was obtained by NucleoSpin Plasmid kit (Macherey Nagel, Düren, Germany) and further transduced into PH5CH cells via lentiviral transduction. After puromycin selection, shRBM39 knockdown cells were established.

3.6 Drug treatment

3.6.1 Poly(I:C) stimulation

Poly (I:C) (HMW) (Invivogen, San Diego, USA) was dissolved in nuclease-free water at concentration of 1µg/µl according to manufacturer's instruction. For poly(I:C) supernatant feeding that specifically activates TLR3 pathway, indicated amount of poly(I:C) was added into the medium. For poly(I:C) transfection that triggers TLR3, RIG-I and MDA5 pathways, indicated amount of poly(I:C) was mixed with 2 µl Lipofectamine 2000 (Thermo Fisher Scientific, Waltham, USA) in OptiMEM (Gibco, USA), and incubated at room temperature for 20 min. The mixture was then dropped into the medium evenly. Medium was changed after 6 h. Cells were collected at indicated time points.

3.6.2 LPS stimulation

LPS (Invivogen, San diego, USA) was dissolved at concentration of 1 µg/ml in nuclease-free water. Indicated amount of LPS was added into the medium of PH5CH cells. Cells were harvested after 24 h.

3.6.3 IFNs stimulation

IFN2α were purchased from PBL (Norwich, USA), IFNλ1 were purchased Peprotech (*Rocky Hill*, USA), respectively. IFN2α and IFNλ1 were added to the medium at the final concentration of 200 IU/ml and 10ng/ml, respectively. After 24 h, cells were collected.

3.6.4 Indisulam treatment

Indisulam (Sigma Aldrich, St. Louis, USA) was dissolved in DMSO at a final concentration of 10 mM. Indicated amount of Indisulam were added to the supernatant, same amount of DMSO was used as control; Cells were cultivated for 48 h and collected.

3.6.5 Bafilomycin A1 treatment

Bafilomycin A1 (BafA) (Sigma-Aldrich, St. Louis, USA) was dissolved in nuclease-free water at concentration of 10 µM. BafA was added into the supernatant at a final concentration of 10 nM, cells were cultivated for 45 min and then used for further experiments.

3.6.6 siRNA transfection

siRNAs were ordered from Horizon Discovery (Cambridge, UK), siMAVS was ordered from Sigma Aldrich (St. Louis, USA). Cells were seeded with 60%-70% confluency one day before the transfection, the next day, 1.5 µM siRNA were mixed with 9 µl/ml Lipofectamine RNAiMax (ThermoFisher scientific, Waltham, USA) in OptiMEM according to manufacturer's instructions and incubated at room temperature for 20 min. Subsequently, the mixture was dropped evenly into the medium. Cells were cultivated for 48 h and used for further experiments.

3.7 RNA detection

3.7.1 Northern blot

The IRF3 probe sequence was amplified by PCR using T7 promoter containing primers #52 and #53. The PCR product was purified by Gel and PCR clean-up kit (Macherey Nagel, Düren, Germany). *In vitro* transcription was conducted using the Dig RNA labeling kit (Roche, Basel, Switzerland) and the reaction was set up as follows:

Components	**Amount**
DNA template	1 µg
10 X Dig RNA labeling mix	2 µl
10 X Transcription buffer	2 µl
20U/µl T7 RNA polymerase	2 µl
RNase-free water	20 µl

The mixture was incubated at 37 °C for 2 h, after that, 4 µl 1U/ul DNase (Promega, Madison, USA) was added into the reaction and incubated at 37°C for 30min. The reaction was stopped by adding 2 µl 0.2M EDTA (pH 8.0). Subsequently, the DIG-labeled probe was boiled at 95 °C for 5 min and rapidly cooled down on ice, stored at – 80 °C, ready-to-use.

RNA was extracted with TRIzol reagent (Invitrogen, Waltham, USA) according to manufacturer's instructions. Gel was prepared as below:

Components	Volume
Formaldehyde	7 ml
10 X MOPS (xxx)	5 ml
Agarose	0.86 g
DEPC-water	45 ml

Subsequently, 2 X RNA loading buffer (95% formamide, 0.025% SDS, 0.025% bromophenol blue, 0.025% xylene cyanol FF, 0.025% ethidium bromide, 0.5 mM EDTA) was mixed with RNA samples and was incubated at 65 °C for 10 min. After that, samples were loaded into each well and run at 150 Volt for around 30 min. A nylon membrane (Roche, Basel, Switzerland) was cut into the size of the gel and soaked in water for 1 min, and then transferred into 20 X SSC (3M sodium chloride, 0.3M sodium citrate, pH 7.0) for 1 min. Transfer device was set as below, RNA was transferred from gel to the nylon membrane for 6 h or overnight.

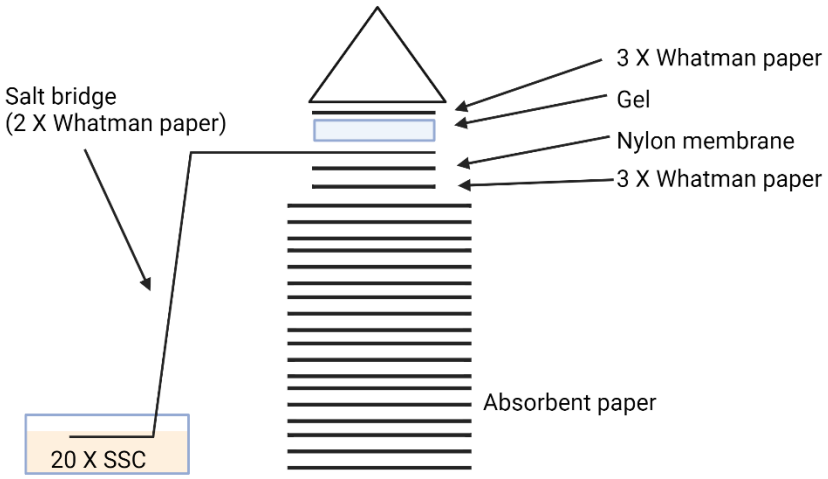

After that, the membrane was fixed at 120 °C for 30 min. 10 ml Easy Hyb was added to a rolling tube at 68 °C for 1 h, then 20 µl probe was added into the tube and incubated overnight. Next day, the membrane was washed by 2 X SSC buffer (with 0.1% SDS), 0.5 X SSC buffer (with 0.1% SDS), 0.1 X SSC buffer (with 0.1% SDS) step by step at 80°C, each wash took 10 min. After that,

the membrane was wash with 1 X DIG-wash buffer (Roche) at room temperature for 5 min and blocked with blocking solution (Roche) at room temperature for 1 h. 1.5 µl DIG-antibody was added into the blocking buffer and incubated for 1 h at room temperature. Subsequently, the membrane was washed 3 times by 1 X DIG-wash buffer for 10 min and incubated in 1 X detection buffer for 5 min. The CSPD solution was added on the membrane in a plastic bag, the membrane was then incubated at 37 °C for 30 min and the luminescence was measured by INTAS imaging system (Intas science imaging, Göttingen, Germany).

3.7.2 Real time quantitative PCR:

mRNA was extracted from cell samples using the NucleoSpin RNA Plus kit (Macherey Nagel, Düren, Germany). Reverse transcription was conducted using High-Capacity cDNA Reverse Transcription Kit (Thermo Fisher Scientific, Waltham, USA) following instruction of the manufacturer, specifically, for IRF3 isoform mRNA, random primers in the kit was replaced by same amount of oligo(dT)18 primers (Thermo Scientific, Waltham, USA). 150 ng mRNA were used as template to produce cDNA. cDNA was diluted with RNase-free water 1:10 for further real-time PCR. The qPCR reaction was set up as below:

Components	**Volume**
Primers_Forward (100 mM)	0.075 µl
Primers_Reverse (100 mM)	0.075 µl
2x iTaq Universal SYBR Green Supermix (Bio-Rad, Hercules, USA)	7.5µl
RNase-free water	2.35 µl
Diluted cDNA	5 µl

The reaction was conducted in CFX96 Touch Real-Time PCR Detection System (Bio-Rad, Hercules, USA) in following conditions: 95°C for 3 minutes, 95°C for 10 and 60°C for 30 seconds, 44 cycles. The fold change of target gene to reference gene was calculated as $2^{-\Delta\Delta Ct}$, the relative expression was further calculated by normalizing the treated samples to control (siNT, DMSO, mock). All mRNA fold change was calculated based on reference gene Glycerinaldehyd-3-phosphat-Dehydrogenase (GAPDH) expression, IRF3 isoforms mRNA fold was based on both GAPDH and Hydroxymethylbilane synthase (HMBS) expression. In particular, IRF3-(228+203)

primers were designed to target both IRF3-228 and IRF3-203, while IRF3 228 primers were designed to target only IRF3-228. The approximate ratio of IRF3-203/total IRF3 mRNA was calculated by following formula:

$$\frac{IRF3-203}{Total\ IRF3} = \frac{IRF3-228 + IRF3-203}{Total\ IRF3} - \frac{IRF3-228}{Total\ IRF3}$$

qPCR primers are listed below:

Target	Forward primer	Reverse primer
RBM39	GCAAGGACAGTCTTCTGTATGC	CGACGAACTCCACATAAGCAA
GAPDH	GAAGGTGAAGGTCGGAGTC	GAAGATGGTGATGGGATTTC
ISG15	CGCAGATCACCCAGAAGATCG	TTCGTCGCATTTGTCCACCA
MxA1	GTTTCCGAAGTGGACATCGCA	CTGCACAGGTTGTTCTCAGC
IFNB1	ATGACCAACAAGTGTCTCCTCC	GGAATCCAAGCAAGTTGTAGCTC
IL6	ACTCACCTCTTCAGAACGAATTG	CCATCTTTGGAAGGTTCAGGTTG
TNFAIP3	TCCTCAGGCTTTGTATTTGAGC	TGTGTATCGGTGCATGGTTTTA
IRF3	TAGAGCTCAGCTGACGGGAA	ACCTACGATGGAAGGTCGG
IFIT1	GAAGCAGGCAATCACAGAAA	TGAAACCGACCATAGTGGAA
IFNLR1	CCCAAGGGTAAGAGCTTCGAT	CCTTCATATTTTACTGACATGGACAAG
IL10RB	TTGCTGTGGTGCGTTTACAAG	CTTTCAGGTGCTGTGGAAGAGA
CXCL10	GGCATTCAAGGAGTACCTCTCTC	TGGACAAAATTGGCTTGCAGGA
SeV-P	CAAAAGTGAGGGCGAAGGAGAA	CGCCCAGATCCTGAGATACAGA
MALAT1	CCTGCAAATTGTTAACAGAA	TCAGCTTCCGCTAAGATGCTAGCTT
IRF3-Total	GACTTTTCCCAGCCAGACAC	TCCAGAATGTCTTCCTGGGTAT
IRF3-203+228	TACCCGGAGCTCCAAGACA	TTCCCATGGTCCGGCCTA
IRF3-228	CCCTTCATTGTAGGCTCCT	CACAGAACCAGAGGGCATAG
IRF3-222	CGACCTTCCATCGTAGGAGTT	GAAGTACTGCCTCCACCATTG
IRF3-202	AGCTACCCGGAGCTCCAA	CTCGGCCCAGGCCTAC
IRF3-219	CCTTCATTGTAGGTGAGTGAG	CCTGAGTTGTTAACCACTGTG

HMBS	TATGGCAAAAGCGGACAAGG	CTTCGCAACATCACCAATGGA
HEV	GGTGGTTTCTGGGGTGAC	AGGGGTTGGTTGGATGAA
HDV	GCGCCGGCYGGGCAAC	TTCCTCTTCGGGTCGGCATG

3.8 Protein detection:

3.8.1 Western blot:

Samples preparation: cells were collected and 30-100 µl lysis buffer (50 mM TRIS HCl pH 7.4, 150 mM NaCl, 1% Triton-X 100, fresh protease inhibitor was added to lysis buffer before use) was added to the cells. The cells were lysed on ice for 45 min, vortexed every 15 min. After that, cell lysates were centrifuged at 14,000 g, 4 °C for 15 min, supernatant was transferred to a new tube and mixed with 6 X Lämmli buffer (0.375M Tris-HCl, 9% SDS, 50% Glycerol, 0.03% Bromophenol Blue, 9% β-mercaptoethanol). The samples were boiled at 95 °C for 5 min, and immediately moved once ice for 2 min. 8%-12% SDS-PAGE gel was prepared as below:

Resolving Gel (2 gels)		Stacking Gel (2 gels)	
Reagents	Volume	Reagents	Volume
miliQ water	2.5 ml	miliQ water	1.9 ml
40% acrylamide	1.25 ml	40% acrylamide	0.25 ml
Tris-HCl pH 8.8 (10% SDS)	1.25 ml	Tris-HCl pH 6.8 (10% SDS)	0.3 ml
TEMED	5 µl	TEMED	2.5 µl
100% Ammonium Persulfate	5 µl	100% Ammonium Persulfate	3.75 µl

Samples were loaded into each well and run at 90 volts for 15 min and switch to 120 volt for around 1.5 h. The polyvinylidene difluoride (PVDF) membranes (Merk Millipore, Burlington USA) was soaked in 20 ml methanol for 1 min and then transferred to western blot transfer buffer (25 mM Tris, 192 mM glycine, pH 8.3, 20% methanol) for 1 min. Blotting was conducted using Wet/Tank Blotting system (Bio-Rad, Hercules, USA). After blotting, the membrane was blocked with 5% milk in PBST (0.05% Tween) or 5% BSA in TBST (0.01% Tween) for 30 min. first antibodies was added afterwards and incubated at room temperature for 2 h or at 4 °C

overnight. The membrane was washed 3 times with 1 X PBS and then incubated with second antibodies for 1 h at room temperature. Membranes were washed again with 1 X PBS for 3 times, incubated with the ECL Plus Western Blotting Detection System (Pierce, GE Healthcare, Little Chalfont, UK) for 1-2 min according to the instructions of the manufacturer, and imaged by Advance ECL Chemocam Imager (Intas Science Imaging, Germany). Western blot imaging was quantified by Fiji software. Antibodies used in the study was listed as follows:

Antibody list:

Antibody	Company	Article number
RBM39	ThermoFisher Scientific, Waltham, USA	PA5-31103
IRF3	Cell Signaling, Danvers, USA	# 11904S
β-actin	Sigma Aldrich, St.Louis, USA	A5441-2ML
p-IRF3	Cell Signaling, Danvers, USA	4947S
GAPDH	Proteintech, Rosemont, USA	60004-1-Ig
H2A.X	ThermoFisher Scientific, Waltham, USA	PA1-41004
Goat anti-rabbit IgG-HRP	Sigma Aldrich, St.Louis, USA	A6154
Goat anti-mouse IgG-HRP	Sigma Aldrich, St.Louis, USA	A4416

3.8.2 ELISA

The LumiKineTMXpress hIFN-β 2.0 kit was purchased by (InvivoGen, San Diego, USA), all procedures are strictly followed the manufacturer's instructions.

3.9 Cell Viability Assay:

Cell viability was performed using CellTiter-Glo® 2.0 Assay (Promega, Madison, USA) according to instructions of the manufacturer.

3.10 Luciferase reporter assay

PH5CH cells were seeded with 90 % confluency in 24 well-plate, luciferase reporters, combined with pRL-Gaussia reference reporter (Promega, Madison, USA), were mixed with 1 µl Lipofectamine 2000 (Thermo Fisher Scientific, USA) in OptiMEM (ThermoFisher, Waltham, USA) and incubated for 20 min. Afterwards, the mixture was dropped into PH5CH cells evenly and cultivated in incubator at 37 °C for 16 h. Subsequently, cells were lysed with Luciferase

lysis buffer (1% Triton X-100, 25mM Glycyl Glycin, 15mM $MgSO_4$, 4mM EGTA, 10% Glycerol, pH7.8, 10mM DTT) for 2 min, cell lysates were loaded into black-bottom plate (Greiner, Kremsmünster, Austria), 300 µl luciferase assay buffer (15 mM $K3PO_4$ pH7.8, 25 mM Glycyl-Glycin pH 7.8, 15 mM $MgSO_4$, 4 mM EGTA, 1mM ATP, 200 µM D-Luciferin for firefly-luciferase, 5µM coelenterazine for Guassia-luciferase) was used to activate luciferase activity. The signal was measured by a Mitras LB940 luminometer (Berthold Technologies, Germany).

3.11 RNA sequencing (RNA seq)

PH5CH cells were silenced with siRBM39 vs siNT or treated with 1 µM Indisulam vs DMSO for 48 h. RNA are extracted by NucleoSpin RNA Plus kit (Macherey Nagel, Düren, Germany). RNA-Sequencing was conduct using the Illumina Hiseq NovaSeq 6000 (RNA seq reads in 2 x 100 bp format) at Genomics and Proteomics Core facility of the German cancer research center (DKFZ). Raw reads were mapped to human reference transcriptome (Human Gencode v40), the transcripts were quantified by the salmon package with GC bias correction. (75). Gene expression was analyzed by DEseq2 (76), the alternative splicing was analyzed by DRIMseq (77). KEGG pathway analysis was performed by GAGE (78). Gene Ontology (GO) analysis was conducted by Gostats package (79).

3.12 Mass spectrometry (MS)

PH5CH cells were transfected with siRBM39 vs siNT or fed with 1 µM Indisulam vs DMSO for 48 h. Cell pellets were collected after centrifugation at 1.000 rpm for 5 min. 300 µl sodium dodecyl sulfate (SDS) lysis buffer (4% SDS, 10 mM DTT, 55 mM IAA, 50 mM Tris-HCl pH 7.5) was added to the cell pellet and inactivated at 95°C for 10 min. The cells then were sonicated 15 times at 4°C, 30s on and 30s off each time. Subsequently, 80% cold acetone was added into cells to precipitate proteins overnight. After that, pellets were dried out and 40 µl thiourea buffer (6 M urea, 2 M thiourea (U/T) in 10 mM HEPES, pH 8.0) was added to resolve it. The concentration of proteins was measured by Pierce™ BCA Protein Assay Kits (ThermoFisher, Waltham, USA) following instructions of the manufacturer. Lysyl endopeptidase (FujiFilm Wako chemicals, Minato, Japan) and trypsin (Promega, Madison, USA) was added into lysates with 1:50 dilution, the digestion was at 25°C, 1200 rpm for 16 h. 1/5 of loading buffer (10% acetonitrile, 3% trifluoroacetic acid) was added to samples for inactivating proteases and enhancing solubility. 3-layer C18 stage tips (3M) were used to desalt peptides, 200 µl methanol was added to equilibrate columns and then 200 µl washing buffer (0.5% acetic acid)

was used for washing. Subsequently, samples were loaded into columns and washed by 200 µl washing buffer twice and then eluted with elution buffer (80% acetonitrile, 0.5% acetic acid). Centrifugation with 500 g at room temperature was applied for all washing steps. Eventually, elute was vacuum-evaporated at 45°C and then resolved in MS buffer (2% acetonitrile, 0.3% trifluoroacetic acid). The concentration of peptide was determined by Nanodrop 2000 (Thermo Scientific, Waltham, USA) and adjusted to 0.25 µg/µl.

The mass spectrometry was conducted in a Q Exactive HF mass spectrometer (ThermoFisher Scientific, Waltham, USA) equipped with a 75 µm x 50 cm analytical column, packing with Reprosil Pur C18-AQ 1.9 µm particles (Dr. Maisch, Entringen, Germany) and an EASY-Nlc 1200 system (ThermoFisher Scientific, Waltham, USA).

Raw data was processed with MaxQuant (version 2.0.1.0) in data dependent acquisition (DDA) mode, default settings and label-free quantification (LFQ) was applied. Forward and reverse sequences of human proteome (Uniprot, Taxon ID 9606) was used for mapping. MaxQuant results was further analyzed by Perseus (version 1.6.15.0).

3.13 Virus infection

3.13.1 Sendai virus (SeV) infection

6 x 10^4 A549 cells were seeded in 24-well plate the day before the infection. The next day, medium was changed to PBS containing 0.3% BSA, SeV (MOI=1) was added to the medium and incubated at room temperature for 1 h. After that, cells were washed 3 time with 500 µl 1 X PBS, then DMEM was changed. Cells were cultivated for indicated time and used for further experiments.

3.13.2 Rift Valley Fever Virus (RVFV) infection

2 x 10^4 A549 cells were seeded into 24-well plates one day before infection. The next day, the cells were inoculated with RVFV-RLuc (MOI of 0.01) in DMEM containing 2% FCS. The cells were cultivated for 24 h and harvested for further analysis.

3.13.3 Hepatitis E virus (HEV) infection

2.5 x 10^4 HepG2/C3A cells were seeded in collagen (500 µg/ml) (Corning, Corning, USA)-coated plates one day before infection. The cells were infected HEV (MOI=4) in MEM with 10% FBS

for 1h. After that, the medium was replaced with fresh MEM. Cells were cultivated for 5 days and harvested for further investigation.

3.13.4 Hepatitis D virus (HDV) infection:

5 x 10^4 HepG2-NTCP Cells were seeded the day before the infection in collagen (500 µg/ml) (Corning, Corning, USA)-coated plates. HDV (MOI=4) was mixed with DMEM with 1.5% DMSO, 4% PEG and was added to cells. Medium was changed after 24 h, cells were cultivated for 5 days and collected for further experiments.

3.13.5 SARS-CoV2 infection:

4x104 A549-ACE2 cells were seeded in a 24 well-plate one day before the infection. The next day, SAR-CoV2 (MOI=1) was added into DMEM with 2% FBS for 1 h. After that, medium was changed and cultivated for 24 h and harvested for further experiments.

3.13.6 VSV pseudovirus experiements:

4 X 10^4 A549-ACE2 cells were seeded one day before the pseudovirus infection. The next day, 150 µl VSVΔG-G was diluted 1:50 in complete DMEM. 100 µl VSVΔG-Spike and 70 µl diluted VSVΔG-G were simultaneously added into cells. After 24 h, cells were collected and used for further experiments.

3.15 Statistical analysis:

Independent biological replicates are denoted with n-numbers. To test for significance, two-tailed unpaired Welch's test, were performed using GraphPad Prism 8 software (GraphPad Software, La Jolla, CA, USA). *p <0.05; **p <0.01; ***p <0.001; ****p <0.0001.

4 Results:

4.1 Identification of TLR3-related innate immune factors in hepatocytes

The CRISPR/Cas9 screen on the TLR3 response in hepatocytes and validation revealed several candidates, such as PCF11, PTPRT, KDM2A and RBM39. PCF11 involves in mRNA maturation of numerous genes and thus was not investigated further in this study. For PTPRT, one siRNA had a very strong phenotype, but was shown to be based on an off-target effect (Figure 12D). The function of KDM2A and RBM39 was waiting for further validation. Therefore, in this thesis, I aimed to identify the PTPRT target and the mode of action of KDM2A and RMB39.

4.1.1 Identification of real target of siPTPRT

Our previous data showed that the use of siPTPRT significantly reduced IFIT1 mRNA expression upon poly(I:C) supernatant feeding (Figure 12D), implying its innate immune function. PTPRT is a tyrosine phosphatase, has been reported to suppress signal transducer and activator of transcription 3 (STAT3) and to be involved in colon cancer (*261, 289*). However, a previous RNA seq analysis in my lab (Betz et al., unpublished data) and literature (*263*) showed that PTPRT was not expressed in PH5CH and Huh7-Lunet cells, indicating an off-target event.

To find the real target of the siRNA used in the experiment, I transfected PH5CH cells and Huh7-Lunet-TLR3 cells with the PTPRT specific siRNA providing the strongest effect on TLR3 response, extracted mRNA and sent them for RNA seq. After analysis, only 18 candidate genes showed reduction in both cell lines, compared to a non-targeting siRNA (Table 2). To further confirm the knockdown of these candidates upon siRNA transfection, I checked their mRNA expression by qPCR. Consistently with RNA seq data, most genes exhibited down-regulation upon siRNA transfection, apart from Glycogenin 2 (GYG2), Leucine Rich Repeat Containing 2 (LRRC2), Prostaglandin-Endoperoxide Synthase 1 (PTGS1) and A-Kinase Anchoring Protein 7 (AKAP7) (Figure 14A).

Table 2. Candidate genes showing reduced mRNA expression in both Huh7-Lunet-TLR3 and PH5CH cells upon siPTPRT knockdown.

Gene name	Log_2 fold change (PH5CH)	Log_2 fold change (Huh7-Lunet-TLR3)	mean
PTGS1	1,18	1,74	1,46

SLC16A9	1,93	0,60	1,27
LRRC2	1,95	0,31	1,13
FTLP3	1,31	0,34	0,83
PARD3B	1,11	0,47	0,79
CPS1	0,71	0,84	0,78
PLEKHG6	0,79	0,59	0,69
LOXL4	0,65	0,72	0,69
CDH1	0,63	0,69	0,66
PCK2	0,94	0,36	0,65
CYB5A	0,64	0,59	0,62
KRCC1	0,82	0,37	0,60
ALDH5A1	0,67	0,50	0,59
PXK	0,80	0,34	0,57
AKAP7	0,61	0,41	0,51
SCNN1A	0,68	0,33	0,51
COL3A1	0,65	0,36	0,51
GYG2	0,62	0,31	0,47

Afterwards, I chose the top 5 most promising candidates that showed the strongest reduction, lysyl oxidase like 4 (LOXL4), solute carrier family 16 member 9 (SLC16A9), lysine rich coiled-coil 1 (KRCC1), collagen type iii alpha 1 chain (COL3A1), sodium channel epithelial 1 subunit alpha (SCNN1A), for further individual siRNA validation. siRNA targeting each gene was transfected into PH5CH cells separately and poly(I:C) was fed to the supernatant to activate the TLR3 pathway. IFIT1 mRNA was measured as a readout of innate immune response. However, none of the candidates attenuated the expression of IFIT1 mRNA upon knockdown (Figure 14B), even with a high knockdown efficiency (Figure 14C), indicating they are not the real target of si'PTPRT'.

Taken together, the attempt to identify the real target of si'PTPRT' by RNA seq failed. A more sophisticated method is required for finding out the target of off-targeted siRNA.

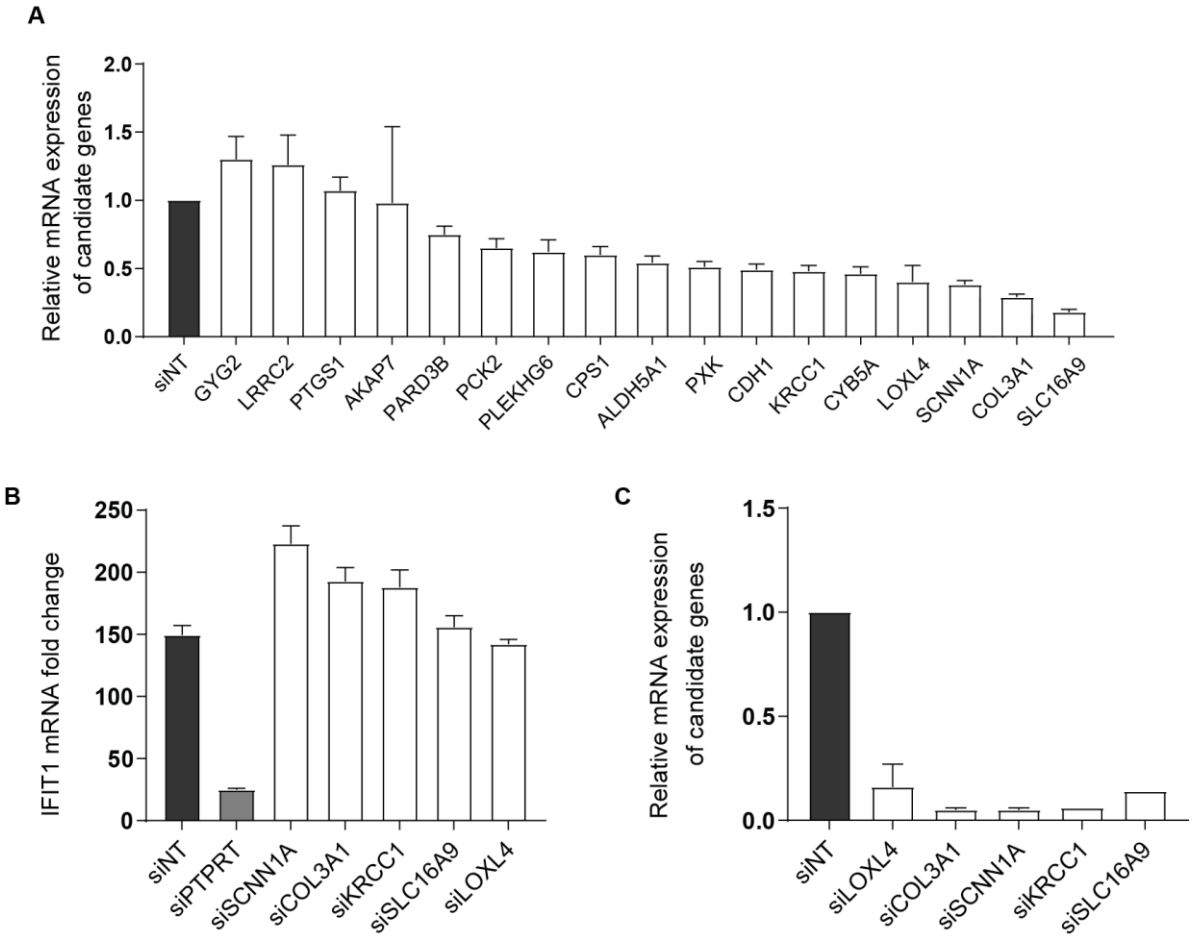

Figure 14. **The validation of potential real targets of si'PTPRT'.** (A) PH5CH cells were transfected with si'PTPRT' or siNT as control for 48 h. Then, mRNA expression of each candidate gene was measured by qPCR. (B to C) PH5CH cells were silenced with si'PTPRT' or siRNA targeting each candidate gene; after 48 h, cells were fed with 50 µg/ml poly(I:C) for 6h. IFIT1 mRNA (B) or other candidate gene mRNA (C) expression was measured by qPCR. The shown data presented the mRNA fold change of gene of interest relative to reference GAPDH. Relative mRNA expression refers to the normalization of mRNA fold change in each condition compared to the siNT control. Error bar indicates the standard deviation from three technical replicates.

4.1.2 KDM2A and KDM2A short form isoform cannot rescue the KDM2A knockdown phenotype

Since the phenotype observed for PTPRT was an off-target effect, I moved to the further validation of KDM2A. KDM2A is a lysine demethylase that demethylates mono- and di-methylated histone 3 lysines (H3K36me1/2) using its N-terminal Jumonji-C demethylase domain, playing a vital role in chromosome remodeling and gene transcription (*264*). To exclude the off-target effect of siKDM2A, a rescue experiment was conducted by the former colleague Arthur Lang. In the experiment, siKDM2A targets the 5' non-coding region of KDM2A, therefore, the ectopic KDM2A without 5' untranslated region (UTR) is already resistant to RNA interference (RNAi). Subsequently, KDM2A was expressed in PH5CH cells via lentiviral

transduction. Then, PH5CH cells expressing KDM2A or empty vector as control were transfected with siKDM2A and fed with poly(I:C) in the supernatant. RNA was extracted and mRNA expression analyzed by qPCR. Overexpression of KDM2A was not able to rescue the IFIT1 mRNA expression in PH5CH cells upon poly(I:C) supernatant feeding (Figure 15A), indicating a possible off-target effect of the siRNA.

An alternative isoform, KDM2A short form (KDM2A-SF), has been reported, lacking the N-terminal demethylase domain but sharing all other functional domains with the KDM2A longer form (KDM2A-LF) (*290*) (Figure 15B). Due to the absence of demethylase function, KDM2A-SF has been reported to play dominant negative role (*290*). To test whether this short isoform was the real target of the siKDM2A, I overexpressed the KDM2A-SF in PH5CH cells via lentiviral transduction. Subsequently, I transfected PH5CH cells expressing KDM2A-SF with siKDM2A and stimulated them with poly(I:C) supernatant feeding. However, the IFIT1 mRNA levels were not restored by KDM2A-SF (Figure 15C), indicating that KDM2A-SF was not the target of the siKDM2A I used. Noticeably, the expression of both KDM2A and KDM2A-SF seems to reduce the IFIT1 mRNA expression even in siNT controls for unknown reason.

All in all, it was concluded that the knockdown phenotype induced by siKDM2A might result from an off-target effect. KDM2A-SF was excluded as the real target of the siRNA.

A

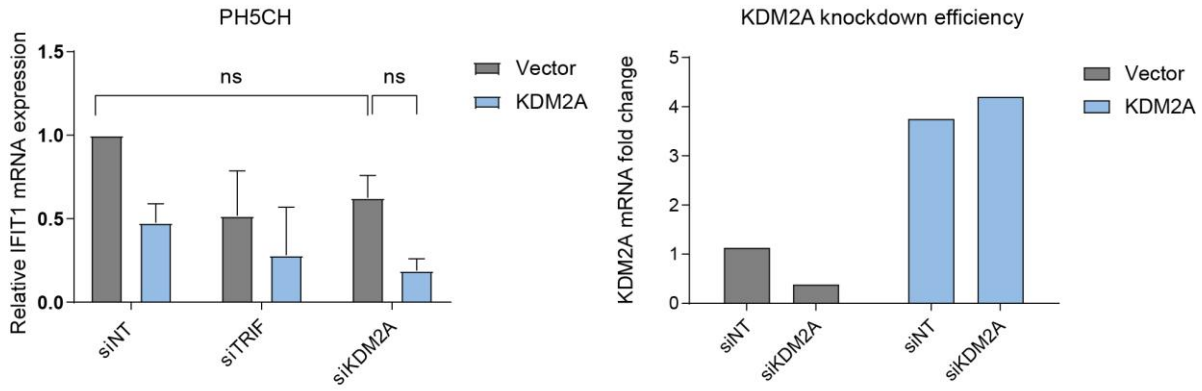
PH5CH
Relative IFIT1 mRNA expression
1.5
1.0
0.5
0.0
ns
ns
Vector
KDM2A
siNT
siTRIF
siKDM2A
KDM2A knockdown efficiency
KDM2A mRNA fold change
5
4
3
2
1
0
Vector
KDM2A
siNT
siKDM2A
siNT
siKDM2A

B

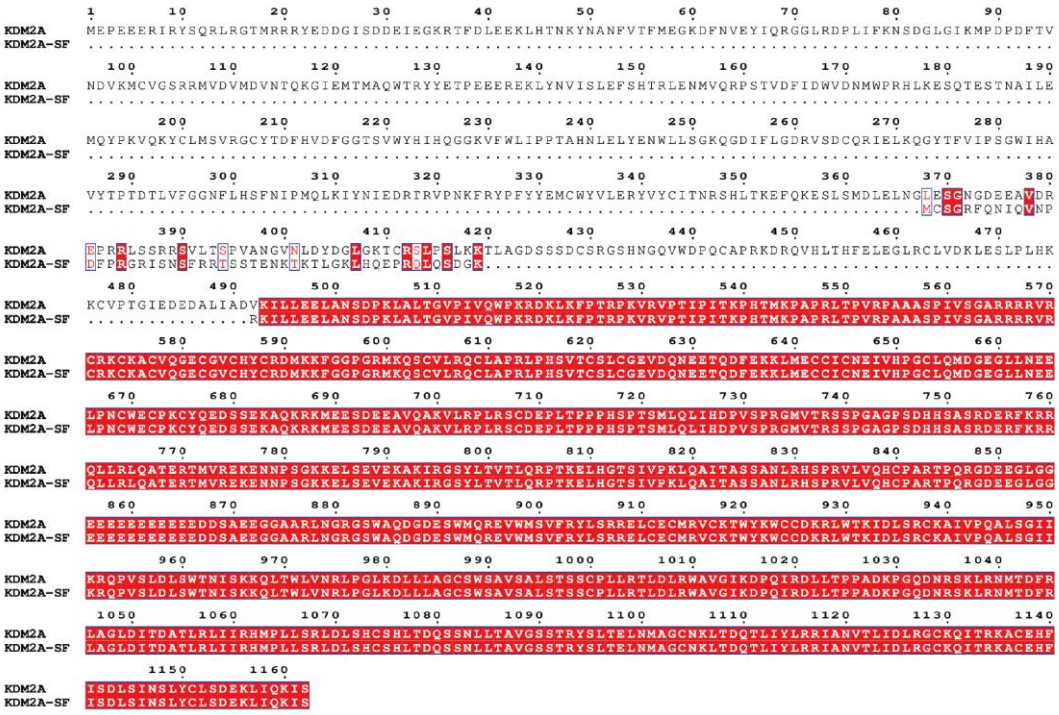
KDM2A
KDM2A-SF

C

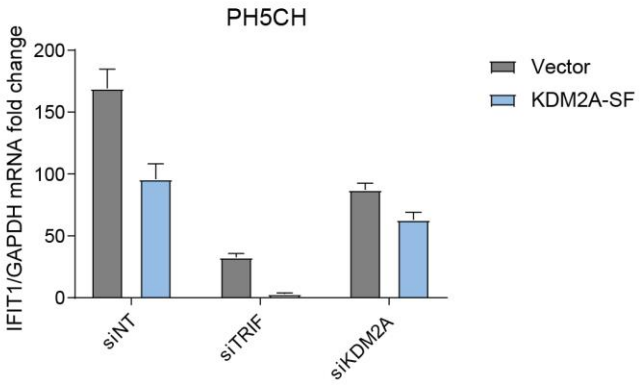
PH5CH
IFIT1/GAPDH mRNA fold change
200
150
100
50
0
Vector
KDM2A-SF
siNT
siTRIF
siKDM2A

Figure 15. KDM2A and KDM2A-SF rescue experiments. (A) PH5CH cells expressing KDM2A or empty vector as control were transfected by siKDM2A for 48h, and then stimulated with 50µg/ml poly(I:C) via supernatant feeding. IFIT1 and KDM2A mRNA expression were measured by qPCR. Experiment performed by Arthur Lang. (B) Amino acid sequence alignment of KDM2A and KDM2A-SF. (C) PH5CH cells expressing empty vector or KDM2A-SF were transfected with siKDM2A for 48h, then stimulated with 50µg/ml poly(I:C) via supernatant feeding. IFIT1 mRNA expression was measured by qPCR. The mRNA expression of each gene was normalized by that of GAPDH, relative mRNA expression was determined by comparing with siNT control. Error bar indicates the standard deviation from three technical replicates.

4.1.3 RBM39 is confirmed as a novel innate immune factor

As both PTPRT and KDM2A exhibited off-target effects, RBM39 remained as the only one promising candidate. To further confirm the phenotype of RBM39, an RBM39 siRNA resistant mutant (RBM39.Esc) was designed by mutating the siRNA targeting region and expressed into PH5CH cells via lentiviral transduction. After siRNA knockdown and specific poly(I:C) stimulation of TLR3, I observed that the overexpression of RBM39.Esc restored the expression of IFIT1 mRNA. (Figure 16A).

To exclude the possibility that RBM39 has a direct effect on IFIT1 expression, I further measured other ISGs, including ISG15 ubiquitin like modifier (ISG15), MX dynamin like GTPase 1 (MxA) and C-X-C motif chemokine ligand 10 (CXCL10). As expected, the knockdown of RBM39 significantly reduced the CXCL10 mRNA level upon poly(I:C) activation, while overexpression of RBM39.Esc rescued the expression of CXCL10 mRNA. It also significantly inhibited ISG15 and MxA mRNA expression, although the rescue effects were not significant (Figure 16B-D). To validate the impact of RBM39 knockdown at protein levels, I also measured secreted IFNβ protein expression in the supernatant by Enzyme-Linked Immunosorbent Assay (ELISA). Consistently, the result showed that the silencing of RBM39 inhibited IFNβ expression at protein level (Figure 16E), further supporting its role in TLR3 signaling.

To further confirm the phenotype in other cell lines, I expressed RBM39.Esc mutant in Huh7-Lunet-TLR3 cells and Huh7.5-TLR3 cells, and then performed siRNA transfection and poly(I:C) supernatant feeding. In both cell lines, RBM39 knockdown significantly inhibited the TLR3-mediated IFIT1 mRNA expression; however, the overexpression of RBM39.Esc only slightly, but not significantly, rescued the IFIT1 mRNA level upon knockdown (Figure 16F and G).

Taken together, I found that RBM39 affects the cell intrinsic innate immune response not only at the level of ISGs mRNA expression, but also regulating the protein expression of IFNβ. In addition, besides impacting these functions in PH5CH cells, RBM39 also plays a role in other

two liver-based cell lines. These evidences strongly support the innate immune regulatory function of RBM39.

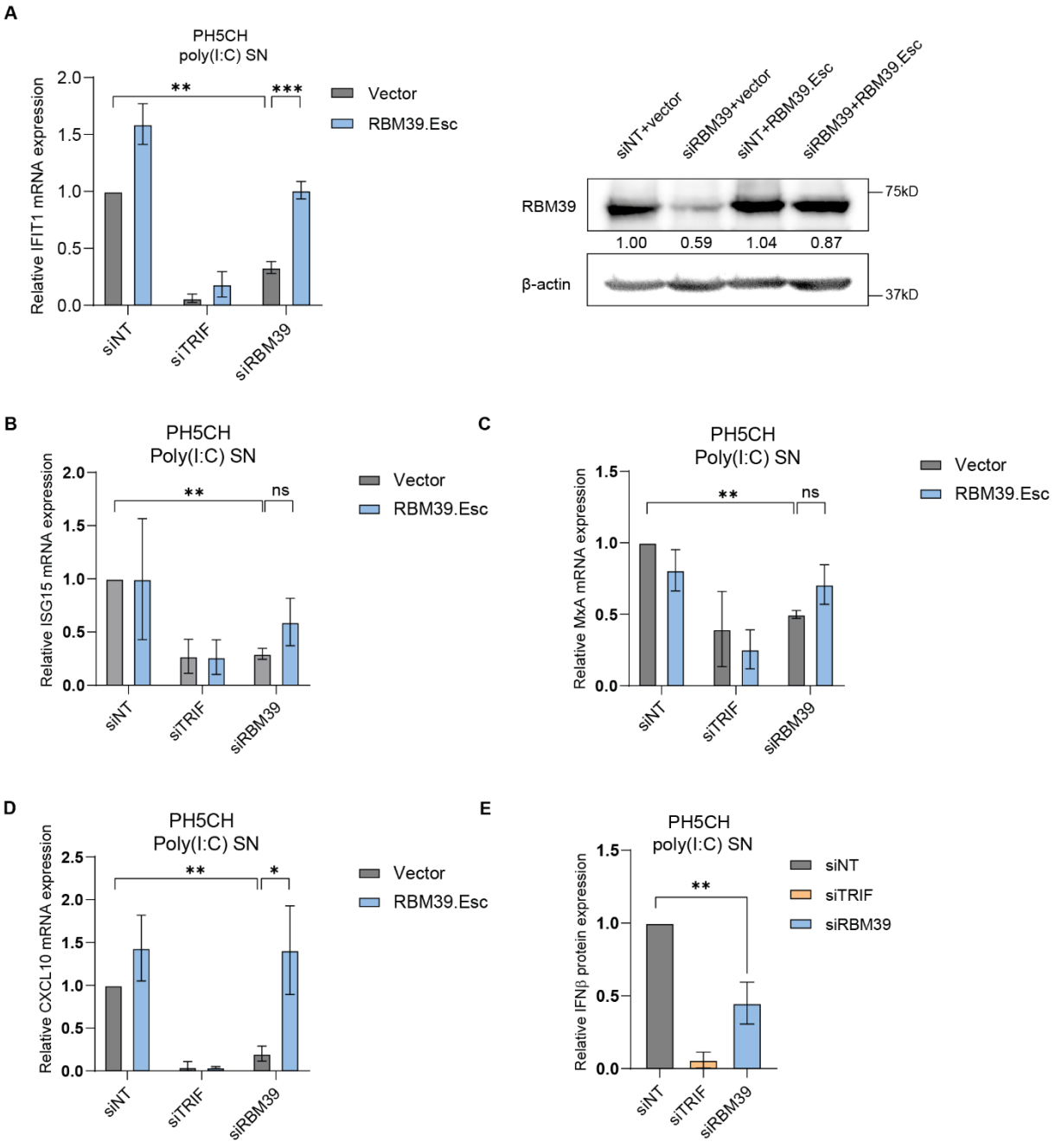

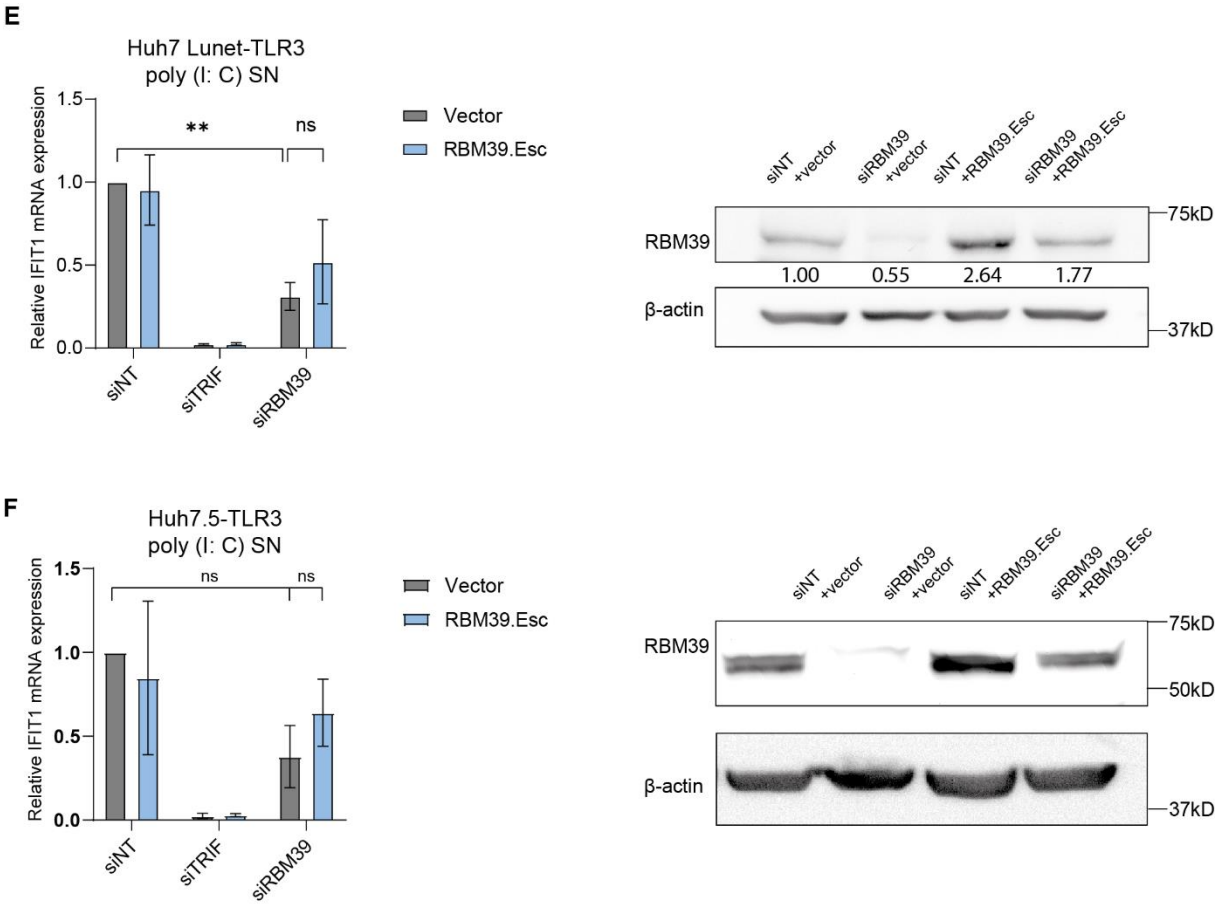

Figure 16. RBM39 affect ISGs expression. (A to E) PH5CH expressing empty vector or RBM39.Esc were transfected with siRBM39 for 48 h and then stimulated by adding 50 µg/ml poly(I:C) in the supernatant. IFIT1 (A), ISG15 (B), MxA (C) and CXCL10 (D) mRNA was measured by qPCR. RBM39 protein level was measured by western blot. Protein expression of IFNβ secreted in the medium was detected via ELISA (E). (F and G) Huh7-Lunet-TLR3 cells (F) or Huh7.5-TLR3 cells (G) with empty vector or RBM39.Esc were treated siRBM39 or siNT as control, and fed with 50 µg/ml poly(I:C) to activate TLR3 pathway. IFIT1 mRNA expression was measured. mRNA fold change was normalized by GAPDH. Shown is relative mRNA expression to siNT control. Data was from biological triplicates. Significance test was performed using two-tailed unpaired Welch's test via GraphPad Prism 8 software (GraphPad Software, La Jolla, CA, USA). *p <0.05; **p <0.01; ***p <0.001. RBM39 and β-actin protein level was determined by western blot. RBM39 protein level was normalized by β-actin, the average number of the relative protein expression to siNT control from three replicates is shown under each band of a representative experiment.

4.1.4 Generation of stable RBM39 knockout and knockdown cells

To achieve a more efficient depletion of RBM39, I decided to knock out (KO) RBM39 via CRISPR/Cas9. 4 oligos were designed to target the 5' CDS of RBM39 and cloned it into a pWPI-vector for lentiviral transduction. After antibiotics selection and expansion of the surviving cells, I obtained 4 RBM39 KO cell pools and validated them by western blot. The result showed that the protein level of RBM39 of pool 1 and pool 2 was slightly reduced, whereas pool 3 and

4 had an increased RBM39 expression (Figure 17A). To further verify the innate immune function of these pools, I stimulated them with poly(I:C) feeding and checked ISGs mRNA expression via qPCR. Surprisingly, the IFIT1 mRNA expression in pool #1, #3 and #4 upon poly(I:C) stimulation were strongly promoted compared to PH5CH WT cells, with only the pool #2 presenting a mild reduction (Figure 17B). Therefore, I seeded pool #2 aiming at obtaining single cell clones. Most single cells did not grow and thereby I was only able to expand a few of them. Eventually, only clone #25 and clone #41 showed a reduced RBM39 protein level, clone #24 seems like knockout phenotype, but the absence of β-actin indicates it was just a technical mistake (Figure 17C). However, the IFIT1 mRNA expression upon poly(I:C) stimulation in these two clones was not affected if compared to that in WT cells (Figure 17D), hinting at unsuccessful knock-out.

In search of another strategy to obtain RBM39 depletion, I employed the Alt-R® CRISPR-Cas9 system to generate PH5CH KO cells. In this method, at least two sgRNAs targeting different regions of RBM39 are required. By transfecting the two sgRNAs into the target at the same time, a short deletion of the target gene can be achieved, resulting in a frameshift and loss-of-function. The efficiency of deletion can be easily detected by PCR and thereby improves efficiency of validation.

To achieve the knockout of RBM39, I transfected two sgRNAs targeting RBM39 along with Cas9 enzyme into PH5CH cells through electroporation, cells then were seeded and expanded for validation. To check the knockout efficiency, I designed primers targeting the deletion region of RBM39, and conducted PCR using genomic DNAs as template. The expected size of deletion is approximately 474 bp and the size of PCR product that only in presence of complete genome should be 439 bp. Indeed, in two PH5CH RBM39 KO pools, the PCR product of the deletion region was dramatically reduced (Figure 17E). Subsequently, I re-seeded pool #1 cells for single KO clone screen. However, only two single cell clones grew and they were expanded. Next, I performed PCR to measure the Cas9-induced deletion of RBM39 in an agarose gel, but the segment supposed to be deleted was still existing (Figure 17F) and western blot also showed strong RBM39 protein levels (Figure 17G) in these two clones, indicating a failure of the knockout.

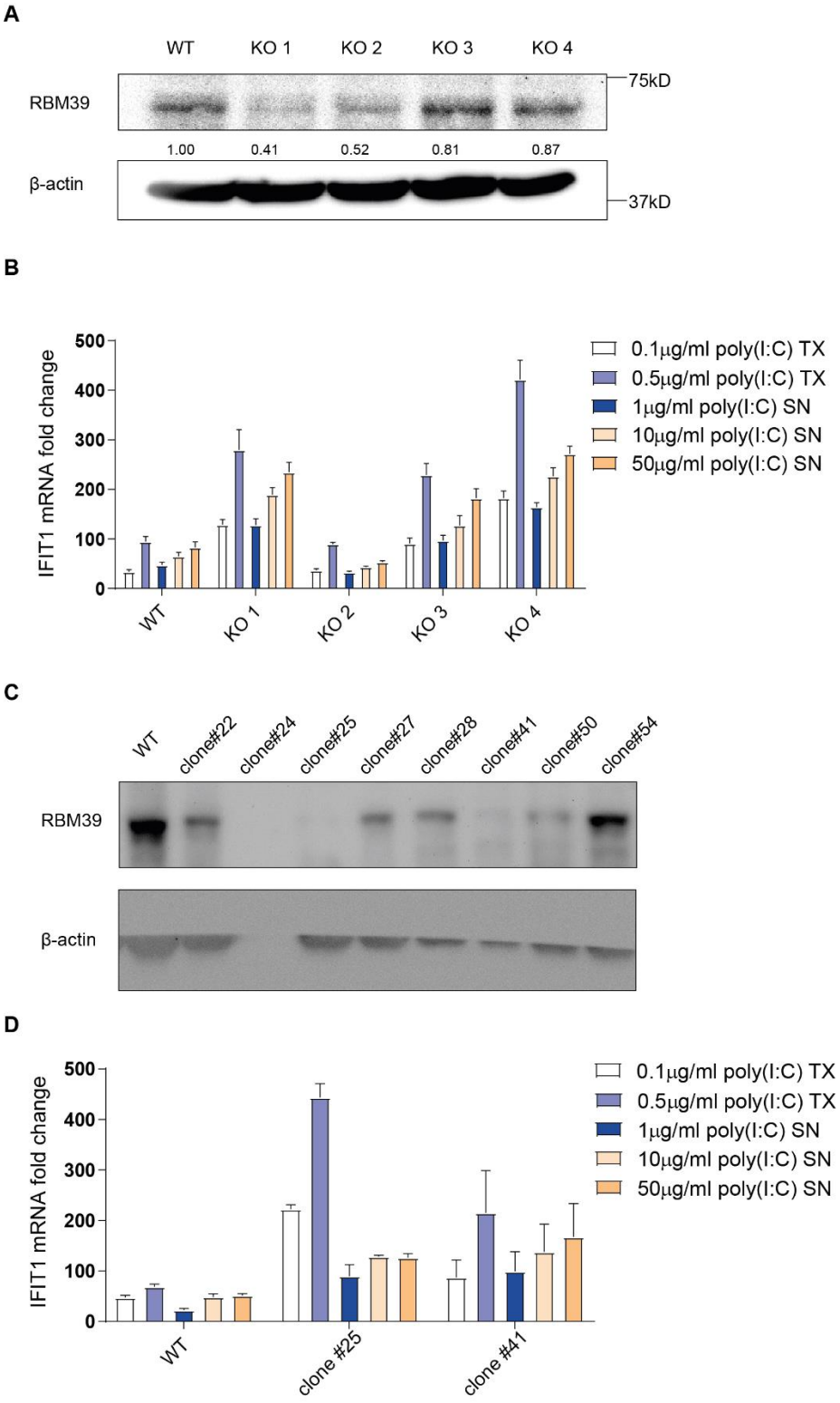
A
WT
KO 1
KO 2
KO 3
KO 4
RBM39
75kD
1.00
0.41
0.52
0.81
0.87
β-actin
37kD
B
IFIT1 mRNA fold change
500
400
300
200
100
0
WT
KO 1
KO 2
KO 3
KO 4
0.1μg/ml poly(I:C) TX
0.5μg/ml poly(I:C) TX
1μg/ml poly(I:C) SN
10μg/ml poly(I:C) SN
50μg/ml poly(I:C) SN
C
WT
clone#22
clone#24
clone#25
clone#27
clone#28
clone#41
clone#50
clone#54
RBM39
β-actin
D
IFIT1 mRNA fold change
500
400
300
200
100
0
WT
clone #25
clone #41
0.1μg/ml poly(I:C) TX
0.5μg/ml poly(I:C) TX
1μg/ml poly(I:C) SN
10μg/ml poly(I:C) SN
50μg/ml poly(I:C) SN

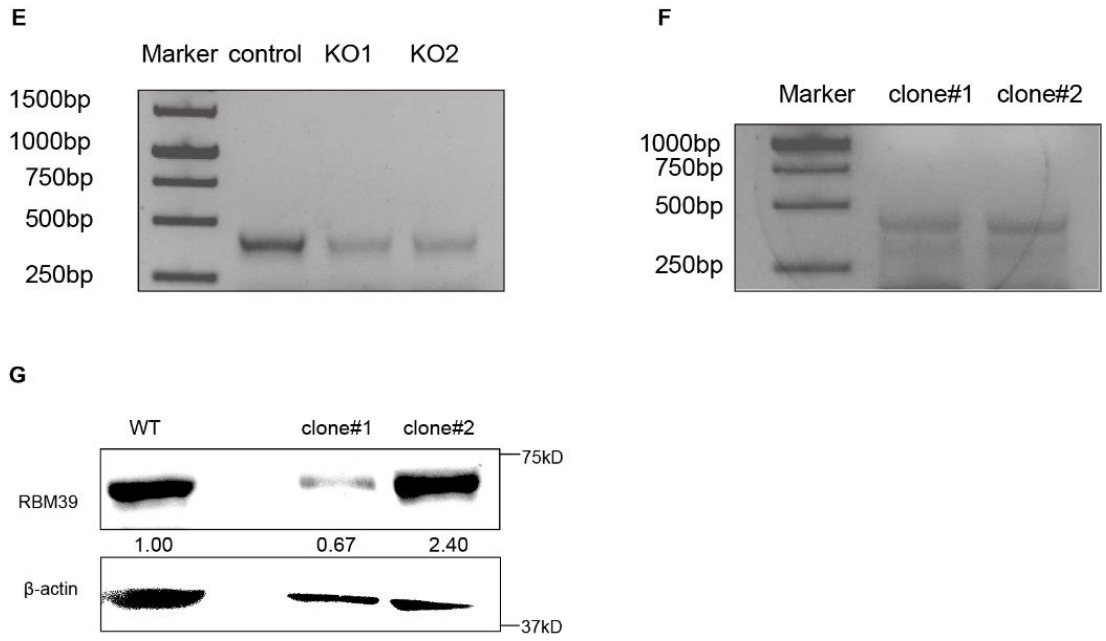

Figure 17. **Generation of RBM39 knockout cells.** (A to D) PH5CH cells were transduced with lentivirus containing sgRNAs to produce PH5CH RBM39 knockout cells. (A) Validation of PH5CH RBM39 knockout pools via western blot. (B) Validation of PH5CH RBM39 knockout pools by qPCR. PH5CH WT or PH5CH RBM39 knockout pools #1-4 were stimulated using poly(I:C) supernatant feeding (SN) or transfection (TX), at the indicated concentrations, for 6 h. IFIT1 mRNA expression as read out was measured by qPCR. (C) Validation of PH5CH RBM39 knockout clones via western blot. Clone #25 and #41 showed knockout phenotype, #24 was not detectable (D) Validation of PH5CH RBM39 knockout clones #25 and #41 via qPCR. PH5CH WT or PH5CH RBM39 knockout clones #25 and #41 were stimulated as indicated with poly(I:C) via supernatant feeding or transfection for 6 h; IFIT1 mRNA levels were determined by qPCR. (E to F) PH5CH cells were electroporated with sgRNA targeting RBM39 to produce knockout cells (E) Validation of PH5CH RBM39 knockout pools #1 and #2 by PCR. The deletion segment of RBM39 was amplified by PCR from genomic DNA and measured by gel electrophoresis. (F) Validation of PH5CH knockout clone #1 and clone #2 by PCR. PCR segment of potential deletion region of RBM39 was amplified by PCR using genomic DNA of Clone #1 and #2 and measured by agarose gel electrophoresis. (G) Validation of PH5CH knockout clone #1 and clone #2 by western blot. mRNA fold change was normalized by GAPDH.

Therefore, I turned to establish shRNA-induced stable RBM39 knockdown cells. Again, three oligos that targeted the 5' CDS of RBM39 were designed and cloned into a pAPM vector. Lentivirus particles were produced and then transduced into PH5CH cells. After antibiotic selection, three cell pools were validated by immunoblotting and qPCR. All three pools showed RBM39 reduction at the protein levels, with pool#3 showing the highest reduction (Figure 18A). Consistently, qPCR results also validated RBM39 mRNA inhibition in three cell pools, with pool #3 exhibiting the strongest phenotype (Figure 18B). Unfortunately, western blot showed the knockdown phenotype was lost after passaging several times (Figure 18C).

Altogether, the establishment of RBM39 KO single clone and stable RBM39 knockdown cell failed, indicating that RBM39 plays a vital role in cell growth. Therefore, from this point on, I stuck to transient siRNA knockdown for the subsequent experiments.

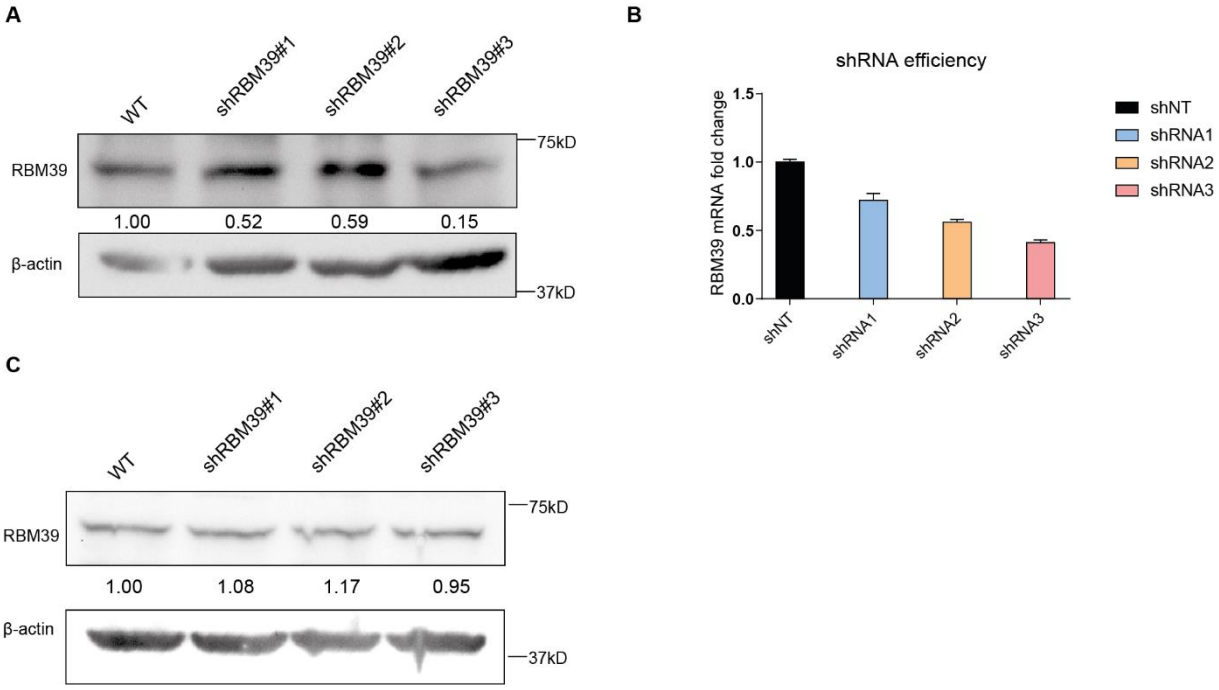

Figure 18. **The generation of stable RBM39 knockdown cells** (A) Validation of the efficiency of shRBM39 #1-3 via western blot. (B) Validation of the efficiency of shRBM39 #1-3 via qPCR. RBM39 mRNA expression of PH5CH cells expressing shRNA #1-#3 was measured by qPCR. The mRNA expression of each gene was normalized by that of GAPDH. Error bar indicates the standard deviation from three technical replicates. The quantification of western blot was performed by Fiji software and presented under each band.

4.1.5 RBM39's function is neither TLR3- nor hepatocyte-specific

My investigation so far focused on the TLR3 pathway. To determine whether RBM39 plays a role in other PRR pathways, I expressed RIG-I and MDA, respectively, in Huh7.5 cells through lentiviral transduction. Huh7.5 is a human hepatoma-derived cell line that does not express TLR3 and MDA5 and contains a loss-of-function mutation in RIG-I (*291*), allowing me to scrutinize the respective pathway upon reconstitution of the individual PRR. Subsequently, I silenced RBM39 by siRNA and stimulated the RIG-I and MDA5 pathway, respectively, by poly(I:C) transfection. Intriguingly, RBM39 knockdown also attenuated the IFIT1 mRNA expression upon RIG-I (Figure 19A) and MDA5 (Figure 19B) activation.

A549, an adenocarcinoma derived human alveolar basal epithelial cell line, lacks the expression of TLR3 but express high level of RIG-I and MDA5 (*292*), making it an ideal model for investigating these pathways. To confirm whether the endogenous RIG-I/MDA5 pathway is also affected by RBM39, I conducted siRNA and poy(I:C) transfection in these cells. Consistently, I found significant inhibition of IFIT1 mRNA upon RBM39 knockdown in A549 cells (Figure 19C), further confirming the role of RBM39 on RIG-I and MDA5 pathways, also indicating its role is not limited to hepatocytes.

Considering the pathways I have investigated so far to be strictly dsRNA-activated, I hypothesized that the function of RBM39 could specifically facilitate RNA recognition. In the previous RNA seq data (Betz et al., unpublished data), I confirmed a high expression of TLR4 in PH5CH cells. To verify whether RBM39 is exclusively activating RNA sensors, I further stimulated RBM39-silenced PH5CH cells with lipopolysaccharide (LPS), a gram-negative bacteria-derived component that triggers the TLR4 pathway and induces ISGs and inflammatory cytokines (*293*). Surprisingly, RBM39 also affected the LPS-induced TLR4 pathway in PH5CH cells (Figure 19D), expanding the role of RBM39 beyond RNA recognition.

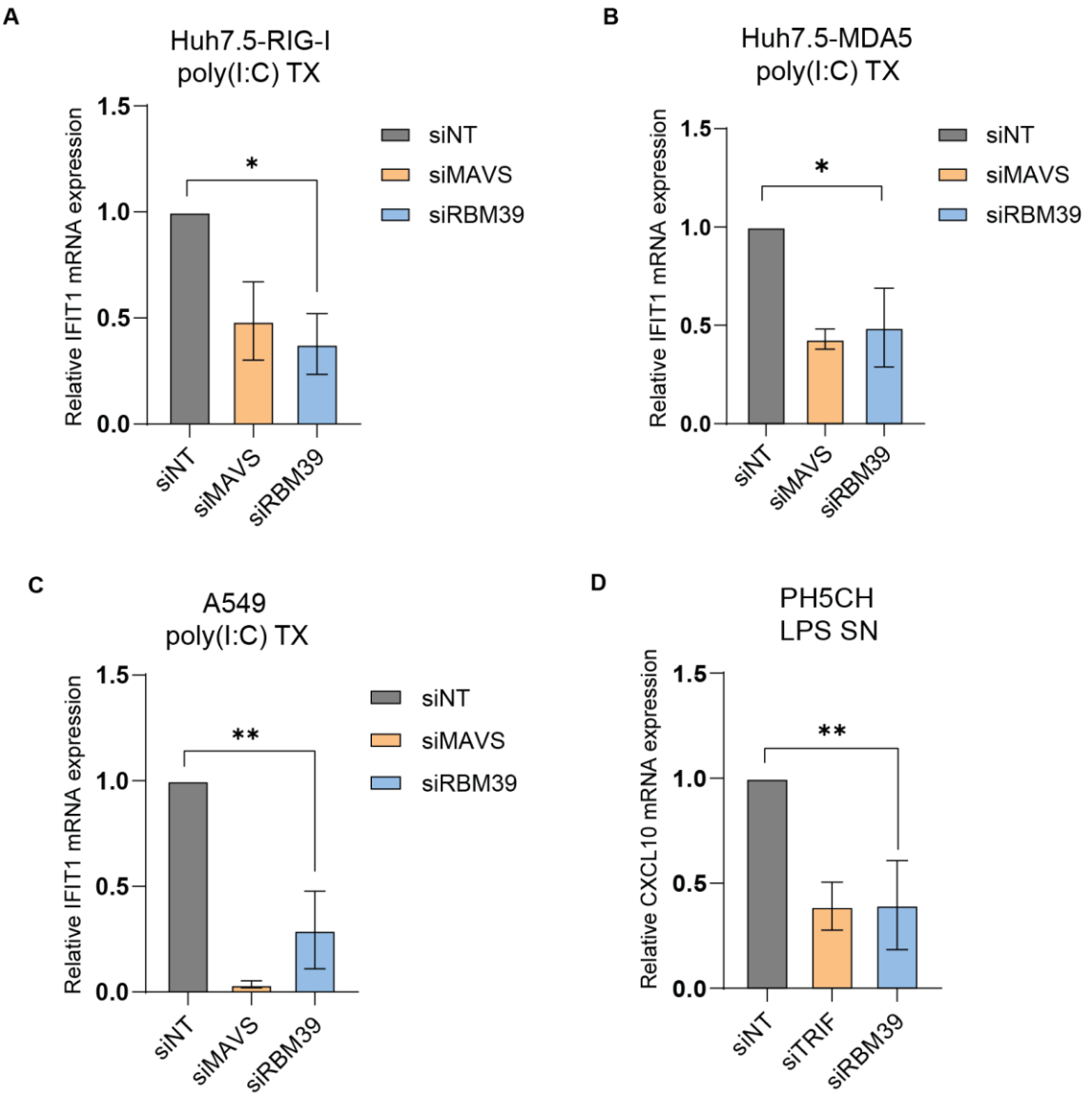

Figure 19. RBM39's function is not limited to TLR3 and hepatocytes. (A to C) Huh7.5-RIG-I (A), Huh7.5-MDA5 (B) and A549 (C) were transfected with corresponding siRNA for 48 h and then transfected with 0.5 µg/ml poly(I:C) for 6 h. IFIT1 mRNA was measured by qPCR. (D) PH5CH cells were silenced with the indicated siRNA for 48 h and 100 ng/ml LPS were added to the supernatant for 24 h; CXCL10 mRNA was then determined by qPCR. mRNA fold change was normalized by GAPDH, shown is relative mRNA expression to siNT control. Data are from three biological replicates, statistics analysis was perform using two-tailed unpaired Welch's test via GraphPad Prism 8 software (GraphPad Software, La Jolla, CA, USA). *p <0.05; **p <0.01; ***p <0.001.

4.1.6 RBM39 specifically participates in type III IFN pathway regulation

To understand in which step of the signaling pathway RBM39 participates, I measured two NF-κB specifically induced genes, TNF alpha induced protein 3 (TNFAIP3) and interleukin 6 (IL6) upon RBM39 knockdown and poly(I:C) supernatant feeding in PH5CH cells. In contrast to the reduction of IRF3-induced ISGs, TNFAIP3 mRNA did not show a significant change (Figure 20A)

while IL6 exhibited a significant but limited reduction (Figure 20B), indicating that RBM39 has no or only a minor effect on the NF-κB pathway, at least in the context of TLR3 induction.

Furthermore, I investigated the influence of RBM39 on downstream IFN signaling pathways. To bypass the IRF3 and NF-κB activation and directly investigate the impact of RBM39 on IFN pathways, I stimulated RBM39-silenced PH5CH cells with IFN2α and IFNλ1 to activate type I and type III IFN pathways, respectively. Interestingly, RBM39 knockdown did not affect the IFN2α-mediated but strongly impaired the IFNλ1-mediated IFIT1 mRNA expression in PH5CH cells (Figure 20C and 20D). The type I and type III IFN pathways share similar downstream signaling but are initiated through distinct receptors. The recognition of type I IFNs involves subunit Interferon alpha and beta receptor subunit 1 (IFNAR1) and interferon alpha and beta receptor subunit 2 (IFNAR2), while the type III IFN receptor consists of the subunit interferon lambda receptor 1 (IFNLR1) and interleukin 10 receptor subunit beta (IL10RB) (*118*). To understand the discrepancy, the mRNA expression of type III IFN receptor subunits upon RBM39 knockdown was measured. Interestingly, qPCR results showed that the mRNA level of IFNLR1 had a significant upregulation, whereas IL10RB mRNA expression exhibited significant decrease upon the knockdown (Figure 20E). This downregulation of IL10RB could contribute to the suppression of innate immune responses mediated by type III IFNs.

To study the contribution of type III IFN pathway to the entire RBM39-mediated innate immune regulation, I determined the innate responses in A549 IFNAR/IFNLR KO cells upon RBM39 knockdown and poly(I:C) stimulation. These cells do not express either type I or type III IFN receptors and thus cannot initiate type I or type III IFN pathways. However, upstream IFNs production, which are mostly not affected, and IFIT1, being induced partly independent of IFNs (*294*), can be measured as readouts. As shown, the silencing of RBM39 still had an inhibitory function on IFIT1 and IFNβ mRNA expression (Figure 20F), hinting that, at least in my experimental settings, type III IFN is dispensable in the RBM39-mediated regulation, and indicating that other important factors upstream of the IFNs were involved in the process.

To sum up, I observed RBM39 was implicated in IRF3-mediated, rather than NF-κB-induced, innate signaling. Additionally, it might have an impact on the type III IFN pathway and probably on some upstream factors.

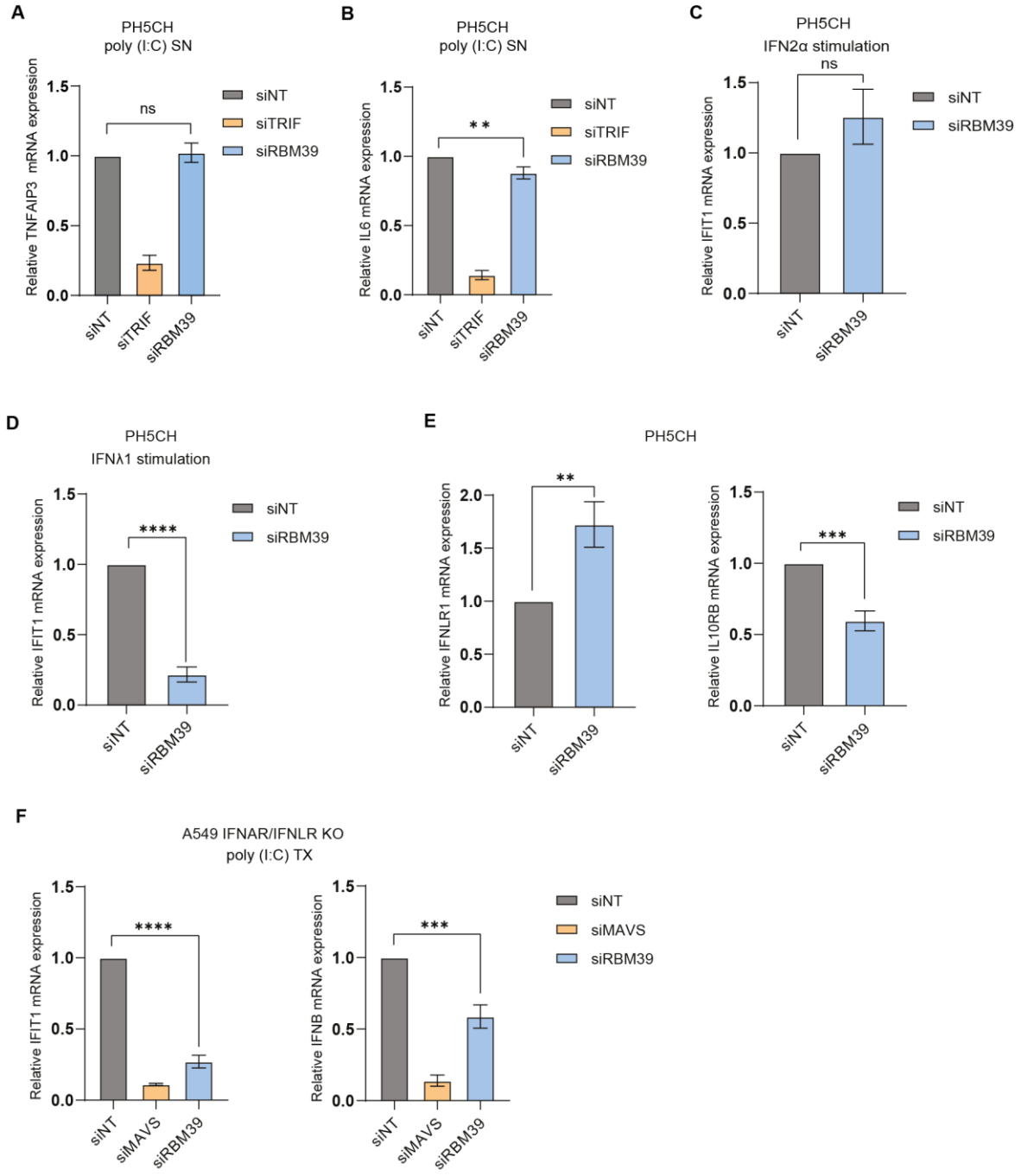

Figure 20. The role of RBM39 in the NF-KB pathway and IFN pathways (A-B) PH5CH cells were treated with the indicated siRNA for 48 h and stimulated with 50 µg/ml poly(I:C) for 6 h; TNFAIP3 (A) and IL6 (B) mRNA expression were measured by qPCR. (C and D) PH5CH cells were silenced with corresponding siRNA for 48 h and stimulated with IFN2α (C) or IFNλ1 (D) for 24 h; IFIT1 mRNA expression was then measured by qPCR. (E) PH5CH were treated with the indicated siRNA for 48 h, IFNLR1 (left) and IL10RB (right) were measured by qPCR. (F) A549 IFNAR/IFNLR KO cells were treated siRNA indicated for 48 h and transfected with 0.5 µg/ml poly(I:C) for 6 h, IFIT1 and IFNB mRNA expression were measured by qPCR. mRNA fold change was normalized by GAPDH, shown is relative mRNA expression to siNT control. Data are from three biological replicates, statistics analysis was perform using two-tailed unpaired Welch's

test via GraphPad Prism 8 software (GraphPad Software, La Jolla, CA, USA). *p <0.05; **p <0.01; ***p <0.001.

4.1.7 RBM39 regulates the basal expression of IRF3

As previously mentioned, RBM39 participates in multiple PRR-mediated pathways but has no impact on NF-κB signaling upon TLR3 stimulation. This observation led me to investigate in-depth the IRF3-mediated signaling. The phosphorylation of IRF3 is a key marker for the activation of the pathway; therefore, I measured the phosphorylated IRF3 (p-IRF3) upon siRNA knockdown and poly(I:C) supernatant feeding in PH5CH cells. As expected, the expression of p-IRF3 was barely detectable in untreated cells but strongly increased upon poly(I:C) stimulation. Moreover, the knockdown of RBM39 inhibited phosphorylation while the overexpression of RBM39.Esc slightly rescued the phenotype. Interestingly, I also observed a significant reduction of the basal expression of IRF3 upon knockdown, indicating that RBM39 participates in the regulation of IRF3 (Figure 21A).

Afterwards, upon literature investigation I found the possibility of a drug-mediated approach: the anti-cancer sulfonamide drug Indisulam was shown to degrade RBM39 in an E3-ligase dependent manner (*283*) and thus could be a useful tool for my study. Firstly, I tested the efficiency of Indisulam in PH5CH. The addition of RBM39 indeed dose dependently degraded RBM39 at protein level in PH5CH cells and, because of the regulatory activity of RBM39, IRF3 expression showed a reduction in the same manner, associated with cytotoxicity at increasing concentrations (Figure 21B). A RBM39 mutant (G268V) was reported to acquire resistance to Indisulam to some extent (*279*). To prove that the down-regulation of IRF3 relies on RBM39 instead of being due to a direct effect of Indisulam, I overexpressed RBM39 G268V, or WT as control, in PH5CH cells and treated the latter with increasing amounts of Indisulam. Comparing with WT, G268V indeed partly rescued RBM39 degradation and, correspondingly, the reduction of IRF3 was weaker in RBM39 G268V-expressing cells (Figure 21C), which supported the evidence of IRF3 being regulated by RBM39.

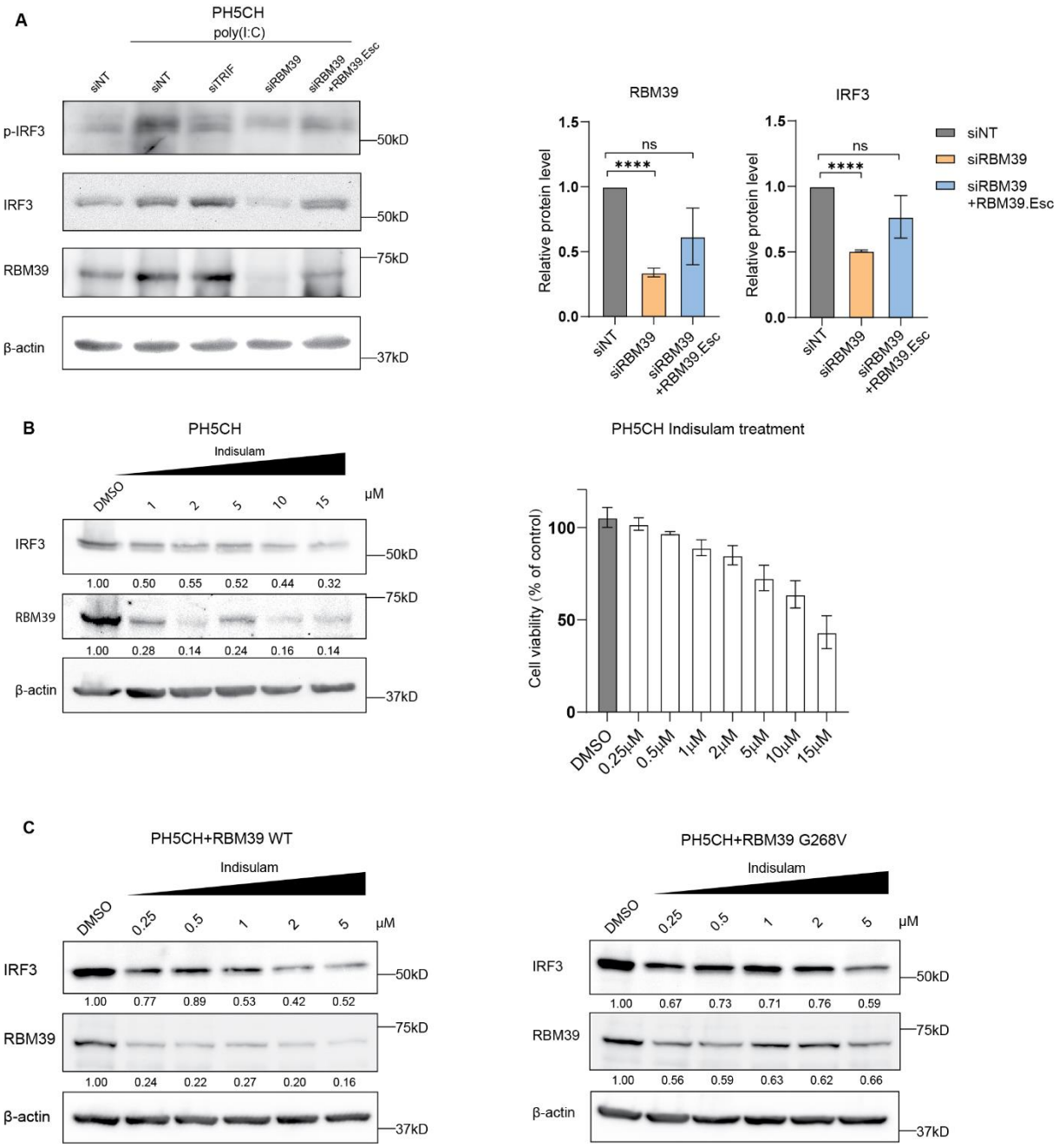

Figure 21. RBM39 regulates the expression of IRF3. (A) PH5CH or PH5CH RBM39.Esc were transfected with indicated siRNA for 48 h to achieve knockdown and then fed with 50 μg/ml poly(I:C) for 6 h. The protein expression of phosphorylated IRF3 (p-IRF3), IRF3, RBM39 and β-actin were measured by western blot. The RBM39, IRF3, p-IRF3 protein level was normalized by β-actin. Quantification was performed by Fiji software, the average number of the relative protein expression to siNT control from three replicates is shown under each lane (right). (B to C) Indisulam, at the indicated concentrations, was added to PH5CH Naïve cells (B), PH5CH RBM39-WT or PH5CH RBM39-G268V cells (C) for 48 h; protein expression of IRF3, RBM39 and β-actin was measured via western blot. Quantification of three biological replicates of western blot was performed by Fiji software and presented under each band.

Same drug treatments were also performed in A549, primary human hepatocytes (PHH) and primary mouse hepatocytes (PMH). Consistently, Indisulam reduced IRF3 protein levels in A549 cells and PHH in a dose-dependent way, but requiring higher doses and associated with

increased cytotoxicity, especially in PHH (Figure 22A and B). However, the addition of Indisulam on PMH did not exert any effect, neither on RBM39 protein abundance (Figure 22C) nor causing cytotoxicity. To understand whether Indisulam was not effective in general for mouse liver cells, I treated another lab-adapted mouse hepatoma cell line, Hep56.1D, with Indisulam. However, indisulam in these cell efficiently degraded RBM39 with a low cytotoxicity (Figure 22D). As shown in literature, the degradation of RBM39 by Indisulam is dependent on the E3 ligase DCAF15 (*283*), therefore the tolerance to Indisulam in PMH was probably due to a lower DCAF15 expression in these mouse cells.

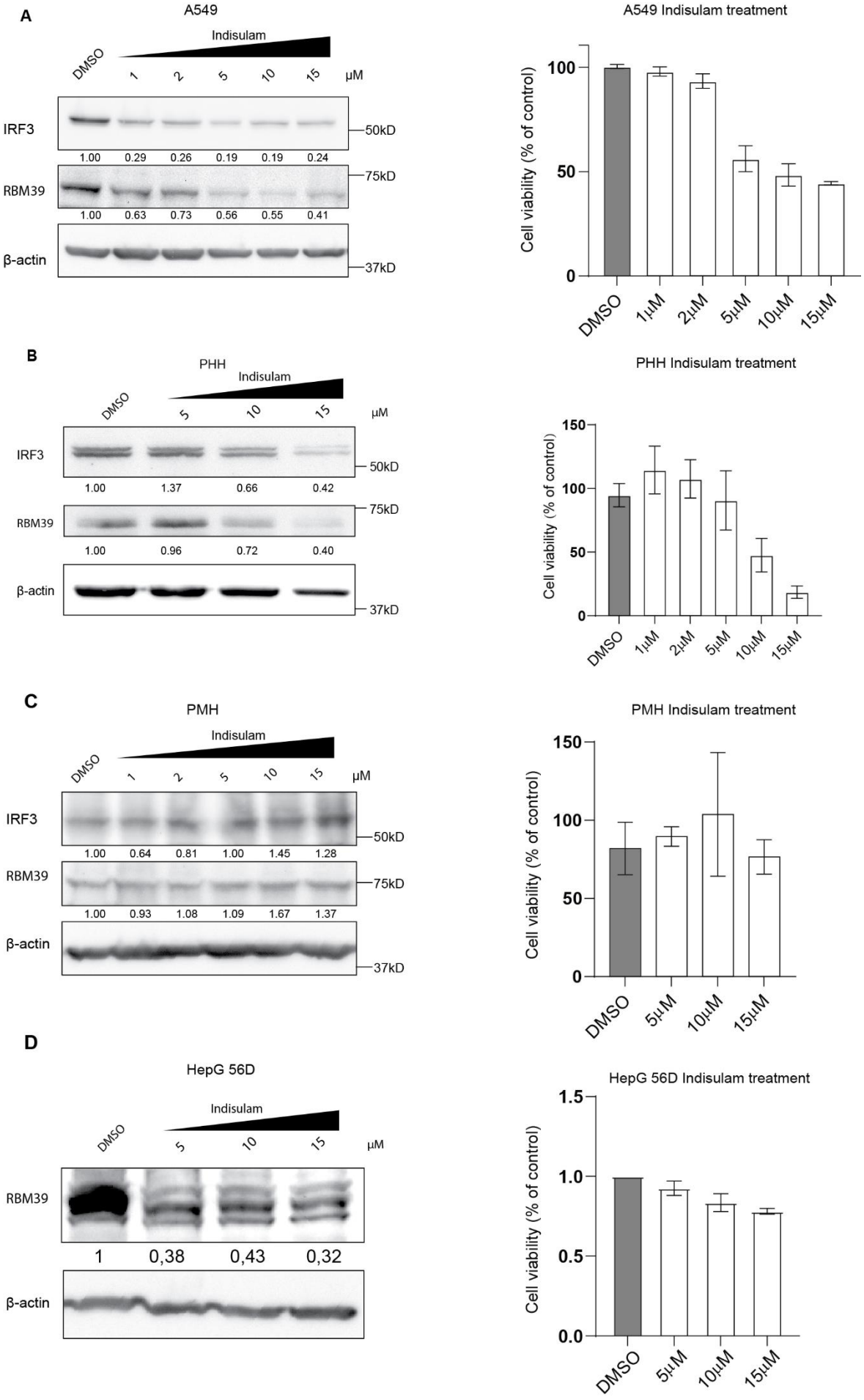
A
A549
Indisulam
DMSO
1
2
5
10
15
μM
IRF3
50kD
1.00 0.29 0.26 0.19 0.19 0.24
RBM39
75kD
1.00 0.63 0.73 0.56 0.55 0.41
β-actin
37kD
A549 Indisulam treatment
Cell viability (% of control)
100
50
0
DMSO
1μM
2μM
5μM
10μM
15μM
B
PHH
Indisulam
DMSO
5
10
15
μM
IRF3
50kD
1.00 1.37 0.66 0.42
RBM39
75kD
1.00 0.96 0.72 0.40
β-actin
37kD
PHH Indisulam treatment
Cell viability (% of control)
150
100
50
0
DMSO
1μM
2μM
5μM
10μM
15μM
C
PMH
Indisulam
DMSO
1
2
5
10
15
μM
IRF3
50kD
1.00 0.64 0.81 1.00 1.45 1.28
RBM39
75kD
1.00 0.93 1.08 1.09 1.67 1.37
β-actin
37kD
PMH Indisulam treatment
Cell viability (% of control)
150
100
50
0
DMSO
5μM
10μM
15μM
D
HepG 56D
Indisulam
DMSO
5
10
15
μM
RBM39
1 0,38 0,43 0,32
β-actin
HepG 56D Indisulam treatment
Cell viability (% of control)
1.5
1.0
0.5
0.0
DMSO
5μM
10μM
15μM

Figure 22. Indisulam treatment in other cell lines. (A to D) Indisulam, at the indicated concentrations, was added to A549 cells (A), PHH (B), PMH (C) or Hep56.1D cells (D) for 48 h; protein expression of IRF3, RBM39 and β-actin was measured using western blot. Quantification was performed by Fiji software from three biological replicates of western blot and presented under each band.

In addition, to further confirm the effect of Indisulam on cell-intrinsic innate immune response, I treated PH5CH cells with Indisulam and stimulated them with poly(I:C) in the supernatant to exclusively trigger the TLR3 pathway. IFIT1 mRNA expression was dramatically reduced even upon low doses of Indisulam, indicating a high sensitivity of these cells to the drug (Figure 23A). Similarly, I stimulated Indisulam-treated A549 cells with poly(I:C) transfection, to address the RLRs-mediated pathways. Consistently, I observed a strong decline of IFIT1 mRNA expression in these cells even upon low concentration of Indisulam (Figure 23B). These observations further supported RBM39's function and indicated Indisulam might be used in clinical settings as an immune inhibitor.

In summary, these evidences supported that RBM39 affects basal IRF3 expression. The anticancer drug, Indisulam, was able to degrade RBM39 in human cell lines, including PH5CH, A549 and PHH, and in mouse hepatoma cell line, Hep56.1D, however, in mouse PMH, it did not show function as a degrader, which prevent further in vivo studies in mice.

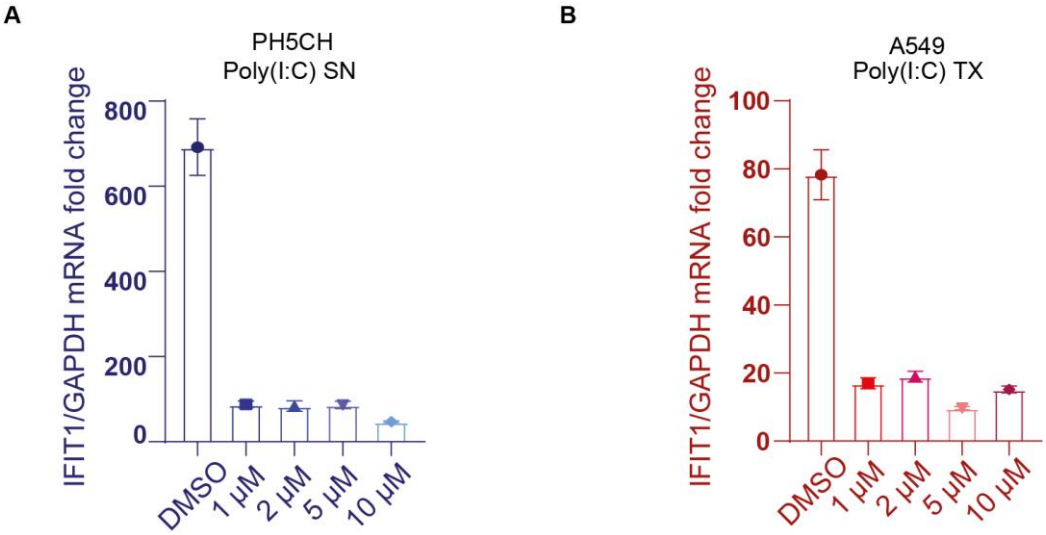

Figure 23. Innate immune response in Indisulam treated cells. (A) PH5CH cells were treated with Indisulam as indicated, or DMSO as control, for 48 h and fed with 50 μg/ml poly(I:C) for 6 h. IFIT1 mRNA was then measured via qPCR. (B) A549 cells were treated with the indicated amounts of Indisulam, or DMSO as control, for 48 h and transfected with poly(I:C) for 6 h. IFIT1 mRNA was determined by qPCR. Shown is the fold change of IFIT1 to GAPDH mRNA from one experiment.

4.1.8 RBM39 affects innate immune activation upon virus infection.

The immunostimulants I used in our experiment so far included poly(I:C), LPS and IFNs. However, whether RBM39 plays a role as well in a more authentic virus infection context remained to be understood. To address this, I initially tested the impact of RBM39 knockdown on Sendai virus (SeV) infection in PH5CH cells. Sendai virus has been reported to trigger the RIG-I pathway (*174*), making it an ideal virus model for studying innate immune responses. As expected, Sendai virus infection strongly upregulated IFIT1 mRNA expression, and notably, the knockdown of RBM39 prior to SeV infection significantly inhibited this response (Figure 24A) even though the virus replication was slight but significant lower 12 h post-infection (Figure 24B). Given that Sendai virus is a pneumotropic virus, I sought to confirm these findings in a more authentic cell model. Therefore, I performed siRNA knockdown followed by Sendai virus infection in A549 cells. Consistently, the knockdown of RBM39 significantly reduced IFIT1 mRNA expression in Sendai virus-infected A549 cells (Figure 24C), correlating with an increased viral replication (Figure 24D).

Subsequently, I extended our investigation by performing Indisulam treatment in A549, HepG2/C3A and HepG2-NTCP cells, followed by infection with River Valley Fever Virus (RVFV), Hepatitis E virus (HEV) and Hepatitis D virus (HDV), respectively, as they all RNA viruses and strong innate immune agonists (*192, 200, 295*). The results demonstrated that RBM39 knockdown significantly suppressed the IFIT1 mRNA expression during RVFV (Figure 24E), HEV (Figure 24F) and HDV (Figure 24G) infection. The replication of RVFV (Figure 24E) and HEV (Figure 24F) upon the knockdown did not change, excluding that the reduced immune response is caused by lower virus replication. Specially, the knockdown even significantly increased HDV replication (Figure 24G).

These experiments collectively support a crucial role of RBM39 in contributing to innate immune responses during virus infection.

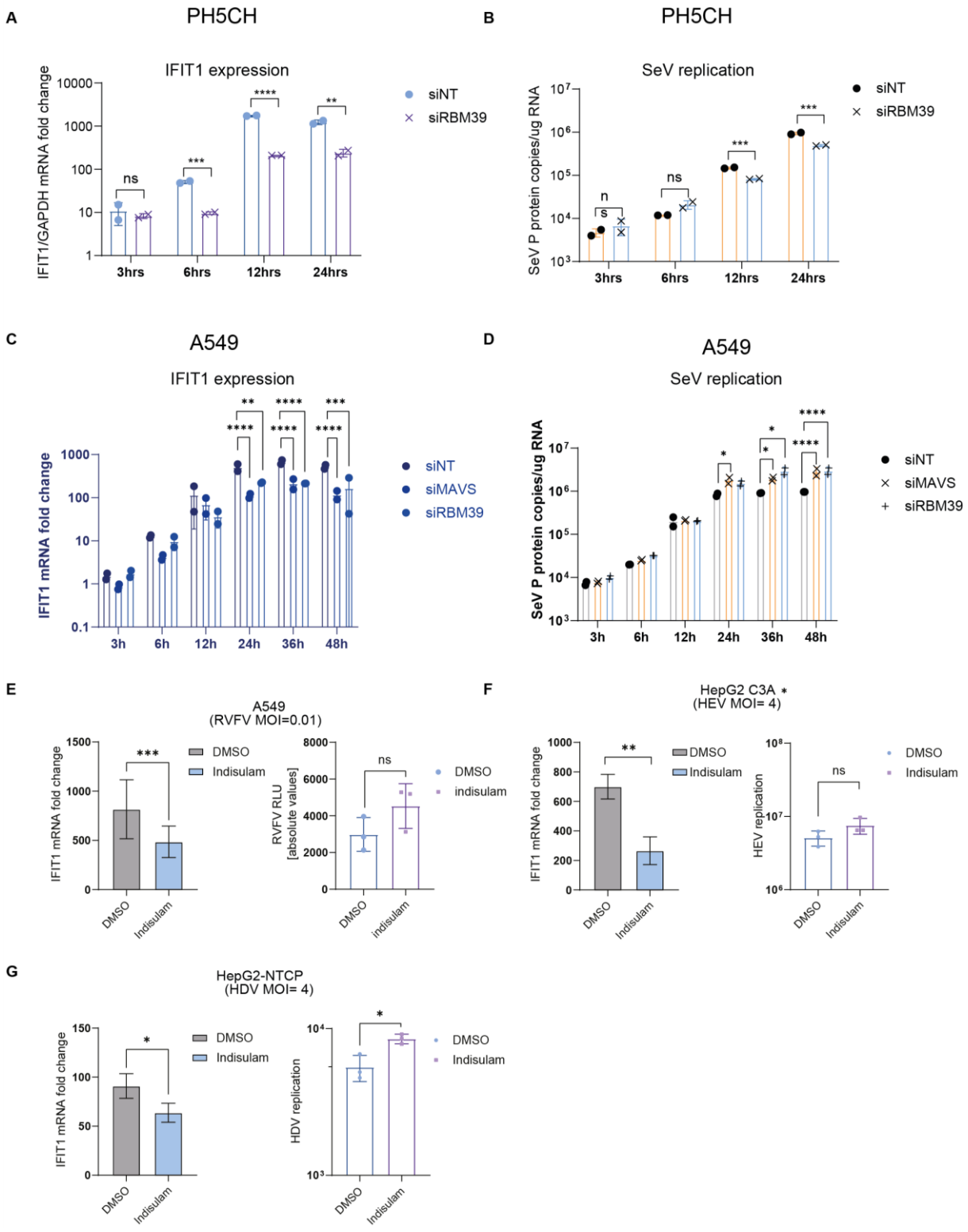

Figure 24. RBM39 affect innate immune activation upon virus infection. (A to D) PH5CH cells (A and B) and A549 cells (C and D) were transfected with indicated siRNA for 48 h and then infected with Sendai virus (MOI=1) for 24 h, IFIT1 mRNA (A and C) and Sendai virus P protein mRNA expression (B and D) was measured by qPCR. (E-G) A549 cells (E), HepG2/C3A cells (F) and HepG2-NTCP cells (G) were treated with 0.1 µM Indisulam or the same amount of DMSO as control. After 48 h, cells were further infected with river valley fever virus (RVFV) (MOI=0.01) for 24 h (B), Hepatitis E virus (MOI=4) (C) and Hepatitis D virus (MOI=4) (D) for 5 days. IFIT1 mRNA and virus replication were measured by qPCR. mRNA fold change was normalized by GAPDH. Shown is relative mRNA expression to DMSO or siNT

control. Data are obtained from three biological replicates, statistics analysis was perform using two-tailed unpaired Welch's test via GraphPad Prism 8 software (GraphPad Software, La Jolla, CA, USA). * p <0.05; **p <0.01; ***p <0.001.

4.1.9 RBM39 is related to SARS-CoV2 infection

SARS-CoV-2 is also an RNA virus that was reported to activate the innate immune response, especially causing strong inflammation (*296*). To investigate whether RBM39 also affected the SARS-CoV-2-related innate immune response, I conducted an infection experiment using SARS-CoV2. I firstly performed RBM39 knockdown via siRNA in A549 cells and then assessed IFIT1 mRNA levels upon SARS-CoV2 replication. Here, ACE2, serving as the receptor for SARS-CoV2, was overexpressed in A549 to enhance infection (*218*). Probably due to the strong inhibitory effect of SARS-CoV2 on the innate immune response (*224*), I did not observe any induction of IFIT1 mRNA, making it challenging to assess the impact of RBM39 on SARS-CoV2-induced innate immune responses (Figure 25A). However, surprisingly, I found a significant decrease in SARS-CoV2 replication in RBM39 knockdown cells (Figure 25B). The qPCR verified a successful RBM39 knockdown (Figure 25C). To corroborate this observation, I alternatively used Indisulam to degrade RBM39 and then infected A549-ACE2 cells. Consistently, I observed a dramatic reduction of SARS-CoV2 replication upon Indisulam treatment as well (Figure 25D).

Evidently, the inhibition of SARS-CoV2 was not related to innate immune function of RBM39, as SARS-CoV2 did not activate it. However, RBM39 expression appeared to be crucial for the virus life cycle. To understand the mechanism, I employed the GFP-VSV pseudovirus system. By replacing the glycoprotein G of VSV by the spike protein of SARS-CoV2 (VSV-S), I could measure entry efficiency by quantifying the GFP signal, while VSV-G served as a control to monitor a general impact on the entry of VSV. A549-ACE2 cells were treated either with siRBM39 or Indisulam for 48 h and infected with VSV-S or VSV-G for control. Using immunofluorescence staining, I observed that both siRBM39 and Indisulam treatment strongly repressed the VSV-S entry (Figure 25E and F). Interestingly, siRBM39 treatment also significantly increased VSV-G infection (Figure 25F), might indicating VSV-G replication is sensitive to innate immunity. Quantification of the images showed that both RBM39 knockdown, or Indisulam-mediated RBM39 degradation, reduced the infection rate of VSV-S, although the reduction was not significant under siRBM39 KD condition (Figure 25F).

In summary, these evidences strongly indicate that RBM39 is crucial for SARS-CoV2 infection, potentially by influencing viral entry.

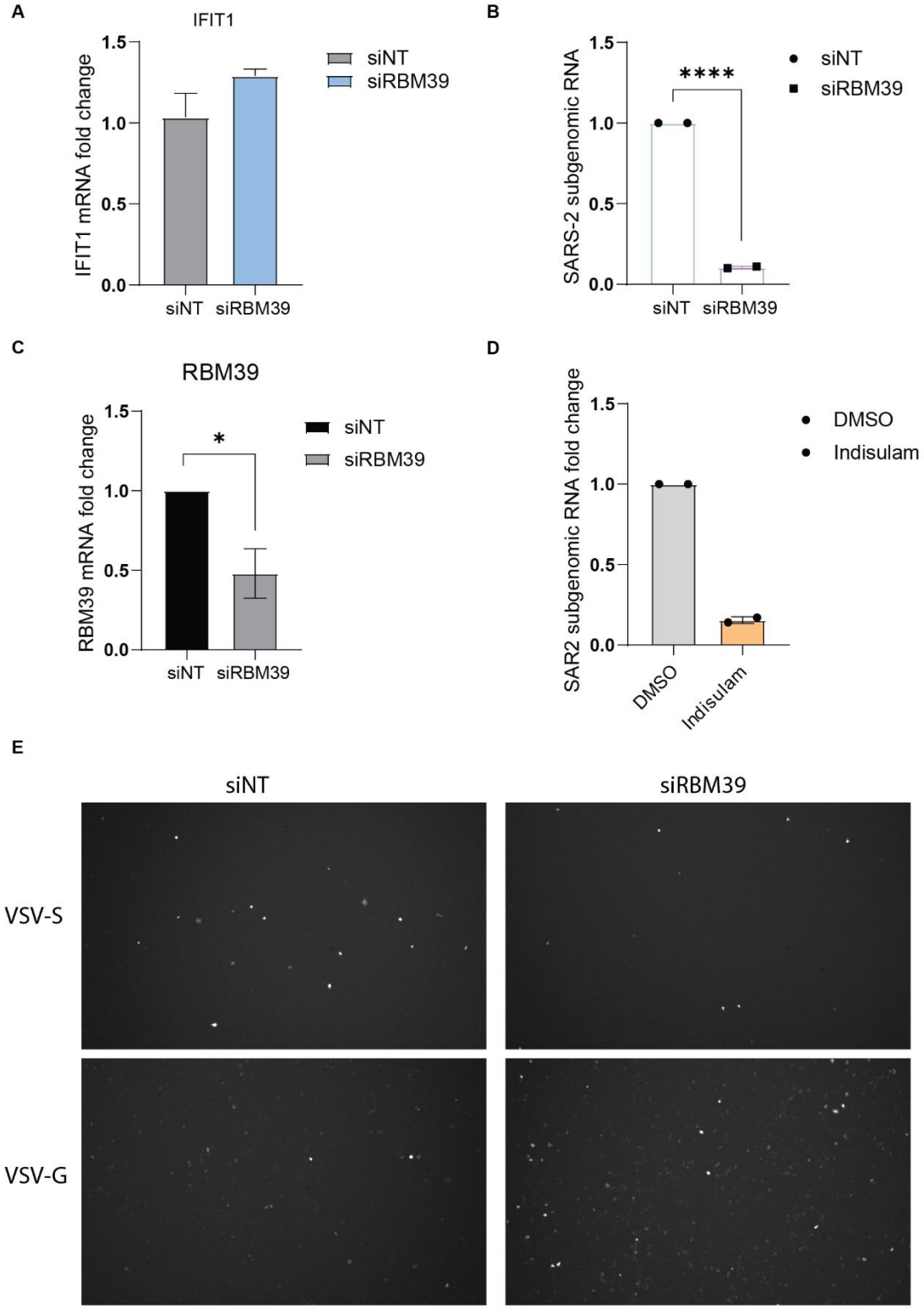

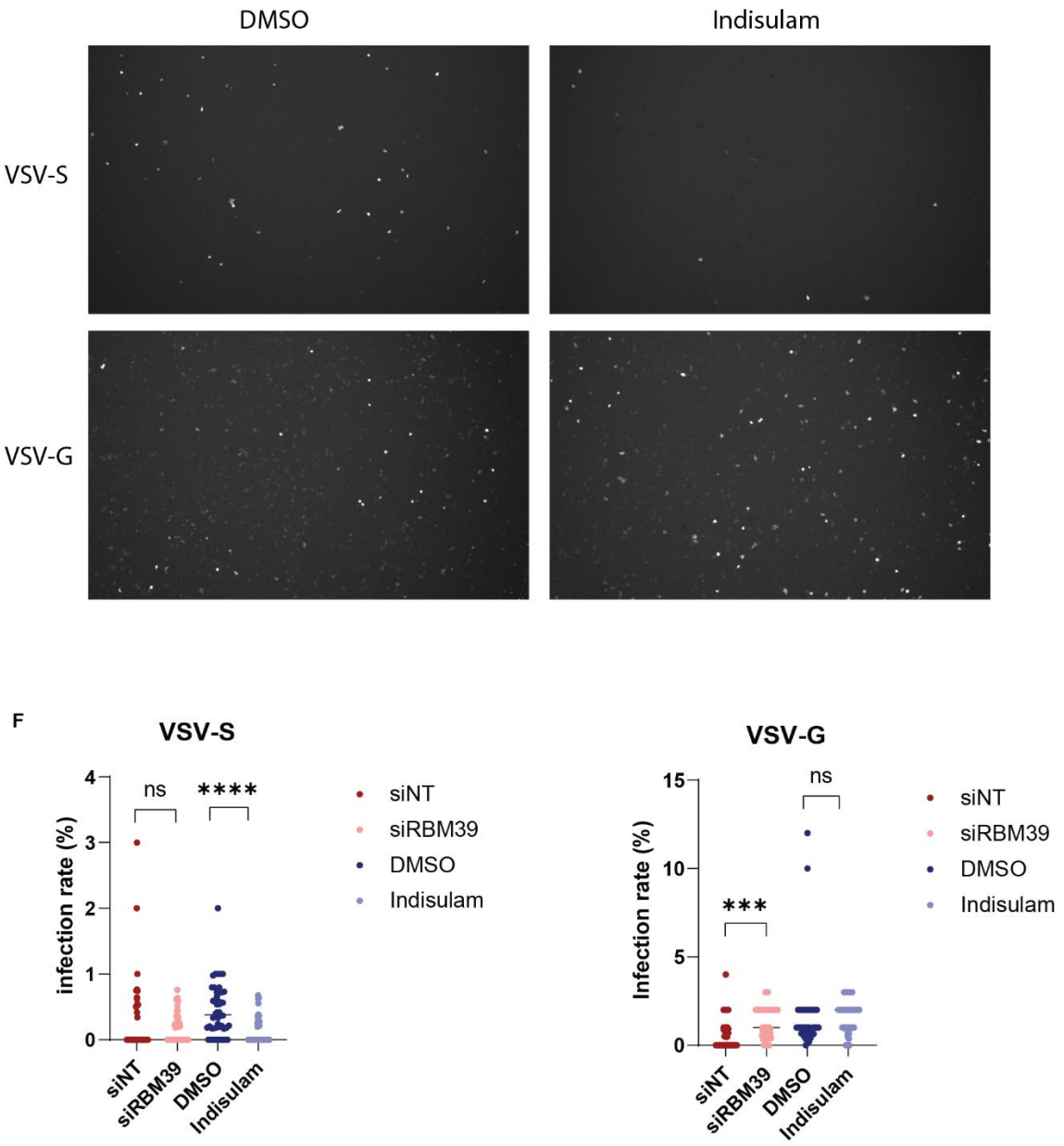

Figure 25. RBM39 is important for SARS-CoV-2 infection. (A to C) A549-ACE2 cells were transfected with siRNA to achieve RBM39 knockdown, after 48 h, cells were further infected with SARS-CoV2 (MOI=1) for 16 h, IFIT1 mRNA (A), SARS-CoV2 subgenomic RNA (B) and RBM39 mRNA (C) were measured by qPCR. (C) A549-ACE2 cells were treated with Indisulam or DMSO for 48 h and then infected with SARS-CoV2 (MOI=1) for 16 h. SARS-CoV2 subgenomic RNA was measured by qPCR. (E) GFP signals of GFP-VSV-S and GFP-VSV-G in A549-ACE2 cells measured by IF. (D) Quantification was performed by cellprofier from 20 IF images. statistics analysis was perform using two-tailed unpaired Welch's test via GraphPad Prism 8 software (GraphPad Software, La Jolla, CA, USA). *p <0.05; **p <0.01; ***p <0.001.

4.1.10 The UHM domain is not required for RBM39's immune function

The structure of RBM39 encompasses a serine/arginine-rich domain (SR), along with three RNA-binding motifs (RRMs). Notably, the last RRM is recognized as a nonclassical RRM and is commonly referred to as the U2AF homology motif (UHM) (Figure 26A). Understanding the

distinct contributions of these domains is essential for unraveling the precise mechanisms underlying RBM39's immune functions.

To investigate which domain was responsible for the innate immune function of RBM39, I firstly generated RBM39 mutant lacking the UHM domain (RBM39-ΔUHM) (Figure 26A). As the antibody I used specifically targeted the UHM domain of RBM39, the RBM39 mutants were not detectable, making it impossible to evaluate the expression of these mutants on the protein level. Therefore, an HA-tag was added at the N-terminus of WT RBM39 and the mutant, and both variants were expressed in PH5CH cells via lentiviral transduction. The expression of these two proteins was confirmed by western blot (Figure 26B). Subsequently, I performed siRBM39 knockdown and poly(I:C) stimulation in PH5CH cells expressing HA-RBM39.Esc or HA-RBM39-ΔUHM. By comparing the rescue effect of mutant proteins with RBM39.Esc, I could determine whether the UHM domain was important for the innate immune function of RBM39. My results showed that the deletion of UHM did not affect the rescue of poly(I:C)-induced IFIT1 mRNA expression, indicating this domain is dispensable (Figure 26C).

However, further experiments with more truncated mutants are still needed to identify the crucial domain for RBM39’s innate immune function.

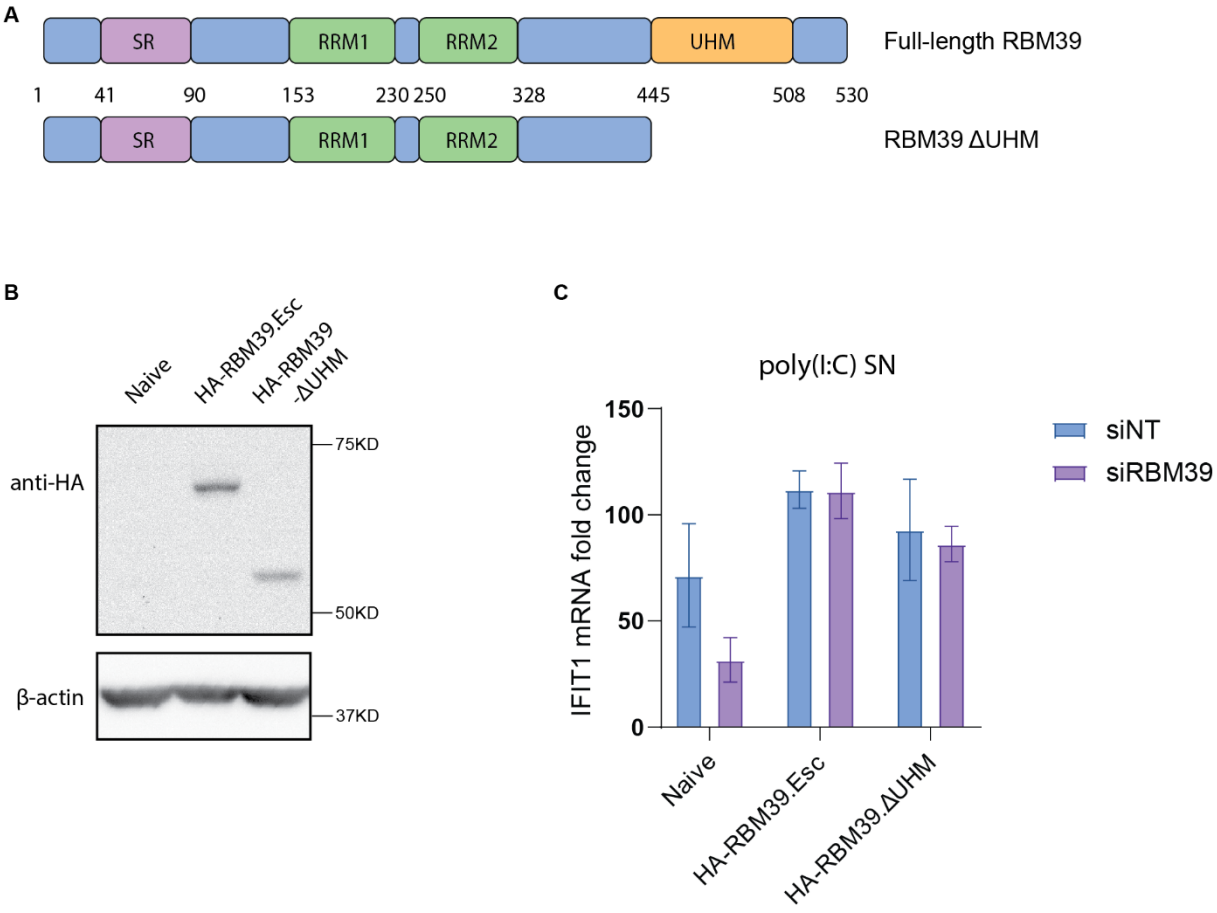

Figure 26. Functional validation of the role of the RBM39 UHM domain in innate immune signaling. (A) Schematic of full-length RBM39 and RBM39- ∆ UHM. (B) The overexpression of HA-RBM39.Esc and HA-RBM39- ∆ UHM in PH5CH cells was measured by immunoblotting. (C) PH5CH cells expressing HA-RBM39.Esc or HA-RBM39- ∆ UHM were silenced by siRBM39 for 48h and stimulated via 50 µg/ml poly(I:C) supernatant feeding for 6 h, IFIT1 mRNA was measured by qPCR.

4.1.11 RBM39-mediated IRF3 regulation is not at the protein level

Despite demonstrating the role of RBM39 in innate immunity across various cell lines and stimuli, including physiological virus infection, and its association with IRF3 expression, the precise mechanism governing this regulation remained unclear so far.

To better understand the RBM39-mediated IRF3 regulation, I firstly looked at the localization of RBM39 in PH5CH cells. Due to the high background issues with the polyclonal RBM39 antibody, I opted for an alternative approach by constructing two HA-tagged RBM39 variants and expressing them into PH5CH through lentiviral transduction. Immunofluorescence staining revealed that both 5'HA-RBM39 and 3'HA-RBM39 predominantly localized in the nucleus, and this subcellular distribution remained unchanged upon poly(I:C) stimulation (Figure 27A and B). Considering that IRF3 protein was primarily located in the cytoplasm in the

absence of stimulation (*297*) but was still regulated by RBM39 (Figure 21 and 22), a direct protein interaction between RBM39 and IRF3 appeared unlikely.

In order to further explore whether RBM39 regulates IRF3 at protein levels, IRF3 was ectopically expressed in IRF3 knockout cells (PH5CH-eIRF3), and the IRF3 protein expression of PH5CH naïve cells and PH5CH-eIRF3 cells following RBM39 knockdown was compared. In PH5CH naïve cells, the silencing of RBM39 resulted in a reduction of IRF3 at protein levels. However, the ectopic IRF3 in PH5CH-eIRF3 cells remained unaffected (Figure 27C). Furthermore, when I stimulated PH5CH-eIRF3 cells with poly(I:C) supernatant feeding after RBM39 knockdown, I observed no impact on IFIT1 mRNA induction (Figure 27D). This clearly demonstrated that RBM39 did not play a role in the regulation of ectopic IRF3. Additionally, the expression of ectopic IRF3 was sufficient to rescue the RBM39 knockdown-mediated IFIT1 mRNA reduction upon TLR3 stimulation, also underscoring the pivotal role of IRF3 in this regulatory process.

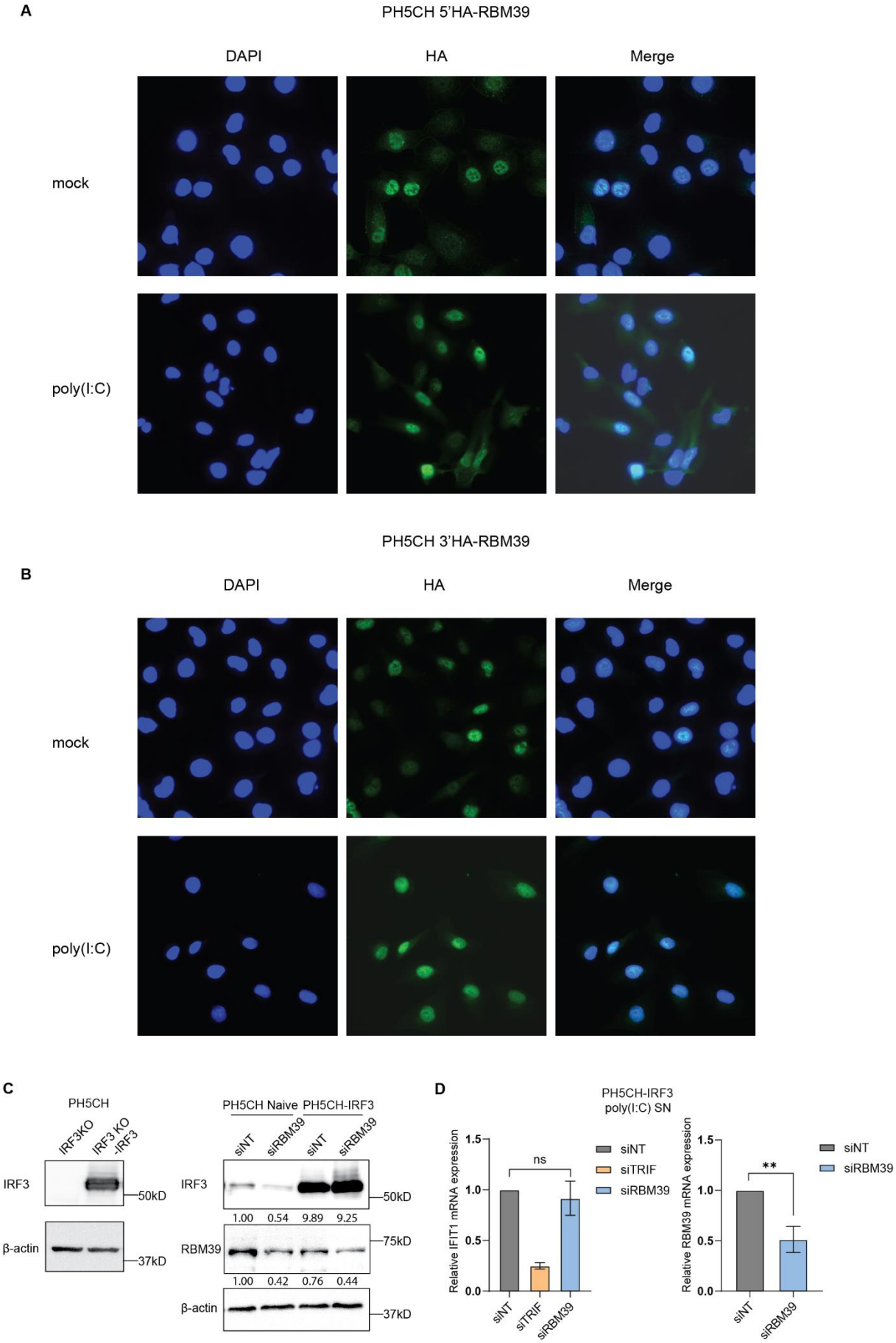
A
PH5CH 5'HA-RBM39
DAPI
HA
Merge
mock
poly(I:C)
B
PH5CH 3'HA-RBM39
DAPI
HA
Merge
mock
poly(I:C)
C
PH5CH
IRF3KO
IRF3 KO -IRF3
IRF3
50kD
β-actin
37kD
PH5CH Naive
PH5CH-IRF3
siNT
siRBM39
siNT
siRBM39
IRF3
50kD
1.00 0.54 9.89 9.25
RBM39
75kD
1.00 0.42 0.76 0.44
β-actin
37kD
D
PH5CH-IRF3
poly(I:C) SN
Relative IFIT1 mRNA expression
1.5
1.0
0.5
0.0
ns
siNT
siTRIF
siRBM39
siNT
siTRIF
siRBM39
Relative RBM39 mRNA expression
1.5
1.0
0.5
0.0
**
siNT
siRBM39
siNT
siRBM39

Figure 27. RBM39-mediated IRF3 regulation is not at the protein level. (A and B) the localization of RBM39 with or without poly(I:C) stimulation in PH5CH cells expressing 5'HA-RBM39 (A)or 3'HA-RBM39 (B) was measured by immunofluorescence. (C) IRF3 protein level in PH5CH IRF3 KO cells with or without the ectopic IRF3 (PH5CH-eIRF3) was measured by immunoblotting (left), PH5CH naïve cells or PH5CH-eIRF3 cells were silenced by siRNA indicated, IRF3, RBM39 and β-actin protein expression was determined via western blot (right). The quantification was performed using Fiji software, the average number of the relative protein expression to siNT control from three replicates is shown under a representative figure. (D) PH5CH-eIRF3 cells were treated with indicated siRNA for knockdown and then stimulated by 50 μg/ml poly(I:C) in the supernatant for 6 h. IFIT1 and RBM39 mRNA levels were measured by qPCR. mRNA fold change was normalized on GAPDH. Data are obtained from biological triplicates. Statistics was conducted via two-tailed unpaired Welch's test by GraphPad Prism 8 software (GraphPad Software, La Jolla, CA, USA). *p <0.05; **p <0.01; ***p <0.001.

4.1.12 RBM39 regulates IRF3 mRNA transcription

Having ruled out a protein-level regulatory function of RBM39 on IRF3 abundance, I further considered the mechanism could rely on mRNA.

Given that RBM39 has previously been identified as a co-transcriptional factor of AP-1, ERα and ERβ (*285*), it was plausible to hypothesize that it may also regulate the transcription of IRF3. To investigate this, I firstly measured IRF3 mRNA expression in RBM39-silenced PH5CH cells, observing a slight but significant reduction of IRF3 mRNA (Figure 28A). To confirm this, I then referred to literature and found two IRF3 promoter sequences that have been evaluated (*298*). The longer sequence contains the full-length IRF3 promoter region (pGL3-982) and the shorter one included only the IRF3 core promoter (pGL3-149), which is the minimal length required for its promoter function (Figure 28B). Subsequently, two luciferase reporters containing the IRF3 promoter sequences were constructed and transfected into RBM39-silenced PH5CH cells. In line with the qPCR results, RBM39 knockdown also inhibited the luciferase activity in both IRF3-based luciferase assays (Figure 28C), supporting the hypothesis that RBM39 is involved in the transcriptional regulation of IRF3.

However, the mild mRNA downregulation could not explain the strong reduction of IRF3 at protein levels. Since RBM39 has an RNA binding function and mainly localizes in the nucleus (Figure 26A), I hypothesized that RBM39 might bind to IRF3 mRNA and promote its translocation from the nucleus to the cytoplasm. To verify this, I isolated the nucleus and cytoplasm, measured IRF3 mRNA and protein expression upon degradation of RBM39 by Indisulam in both fractions. As expected, the Indisulam treatment dramatically degraded RBM39 in the nucleus and thus decreased IRF3 protein levels in the cytoplasm (Figure 28D). Our markers, H2A.X and GAPDH, only expressed in nucleus and cytoplasm (*299, 300*),

respectively, and MALAT1 as a non-coding RNA expressing in nuclear speckles was used as a control (*301*), ensured specificity during the isolation. Regardless, the IRF3 cytoplasmic/nucleic mRNA ratio did not change upon Indisulam treatment (Figure 28E), demonstrating that IRF3 mRNA translocation is not modified by RBM39.

To sum up, I excluded the possibility of RBM39 regulating IRF3 on the protein level and revealed that transcription of IRF3 mRNA is affected by RBM39.

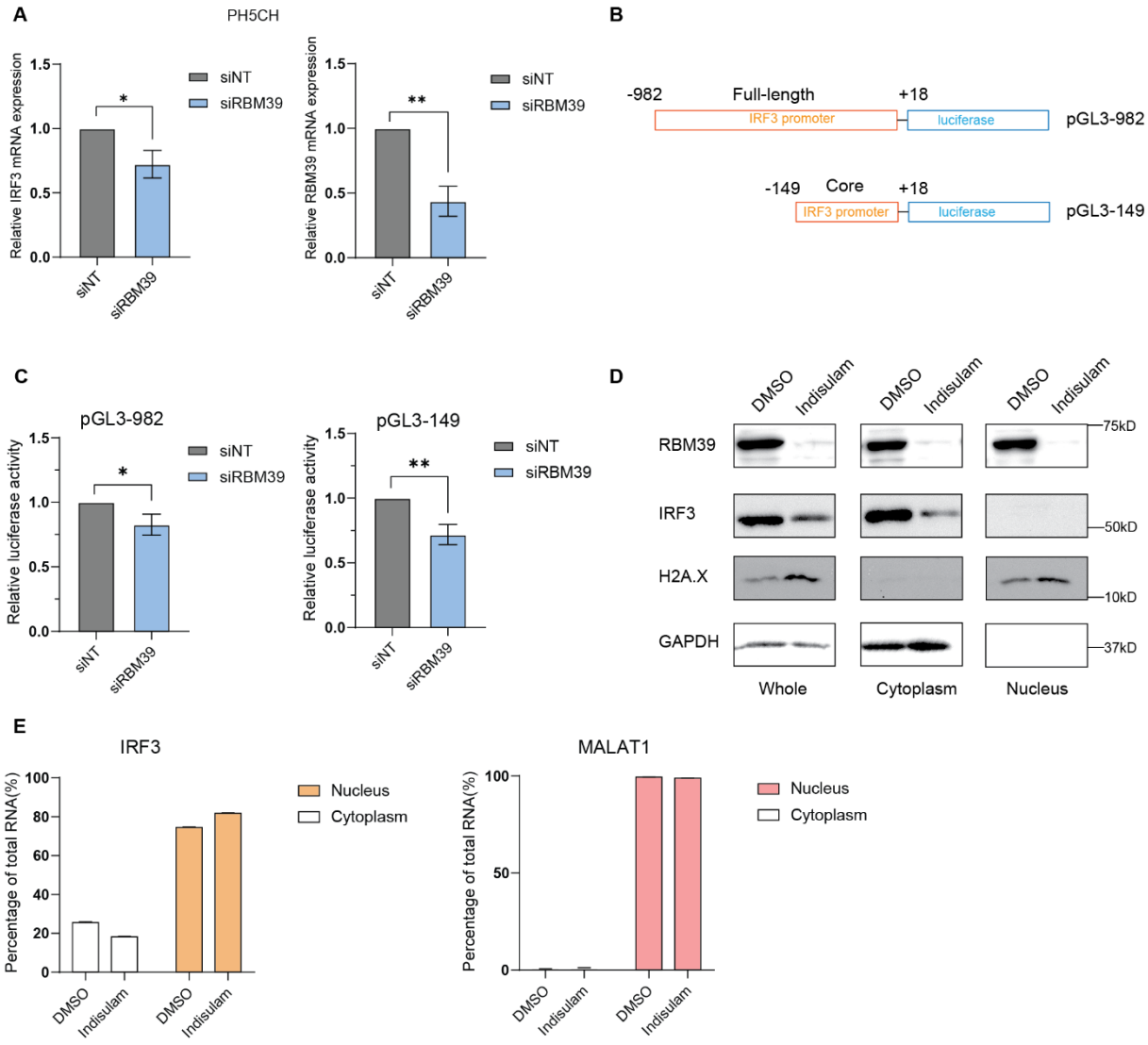

Figure 28. RBM39 regulates IRF3 mRNA transcription. (A) PH5CH cells were transfected with siRBM39. After 48h, IRF3 mRNA and RBM39 mRNA were measured by RT-qPCR. (B) Schematic of IRF3-based luciferase reporter. The full-length IRF3 promoter sequence with 982 bp (pGL3-982) and core IRF3 promoter (pGL3-149) were inserted into the pGL3-firefly luciferase reporter. (C) PH5CH cells were silenced with the indicated siRNA. pGL3-982 and pGL3-149 firefly luciferase reporters, respectively, together with a CMV-driven Gaussia luciferase reporter, were transfected into the cells after 48 h. 24 hours later, luciferase activity was measured. Relative luciferase was determined by normalizing firefly luciferase activity on Gaussia luciferase activity. (D and E) The cytoplasm and nucleus of PH5CH cells were isolated, RBM39 and IRF3 protein expression in each fraction was assessed by western blot. H2A.X and GAPDH were used as nucleus marker and cytoplasm maker, respectively (D). IRF3 and

MALAT1 mRNA in each fraction was measured by qPCR, shown is the ratio of mRNA in each fraction to the total mRNA. MALAT1 served as a nucleus marker.

4.1.13 RBM39 governs the alternative splicing of IRF3

RBM39 regulated the IRF3 promoter activity, but the effect was limited. Given that RBM39 is also a splicing factor that interacts with the spliceosome and facilitates the splicing process (*302*), I further investigated whether RBM39 maintains the splicing of IRF3 mRNA.

To achieve this, I attempted to identify the IRF3 isoforms in PH5CH cells upon RBM39 knockdown via RT-PCR, using primers targeting the full length IRF3. Indeed, the IRF3 isoform pattern showed differences comparing siNT and siRBM39-treated samples (Figure 29A). However, the observed patterns were not reproducible and depended on the PCR conditions. To have an alternative approach, I designed an RNA probe targeting IRF3 exon 8, which is presence in most isoforms, and measured IRF3 isoform mRNA via northern blot. Here, I only observed a single IRF3 band (Figure 29B), suggesting a failure of identifying mRNAs of IRF3 isoforms.

To improve the sensitivity and reliability, I conducted a RBM39 knockdown using siRNA and Indisulam treatment to degrade RBM39, respectively, in PH5CH cells, and then extracted the mRNA and performed RNA sequencing (RNA seq). The intensive bioinformatic analysis was conducted by my colleague Paul Rothhaar. The RNA counts of GAPDH did not significantly change after the knockdown or Indisulam-mediated degradation of RBM39, indicating the absence of strong toxicity (Figure 29C). In contrast, RBM39 RNA counts showed a significant reduction in RBM39 knockdown cells as expected, confirming the efficacy of the knockdown (Figure 29D). Interestingly, RBM39 mRNA expression exhibited a robust increase in the Indisulam-treated condition, probably hinting an auto-regulation of mRNA abundance upon depletion of the protein. A slight suppression of IRF3 mRNA was also observed in both RBM39 knockdown and Indisulam treatment conditions, consistent with the qPCR results, although it was not statistically significant in this analysis (Figure 29E).

Furthermore, IRF3 mRNA isoform expression was analyzed in both conditions. Many IRF3 isoforms have been already discovered and extensively studied, for example, IRF3-203 has been reported as the only functional isoform, while other isoforms such as IRF3-228 are dysfunctional and inhibitory to innate immune responses (*303*). Several IRF3 isoforms in PH5CH cells under the experimental conditions were identified. In both conditions, the ratio

of isoform IRF3-203 to total IRF3 decreased while the ratio of other isoforms to total IRF3, including IRF3-228, IRF3-202 and IRF3-219 increased (Figure 29F). The absolute mRNA counts, reflecting the combined effect on both transcription and alternative splicing, revealed a more pronounced attenuation on the functional IRF3-203 isoform and an elevation of other non-functional isoforms (Figure 29G). Particularly, IRF3-228 has been reported as an innate immune inhibitor (*303*), therefore, the upregulation of this isoform and the decrease of functional isoform IRF-203 could collectively contribute to the suppression of innate immune signaling.

To confirm the phenotype observed in the RNA seq data, primers that targeted the IRF3 isoforms were designed and their expression upon RBM39 knockdown was measured by RT-qPCR. Most primers were designed targeting specific regions of isoforms (Figure 29H), as most isoforms had unique intron insertion or exon skipping. However, IRF3-203 and IRF3-228 had only a 16 bp difference in their nucleic acid sequence, making it challenging to distinguish. As an alternative, primers were designed specifically targeting the 16 bp sequence of IRF3-228 (primers 228) and targeting both IRF3-228 and IRF3-203 (primers 203+228), the ratio of IRF3-203 to total IRF3 could then be obtained by calculation. Subsequently, RBM39 knockdown was performed in PH5CH cells and IRF3 isoforms mRNA expression was determined via RT-qPCR. The results showed a similar pattern as the RNA seq data, with IRF3-203/total IRF3 significantly decreasing while IRF3-228/total IRF3 exhibited a significant increase upon reduced RBM39 levels; other isoforms either slightly increased or decreased, but not significantly (Figure 29I).

Overall, the splicing analysis of the RNA seq data revealed that the downregulation of RBM39 caused alternative splicing of IRF3 mRNA, switching the functional IRF3 isoform to other non-functional ones. This was further verified by qPCR and could represent the main reason contributing to the suppression of innate immune sensing.

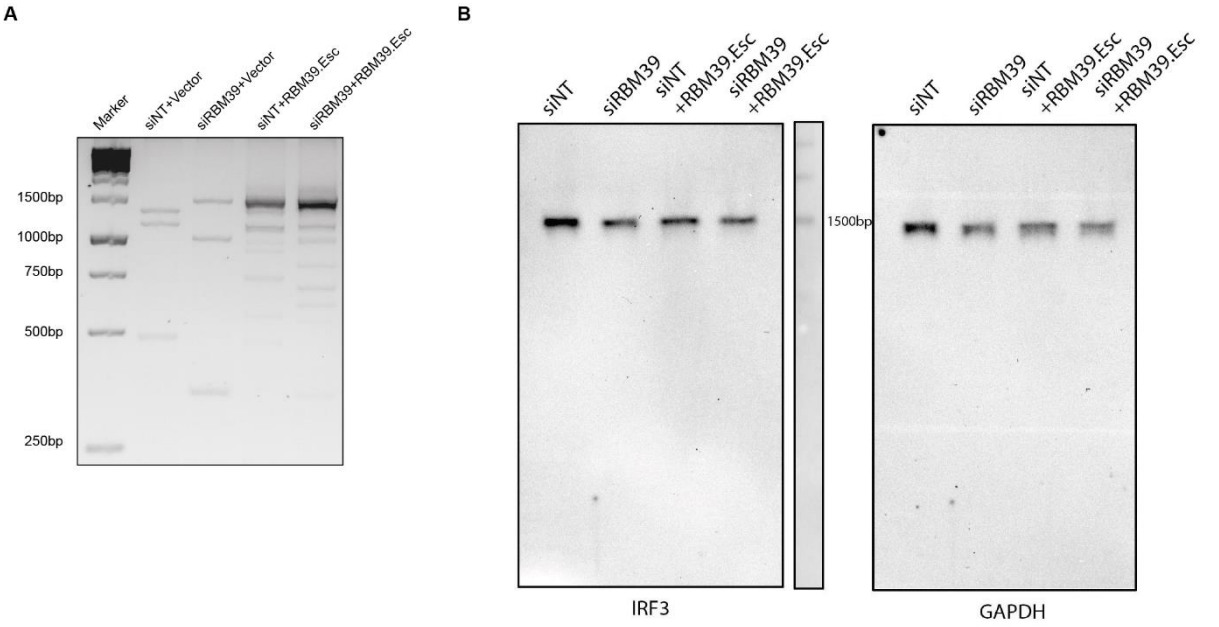
A
Marker
siNT+Vector
siRBM39+Vector
siNT+RBM39.Esc
siRBM39+RBM39.Esc
1500bp
1000bp
750bp
500bp
250bp
B
siNT
siRBM39
siNT +RBM39.Esc
siRBM39 +RBM39.Esc
1500bp
IRF3
GAPDH

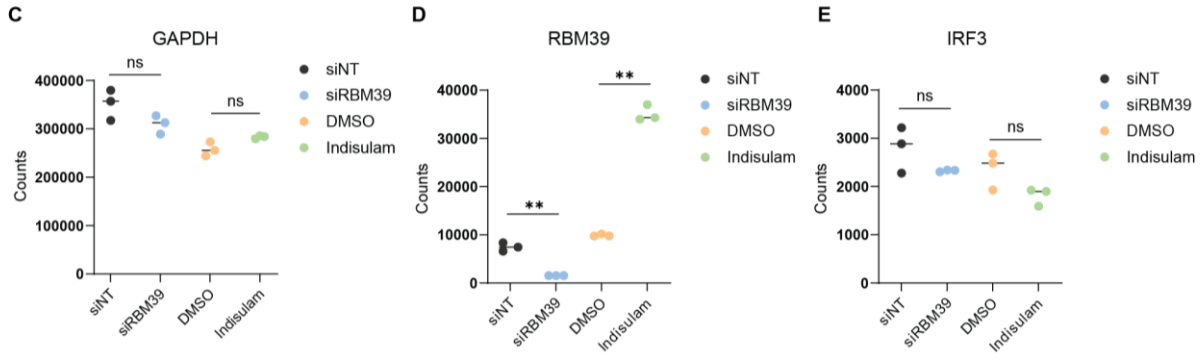
C
GAPDH
Counts
ns
siNT
siRBM39
DMSO
Indisulam
D
RBM39
**
E
IRF3

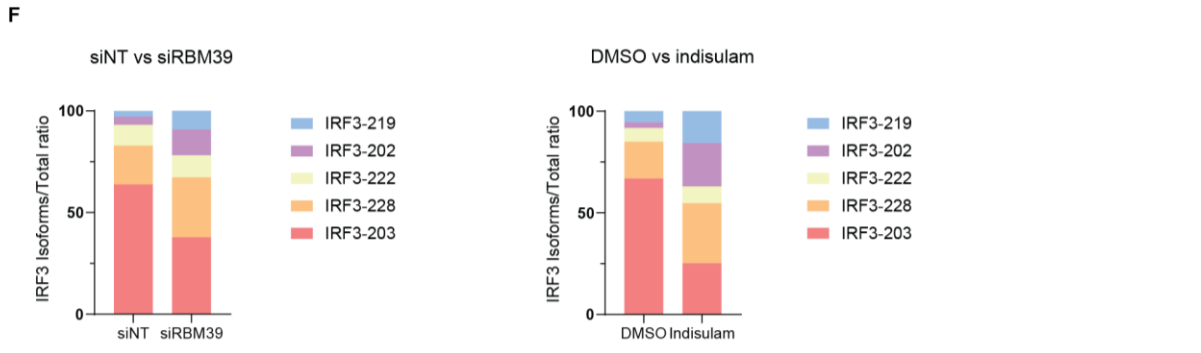
F
siNT vs siRBM39
DMSO vs indisulam
IRF3 Isoforms/Total ratio
IRF3-219
IRF3-202
IRF3-222
IRF3-228
IRF3-203

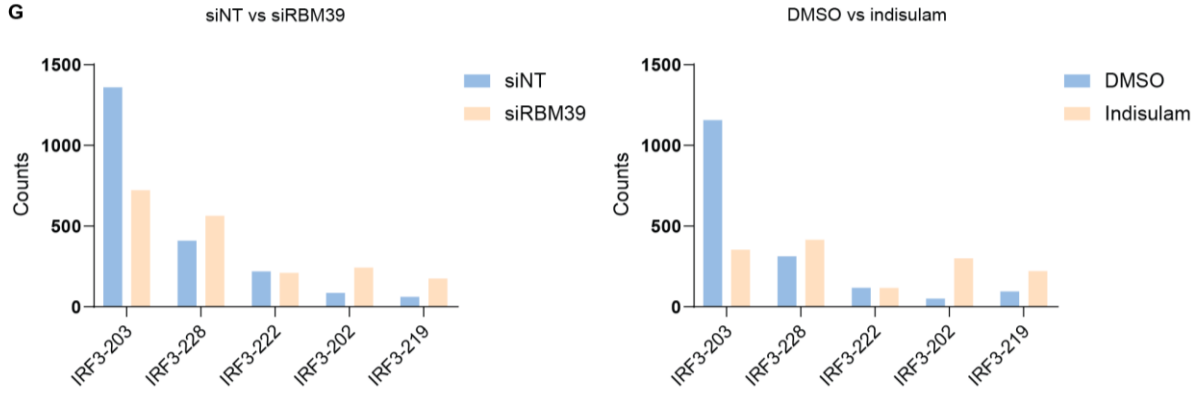
G
siNT vs siRBM39
DMSO vs indisulam
Counts
siNT
siRBM39
DMSO
Indisulam
IRF3-203
IRF3-228
IRF3-222
IRF3-202
IRF3-219

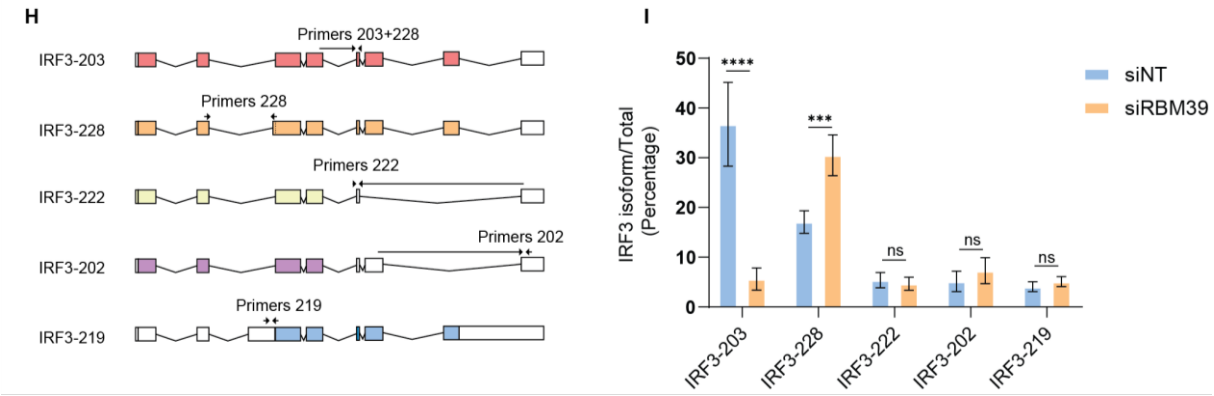

Figure 29. RBM39 governs the alternative splicing of IRF3 (A) The expression IRF3 isoforms in PH5CH cells was measured by RT-PCR using primer targeting the exon1 and exon8 of IRF3 mRNA. (B) PH5CH and PH5CH cells expressing RBM39.Esc were treated with siRBM39 or siNT as controls for 48 h. 10 µg of total RNA were subjected to northern blot analysis, using formaldehyde-agarose gel electrophoresis. RNA probe targeting full-length IRF3 was generated by in vitro transcription. The IRF3 isoform expression in PH5CH cells was measured by northern blot. (C to E) Differential expressed gene (DEG) analysis of the RNA seq data was performed by DESeq2. GAPDH (C), RBM39 (D) and IRF3 (E) mRNA counts in PH5CH cells treated with siRBM39 or Indisulam are shown (F to G). Different transcript usage (DTU) analysis of the RNA seq data was conducted using DRIMseq. Shown are IRF3 isoforms/total mRNA ratio (F) and absolute mRNA counts (G) in PH5CH treated with siRBM39 or Indisulam. (H) Schematic of IRF3 isoforms, exons or introns that are kept in the isoforms are shown in boxes, colored boxes indicate coding sequence. Specific primers targeting different isoforms are shown as arrows. (I) IRF3 isoforms mRNA expression in PH5CH cells was identified by RT-qPCR. Shown is the ratio of the IRF3 isoforms/total mRNA.

4.1.14 Global transcriptomic and proteomic analysis highlight the role of RBM39 in innate immunity

To comprehensively understand the regulatory network of RBM39, global transcriptomic analysis was also conducted.

The analysis identified 2719 differential expression genes (DEGs) in siRBM39 knockdown samples and 2858 DEGs in Indisulam-treated samples. 1500 DEGs overlapped in both conditions, comprising 39% of the total DEGs (Figure 30A). 2833 differential transcript usages (DTUs) were identified in siRBM39 treated samples and 3197 DTUs was triggered by Indisulam-treatment, consisting of 49% of the total DTUs (Figure 30A). The relatively high overlap of the two settings also proved the reliability of our analysis.

Noticeably, DEGs analysis not only showed 1586 and 1634 down-regulated genes, but also displayed 1133 and 1224 up-regulated genes in siRBM39 or Indisulam-treated samples, respectively. A total of 978 genes exhibited down-regulation and 585 genes was promoted in both conditions (Figure 30B). The volcano plot showed all DEGs in RBM39 knockdown and

Indisulam-treated samples, respectively. DEGs with fold change >2 or <0.5 and p-value <0.05 was considered significant and was marked (Figure 30C). The gene ontology analysis also revealed that the most involved biological processes in combined conditions, with organic acid metabolic, oxoacid metabolic and small molecule metabolic processes being the top three. However, biological processes related to innate immunity were not significant in the analysis (Figure 30D), explaining why this effect might have been missed in previous transcriptomic studies.

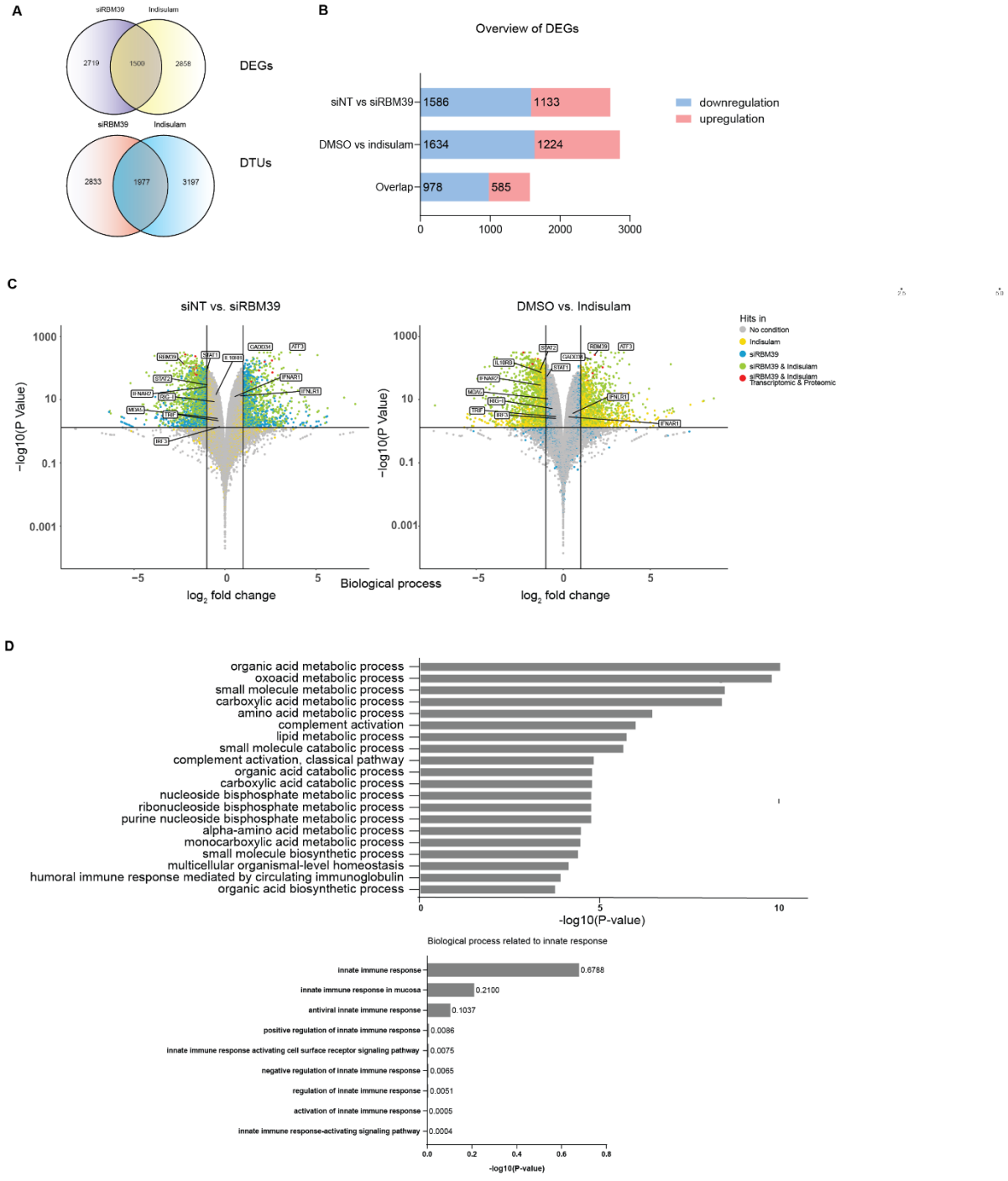

Figure 30. Overview of the global transcriptome and splicing analysis in siRBM39 or Indisulam-treated PH5CH cells. (A) DEG analysis and DTU analysis. Numbers indicate the events in each condition and overlapped condition. (B) Overview of DEGs, up-regulated and down-regulated gene numbers in each condition and overlapped condition are shown. (C) Volcano plot of the DEG analysis. Genes with fold change >2 or < 0.5, p-value < 0.05 only in siRBM39 treatment condition are marked with a blue dot, only in Indisulam treatment condition are highlighted with yellow, and overlapping genes are colored in green. (D) Gene ontology analysis of RBM39 regulated biological processes. P-value was obtained from combined conditions.

4.1.15 RNA seq revealed other innate immune factors involved in RBM39 regulatory network

Here, my focus was specifically on innate immune factors, and their transcription and splicing were analyzed with the help of Paul Rothhaar based on the RNAseq data. RIG-I and MDA5, crucial PRRs for dsRNA recognition, showed significant reduction in mRNA abundance in both conditions while only the RIG-I functional isoform exhibited decrease in DTU analysis, arguing for differential splicing regulated by RBM39 (Figure 31A and B). To confirm the functional significance of RIG-I/MDA5 depletion, I used Bafilomycin A1 (BafA) to pre-treat PH5CH-eIRF3 cells with stable, ectopic IRF3 expression. BafA abrogates the acidification of the endosome thereby abrogating endosomal TLR signaling, including TLR3 (*292*). Subsequently, I measured the IFIT1 mRNA expression upon knockdown of RBM39 and RIG-I/MDA5 activation by poly(I:C) transfection. In contrast to the rescue of TLR3 signaling by IRF3 overexpression (Figure 27D), the overexpression of IRF3 was unable to rescue RIG-I/MDA5-induced IFIT1 mRNA upon knockdown, confirming the involvement of upstream RIG-I/MDA5 in mediating the effect of RBM39 on innate immunity (Figure 31C).

TRIF, the adaptor protein of TLR3, exhibited slight attenuation in Indisulam-treated samples but not in siRBM39-treated samples (Figure 31D). However, the expression of eIRF3 was sufficient to rescue the knockdown of RBM39 (Figure 27D), excluding the participation of TRIF. Consistently, the splicing of TRIF did not show any change in both conditions (Figure 31D).

Given our earlier observation of the impact of RBM39 on the type III IFN pathway, I next checked the expression and splicing of IFNLR1 and IL10RB. Similar to what observed previously (Figure 20E), IFNLR1 mRNA showed an increase while IL10RB mRNA reduced significantly in both conditions. However, the splicing did not show significant changes for both genes (Figure 31E and F). This downregulation of IL10RB could have contributed to RBM39-mediated type III IFN-specific innate immune inhibition.

Surprisingly, the expression of type I IFN receptors, IFNAR1, exhibited a significant increase, whereas the expression of IFNAR2 was significantly reduced (Figure 31G and H), although their splicing did not show significant changes. More importantly, the vital components of the JAK-STAT pathway, STAT1 and STAT2 also exhibited suppression in the DEG analysis, with STAT1 also showing alternative splicing (Figure 31I and J), suggesting a general downregulation on both type I and type III IFN pathways, which was in contrast to our previous observations. However, it has been reported that the activation of type I IFN was partly independent of IFNAR2 (*129*). Considering the observed increase in IFNAR1, the reduction in IFNAR2 expression might be functionally compensated by the increase of IFNAR1.

Overall, the transcriptomic and splicing analysis further supports that RBM39 regulates other innate immune factors, including PRRs like RIG-I and MDA5, and JAK-STAT pathway factors, IFNAR1, IFNLR1, STAT1 and STAT2, highlighting its role in innate immune regulation.

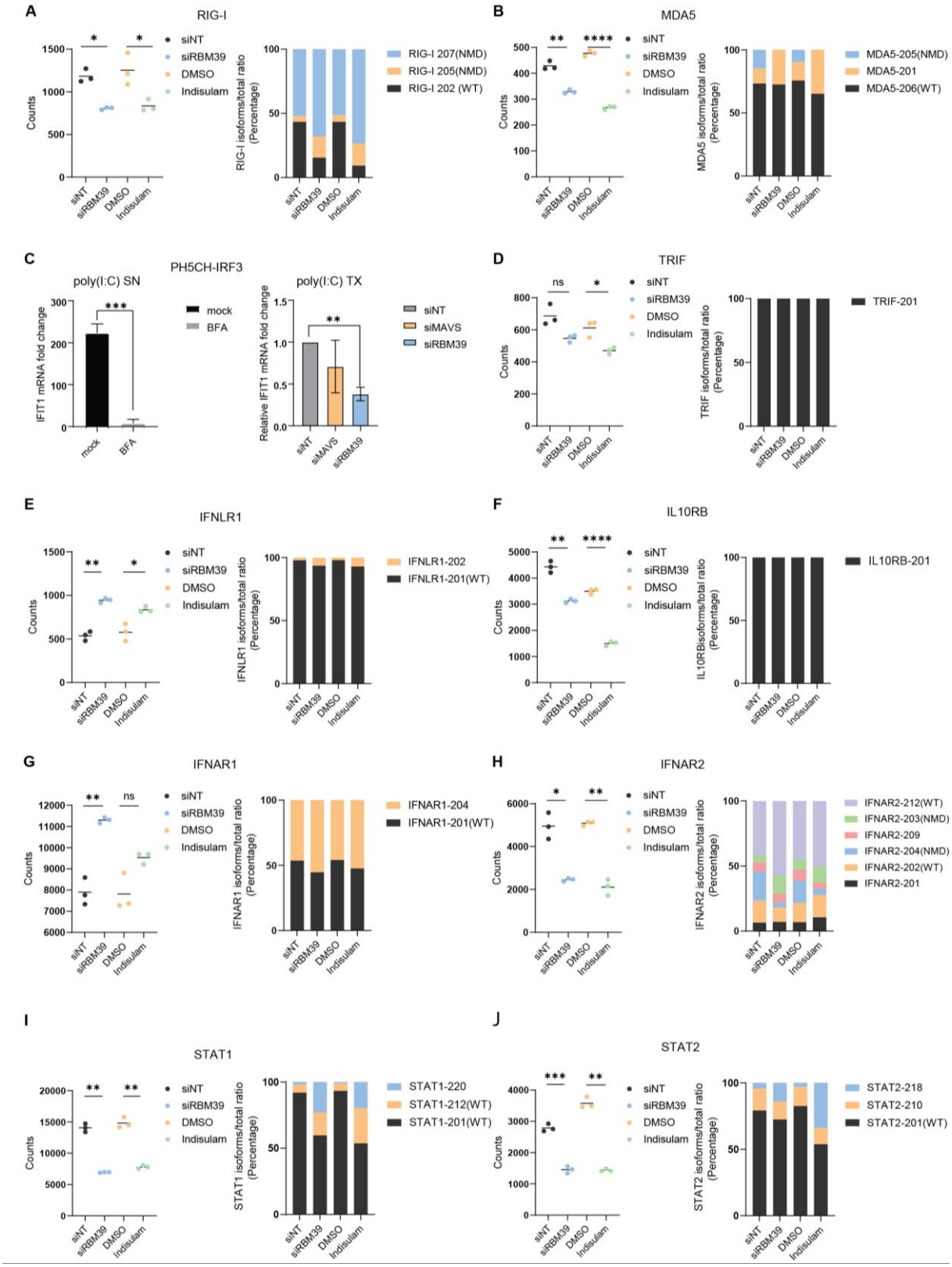

Figure 31. Other innate immune factors in the transcriptomic and alternative splicing analysis. (A to B and D to J) DEG analysis (left) and DTU analysis (right) of siRBM39 or Indisulam-treated PH5CH samples. (C) PH5CH-eIRF3 were transfected with the indicated siRNA for 48 h and treated with 10 nM

baflomycin for 45 min, subsequently cells were stimulated with 0.5µg/ml poly(I:C) by transfection. IFIT1 mRNA expression was measured by qPCR.

4.1.16 Mass spectrometry further confirms the RBM39 regulatory network

Next, to investigate the consequence of the transcriptomic and splicing regulation mediated by RBM39, I also performed mass spectrometry (MS), with the help of my collaborators Antonio Piras and Andreas Pichlmair from Munich, to analyze the global changes on the protein level in PH5CH cells upon knockdown of RBM39 or Indisulam treatment. In the bioinformatic analysis proteins with fold change >2 or < 0.5, p-value < 0.05 were considered as significant. In general, only 135 proteins showed significant change (76 upregulation, 59 downregulation) in siRBM39-treated samples compared to siNT control, while 255 proteins exhibited significant change (96 upregulation, 159 downregulation) in Indisulam-treated samples compared to the DMSO control. 33 proteins overlapped in both conditions, among them, 13 were up-regulated and 20 were decreased (Figure 32A and B). As the quality control, the protein levels of RBM39 in both RBM39 knockdown and Indisulam treatment conditions experienced a similar decrease of approximately 70% (Figure 32C), which proved the efficiency of our treatment. Paradoxically, the expression of IRF3 did not show significant difference (Figure 32D), which could be due to the limitation of the mass spectrometry to distinguish isoforms and/or the limited sensitivity of the approach, indicated by the low number of hits.

However, some key innate immune factors related to PRRs-mediated signaling were still found. A significant reduction of STAT2 was observed in both siRBM39 and Indisulam-treated samples compared to their respective controls (Figure 32E), which was consistent with the transcriptomic analysis (Figure 32J) and further provided robust evidence on protein level. Likewise, STAT1 protein expression also showed significant attenuation in both conditions (Figure 32F) but not as strong as what I observed at the mRNA level (Figure 32I). Interestingly, the protein level of RIG-I did not change in RBM39 knockdown samples but significantly reduced in Indisulam-treated samples, also partly in line with RNA seq data (Figure 32G).

Overall, the transcriptomic, splicing and proteomic analysis revealed that not only IRF3, but also other key innate immune factors, such as RIG-I, MDA5, STAT1 and STAT2, might contribute to the regulatory network of RBM39, and collaboratively contributing to cell intrinsic innate immune signaling. This highlights the role of RBM39 in immunity.

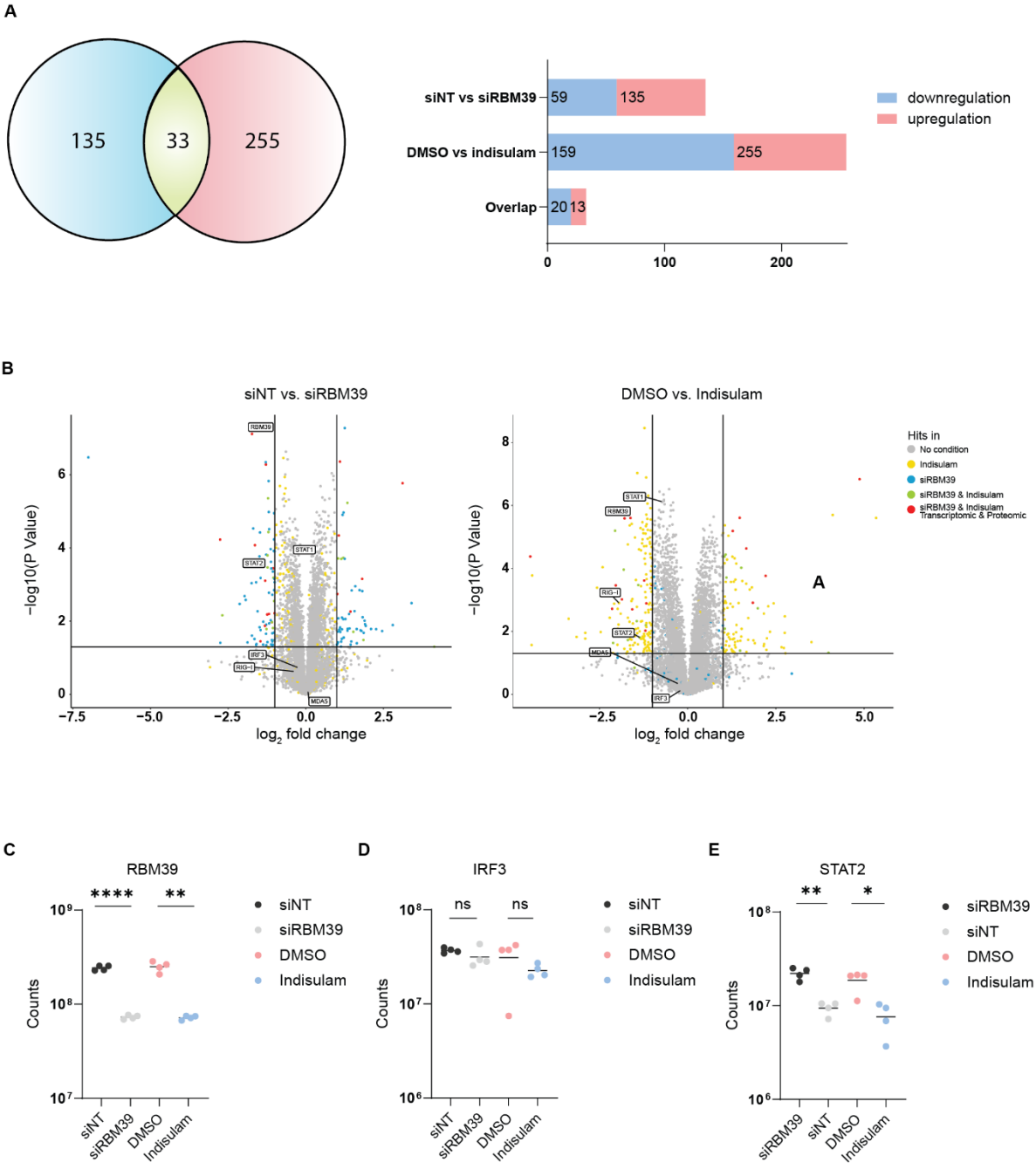
A
135
33
255
siNT vs siRBM39
DMSO vs indisulam
Overlap
59
135
159
255
20
13
0
100
200
downregulation
upregulation
B
siNT vs. siRBM39
DMSO vs. Indisulam
−log10(P Value)
log2 fold change
Hits in
No condition
Indisulam
siRBM39
siRBM39 & Indisulam
siRBM39 & Indisulam Transcriptomic & Proteomic
RBM39
STAT1
STAT2
IRF3
RIG-I
MDA5
A
C
RBM39
D
IRF3
E
STAT2
Counts
****
**
ns
*
siNT
siRBM39
DMSO
Indisulam

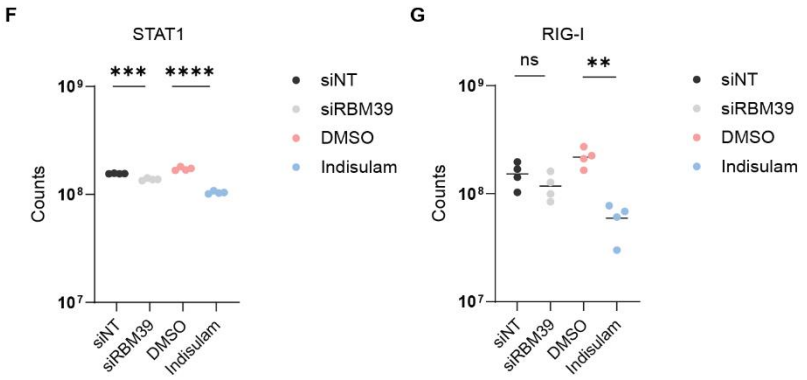

Figure 32. Proteomic analysis in RBM39-downregulated PH5CH cells. The mass spectrometry was performed in PH5CH treated with siRBM39 or 1µM Indisulam for 48 h. Raw data was analyzed by Perseus. (A) The overview of the proteomic analysis. Up-regulated and down-regulated proteins are shown. (B) Volcano plot of the proteome in siRBM39 vs siNT and Indisulam vs DMSO treated cells. Significantly changed proteins in siRBM39-treated samples are marked in blue, in Indisulam-treated samples in yellow and overlapping proteins are colored in green. (C-G) Protein expression of RBM39 (C), IRF3 (D), STAT2 (E), STAT1 (F) and RIG-I (G) in both conditions.

4.2 Functional study of TLR3 single nucleotide polymorphisms (SNPs)

4.2.1 TLR3 SNPs are potentially associated with infectious diseases

TLR3 is an important pattern recognition receptor (PRR) in innate immune sensing, and its impaired function is often associated with diseases, particularly infection-related diseases (*304*). In this project, I gathered all disease-related TLR3 SNPs identified so far, excluded the ones with synonymous mutations and nonsense mutations, and finally filtered 14 TLR3 SNPs for further analysis (Table 3). Our goal was to analyze the functional implications of these SNPs, with a particular focus on understanding the role of TLR3 in hepatocytes.

Table 3. List of the 14 TLR3 SNPs.

No	Rs number	Mutation	AA change	Related-disease reported
1	rs5743316	851 A>T	N284I	herpes simplex encephalitis (*305*)
2	rs35311343	889C>G	L297V	herpes simplex encephalitis (*226*)
3	rs768091235	1079T>C	L360P	herpes simplex encephalitis (*227*)
4	rs3775291	1234C>T	L412F	Japanese encephalitis (*231*) Zika virus microcephaly (*229*) influenza-associated pneumonia (*306*) chronic HCV (*307*) HCMV infection (*308*)
5	rs121434431	1660C>T	P554S	Influenza Pneumonia (*235*) herpes simplex encephalitis (*227*)
6	rs754289571	2227G>A	G743S	(G743D) in literature herpes simplex encephalitis (*227*)
7	rs746041651	2433A>T	R811S	(Arg811I) in literature herpes simplex encephalitis (*227*)
8	rs199768900	2600G>A	R867Q	herpes simplex encephalitis (*227*)
9	rs753482575	597A>T	L199F	Varicella-Zoster virus encephalitis (*225*)
10	NA	908T>C	F303S	Influenza encephalitis (*228*)
11	rs3775290	1377C>A	F459L	HBV and HCV infection (*309*) Chronic HCV (*236*)
12	NA	2039C>T	P680L	Influenza pneumonitis (*235*)

13	rs147431766	2224C>T	L742F	PUUV-hantavirus encephalitis (*310*)
14	NA	2608A>G	M870V	COVID-19 (*237*)

4.3 Poly(I:C) titration and time course of TLR mediated ISG induction in Huh7.5 cells

Huh7.5 is considered a clean cell model for investigating the TLR3 pathway, as it is immune-deficient and does not endogenously express RNA recognition PRRs like TLR3 and MDA5. At the same time, an intrinsic mutation in one RIG-I allele with dominant negative effect also renders this PRR unfunctional in this cell line (*291*). To validate the lack of innate immune response in Huh7.5 cells, I performed poly(I:C) titration stimulation in Huh 7.5 naïve cells and Huh 7.5 cells expressing TLR3 for 6 h. Poly(I:C) supernatant feeding specifically activates the TLR3 pathway, while poly(I:C) transfection triggers both the TLR3 and RIG-I/MDA5 pathways. Poly(I:C) supernatant feeding indeed basically did not induce IFIT1 mRNA expression in Huh7.5 naïve cells, although poly(I:C) transfection still induced IFIT1 mRNA expression, especially at high concentrations (Figure 33A), indicating a residual endogenous cytoplasmic PRR sensing. On the contrary, in Huh7.5 cells expressing wild-type (WT) TLR3, the IFIT1 mRNA induction was much stronger compared to naïve cells in both poly(I:C) supernatant feeding and transfection conditions (Figure 33B). In general, IFIT1 mRNA levels increased proportionally to the increase of poly(I:C) concentration. However, I also noticed that 100 µg/ml poly(I:C) for the supernatant feeding and 5 µg/ml poly(I:C) transfection were sufficient to achieve maximal induction levels; higher poly(I:C) concentration did not profoundly increase the IFIT1 production (Figure 33A and B). Therefore, these two conditions were applied for further experiments.

Next, I also performed the poly(I:C) stimulation experiments in the above mentioned two cell lines at different time points to determine the optimal condition for stimulation, considering the plan to express potential TLR3 loss of function mutants in this model. In Huh7.5 naïve cells, poly(I:C) supernatant feeding did not induce IFIT1 expression at any time point tested, whereas in case of poly(I:C) transfection IFIT1 mRNA induction became detectable at 12 h and the induction increased significantly at 24 h (Figure 33C). As expected, poly(I:C) stimulation triggered higher IFIT1 production in Huh7.5-TLR3 WT cells. The IFIT1 mRNA levels reached a

peak at 6 h for supernatant feeding and at 12 h for transfection (Figure 33D). As ISGs, RIG-I and MDA5 can also be induced by IFNs or PRR stimulation and thereby initiate an enhanced second round innate immune sensing. To check the possible interference of second round activation induced by IFNs, I also measured mRNA expression of IFNβ. In Huh7.5 naïve cells, I observed that poly(I:C) supernatant feeding marginally induced IFNβ after 12 h. In contrast, poly(I:C) transfection clearly induced IFNβ mRNA to a larger extend, becoming clearly detectable at 24 h (Figure 33E). Surprisingly, in Huh7.5 TLR3 WT cells IFNβ mRNA level did not significantly change upon poly(I:C) supernatant feeding while showing a strong increase already at 6 h after poly(I:C) transfection (Figure 33F). The absence of IFNβ expression in Huh7.5 naïve and Huh7.5 TLR3 WT cells upon poly(I:C) supernatant feeding excluded the involvement of a second round of innate immune response.

In conclusion, I decided to use 100 µg/ml and 5 µg/ml poly(I:C) for supernatant feeding and transfection, respectively, to achieve saturated stimulation, and to collect samples at 6 h to avoid innate immune response originating from the boosted endogenous TLR3, RIG-I and MDA5 expression.

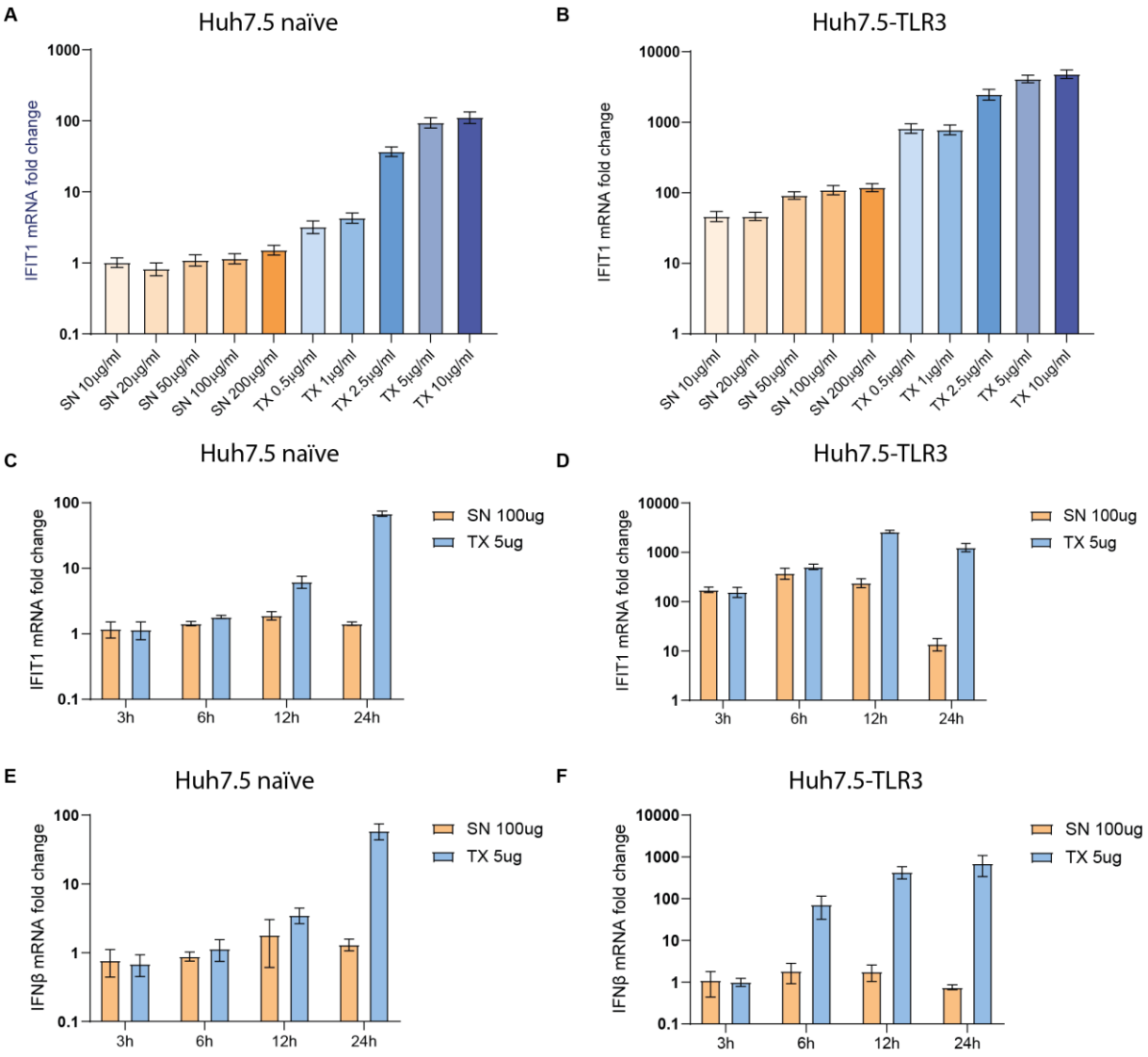

Figure 33. Poly(I:C) titration and time course of ISG induction in Huh7.5 cells. (A and B) The poly(I:C) titration experiment in Huh7.5 naïve cells (A) and Huh7.5 TLR3 WT cells (B) was analyzed at 6 h after supernatant feeding (SN) or transfection (TX) of the indicated amounts of poly(I:C). IFIT1 mRNA was measured by qPCR. (C to F) Kinetics of poly(I:C) stimulation in Huh7.5 naïve and Huh7.5 TLR3 WT cells. IFIT1 mRNA (C and D) and IFNβ mRNA were measured by qPCR. Fold change was normalized on GAPDH.

4.4 Investigation of endogenous PRR expression after stimulation in Huh7.5 cells

Given that TLR3, RIG-I and MDA5 as ISGs can be induced by first-round IFN activation and directly by stimulation of these PRRs, I performed poly(I:C) stimulation by using the abovementioned conditions, and measured mRNA and protein expression of TLR3, RIG-I and MDA5, to monitor the endogenous expression of TLR3, RIG-I and MDA5.

TLR3 mRNA expression increased around 4 folds after poly(I:C) stimulation at all time points in Huh7.5-TLR3 cells although the ectopic TLR3 expression was already high (Figure 34A). In contrast, the protein level of TLR3 upon poly(I:C) supernatant feeding or transfection was not significantly affected at all time points tested (Figure 34B), supporting a low background of endogenous TLR3 expression. However, from 3 h onwards, I observed an induction of RIG-I mRNA upon both poly(I:C) stimulation conditions. Similar to the IFIT1 mRNA expression, RIG-I mRNA levels peaked at 6 h upon the poly(I:C) supernatant feeding. However, in poly(I:C) transfected samples, it continuously increased, peaking at 12 h, and then decreased after 24 h (Figure 34C). The protein production slightly lagged behind the mRNA, with RIG-I protein expression observed after 6 h, peaking at 12 h upon the poly(I:C) supernatant feeding and at 24 h upon the poly(I:C) transfection, respectively (Figure 34D). MDA5 mRNA expression significantly increased from 6 h and peaked at 12 h for both poly(I:C) supernatant feeding and transfection (Figure 34E). Similarly, MDA5 protein expression exhibited a similar pattern, induced from 6 h and 12 h upon the poly(I:C) supernatant feeding and transfection, respectively, and reaching a peak at 12 h and 24 h, respectively (Figure 34F).

Taken together, despite Huh7.5 cells expressing low levels of TLR3, RIG-I and MDA5, in Huh7.5 cells expressing ectopic TLR3, activation of the TLR3 pathway can induce high levels of endogenous RIG-I and MDA5, especially at later time points, possibly interfering the TLR3-specific signaling.

Figure 13

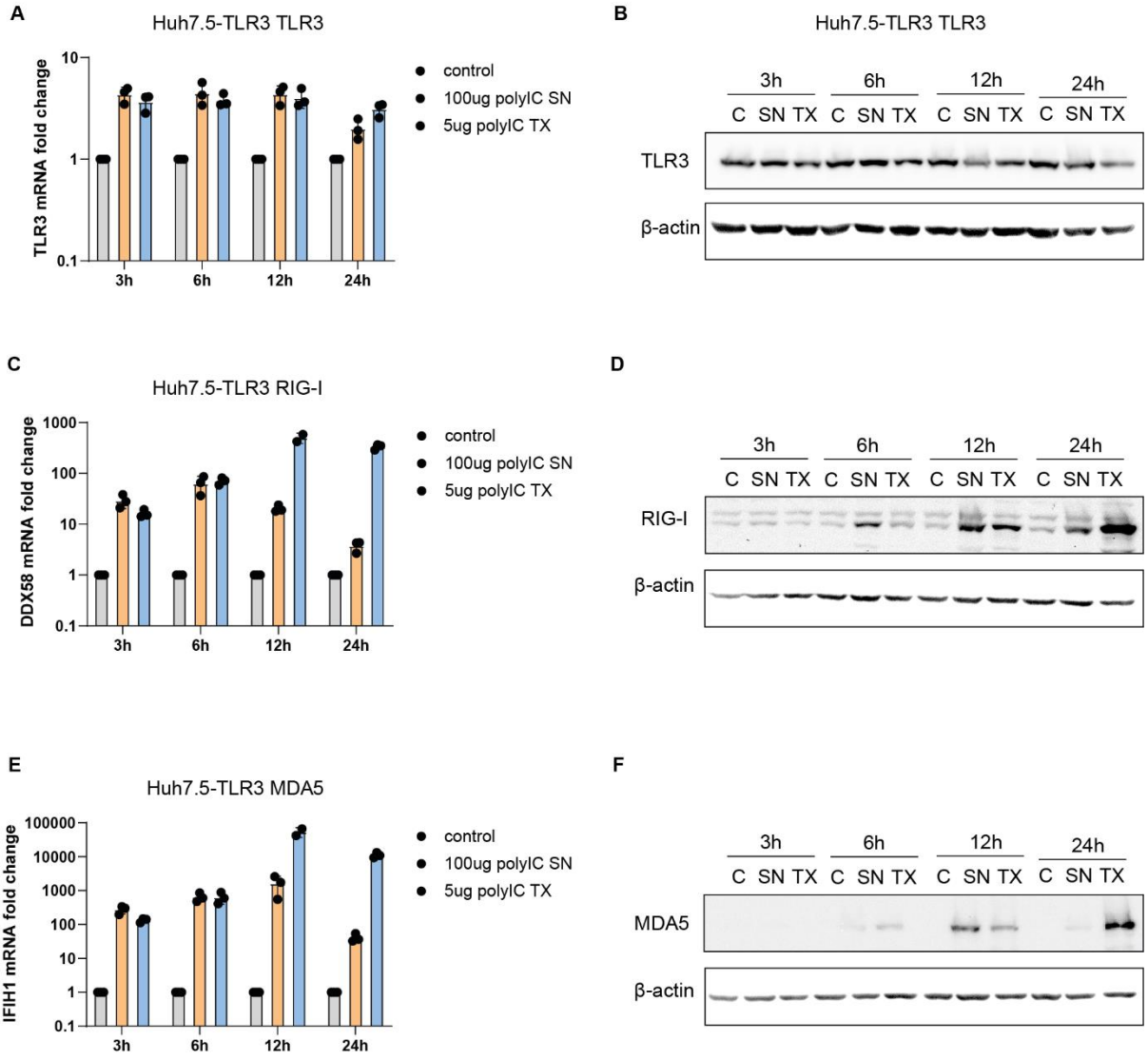

Figure 34. endogenous TLR3, RIG-I and MDA5 expression upon stimulation in Huh7.5-TLR3 cells. (A-F) Huh7.5-TLR3 cells were stimulated with poly(I:C) by supernatant feeding and transfection at indicated time points. TLR3 mRNA (A), RIG-I mRNA (C) and MDA5 mRNA were measured by RT-qPCR. TLR3 protein (B), RIG-I protein (D) and MDA5 protein (E) were assessed via western blot, respectively. Date are obtained from three replicates.

4.5 TLR3 SNPS have impaired function upon poly(I:C) stimulation

After determining the optimal conditions for poly(I:C) stimulation, I initiated the investigation of naturally occuring SNPs in TLR3 associated with diseases (Table 3). Initially, I expressed these TLR3 SNPs into Huh7.5 cells via lentiviral transduction individually. After antibiotic selection, stable Huh7.5 cell lines expressing TLR3 WT and SNPs were obtained. Western blot analysis confirmed the absence of TLR3 protein expression in Huh7.5 naïve cells, while TLR3 WT and SNPs proteins were comparable in their ectopic expression (Figure 35A). RT-qPCR

results further indicated the successful expression of TLR3 WT and SNPs in Huh7.5 cells (Figure 35B).

Subsequently, I performed poly(I:C) stimulation in Huh7.5 TLR3 SNPs cells at early time points to avoid the second round innate immune activation by IFNs and endogenous RIG-I/MDA5 expression. After 6 h stimulation, IFIT1 mRNA was strongly induced in most cell lines; However, IFIT1 mRNA expression was strongly impaired in Huh7.5 cells expressing TLR3 SNPs L360P, P680L, L742F, G743S, R811S, R867Q and M870, compared with Huh7.5-TLR3 WT cells. Especially in Huh7.5-TLR3 L360P cells, the IFIT1 mRNA production was almost completely blocked (Figure 35C). Importantly, I compared IFIT1 inductionat low and at saturating poly(I:C) concentrations, but the pattern did not show significant differences, indicating that minor differences in TLR3 SNPs expression did not significantly affect the TLR3 pathway activation. To reveal whether these SNPs showed the same differences in inducing NF-κB specific inflamatory cytokines, I also measured TNFα expression upon the activation of TLR3 pathway in these cells. Similary, I observed a reduction of TNFα mRNA expression in Huh7.5-TLR3 L360P, P680L, L742F, G743S, R811S, R867Q and M870V cells, but not in case of the other mutants (Figure 35D).

Overall, this experiment demonstrated that most of the TLR3 SNPs exhited impaired function in trigerring innate immune signaling. Further analyses will be required to investigate the role of these SNPs during virus infection in hepatocytes and the underlying mechnisms.

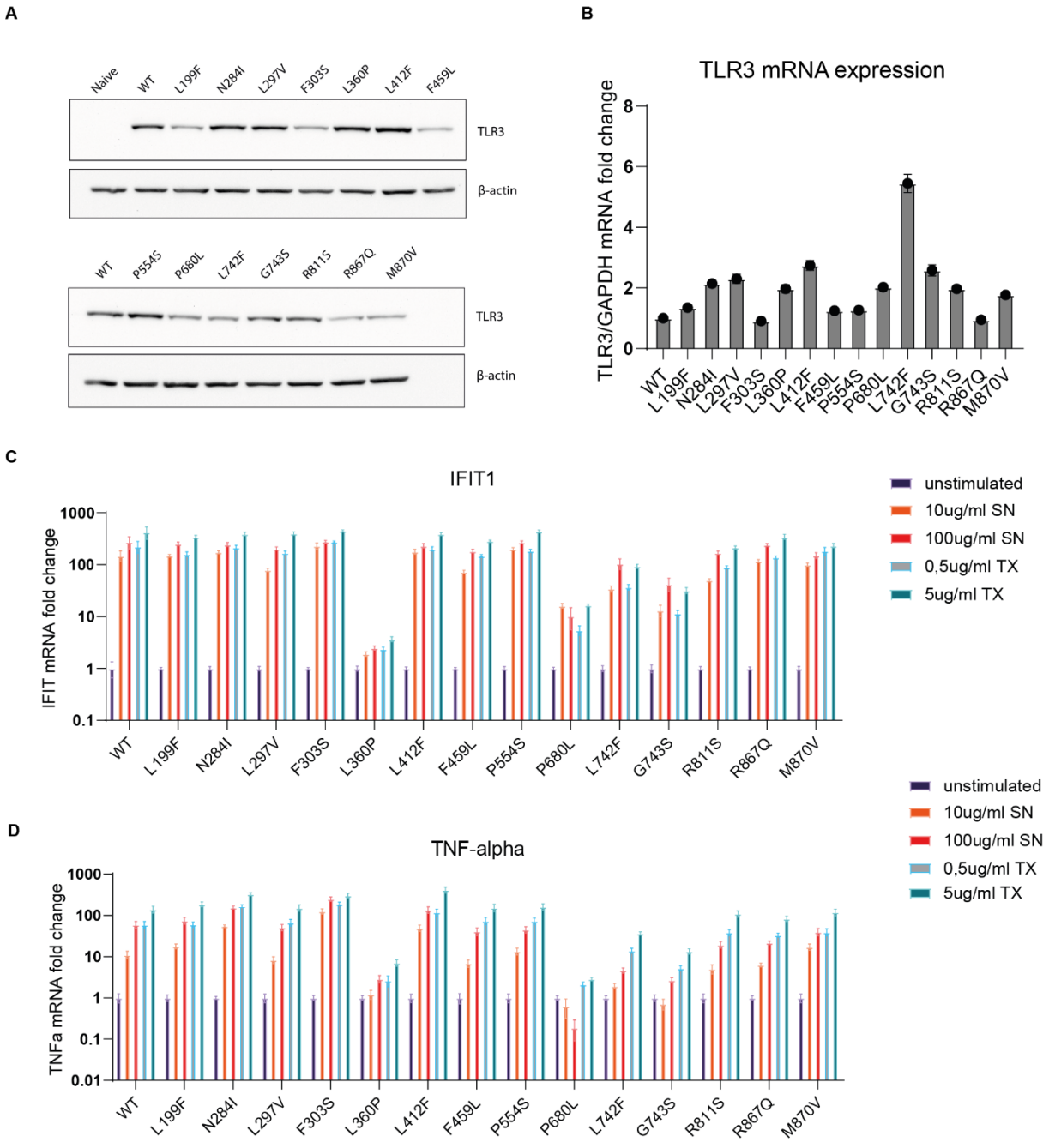

Figure 35. Functional validation of TLR3 SNPs. (A) Huh7.5 cells were transduced with lentiviral vectors encoding the indicated TLR3 variants. Protein expression of TLR3 SNPs in Huh7.5 cells was measured by immunoblotting. (B) mRNA expression of TLR3 SNPs in Huh7.5 cells was measured by RT-qPCR. (C and D) Huh7.5 cells with WT or TLR3 SNPs was stimulated with poly(I:C) supernatant feeding or transfection at indicated concentrations for 6 h. IFIT1 mRNA (C) and TNF-α mRNA (D) were measured by RT-qPCR. Data were normalized to siNT control. One experiment was presented.

5 Discussion:

The first part of my thesis was focusing on the identification of TLR3-related innate immune factors in hepatocytes. To achieve that, a genome-wide CRISPR/Cas9 screen was performed by my previous colleagues, Jannik Traut and Oliver Grünvogel (Detailed information can be found in Jannik Traut's Master's thesis).

CRISPR/Cas9 is widely used as a powerful tool for genome-wide screening to identify innate immune factors. While previous studies have predominantly focused on immune cells such as dendritic cells (*311*) and macrophages (*312*), research in hepatocytes is relatively limited. In this particular study, the CRISPR/Cas9 screen was executed in two hepatocyte cell lines, Huh7-Lunet-TLR3 cells and PH5CH cells, providing insight into innate immune regulation in the liver.

Following the screening, a comprehensive large-scale siRNA validation was carried out by my colleagues, Santa Mariela Olivera Ugarte and Arthur Lang (details are described in Arthur Lang's MD thesis). This validation ultimately led to the identification of Protein tyrosine phosphatase receptor type T (PTPRT), (Lysine demethylase 2A(KDM2A) and RNA binding motif protein 39 (RBM39) as promising candidates.

5.1 PTPRT

PTPRT, as a tyrosine phosphatase, has been described to dephosphorylate signal transducer and activator of transcription 3 (STAT3), leading to the attenuation of the STAT3 pathway activation (*261*). This function is linked to the inhibition of tumorigenesis in colorectal cancer cells (*289*). In previous study, the knockdown of PTPRT demonstrated a suppressive effect on TLR3 signaling in two liver-based cell lines, Huh7-Lunet-TLR3 and PH5CH cells (Figure 12), suggesting a potential role in this pathway. However, previous study reported that PTRPT is primarily expressed in the brain and is involved in synapse formation (*263*). An earlier transcriptome analysis of hepatocytes in my lab also confirmed the absence of PTRPT expression in the liver. Consequently, I concluded that the observed phenotype was likely an off-target effect.

Considering the robust inhibitory effect of this knockdown on TLR3 activation, I conducted a knockdown using the off-targeting siRNA in both Huh7-Lunet-TLR3 and PH5CH cells. Subsequently, I performed RNA seq to identify the real target among the downregulated genes. Following this, a set of genes displaying reduced expression in the RNA-seq data was

individually validated with corresponding siRNAs. Unfortunately, none of these genes exhibited a similar inhibitory function on TLR3 activation (Figure 14), pointing towards the conclusion of an off-target effect.

5.2 KDM2A

Another candidate, KDM2A, is known to function as a histone demethylase, specially demethylating Lys36 of histone 3 (H3K36), and acts as a tumor suppressor (*264*). In my experiments, the knockdown of KDM2A by siRNA significantly reduced activation of the TLR3 pathway in both Huh7-Lunet-TLR3 and PH5CH cells (Figure 12). However, the attempts to rescue the phenotype through overexpression of KDM2A were unsuccessful (Figure 15A). A previous study identified an isoform of KDM2A, SF-KDM2A, lacking the N-terminal demethylation domain, which acts as a competitor to KDM2A and exhibits the function of KDM2A (*290*). However, overexpression of SF-KDM2A did not restore the knockdown phenotype either, suggesting the occurrence of an off-target event here as well (Figure 15C).

5.3 RBM39

RBM39 belongs to the arginine-serine rich RNA-binding protein family and has been reported as a co-activator of activating protein 1 (AP-1), estrogen receptor (ER) α and ERβ (*285*). Additionally, RBM39 function as a splicing factor, participating in alternative splicing (*272*). It contributes to multiple biological processes, including cell cycle control (*269*), cell metabolism (*287*), and tumorigenesis (*270*). However, the role of RBM39 in immunity is not well understood. A recent study reported that porcine RBM39, rather than human RBM39, inhibits the AP-1 pathway by dephosphorylating the key transcription factor, c-Jun, leading to reduced expression of IFNβ and several cytokines (*313*). This finding contrasts with my results, as the knockdown of RBM39 in my experiment significantly reduced the expression of IFNβ and ISGs, indicating its pro-immunity role (Figure 16). This discrepancy may indicate an intrinsic difference of RBM39 between porcine and human.

Fortunately, the overexpression of a siRNA-resistant RBM39 mutant restored the impaired innate immune response caused by RBM39 knockdown, confirming its on-target effect (Figure 16A). Therefore, I focused on this factor for further analysis.

5.4 Off-target effect of siRNA

As abovementioned, two of three candidates in the siRNA validation showed strong phenotype, but unfortunately, off-target effect were observed in these cases.

There are three potential reasons for off-target effect of siRNA: (1) Mis-assembly of siRNA into microRNA (miRNA) machinery: siRNA and miRNA are distinct but similar small regulatory RNAs. Proper siRNA function requires a perfect match between the 19 bp of siRNA and the target sequence, which leads to a cleavage on target and mRNA downregulation. In contrast, miRNA only needs only a 6 bp complementary sequence to inhibit the translation of or to degrade the target mRNA (*314*). When siRNA behaves like miRNA and is incorporated into miRNA machinery, it might not necessarily cause a reduction in its target at the mRNA level. This could explain the difficulty in identifying the real target of "siPTPRT" by RNA-seq. (2) Activation of innate immune response: in mammalian cells, double stranded RNA (dsRNA) longer than 23 bp can trigger a strong innate immune response, resulting in increased expression of hundreds of interferon-stimulated genes (ISGs), including interferons (IFNs), potentially interfering with the experimental readout (*315*). In this study, as the siRNA sequences used are less than 23 bp, and significant innate immune activation was not observed after the knockdown, this reason is ruled out. (3) Saturation of siRNA: since siRNA and miRNA use similar machinery for silencing or downregulation, a high concentration of siRNA could occupy the machinery of miRNA and disturb gene expression in a miRNA-like manner, leading to an off-target event (*316*).

Given these reasons, predicting the target of an off-target siRNA is challenging and requires more sophisticated techniques. The crosslinking, ligation and sequencing of hybrids (CLASH) method, which identify RNA-protein interactome between miRNA machinery and RNA targets, that has been previously described (*317*), could be optimized and adapted for siRNA target search in the future.

5.5 CRISPR/Cas9 knockout and stable knockdown of RBM39

For the purpose of facilitating further investigation into RBM39, I endeavored to perform a knockout of RBM39 in PH5CH cells using CRISPR/Cas9 (Figure 17). While the knockout did results in a reduction of RBM39 expression to some extent in the knockout cell pools (Figure 17 A-D), the single clones failed to grow and proliferate. As an alternative approach, I also designed shRNAs targeting RBM39 and introduced them into PH5CH cells via lentiviral

transduction, aiming to establish stable RBM39 knockdown cells (Figure 17E-G). Unfortunately, this method also proved unsuccessful, as the cells could not consistently maintain the knockdown phenotype upon passaging (Figure 18C). Previous reports have indicated the degradation of RBM39 inhibits cell proliferation in various cancer cells, such as gastric cancer cells (*318*) and leukemia cells (*279*). Another study demonstrated that the depletion of RBM39 arrests cells in the G1 phase by inhibiting the activation of cyclin-dependent kinases CDK4 and CDK6 (*319*). These findings collectively underscore the significance of RBM39 in the control of the cell cycle, rendering it challenging to establish stable RBM39 knockout cells or RBM39 knockdown cells.

5.6 RBM39 is involved in multiple pathways and not limited to hepatocytes

Due to the off-target effects observed in two other candidate genes and the challenges in establishing stable RBM39 knockout or knockdown cells, I redirected my focus towards a more in-depth investigation of RBM39 using siRNA transient siRNA knockdown in subsequent experiments. All stimulation experiments conducted so far involved poly(I:C) supernatant feeding, which selectively activates the TLR3 pathway without affecting other RNA sensors like RIG-I and MDA5. Endogenous TLR3 and MDA5 are expressed to a very low degree (Betz et al., unpublished data) and RIG-I is non-functional in Huh7.5 cells (*139*).To assess the specificity of RBM39, I examined the impact of RBM39 knockdown on the RIG-I and MDA5 pathways in Huh7.5 cells expressing ectopic RIG-I and MDA5, respectively (Figure 19A and B). A549 cells exhibit low expression of TLR3 but express high levels of RIG-I and MDA5 (*320, 321*). To investigate RBM39's role in endogenous RIG-I/MDA5 pathways, its function was assessed in A549 cells (Figure 19C). Upon poly(I:C) transfection to activate RIG-I and MDA5, all three cell types showed reduced IFIT1 mRNA expression upon RBM39 knockdown, suggesting the involvement of RIG-I/MDA5 pathway in RBM39-mediated regulation. In addition, I explored the role of RBM39 in TLR4 pathway and obtained similar results (Figure 19D). TLR4, unlike TLR3, RIG-I and MDA5, reacts to lipopolysaccharide (LPS), a bacterial component (*36*). The observed effect of RBM39 in the TLR4 pathway excludes its participation in RNA recognition, highlighting its non-specific role in various cell intrinsic innate immune pathways. Noticeably, the confirmation of RBM39's function in A549 cells, a human lung adenocarcinoma cell line (*322*), also suggesting its general involvement in different tissues and highlighting its role in different pathways.

Another study suggested that RBM39 can interact with a viral NF-κB homologue, v-Rel, and suppresses its transformation activity (*286*). However, whether RBM39 interacts with other human NF-κB members, such as p50 or p105, to inhibit the inflammatory cytokines, has not been investigated. In my study, I measured the expression of two NF-κB specific genes, TNF alpha induced protein 3 (TNFAIP3) and interleukin 6 (IL6), upon RBM39 silencing. I observed only minor effect on IL6 and no significant impact on TNFAIP3 expression (Figure 20A and B), implying that RBM39 does not play a regulatory role in the NF-κB pathway.

5.7 Type III IFN is regulated by RBM39

Type II IFN is expressed only in immune cells, such as natural killer cells, macrophages (*323*), thereby it will not be discussed in this study. However, type I and type III IFNs are present in the cell lines I used, including hepatocytes and lung epithelial cells (*324, 325*). By stimulating cells with type I (IFN2α) and type III IFNs (IFNλ1), I investigated the role of RMBM39 in the downstream IFN pathways. Surprisingly, I observed a strong inhibition of type III IFN pathway, but not of the type I IFN pathway upon RBM39 silencing (Figure 20C and D). While both pathways share most components and signaling, they differ in the usage of receptors. Type I IFN receptor is composed of IFNAR1 and IFNAR2 subunits, whereas type III IFN receptor comprises IFNLR1 and IL10RB (*118*). Consistent with the results, one receptor unit of type III IFN, IL10RB, showed a significant reduction upon RBM39 knockdown (Figure 20E), which could explain the attenuation of type III IFN activation. However, detecting type III IFN receptors at protein level is challenging due to the unavailability of commercial antibodies.

Stimulation by IFNs increases the expression of ISGs, including some PRRs, such as RIG-I and MDA5, which in turn enhance the ligand sensing, and interferon regulatory factors, such as IRF7, promoting the second-round production of IFNs and ISGs (*326*). To exclude the interference of second-round activation, I performed RBM39 knockdown and poly(I:C) stimulation in A549 IFNAR/IFNLR KO cells. In these cells, receptors of both type I and type III IFNs are knocked-out via CRISPR/Cas9, blocking the downstream IFN pathway and avoiding the second-round innate immune responses. In contrast, upstream IFNs production is not affected in these cells, and IFIT1 can be induced via IRF3 in an IFN-independent way (*294*). By measuring IFIT1 and IFNβ expression, I observed a reduction of innate immune response in these KO cells (Figure 20F). Interestingly, the decrease observed in A549 KO out cells is comparable to that in A549 WT cells (Figure 19C), indicating that the suppression of the type

III IFN pathway might not the major process regulated by RBM39, and upstream factors are also monitored by RBM39.

5.8 IRF3 regulation mediated by RBM39

To identify the upstream factors regulated by RBM39, I initially examined the phosphorylation of IRF3. IRF3 is a key transcription factor in cell intrinsic innate immune pathways. The phosphorylation and dimerization of IRF3 lead to the production of IFNs (*297*). In RBM39 knockdown PH5CH cells, IRF3 phosphorylation was reduced (Figure 21A), consistent with the attenuated innate immune responses (Figure 16 and 19). Interestingly, the RBM39 knockdown decreased the basal levels of IRF3 as well (Figure 21A). IRF3 is not an ISG, a previous RNA-seq data in my lab showed that its expression is not affected by poly(I:C) stimulation (Betz et al., unpublished data). Therefore, the basal IRF3 expression is mediated by RBM39, instead of downregulated IFNs.

To further confirm this, a sulfonamide, Indisulam, was utilized as alternative method of siRNA knockdown. Indisulam is widely used in the studies of RBM39 in cancer research (*279, 281, 282*). It functions as a molecular glue mediating the interaction between RBM39 and the E3 ligase DCAF15, resulting in the ubiquitination and proteasomal degradation of RBM39 (*283*). I tested the efficiency of Indisulam in several cell lines, including PH5CH cells, A549 cells, primary human hepatocytes (PHH), primary mouse hepatocytes (PMH) and HepG 56D. In PH5CH cells, A549 cells and PHH, RBM39 was effectively degraded by Indisulam in a dose-dependent manner, and the IRF3 levels correspondingly decreased, with relatively low toxicity at low concentration (Figure 21B, 22A-B). The innate immune response upon poly(I:C) stimulation in PH5CH cells and A549 cells was also significantly suppressed by Indisulam (Figure 23A and B), allowing me to alternatively downregulate RBM39 and make a comparative investigation on RBM39. Moreover, a mutation (G268V) in RBM39 was reported to provide resistance to Indisulam in a previous study (*302*). This mutation partly rescued IRF3 expression in PH5CH cells, confirming that IRF3 reduction is indeed mediated via RBM39 (Figure 21C). However, in PMH, RBM39 degradation and IRF3 reduction were not observed, but in lab adapted mouse hepatoma cell line, HepG 56D, significant RBM39 degradation was observed. Therefore, the lack of responsiveness to Indisulam of PMH probably due to low levels of DCAF15 in the mouse liver (*327*). This observation aligns with another in vivo study reporting that Indisulam had no effect on the mouse liver, lung and heart of humanized

chimeric mice but still degraded RBM39 in the mouse kidney and grafted human tumors (*282*). Further investigations on the innate immune function of RBM39 conducted in the mouse kidney or using this chimeric mouse model could be helpful for the better understanding of the role of RBM39 in vivo.

A previous study has reported that IRF3 is essential in establishing autoimmune encephalomyelitis in the central neuron system (*328*). Another study also showed that IRF3 is associated with T cell autoimmune disease (*329*). Therefore, the application of Indisulam as an innate immune inhibitor, particularly in suppression of IRF3, offers a potential treatment to autoimmune disorders. Moreover, this targeted protein degradation (TPD) can be modulated by proteolysis-targeting chimeras (PROTACs), in which E3 ligase binding domain is linked with a changeable target binding domain. These methods have gained increasing attention in the field of targeted therapies (*330*).

5.9 The role of RBM39 in authentic virus infection models

The abovementioned investigation has predominantly centered around poly(I:C) stimulation. However, whether RBM39 exhibits a similar phenotype during virus infection remained unclear. To this end, 5 viruses were used as stimuli to activate cell intrinsic innate immune pathways in RBM39-downregulated cells.

Sendai viral 5’ triphosphate RNA is known to be recognized by RIG-I, inducing robust innate immune responses (*174*). In this study, strong IFIT1 mRNA expression was observed in both PH5CH and A549 cells upon Sendai virus infection. Specifically, a notable suppression of innate immune response upon RBM39 knockdown was observed at 6 hours post infection in PH5CH cells and 24 hours in A549 cell (Figure 24A-D). Conversely, RBM39 knockdown significantly increased Sendai virus replication at 12 h in PH5CH cells and at 24 h in A549 cells (Figure 24B and D). MAVS was used as a positive control, given its role as the key adaptor protein of the RIG-I pathway (*163*). Interestingly, the IFIT1 mRNA inhibition in RBM39 knockdown cells was comparable to that in MAVS knockdown cells, underscoring the critical role of RBM39 in virus-induced innate immune response. However, either MAVS or RBM39 knockdown only slight boosted the virus replication, suggesting innate immunity may not be the most crucial restriction factor for Sendai virus replication.

RVFV has been reported to be specifically recognized by RIG-I (*295*). In this study, A549 cells were infected with RVFV virus after treatment of Indisulam or DMSO control. Following

transfection, a strong innate immune response was observed in A549 cells (Figure 16E). The effect of Indisulam mirrored that of siRNA knockdown, reducing the innate activation of A549 cells and marginally increasing virus replication, although the increase was not statistically significant (Figure 16E), probably due to the inhibitory effect of NSs to type I IFNs (*186*).

HEV genomic RNA is a potent innate immune agonist; a previous study has ruled out the role of RIG-I, MDA5 and TLR3 in the recognition of HEV and indicated that the single stranded genomic RNA is sufficient to trigger the interferon response (*200*). However, the specific PRR responsible for this recognition remains unknown. In this study, the innate immune induction upon HEV in HepG2/C3A is robust (Figure 24F). The depletion of RBM39 by Indisulam significantly inhibited the innate immune responses induced by HEV but did not enhance the virus replication (Figure 24F), possibly explained by its resistance to IFNs (*331*).

HDV is recognized by MDA5, triggering strong innate response in HepG2-NTCP cells, with LGP2 being required for this recognition (*192*). Similar to the RVFV experiments, HepG2-NTCP cells were treated with Indisulam or DMSO control and then infected with HDV virus. RBM39 degradation suppressed the IFIT1 mRNA expression induced by HDV and enhanced the virus replication slightly and statistically significant (Figure 24G). This result is also in line with a previous finding that HDV replication is not significantly reduced after IFNs treatment (*192*),

It is noteworthy that the measurement of the IFIT1 and virus mRNA in HEV and HDV infection experiments were conducted 5 days post-infection; the phenotype at earlier time point may differ and requires further investigation.

While MDA5 and LGP2 have reported as key RNA sensors that initiate the antiviral innate immunity during SARS-CoV-2 infection (*222*), the role of RIG-I in SARS-CoV-2 sensing is still controversial (*222, 223*). In addition, inborn errors with TLR3 mutation have been linked to severe infection of SARS-CoV-2 (*237*), but whether TLR3 is responsible for the sensing remains unclear. Previous study has shown that the expression of several cytokines, including IFNβ, is boosted in patients with COVID-19 (*332*). However, in this study, SARS-CoV-2 infection in A549 cells did not induce an innate immune response at all (Figure 25A). This difference may due to distinct cell-types and strong innate immune evasion caused by various viral proteins (*224*). Interestingly, I observed a dramatic decrease of SARS-CoV-2 subgenomic RNA replication upon RBM39 knockdown (Figure 25B) or RBM39 degradation mediated by Indisulam (Figure 25D). This phenotype is obviously not dependent on innate immunity since its activation was

described to be blocked by various viral proteins (*296*). As VSV pseudovirus with SARS-CoV-2 spike protein showed a reduction in infection rate in RBM39 downregulated cells (Figure 25E and F), indicating that RBM39 could regulate key factors for virus entry. However, more experiments are still required to confirm this phenotype and the underlying mechanism needs further investigation.

In summary, the virus infection experiments have demonstrated that RBM39 is critical in establishing antiviral immune responses during several virus infections but not necessarily important for virus replication due to potential virus evasion mechanisms. One exception here is SAR-CoV-2, downregulation of RBM39 dramatically reduced its replication independent of innate immunity. However, the precise mechanism in this process remains unknown, and whether Indisulam can be applied as an antiviral drug after the establishment of SAR-CoV-2 infection has not been tested. Additionally, the function of RBM39 in immune cells and infection *in vivo* is also unclear and requires further investigation.

5.10 RBM39 regulates IRF3 at mRNA level

RBM39 primarily localizes in the nucleus, as confirmed by immunofluorescence (Figure 27A and B). IRF3, on the contrary, is expressed in the cytoplasm and translocated into the nucleus upon stimulation (*333*). Given the distinct subcellular localization of RBM39 and IRF3, it is unlikely that RBM39 regulates IRF3 through a protein-protein interaction. To validate this, ectopic IRF3 was expressed in PH5CH IRF3 KO cells. This ectopic IRF3, containing only the CDS of IRF3, allowed an investigation into the interaction between IRF3 and RBM39 at protein level. The result showed that, in PH5CH cells expressing ectopic IRF3, RBM39 had no effect on the expression of IRF3 (Figure 27C), excluding the possibility of a regulation at protein levels.

This observation prompted an exploration of the potential regulatory function of RBM39 at mRNA level. Indeed, in RBM39-silenced PH5CH cells, the mRNA expression of IRF3 exhibited a mild but significant reduction (Figure 28A). Considering RBM39 function as a coactivator of AP-1, ERα and ERβ (*285*), further investigation was conducted to determine whether RBM39 also function as a coactivator of IRF3. Luciferase assays were performed using two IRF3-promoter-based luciferase reporters: a longer reporter containing the full-length IRF3 promoter sequence and a shorter one with only the minimum IRF3 base pairs required for IRF3 promoter function. Two promoter sequences have been reported and validated in a previous study (*298*). Although the reduction was modest, the RBM39 knockdown resulted in

decrease luciferase activity of IRF3 promoters (Figure 28C), suggesting a potential regulation on IRF3 mRNA transcription by RBM39. However, as mentioned earlier, both IRF3 mRNA and the IRF3 promoter activity were only mildly influenced by RBM39 compared to the protein level. Therefore, additional mechanisms, like transcription and post-transcription modification, must be considered.

5.11 RBM39 regulates IRF3 splicing

As mentioned earlier, RBM39 primarily localizes in the nucleus, and in a previous study using crosslinking and immunoprecipitation (CLIP) assay demonstrated an interaction between IRF3 mRNA and RBM39 (*279*). I hypothesized that RBM39, as an RNA-binding protein, might bind to IRF3 mRNA and facilitate its export from the nucleus. To investigate this, I isolated the cytoplasm and nucleus fractions, and measured the expression of IRF3 mRNA in each fraction with or without RBM39 degradation. However, I observed that the expression of IRF3 mRNA in cytoplasm and nucleus remained unchanged upon RBM39 degradation (Figure 28D and E), ruling out my hypothesis of RBM39 being involved in mRNA export.

Given that RBM39 is a splicing factor that interacts with the spliceosome and collectively participates in alternative splicing processes (*272*). It is plausible that RBM39 may influence the splicing of IRF3. To explore the possibility, I firstly detected IRF3 isoforms in RBM39 knockdown cells via RT-PCR using specific primers targeting the exon1 and exon 8 of IRF3 (Figure 29A). While different expression patterns of IRF3 isoforms were observed upon RBM39 knockdown, these patterns were not reproducible and varied depending on the template concentration and PCR cycles. As the full-length IRF3 band was not detected in the siNT control, but appeared in RBM39 knockdown samples, I concluded that this result could be artificial, possibly caused by sample contamination or degradation. Alternatively, I also designed RNA probe that targets the exon shared by all IRF3 isoforms, exon 8, and perform northern blot to identify the splicing events of IRF3. Unfortunately, only the full-length IRF3 was observed (Figure 29B), probably due to the low abundance of other isoforms or the instability the RNA samples.

Considering the limitations of RT-PCR and northern blot, a more sensitive and stable method, RNA-sequencing, was employed. PH5CH cell was either silenced with siRBM39 or treated with Indisulam to abrogate RBM39. The reference gene GAPDH mRNA did not show significant changes in both treatments (Figure 29C), while RBM39 mRNA in RBM39 knockdown samples

exhibited a significant decrease (Figure 29D), confirming the reliability of the experiment. Surprisingly, RBM39 mRNA in Indisulam-treated samples showed a dramatic increase (Figure 29D), which is inconsistent with the expected function of Indisulam as a degrader. This unexpected increase in RBM39 mRNA in response to Indisulam treatment might hint at a self-regulation mechanism of RBM39. According to this hypothesis, Indisulam degrades RBM39 protein, triggering the alternative splicing of anther unknown factor that in turn increases the transcription of RBM39 mRNA. In contrast, in siRNA treated samples, RNA interference constantly degrades RBM39 mRNA, preventing the self-regulatory function of RBM39.

Subsequently, I focused on IRF3 isoforms. Several IRF3 isoforms have already been reported and investigated in vitro (*303, 334, 335*). In this study, five major IRF3 isoforms were identified, including IRF3-203, IRF3-228, IRF3-222, IRF3-202, IRF3-219 (Figure 29F and G). Among these, IRF3-203 is the major isoform and the only functional isoform, composed of 8 exons. IRF3-228 shared a similar structure with IRF3-203 but featured an additional 16 bp in exon 7, leading to a frame shift and encoding an extended C-terminus. This elongation renders IRF3-228 inhibitory, as it competes with IRF3-203 in innate signaling (*303*). IRF3-228 is the second abundant isoform in PH5CH cells, the 16 bp difference might also explain why it is challenging to separate IRF3 isoforms in gels in RT-PCR and northern blot experiments. On the contrary, IRF3-222 lacks exon 1 and 2, whereas IRF3-202 only lacks exon 1; both encode a short, non-functional isoform. IRF3-219 exhibited intron 1 retention and contains part of intron 6. According to Ensembl (www.ensembl.org), a genome browser predict transcripts, this mRNA harbors a premature termination codon (PTC), triggering its degradation via non-sense mediated decay (NMD).

The RNA-seq data revealed a decrease in the ratio of IRF3-203 to total IRF3 mRNA (Figure 29F) and a reduction in the absolute IRF3-203 RNA reads (Figure 29G), while other isoforms, including IRF3-228, IRF3-202, and IRF3-219, exhibited an opposite trend upon RBM39 knockdown and RBM39 degradation. Consistency between the two treatments prove the effectiveness of the method. Additionally, qPCR validation using specific primers targets for each isoform confirmed a similar pattern of isoform switches (Figure 29H and I).

In conclusion, downregulation of RBM39 altered the splicing of IRF3 mRNA, shifting from the IRF3-203 isoform to other non-functional isoforms. Notably, IRF3-228 emerged as a

suppressor of IRF3-203, and the increase of IRF3-219, an instable isoform undergoing NMD, probably contributing to the transcriptional decrease of IRF3 mRNA (Figure 28A-C).

5.12 RNA seq analysis identified other factors that regulated by RBM39

Genome-wide transcriptome and alternative splicing in breast cancer cell line, leukemia cell lines have already been described in previous studies (*279, 336*). In this study, a comprehensive analysis of the transcriptome and alternative splicing was conducted in an innate immune-competent hepatocyte, PH5CH cells, providing novel insights into splicing regulation in liver cells with the focus primarily on innate immune factors. Another two RNA sensors, RIG-I and MDA5, were identified as different expression genes (DEGs). Transcriptome analysis revealed a significant reduction in RIG-I and MDA5 mRNA levels in RBM39-downregulated PH5CH cells (Figure 31A and B). Alternative splicing further identified different transcript usages (DTUs) of RIG-I, with a substantial decrease in the functional RIG-I-202 isoform and an increase in other isoforms, including RIG-I-207 and RIG-205 (Figure 31A). In contrast, MDA5 exhibited only transcriptional changes (Figure 31B).

As most experiments in this study were based on TLR3 activation with poly(I:C) supernatant feeding, these phenotypes were not identified previously. To validate the specific regulation of RBM39 in RIG-I and MDA5, a TLR3 inhibitor, Bafilomycin A1, was used. Bafilomycin A1 blocks the acidification of the endosome, inhibiting endosomal TLR signaling (*292*). Previous experiment has shown that the overexpression of IRF3 was able to rescue the TLR3 inhibition mediated by RBM39 knockdown in PH5CH cells (Figure 27D), suggesting IRF3 is the key factor affected by RBM39 in TLR3 signaling. To prove that RIG-I and MDA5 is regulated by RBM39, I pre-treated the PH5CH-eIRF3 cells with bafilomycin A1 to block TLR3 activation and measured the innate immune responses specifically induced by RIG-I and MDA5. Interestingly, the inhibition induced by RBM39 knockdown was not restored by overexpression of IRF3 (Figure 31C), further implying the involvement of RIG-I and MDA5.

In previous experiments, RBM39 was also observed to specifically affect type III IFN pathway but not type I IFN pathway, and the decrease of type III IFN receptor subunit, IL10RB could contributed to this effect (Figure 20B-E). The RNA-seq data further confirmed this hypothesis, showing an increase in IFNLR1 and a reduction of IL10RB (Figure 31F). However, intriguingly, the transcriptomic analysis revealed a significant upregulation of type I IFN receptor subunit, IFNAR2, along with an increase in IFNAR1 (Figure 31G and H). Moreover, STAT1 and STAT2

were also downregulated at the RNA level, with STAT1 specially undergoing alternative splicing (Figure 31I and J).

These evidences suggest that type I IFN pathway may also be monitored by RBM39, since type I IFN pathway utilizes IFNAR1 and IFNAR2 as receptors and share downstream components like STAT1 and STAT2 with the type III IFN pathway to activate the JAK-STAT pathway (*118*). However, in my experiments, RBM39 did not show any effect on IFN2α-stimulated type I IFN pathway (Figure 20B). IFNβ has been reported to interact to IFNAR1 with high affinity, allowing a IFNAR2-indepent activation of type I IFN pathway (*129, 130*). This is might also be the case for IFNα. Additionally, the effect of STAT1 and STAT2 reduction might be compensated by the increase of IFNAR1. Further investigation is still required to clarify this aspect.

5.13 Proteome of RBM39-downregulated cells

In addition, to confirm the consequence on of these transcriptional and splicing changes mediated by RBM39, mass-spectrometry was conducted with the same conditions as RNA-seq in PH5CH cells. While transcriptomic analysis revealed the significant impact of RBM39 on thousands of genes, the proteomic analysis identified fewer proteins with significant changes, showing only hundreds of affected proteins, and with only 33 proteins overlapping between the two conditions (Figure 32A). The RBM39 protein levels showed significant decrease in two conditions, serving as a quality control (Figure 32C). Reduction of STAT1, STAT2 and RIG-I was observed (Figure 32E and G), consistent with the transcriptomic data (Figure 32I and J). However, certain membrane proteins of interest, including IFNAR1, IFNAR2, IFNLR1 and IL10RB were not detectable in the analysis, likely due to their low abundance and limited solubility (*337*). As mass spectrometry does not directly measure the entire protein sequence but rather peptides generated from proteins via enzymatic cleavage, the isoforms that share high similarity and lacks unique features are often challenging to distinguish (*338*). The failure of identifying IRF3 isoforms is a good example (Figure 32D). To identify isoforms, a targeted mass spectrometry such as selected reaction monitoring (SRM) is required, especially for the purpose of this study (*339*).

5.14 RBM39 domains and its function

RBM39 consists of a serine-arginine rich (SR) domain and three RNA-binding domains (RRMs), with the last RRM also known as the U2AF65 homologous motif (UHM) (*272*). The functions of different domains have been reported: amino acids 406-530 are responsible for binding

with ASC-2, potentially recruiting RRM domain-containing proteins, while residues 291-400 and 356-400 are involved in c-Jun and ER coactivator functions, respectively (*285*). The region spanning 1-291 interacts with v-Rel, inhibiting its transformation ability (*286*) , and a segment near the RS domain interacts with the tyrosine kinase c-Abl, leading to RBM39 phosphorylation and enhanced activity (*340*). However, the domain responsible for its innate immune function remains unknown. In this study, the role of the UHM was investigated and found not to be essential for RBM39's innate immune function (Figure 26). This region has also been reported as crucial for the interaction between RBM39 and other splicing factors, including U2AF65 (*272*). The lack of involvement of the UHM domain suggests that RBM39's splicing function may be partially independent of U2AF65. Further investigations into these domains are still required.

The second part of the thesis focuses on the functional validation of TLR3 single nucleotide polymorphisms (SNPs) in hepatocytes. This study searched all TLR3 SNPs has been reported until 2019, nonsense mutations and synonymous mutations are excluded (Table 3). Although these SNPs are associated with infectious diseases, their role in hepatocytes, particularly during infection, have not been investigated so far.

5.15 The cell intrinsic innate immune response in Huh7.5 cells

To investigate the function of TLR3 SNPs in hepatocytes in vitro, Huh7.5 cells were chosen as *in vitro* cell culture model. Huh7.5 cell line is a subclone of human hepatoma cell line Huh7 (*253*). As it lacks endogenous TLR3 and MDA5 expression, and expresses a mutated RIG-I with impaired function (*139, 291*), Huh7.5 is considered an immune-incompetent cell line. This characteristic allows for the specific investigation of the role of TLR3 SNPs by ectopically expressing them into the cell line.

In the initial experiments, the innate immune response was assessed at 6 hours in both Huh7.5 naïve cells and Huh7.5 cells expressing wild-type (WT) TLR3. In Huh7.5 naïve cells, the poly(I:C) supernatant feeding did not induce the expression of IFIT1 mRNA even at high concentrations. However, high concentrations of poy(I:C) transfection still triggered innate immune responses (Figure 33A). As MDA5 is an interferon stimulated gene (ISG), these phenotypes indicated that the endogenous MDA5 could be induced only upon poly(I:C) transfection in these cells and in turn facilitated the activation. In Huh7.5-TLR3-WT cells, the poly(I:C) stimulation showed saturation at 100 μg/ml and 5 μg/ml for supernatant feeding and transfection, respectively

(Figure 33B). In addition, a time-course experiment using saturating concentration of poly(I:C) in Huh7.5-TLR3-WT cells revealed a peak response at 6 hours for supernatant feeding and 12 hours for transfection (Figure 33C-F).

As the impact of endogenous of PRRs has not been determined, RIG-I, MDA5 and TLR3 mRNA expression were measured by quantitative PCR (qPCR). TLR3 expression did not significantly change upon stimulation but RIG-I and MDA5 mRNA were significantly increased even at an early time point (3 h) (Figure 34A, C and E). This was further confirmed at the protein level by western blot analysis, where TLR3 expression remained constant, while RIG-I and MDA5 showed an increase over time (Figure 34B, F and G). As RIG-I is mutated, it should not be involved in the signaling. However, endogenous MDA5 was highly expressed after 6 h, interfering the validation of TLR3 pathway. Considering these findings, the 6 hours timepoint was chosen for subsequent experiments to avoid the interference from endogenous MDA5-induce innate signaling.

5.16 TLR3 SNPs functional validation

After determining the experiment conditions, various TLR3 SNPs were expressed in Huh7.5 cells, and their innate immune functions were compared with those of TLR3 WT (Figure 35A and B). Among the 14 TLR3 SNPs, L360P, P680L, L742F, G743S, R811S, R867Q, M870V showed significant impairment in function (Figure 35C and D).

L360P and P680L are located at the ectodomain of TLR3. This horse-shoe shaped domain is composed of 23 leucine-rich (LRRs) and is responsible for the ligand binding and oligomerization (*341*). Cleavage of ectodomain was reported as an essential step for the signaling (*68*). The mutation L360P, near the cleavage site (323-356) of ectodomain, was reported as uncleaved and loss-of-function (*227*), which is line with the observed abrogation of IFIT1 mRNA and TNFα expression (Figure 35C and D). P680L was reported to be unable to dimerize and binds to dsRNA, and impaired in activating NF-κB in HEK293T cells (*342*), which is also consistent with the phenotype in this study (Figure 35C and D).

L742F and G743S are situated in the linker region bridging the transmembrane domain and Toll/interleukin-1 receptor (TIR) domain. The impaired function of L742 and G743S suggests the importance of this region for structural stability.

R811S, R867Q and M870V are located in the TIR domain, critical for recruiting TRIF and initiating downstream signaling. Previous reports showed that R811S and R867Q were partly impaired (*227*), aligning with this study. The mechanism of action for R811S, R867Q, M870V may involve interactions with TRIF.

Consistent with previous study that showed N284I and L412F was functional in P2.1 cells (*305*), in this study, N284 and L412F was not impaired (Figure 35C and D). It was also reported that PBMCs cell from patient carrying L297V mutation did not show lower responsiveness to poly(I:C) (*226*), this was also confirmed in hepatocyte in this study (Figure 35C and D). F303S was reported as loss-of-function in HEK293T cells (*228*) and P554S was loss-of-function in P2.1 cells (*235*). In contrary, impairment of function was not observed in this study (Figure 35C and D), probably indicating cell-type specific mechanism. In addition, L199F, found in Vricella-Zoster virus encephalitis patient (*225*) and F459L, associated with chronic HCV (*236*) have never been tested before and showed normal function in this study (Figure 35C and D).

Together, further details about the specific effects of these mutations on TLR3-mediated signaling and immune responses in hepatocytes would be critical for understanding their roles in the corresponding diseases and may provide insights into potential therapeutic strategies.

6 Abbreviation

PRR	Pattern recognition receptors
PAMP	Pathogen-associated molecular pattern
IFN	Interferon
ISG	Interferon-stimulated gene
TLR3	Toll-like receptor 3
PTPRT	Protein tyrosine phosphatase receptor type T
KDM2A	Lysine demethylase 2A
RBM39	RNA binding motif protein 39
poly(I:C)	Polyinosinic-polycytidylic acid
RNA seq	RNA sequencing
SNP	Single nucleotide polymorphism
NK cells	Natural killer cells
DCs	Dendritic cells
LPS	Lipopolysaccharide
TLRs	Toll-like receptors
CLRs	C-type lectin receptors
NLRs	Nucleotide binding oligomerization domain -like receptors
AIM2	Absent in melanoma 2
ALRs	Absent in melanoma 2 (AIM2)-like receptors
RIG-I	Retinoic acid-inducible gene
RLRs	Retinoic acid-inducible gene (RIG)-I-like receptors
LRR	Leucine-rich repeat
TIR	Toll/interleukin 1 (IL-1) receptor
ds	Double-stranded
ss	Single-stranded
CpG	Cytidine-phosphate-guanosine
pDCs	Plasmacytoid dendritic cells
HIV-1	Human immunodeficiency virus-1
gp41	Glycoprotein 41
TIRAP	TIR domain-containing adaptor protein
MyD88	Myeloid differentiation primary response protein 88
TRIF	TIRAP-inducing IFN-β
TRAM	TRIF-related adaptor molecule
SARM	Sterile-alpha and armadillo motif-containing protein
IRAK	IL-1 receptor-associated kinase
TNF	Tumor necrosis factor
TRAF6	Tumor necrosis factor (TNF) receptor-associated factor 6
TAK1	Transforming growth factor (TGF)-β-activated kinase 1
TAB	TAK1-binding protein
IKK	IκB kinase
MAPK	Mitogen-activated protein kinase

NF-κB	Nuclear factor k-light-chain-enhancer of activated B cells
NEMO	NF-κB essential modulator
CREB	Cyclic AMP-responsive element-binding protein
CRE	cAMP response elements
JNKs	c-Jun N-terminal kinases
ERK	Extracellular signal-regulated protein kinase
AP-1	Activating activator protein 1
RIP1	Recruiting receptor-interacting protein 1
UC93B1	Unc-93 homolog B1
ER	Endoplasmic reticulum
CTLDs	C-type lectin-like domains
ITAMs	Immunoreceptor tyrosine-based activation motifs
SYK	Spleen tyrosine kinase
CARD9	Complex containing caspase-recruitment domain protein 9
BCL-10	B cell lymphoma/leukaemia 10
MALT1	Mucosa-associated lymphoid tissue lymphoma translocation protein 1
MICL	Myeloid inhibitory C-type lectin
SHIP1	Src homology 2 (SH2) domain containing inositol polyphosphate 5-phosphatase 1
LRR	Leucin-rich repeat
CIITA	MHC-II transactivator
BIR	Baculoviral inhibition of apoptosis protein repeat
XIAP	X-linked inhibitor of apoptosis
ISGF3	Interferon stimulated gene factor 3
IFI	Interferon gamma inducible protein
MNDA	Myeloid cell nuclear differentiation antigen
HIN200	Hematopoietic interferon-inducible nuclear protein with 200-amino-acid repeats
STING	Interferon response Cyclic guanosine monophosphate–adenosine monophosphate (cGAMP) interactor
MDA5	Melanoma differentiation-associated protein
LGP2	Laboratory of genetics and physiology 2
CTD	Carboxy- terminal domain
CARDs	Caspase activation and recruitment domain
PPP	Triphosphate
TRIM25	Tripartite motif-containing protein 25
Riplet	RING-finger protein leading to RIG-I activation
MEX3C	Mex-3 RNA binding family member C
MAVS	Mitochondrial antiviral signaling protein
IKKε	Inhibitor of nuclear factor kappa-B kinase subunit epsilon

cGAS	cyclic guanosine monophosphate (GMP)-adenosine monophosphate (AMP) (cGAMP) synthase
PKR	Protein kinase R
eIF2	Eukaryotic initiation factor 2
IRF	Interferon regulatory factor
ISREs	IFN-stimulated response elements
IFIT1	Interferon-induced protein with tetratricopeptide repeats 1
MxA	Myxovirus resistance protein 1
CXCL10	Chemokine interferon-γ inducible protein 10 kDa
MEFs	Mouse embryonic fibroblasts
NDV	Newcastle disease virus
VSV	Vesicular stomatitis Virus
SeV	Sendai virus
JEV	Japanese encephalitis virus
WT	Wild-type
HEV	Hepatitis E virus
EMCV	Encephalomyocarditis virus
HAV	Hepatitis A virus
DENV	Dengue virus
WNV	West Nile virus
CVB3	Coxsackievirus B subtype 3
HSV-1	Herpes simplex virus 1
IAV	Influenza A virus
PTV	Punta Toro virus
HCV	Hepatitis C virus
SARS-CoV-2	Severe acute respiratory syndrome coronavirus type 2
EV71	Enterovirus 71
FMDV	Foot-and-mouth disease virus
HN	Hemagglutinin neuraminidase
RVFV	Rift Valley fever virus
RdRp	RNA-dependent RNA polymerase
RIOK3	RIO kinase 3
HDV	Hepatitis D virus
HBV	Hepatitis B virus
HBSAg	Hepatitis B virus (HBV) surface antigen
NTCP	Sodium taurocholate co-transporting polypeptide
RNP	Ribonucleoprotein
ADAR1	Adenosine deaminase acting on RNA 1
ORF	Open reading frames
NSP	Non-structural protein
HSE	Herpes simplex encephalitis
PBMCs	Peripheral blood mononuclear cells
CMV	Cytomegalovirus
CRISPR	Clustered regulatory interspaced short palindromic repeats
tracrRNA	Transactivating CRISPR RNA

DSB	Double strand break
HDR	Homology-directed repair
NHEJ	Nonhomologous end-joining
Indels	Insertions or deletions
tBID	Truncated BH3 Interacting domain death agonist
BAX	B-Cell CLL/Lymphoma 2 (BCL2) Associated X
BAK	BCL2 Antagonist/Killer 1
APAF-1	Apoptotic protease activating factor 1
PCF11	Cleavage and polyadenylation factor II subunit
STAT3	Signal transducer and activator of transcription 3
H3K36	Demethylating lysine 36 of histone 3
HCC1	Hepatocellular carcinoma 1
ERs	Estrogen receptors
RBP	RNA binding protein
RRM	RNA recognition motifs
UHM	U2AF homology motif
ULM	UHM-ligand motif
PTCs	Premature termination codons
NMD	Nonsense-mediated mRNA decay
DCAF15	DDB1 and CUL4 associated factor 15
PCR	Polymerase chain reaction
LB	Lysogeny Broth
PEI	Polyethylenimine
CIP	Calf-intestinal alkaline phosphatase
BafA	Bafilomycin A1
GAPDH	Glycerinaldehyd-3-phosphat-Dehydrogenase
HMBS	Hydroxymethylbilane synthase
GYG2	Glycogenin 2
LRRC2	Leucine rich repeat containing 2
PTGS1	Prostaglandin-endoperoxide synthase 1
AKAP7	A-Kinase Anchoring Protein 7
LOXL4	Lysyl oxidase like 4
SLC16A9	Solute carrier family 16 member 9
KRCC1	Lysine rich coiled-coil 1
COL3A1	Collagen type iii alpha 1 chain
SCNN1A	Sodium channel epithelial 1 subunit alpha
UTR	Untranslated region
RNAi	RNA interference
KDM2A-SF	KDM2A short form
ELISA	Enzyme-Linked Immunosorbent Assay
KO	Knock out
TNFAIP3	TNF alpha induced protein 3
IL6	interleukin 6
IFNAR	Interferon alpha and beta receptor subunit
IFNL1	Interferon lambda receptor
IL10RB	Interleukin 10 receptor subunit bet
p-IRF3	phosphorylated IRF3

MS	Mass spectrometry
miRNA	microRNA
PHH	Primary human hepatocytes
PMH	Primary mouse hepatocytes
CLIP	Crosslinking and immunoprecipitation
NMD	Non-sense mediated decay
DEGs	Different expression genes
DTUs	Different transcript usages
SRM	Selected reaction monitoring
SR	Serine-arginine rich

7 Acknowledgements

Firstly, I want to thank my mentor, Prof. Volker Lohmann, who gave me the opportunity to work and study under his supervision. His patience, calm and stability made the challenging PhD easier, his caution and hardworking also showed me the way to do science.

I would like to thank Dr. Frauke Müksch and Prof. Friedrich Frischknecht for being part of my defense examination committee. I further want to thank Prof. Ralf Bartenschlager for being my first examiner and also for his constructive comments and advices in Friday meetings and retreats of the department during these four years.

For the same reason, I would like to thank all PIs, students and postdocs in CIID who contributed to this work. And I specially thank my collaborators inside and outside, Nelson, Dr. Marco Binder, Vladimir, Dr. Viet Loan Dao Thi, Ann- Kathrin, Prof. Stephan Urban, Eva, Prof. Andreas Pichmair, Antonio, Dr. Dirk Wohlleber, Emely, Prof. Martina Muckenthaler, Ruiyue, Prof. Matthias Schlesner and Jeongbin Park.

I need to specially thank all colleagues in Lohmann lab including Ombretta, Cong Si, Hao-En (Helen), Paul, Rahel, Marit, Philipp, Lucija and former colleagues Arthur, Andreas, Oliver, Santa, Tomke, Noemi for providing a friendly atmosphere in the lab. Thanks to Paul for the bioinformatics analysis in this work. Thanks to Arthur, Oliver and Santa for building up the project. And especially thank to Ombretta and Cong Si not only for the support in the lab but also for encouragements during my difficult times. I also want to thank all technicians including Rahel, Uli, Marie for their contribution to lab organization and reagent ordering. Thanks to Fredy for IT support. Thanks Pilar and Dr. Sandra Bühler for paper works. Thanks all my friends for hearing my complaints about terrible foods and weather.

Last but not least, I would also need to thank my parents for always supporting my idea, including going abroad for study, even though they do not fully understand it.

8 Reference

1. J. Parkin, B. Cohen, An overview of the immune system. *Lancet* **357**, 1777-1789 (2001).
2. K. Buchmann, Evolution of Innate Immunity: Clues from Invertebrates via Fish to Mammals. *Front Immunol* **5**, 459 (2014).
3. N. A. Mitchison, T-cell-B-cell cooperation. *Nat Rev Immunol* **4**, 308-312 (2004).
4. L. W. Peterson, D. Artis, Intestinal epithelial cells: regulators of barrier function and immune homeostasis. *Nat Rev Immunol* **14**, 141-153 (2014).
5. T. A. Kufer, P. J. Sansonetti, NLR functions beyond pathogen recognition. *Nat Immunol* **12**, 121-128 (2011).
6. S. Akira, S. Uematsu, O. Takeuchi, Pathogen recognition and innate immunity. *Cell* **124**, 783-801 (2006).
7. M. Zasloff, Antimicrobial peptides of multicellular organisms. *Nature* **415**, 389-395 (2002).
8. V. M. Holers, Complement and its receptors: new insights into human disease. *Annu Rev Immunol* **32**, 433-459 (2014).
9. M. J. Holtzman, D. E. Byers, J. Alexander-Brett, X. Wang, The role of airway epithelial cells and innate immune cells in chronic respiratory disease. *Nat Rev Immunol* **14**, 686-698 (2014).
10. N. K. Bjorkstrom, B. Strunz, H. G. Ljunggren, Natural killer cells in antiviral immunity. *Nat Rev Immunol* **22**, 112-123 (2022).
11. J. S. Marshall, D. M. Jawdat, Mast cells in innate immunity. *J Allergy Clin Immunol* **114**, 21-27 (2004).
12. H. L. Twigg, 3rd, Macrophages in innate and acquired immunity. *Semin Respir Crit Care Med* **25**, 21-31 (2004).
13. J. Banchereau, R. M. Steinman, Dendritic cells and the control of immunity. *Nature* **392**, 245-252 (1998).
14. P. Parham, *The immune system*. (Garland Science, 2014).
15. A. E. Mayer, Wake Forest University, (2015).
16. K. Hoebe *et al.*, Upregulation of costimulatory molecules induced by lipopolysaccharide and double-stranded RNA occurs by Trif-dependent and Trif-independent pathways. *Nat Immunol* **4**, 1223-1229 (2003).
17. W. K. Ip, K. Takahashi, K. J. Moore, L. M. Stuart, R. A. Ezekowitz, Mannose-binding lectin enhances Toll-like receptors 2 and 6 signaling from the phagosome. *J Exp Med* **205**, 169-181 (2008).
18. Y. Olguin *et al.*, Detection of flagellin by interaction with human recombinant TLR5 immobilized in liposomes. *Anal Bioanal Chem* **405**, 1267-1281 (2013).
19. H. Hara *et al.*, The NLRP6 Inflammasome Recognizes Lipoteichoic Acid and Regulates Gram-Positive Pathogen Infection. *Cell* **175**, 1651-1664 e1614 (2018).
20. H. Hemmi *et al.*, A Toll-like receptor recognizes bacterial DNA. *Nature* **408**, 740-745 (2000).
21. U. Ohto *et al.*, Structural basis of CpG and inhibitory DNA recognition by Toll-like receptor 9. *Nature* **520**, 702-705 (2015).
22. S. S. Diebold, T. Kaisho, H. Hemmi, S. Akira, C. Reis e Sousa, Innate antiviral responses by means of TLR7-mediated recognition of single-stranded RNA. *Science* **303**, 1529-1531 (2004).
23. L. Alexopoulou, A. C. Holt, R. Medzhitov, R. A. Flavell, Recognition of double-stranded RNA and activation of NF-kappaB by Toll-like receptor 3. *Nature* **413**, 732-738 (2001).
24. A. Pichlmair *et al.*, RIG-I-mediated antiviral responses to single-stranded RNA bearing 5'-phosphates. *Science* **314**, 997-1001 (2006).
25. H. S. Goodridge *et al.*, Activation of the innate immune receptor Dectin-1 upon formation of a 'phagocytic synapse'. *Nature* **472**, 471-475 (2011).
26. X. He *et al.*, LYSMD3: A mammalian pattern recognition receptor for chitin. *Cell Rep* **36**, 109392 (2021).
27. O. Takeuchi, S. Akira, Pattern recognition receptors and inflammation. *Cell* **140**, 805-820 (2010).

28. B. Opitz, S. Hippenstiel, J. Eitel, N. Suttorp, Extra- and intracellular innate immune recognition in endothelial cells. *Thromb Haemost* **98**, 319-326 (2007).
29. J. Yang, H. Yan, Mucosal epithelial cells: the initial sentinels and responders controlling and regulating immune responses to viral infections. *Cell Mol Immunol* **18**, 1628-1630 (2021).
30. K. V. Anderson, G. Jurgens, C. Nusslein-Volhard, Establishment of dorsal-ventral polarity in the Drosophila embryo: genetic studies on the role of the Toll gene product. *Cell* **42**, 779-789 (1985).
31. B. Lemaitre, E. Nicolas, L. Michaut, J. M. Reichhart, J. A. Hoffmann, The dorsoventral regulatory gene cassette spatzle/Toll/cactus controls the potent antifungal response in Drosophila adults. *Cell* **86**, 973-983 (1996).
32. R. Medzhitov, P. Preston-Hurlburt, C. A. Janeway, Jr., A human homologue of the Drosophila Toll protein signals activation of adaptive immunity. *Nature* **388**, 394-397 (1997).
33. T. Duan, Y. Du, C. Xing, H. Y. Wang, R. F. Wang, Toll-Like Receptor Signaling and Its Role in Cell-Mediated Immunity. *Front Immunol* **13**, 812774 (2022).
34. M. S. Jin *et al.*, Crystal structure of the TLR1-TLR2 heterodimer induced by binding of a tri-acylated lipopeptide. *Cell* **130**, 1071-1082 (2007).
35. J. Y. Kang *et al.*, Recognition of lipopeptide patterns by Toll-like receptor 2-Toll-like receptor 6 heterodimer. *Immunity* **31**, 873-884 (2009).
36. B. S. Park *et al.*, The structural basis of lipopolysaccharide recognition by the TLR4-MD-2 complex. *Nature* **458**, 1191-1195 (2009).
37. F. Hayashi *et al.*, The innate immune response to bacterial flagellin is mediated by Toll-like receptor 5. *Nature* **410**, 1099-1103 (2001).
38. C. Y. Chen, H. Y. Liu, Y. P. Hsueh, TLR3 downregulates expression of schizophrenia gene Disc1 via MYD88 to control neuronal morphology. *EMBO Rep* **18**, 169-183 (2017).
39. C. Stoss *et al.*, TLR3 promotes hepatocyte proliferation after partial hepatectomy by stimulating uPA expression and the release of tissue-bound HGF. *FASEB J* **34**, 10387-10397 (2020).
40. F. Heil *et al.*, Species-specific recognition of single-stranded RNA via toll-like receptor 7 and 8. *Science* **303**, 1526-1529 (2004).
41. P. Ahmad-Nejad *et al.*, Bacterial CpG-DNA and lipopolysaccharides activate Toll-like receptors at distinct cellular compartments. *Eur J Immunol* **32**, 1958-1968 (2002).
42. B. M. Henrick *et al.*, TLR10 Senses HIV-1 Proteins and Significantly Enhances HIV-1 Infection. *Front Immunol* **10**, 482 (2019).
43. M. Oosting *et al.*, Human TLR10 is an anti-inflammatory pattern-recognition receptor. *Proc Natl Acad Sci U S A* **111**, E4478-4484 (2014).
44. T. Horng, G. M. Barton, R. Medzhitov, TIRAP: an adapter molecule in the Toll signaling pathway. *Nat Immunol* **2**, 835-841 (2001).
45. K. A. Fitzgerald *et al.*, Mal (MyD88-adapter-like) is required for Toll-like receptor-4 signal transduction. *Nature* **413**, 78-83 (2001).
46. S. C. Lin, Y. C. Lo, H. Wu, Helical assembly in the MyD88-IRAK4-IRAK2 complex in TLR/IL-1R signalling. *Nature* **465**, 885-890 (2010).
47. P. G. Motshwene *et al.*, An oligomeric signaling platform formed by the Toll-like receptor signal transducers MyD88 and IRAK-4. *J Biol Chem* **284**, 25404-25411 (2009).
48. K. S. Bonham *et al.*, A promiscuous lipid-binding protein diversifies the subcellular sites of toll-like receptor signal transduction. *Cell* **156**, 705-716 (2014).
49. M. Windheim, M. Stafford, M. Peggie, P. Cohen, Interleukin-1 (IL-1) induces the Lys63-linked polyubiquitination of IL-1 receptor-associated kinase 1 to facilitate NEMO binding and the activation of IkappaBalpha kinase. *Mol Cell Biol* **28**, 1783-1791 (2008).
50. L. Hu *et al.*, Oligomerization-primed coiled-coil domain interaction with Ubc13 confers processivity to TRAF6 ubiquitin ligase activity. *Nat Commun* **8**, 814 (2017).

51. B. Lamothe *et al.*, Site-specific Lys-63-linked tumor necrosis factor receptor-associated factor 6 auto-ubiquitination is a critical determinant of I kappa B kinase activation. *J Biol Chem* **282**, 4102-4112 (2007).
52. K. A. Fitzgerald *et al.*, IKKepsilon and TBK1 are essential components of the IRF3 signaling pathway. *Nat Immunol* **4**, 491-496 (2003).
53. M. C. Walsh, G. K. Kim, P. L. Maurizio, E. E. Molnar, Y. Choi, TRAF6 autoubiquitination-independent activation of the NFkappaB and MAPK pathways in response to IL-1 and RANKL. *PLoS One* **3**, e4064 (2008).
54. K. Clark, S. Nanda, P. Cohen, Molecular control of the NEMO family of ubiquitin-binding proteins. *Nat Rev Mol Cell Biol* **14**, 673-685 (2013).
55. N. Kanarek, N. London, O. Schueler-Furman, Y. Ben-Neriah, Ubiquitination and degradation of the inhibitors of NF-kappaB. *Cold Spring Harb Perspect Biol* **2**, a000166 (2010).
56. G. L. Johnson, R. Lapadat, Mitogen-activated protein kinase pathways mediated by ERK, JNK, and p38 protein kinases. *Science* **298**, 1911-1912 (2002).
57. K. Honda *et al.*, Spatiotemporal regulation of MyD88-IRF-7 signalling for robust type-I interferon induction. *Nature* **434**, 1035-1040 (2005).
58. K. Honda *et al.*, IRF-7 is the master regulator of type-I interferon-dependent immune responses. *Nature* **434**, 772-777 (2005).
59. A. Takaoka *et al.*, Integral role of IRF-5 in the gene induction programme activated by Toll-like receptors. *Nature* **434**, 243-249 (2005).
60. M. Yamamoto *et al.*, TRAM is specifically involved in the Toll-like receptor 4-mediated MyD88-independent signaling pathway. *Nat Immunol* **4**, 1144-1150 (2003).
61. A. M. Lundberg *et al.*, Toll-like receptor 3 and 4 signalling through the TRIF and TRAM adaptors in haematopoietic cells promotes atherosclerosis. *Cardiovasc Res* **99**, 364-373 (2013).
62. M. Yamamoto *et al.*, Role of adaptor TRIF in the MyD88-independent toll-like receptor signaling pathway. *Science* **301**, 640-643 (2003).
63. T. Kawasaki, T. Kawai, Toll-like receptor signaling pathways. *Front Immunol* **5**, 461 (2014).
64. S. M. McWhirter *et al.*, IFN-regulatory factor 3-dependent gene expression is defective in Tbk1-deficient mouse embryonic fibroblasts. *Proc Natl Acad Sci U S A* **101**, 233-238 (2004).
65. S. Sharma *et al.*, Triggering the interferon antiviral response through an IKK-related pathway. *Science* **300**, 1148-1151 (2003).
66. Y. M. Kim, M. M. Brinkmann, M. E. Paquet, H. L. Ploegh, UNC93B1 delivers nucleotide-sensing toll-like receptors to endolysosomes. *Nature* **452**, 234-238 (2008).
67. S. E. Ewald *et al.*, Nucleic acid recognition by Toll-like receptors is coupled to stepwise processing by cathepsins and asparagine endopeptidase. *J Exp Med* **208**, 643-651 (2011).
68. A. Garcia-Cattaneo *et al.*, Cleavage of Toll-like receptor 3 by cathepsins B and H is essential for signaling. *Proc Natl Acad Sci U S A* **109**, 9053-9058 (2012).
69. B. Park *et al.*, Proteolytic cleavage in an endolysosomal compartment is required for activation of Toll-like receptor 9. *Nat Immunol* **9**, 1407-1414 (2008).
70. G. D. Brown, J. A. Willment, L. Whitehead, C-type lectins in immunity and homeostasis. *Nat Rev Immunol* **18**, 374-389 (2018).
71. M. Bermejo-Jambrina *et al.*, C-Type Lectin Receptors in Antiviral Immunity and Viral Escape. *Front Immunol* **9**, 590 (2018).
72. S. Ye *et al.*, Dectin-1 Acts as a Non-Classical Receptor of Ang II to Induce Cardiac Remodeling. *Circ Res* **132**, 707-722 (2023).
73. M. J. Robinson *et al.*, Dectin-2 is a Syk-coupled pattern recognition receptor crucial for Th17 responses to fungal infection. *J Exp Med* **206**, 2037-2051 (2009).
74. P. Redelinghuys, G. D. Brown, Inhibitory C-type lectin receptors in myeloid cells. *Immunol Lett* **136**, 1-12 (2011).
75. L. Quatrini *et al.*, Ubiquitin-dependent endocytosis of NKG2D-DAP10 receptor complexes activates signaling and functions in human NK cells. *Sci Signal* **8**, ra108 (2015).

76. E. V. Koonin, L. Aravind, The NACHT family - a new group of predicted NTPases implicated in apoptosis and MHC transcription activation. *Trends Biochem Sci* **25**, 223-224 (2000).
77. K. Schroder, J. Tschopp, The inflammasomes. *Cell* **140**, 821-832 (2010).
78. J. P. Ting *et al.*, The NLR gene family: a standard nomenclature. *Immunity* **28**, 285-287 (2008).
79. B. Mach, V. Steimle, E. Martinez-Soria, W. Reith, Regulation of MHC class II genes: lessons from a disease. *Annu Rev Immunol* **14**, 301-331 (1996).
80. V. Steimle, L. A. Otten, M. Zufferey, B. Mach, Complementation cloning of an MHC class II transactivator mutated in hereditary MHC class II deficiency (or bare lymphocyte syndrome). *Cell* **75**, 135-146 (1993).
81. E. M. Kofoed, R. E. Vance, Innate immune recognition of bacterial ligands by NAIPs determines inflammasome specificity. *Nature* **477**, 592-595 (2011).
82. A. B. Molofsky *et al.*, Cytosolic recognition of flagellin by mouse macrophages restricts Legionella pneumophila infection. *J Exp Med* **203**, 1093-1104 (2006).
83. S. E. Girardin *et al.*, Nod1 detects a unique muropeptide from gram-negative bacterial peptidoglycan. *Science* **300**, 1584-1587 (2003).
84. S. E. Girardin *et al.*, Nod2 is a general sensor of peptidoglycan through muramyl dipeptide (MDP) detection. *J Biol Chem* **278**, 8869-8872 (2003).
85. V. Motta, F. Soares, T. Sun, D. J. Philpott, NOD-like receptors: versatile cytosolic sentinels. *Physiol Rev* **95**, 149-178 (2015).
86. K. Kobayashi *et al.*, RICK/Rip2/CARDIAK mediates signalling for receptors of the innate and adaptive immune systems. *Nature* **416**, 194-199 (2002).
87. M. J. Bertrand *et al.*, Cellular inhibitors of apoptosis cIAP1 and cIAP2 are required for innate immunity signaling by the pattern recognition receptors NOD1 and NOD2. *Immunity* **30**, 789-801 (2009).
88. R. B. Damgaard *et al.*, The ubiquitin ligase XIAP recruits LUBAC for NOD2 signaling in inflammation and innate immunity. *Mol Cell* **46**, 746-758 (2012).
89. A. Krieg *et al.*, XIAP mediates NOD signaling via interaction with RIP2. *Proc Natl Acad Sci U S A* **106**, 14524-14529 (2009).
90. N. Watanabe, H. Osada, Phosphorylation-dependent protein-protein interaction modules as potential molecular targets for cancer therapy. *Curr Drug Targets* **13**, 1654-1658 (2012).
91. A. Fontalba, O. Gutierrez, J. L. Fernandez-Luna, NLRP2, an inhibitor of the NF-kappaB pathway, is transcriptionally activated by NF-kappaB and exhibits a nonfunctional allelic variant. *J Immunol* **179**, 8519-8524 (2007).
92. K. L. DeYoung *et al.*, Cloning a novel member of the human interferon-inducible gene family associated with control of tumorigenicity in a model of human melanoma. *Oncogene* **15**, 453-457 (1997).
93. J. A. Trapani *et al.*, A novel gene constitutively expressed in human lymphoid cells is inducible with interferon-gamma in myeloid cells. *Immunogenetics* **36**, 369-376 (1992).
94. Y. Ding *et al.*, Antitumor activity of IFIX, a novel interferon-inducible HIN-200 gene, in breast cancer. *Oncogene* **23**, 4556-4566 (2004).
95. G. R. Burrus, J. A. Briggs, R. C. Briggs, Characterization of the human myeloid cell nuclear differentiation antigen: relationship to interferon-inducible proteins. *J Cell Biochem* **48**, 190-202 (1992).
96. M. Albrecht, D. Choubey, T. Lengauer, The HIN domain of IFI-200 proteins consists of two OB folds. *Biochem Biophys Res Commun* **327**, 679-687 (2005).
97. V. Hornung *et al.*, AIM2 recognizes cytosolic dsDNA and forms a caspase-1-activating inflammasome with ASC. *Nature* **458**, 514-518 (2009).
98. L. Unterholzner *et al.*, IFI16 is an innate immune sensor for intracellular DNA. *Nat Immunol* **11**, 997-1004 (2010).
99. E. E. Gray *et al.*, The AIM2-like Receptors Are Dispensable for the Interferon Response to Intracellular DNA. *Immunity* **45**, 255-266 (2016).

100. P. H. Wang *et al.*, Inhibition of AIM2 inflammasome activation by a novel transcript isoform of IFI16. *EMBO Rep* **19**, (2018).
101. M. Uhlen *et al.*, Proteomics. Tissue-based map of the human proteome. *Science* **347**, 1260419 (2015).
102. Y. M. Loo, M. Gale, Jr., Immune signaling by RIG-I-like receptors. *Immunity* **34**, 680-692 (2011).
103. M. Yoneyama *et al.*, Shared and unique functions of the DExD/H-box helicases RIG-I, MDA5, and LGP2 in antiviral innate immunity. *J Immunol* **175**, 2851-2858 (2005).
104. V. Hornung *et al.*, 5'-Triphosphate RNA is the ligand for RIG-I. *Science* **314**, 994-997 (2006).
105. H. Kato *et al.*, Length-dependent recognition of double-stranded ribonucleic acids by retinoic acid-inducible gene-I and melanoma differentiation-associated gene 5. *J Exp Med* **205**, 1601-1610 (2008).
106. A. Peisley *et al.*, Kinetic mechanism for viral dsRNA length discrimination by MDA5 filaments. *Proc Natl Acad Sci U S A* **109**, E3340-3349 (2012).
107. M. U. Gack *et al.*, TRIM25 RING-finger E3 ubiquitin ligase is essential for RIG-I-mediated antiviral activity. *Nature* **446**, 916-920 (2007).
108. H. Oshiumi, M. Matsumoto, S. Hatakeyama, T. Seya, Riplet/RNF135, a RING finger protein, ubiquitinates RIG-I to promote interferon-beta induction during the early phase of viral infection. *J Biol Chem* **284**, 807-817 (2009).
109. K. Kuniyoshi *et al.*, Pivotal role of RNA-binding E3 ubiquitin ligase MEX3C in RIG-I-mediated antiviral innate immunity. *Proc Natl Acad Sci U S A* **111**, 5646-5651 (2014).
110. H. M. Liu *et al.*, The mitochondrial targeting chaperone 14-3-3epsilon regulates a RIG-I translocon that mediates membrane association and innate antiviral immunity. *Cell Host Microbe* **11**, 528-537 (2012).
111. G. Liu, M. U. Gack, Distinct and Orchestrated Functions of RNA Sensors in Innate Immunity. *Immunity* **53**, 26-42 (2020).
112. T. Saito *et al.*, Regulation of innate antiviral defenses through a shared repressor domain in RIG-I and LGP2. *Proc Natl Acad Sci U S A* **104**, 582-587 (2007).
113. A. Komuro, C. M. Horvath, RNA- and virus-independent inhibition of antiviral signaling by RNA helicase LGP2. *J Virol* **80**, 12332-12342 (2006).
114. A. Murali *et al.*, Structure and function of LGP2, a DEX(D/H) helicase that regulates the innate immunity response. *J Biol Chem* **283**, 15825-15833 (2008).
115. A. M. Bruns, G. P. Leser, R. A. Lamb, C. M. Horvath, The innate immune sensor LGP2 activates antiviral signaling by regulating MDA5-RNA interaction and filament assembly. *Mol Cell* **55**, 771-781 (2014).
116. X. Zhang, X. C. Bai, Z. J. Chen, Structures and Mechanisms in the cGAS-STING Innate Immunity Pathway. *Immunity* **53**, 43-53 (2020).
117. Y. Kim *et al.*, PKR Senses Nuclear and Mitochondrial Signals by Interacting with Endogenous Double-Stranded RNAs. *Mol Cell* **71**, 1051-1063 e1056 (2018).
118. H. M. Lazear, J. W. Schoggins, M. S. Diamond, Shared and Distinct Functions of Type I and Type III Interferons. *Immunity* **50**, 907-923 (2019).
119. L. Prokunina-Olsson *et al.*, A variant upstream of IFNL3 (IL28B) creating a new interferon gene IFNL4 is associated with impaired clearance of hepatitis C virus. *Nat Genet* **45**, 164-171 (2013).
120. E. Alspach, D. M. Lussier, R. D. Schreiber, Interferon gamma and Its Important Roles in Promoting and Inhibiting Spontaneous and Therapeutic Cancer Immunity. *Cold Spring Harb Perspect Biol* **11**, (2019).
121. A. Pichlmair *et al.*, IFIT1 is an antiviral protein that recognizes 5'-triphosphate RNA. *Nat Immunol* **12**, 624-630 (2011).
122. P. S. Mitchell *et al.*, Evolution-guided identification of antiviral specificity determinants in the broadly acting interferon-induced innate immunity factor MxA. *Cell Host Microbe* **12**, 598-604 (2012).

123. X. Zhang *et al.*, CXCL10 plays a key role as an inflammatory mediator and a non-invasive biomarker of non-alcoholic steatohepatitis. *J Hepatol* **61**, 1365-1375 (2014).
124. A. Ichikawa *et al.*, CXCL10-CXCR3 enhances the development of neutrophil-mediated fulminant lung injury of viral and nonviral origin. *Am J Respir Crit Care Med* **187**, 65-77 (2013).
125. H. X. Shi *et al.*, Positive regulation of interferon regulatory factor 3 activation by Herc5 via ISG15 modification. *Mol Cell Biol* **30**, 2424-2436 (2010).
126. J. V. Dzimianski, F. E. M. Scholte, E. Bergeron, S. D. Pegan, ISG15: It's Complicated. *J Mol Biol* **431**, 4203-4216 (2019).
127. S. Crotta *et al.*, Type I and type III interferons drive redundant amplification loops to induce a transcriptional signature in influenza-infected airway epithelia. *PLoS Pathog* **9**, e1003773 (2013).
128. S. E. Doyle *et al.*, Interleukin-29 uses a type 1 interferon-like program to promote antiviral responses in human hepatocytes. *Hepatology* **44**, 896-906 (2006).
129. N. A. de Weerd *et al.*, Structural basis of a unique interferon-beta signaling axis mediated via the receptor IFNAR1. *Nat Immunol* **14**, 901-907 (2013).
130. N. A. de Weerd *et al.*, A hot spot on interferon alpha/beta receptor subunit 1 (IFNAR1) underpins its interaction with interferon-beta and dictates signaling. *J Biol Chem* **292**, 7554-7565 (2017).
131. S. V. Kotenko, J. E. Durbin, Contribution of type III interferons to antiviral immunity: location, location, location. *J Biol Chem* **292**, 7295-7303 (2017).
132. E. O. Glocker *et al.*, Inflammatory bowel disease and mutations affecting the interleukin-10 receptor. *N Engl J Med* **361**, 2033-2045 (2009).
133. G. W. He *et al.*, Optimized human intestinal organoid model reveals interleukin-22-dependency of paneth cell formation. *Cell Stem Cell* **29**, 1333-1345 e1336 (2022).
134. J. H. Tremaine, D. E. Goldsack, The structure of regular viruses in relation to their subunit amino acid composition. *Virology* **35**, 227-237 (1968).
135. E. Harvey, E. C. Holmes, Diversity and evolution of the animal virome. *Nat Rev Microbiol* **20**, 321-334 (2022).
136. H. Kato *et al.*, Cell type-specific involvement of RIG-I in antiviral response. *Immunity* **23**, 19-28 (2005).
137. H. Kato *et al.*, Differential roles of MDA5 and RIG-I helicases in the recognition of RNA viruses. *Nature* **441**, 101-105 (2006).
138. P. B. Devhare, S. Desai, K. S. Lole, Innate immune responses in human hepatocyte-derived cell lines alter genotype 1 hepatitis E virus replication efficiencies. *Sci Rep* **6**, 26827 (2016).
139. O. Colasanti *et al.*, Comparison of HAV and HCV infections in vivo and in vitro reveals distinct patterns of innate immune evasion and activation. *J Hepatol* **79**, 645-656 (2023).
140. N. Gillich, Z. Zhang, M. Binder, S. Urban, R. Bartenschlager, Effect of variants in LGP2 on MDA5-mediated activation of interferon response and suppression of hepatitis D virus replication. *J Hepatol* **78**, 78-89 (2023).
141. S. A. McCartney *et al.*, MDA-5 recognition of a murine norovirus. *PLoS Pathog* **4**, e1000108 (2008).
142. Y. M. Loo *et al.*, Distinct RIG-I and MDA5 signaling by RNA viruses in innate immunity. *J Virol* **82**, 335-345 (2008).
143. B. L. Fredericksen, B. C. Keller, J. Fornek, M. G. Katze, M. Gale, Jr., Establishment and maintenance of the innate antiviral response to West Nile Virus involves both RIG-I and MDA5 signaling through IPS-1. *J Virol* **82**, 609-616 (2008).
144. H. Negishi *et al.*, A critical link between Toll-like receptor 3 and type II interferon signaling pathways in antiviral innate immunity. *Proc Natl Acad Sci U S A* **105**, 20446-20451 (2008).
145. S. Y. Zhang *et al.*, TLR3 deficiency in patients with herpes simplex encephalitis. *Science* **317**, 1522-1527 (2007).
146. T. Wang *et al.*, Toll-like receptor 3 mediates West Nile virus entry into the brain causing lethal encephalitis. *Nat Med* **10**, 1366-1373 (2004).

147. B. D. Rudd, E. Burstein, C. S. Duckett, X. Li, N. W. Lukacs, Differential role for TLR3 in respiratory syncytial virus-induced chemokine expression. *J Virol* **79**, 3350-3357 (2005).
148. R. Le Goffic *et al.*, Detrimental contribution of the Toll-like receptor (TLR)3 to influenza A virus-induced acute pneumonia. *PLoS Pathog* **2**, e53 (2006).
149. B. B. Gowen *et al.*, TLR3 deletion limits mortality and disease severity due to Phlebovirus infection. *J Immunol* **177**, 6301-6307 (2006).
150. M. Wornle *et al.*, Novel role of toll-like receptor 3 in hepatitis C-associated glomerulonephritis. *Am J Pathol* **168**, 370-385 (2006).
151. Y. F. Lee, A. Nomoto, B. M. Detjen, E. Wimmer, A protein covalently linked to poliovirus genome RNA. *Proc Natl Acad Sci U S A* **74**, 59-63 (1977).
152. W. B. Cardenas *et al.*, Ebola virus VP35 protein binds double-stranded RNA and inhibits alpha/beta interferon production induced by RIG-I signaling. *J Virol* **80**, 5168-5178 (2006).
153. N. R. Donelan, C. F. Basler, A. Garcia-Sastre, A recombinant influenza A virus expressing an RNA-binding-defective NS1 protein induces high levels of beta interferon and is attenuated in mice. *J Virol* **77**, 13257-13266 (2003).
154. L. Uchida *et al.*, The dengue virus conceals double-stranded RNA in the intracellular membrane to escape from an interferon response. *Sci Rep* **4**, 7395 (2014).
155. C. J. Neufeldt *et al.*, Hepatitis C virus-induced cytoplasmic organelles use the nuclear transport machinery to establish an environment conducive to virus replication. *PLoS Pathog* **9**, e1003744 (2013).
156. K. Knoops *et al.*, SARS-coronavirus replication is supported by a reticulovesicular network of modified endoplasmic reticulum. *PLoS Biol* **6**, e226 (2008).
157. J. Stack *et al.*, Vaccinia virus protein A46R targets multiple Toll-like-interleukin-1 receptor adaptors and contributes to virulence. *J Exp Med* **201**, 1007-1018 (2005).
158. W. Riedl *et al.*, Zika Virus NS3 Mimics a Cellular 14-3-3-Binding Motif to Antagonize RIG-I- and MDA5-Mediated Innate Immunity. *Cell Host Microbe* **26**, 493-503 e496 (2019).
159. J. Andrejeva *et al.*, The V proteins of paramyxoviruses bind the IFN-inducible RNA helicase, mda-5, and inhibit its activation of the IFN-beta promoter. *Proc Natl Acad Sci U S A* **101**, 17264-17269 (2004).
160. M. U. Gack *et al.*, Influenza A virus NS1 targets the ubiquitin ligase TRIM25 to evade recognition by the host viral RNA sensor RIG-I. *Cell Host Microbe* **5**, 439-449 (2009).
161. H. Oshiumi, M. Miyashita, M. Matsumoto, T. Seya, A distinct role of Riplet-mediated K63-Linked polyubiquitination of the RIG-I repressor domain in human antiviral innate immune responses. *PLoS Pathog* **9**, e1003533 (2013).
162. A. Mukherjee *et al.*, The coxsackievirus B 3C protease cleaves MAVS and TRIF to attenuate host type I interferon and apoptotic signaling. *PLoS Pathog* **7**, e1001311 (2011).
163. Q. Feng *et al.*, Enterovirus 2Apro targets MDA5 and MAVS in infected cells. *J Virol* **88**, 3369-3378 (2014).
164. E. Meylan *et al.*, Cardif is an adaptor protein in the RIG-I antiviral pathway and is targeted by hepatitis C virus. *Nature* **437**, 1167-1172 (2005).
165. C. Wei *et al.*, The hepatitis B virus X protein disrupts innate immunity by downregulating mitochondrial antiviral signaling protein. *J Immunol* **185**, 1158-1168 (2010).
166. L. Sun *et al.*, Viral protease cleavage of MAVS in genetically modified mice with hepatitis A virus infection. *J Hepatol* **78**, 271-280 (2023).
167. Y. Yang *et al.*, Disruption of innate immunity due to mitochondrial targeting of a picornaviral protease precursor. *Proc Natl Acad Sci U S A* **104**, 7253-7258 (2007).
168. M. R. Pulido, E. Martinez-Salas, F. Sobrino, M. Saiz, MDA5 cleavage by the Leader protease of foot-and-mouth disease virus reveals its pleiotropic effect against the host antiviral response. *Cell Death Dis* **11**, 718 (2020).
169. M. Bitzer, S. Armeanu, U. M. Lauer, W. J. Neubert, Sendai virus vectors as an emerging negative-strand RNA viral vector system. *J Gene Med* **5**, 543-553 (2003).

170. R. Sedlmeier, W. J. Neubert, The replicative complex of paramyxoviruses: structure and function. *Adv Virus Res* **50**, 101-139 (1998).
171. A. Ali, D. P. Nayak, Assembly of Sendai virus: M protein interacts with F and HN proteins and with the cytoplasmic tail and transmembrane domain of F protein. *Virology* **276**, 289-303 (2000).
172. C. M. Sanderson, R. Avalos, A. Kundu, D. P. Nayak, Interaction of Sendai viral F, HN, and M proteins with host cytoskeletal and lipid components in Sendai virus-infected BHK cells. *Virology* **209**, 701-707 (1995).
173. M. K. Hasan *et al.*, Versatility of the accessory C proteins of Sendai virus: contribution to virus assembly as an additional role. *J Virol* **74**, 5619-5628 (2000).
174. J. Rehwinkel *et al.*, RIG-I detects viral genomic RNA during negative-strand RNA virus infection. *Cell* **140**, 397-408 (2010).
175. A. Baum, R. Sachidanandam, A. Garcia-Sastre, Preference of RIG-I for short viral RNA molecules in infected cells revealed by next-generation sequencing. *Proc Natl Acad Sci U S A* **107**, 16303-16308 (2010).
176. T. Irie, K. Kiyotani, T. Igarashi, A. Yoshida, T. Sakaguchi, Inhibition of interferon regulatory factor 3 activation by paramyxovirus V protein. *J Virol* **86**, 7136-7145 (2012).
177. T. Irie, N. Nagata, T. Igarashi, I. Okamoto, T. Sakaguchi, Conserved charged amino acids within Sendai virus C protein play multiple roles in the evasion of innate immune responses. *PLoS One* **5**, e10719 (2010).
178. M. Pepin, M. Bouloy, B. H. Bird, A. Kemp, J. Paweska, Rift Valley fever virus(Bunyaviridae: Phlebovirus): an update on pathogenesis, molecular epidemiology, vectors, diagnostics and prevention. *Vet Res* **41**, 61 (2010).
179. M. Spiegel, T. Plegge, S. Pohlmann, The Role of Phlebovirus Glycoproteins in Viral Entry, Assembly and Release. *Viruses* **8**, (2016).
180. N. Lopez, R. Muller, C. Prehaud, M. Bouloy, The L protein of Rift Valley fever virus can rescue viral ribonucleoproteins and transcribe synthetic genome-like RNA molecules. *J Virol* **69**, 3972-3979 (1995).
181. T. Ikegami, C. J. Peters, S. Makino, Rift valley fever virus nonstructural protein NSs promotes viral RNA replication and transcription in a minigenome system. *J Virol* **79**, 5606-5615 (2005).
182. L. Liu, C. C. Celma, P. Roy, Rift Valley fever virus structural proteins: expression, characterization and assembly of recombinant proteins. *Virol J* **5**, 82 (2008).
183. G. W. Anderson, Jr., J. F. Smith, Immunoelectron microscopy of Rift Valley fever viral morphogenesis in primary rat hepatocytes. *Virology* **161**, 91-100 (1987).
184. M. Habjan *et al.*, Processing of genome 5' termini as a strategy of negative-strand RNA viruses to avoid RIG-I-dependent interferon induction. *PLoS One* **3**, e2032 (2008).
185. F. Alem *et al.*, Exosomes originating from infection with the cytoplasmic single-stranded RNA virus Rift Valley fever virus (RVFV) protect recipient cells by inducing RIG-I mediated IFN-B response that leads to activation of autophagy. *Cell Biosci* **11**, 220 (2021).
186. P. Jansen van Vuren, C. T. Tiemessen, J. T. Paweska, Anti-nucleocapsid protein immune responses counteract pathogenic effects of Rift Valley fever virus infection in mice. *PLoS One* **6**, e25027 (2011).
187. K. E. Havranek, L. A. White, T. C. Bisom, J. M. Lanchy, J. S. Lodmell, The Atypical Kinase RIOK3 Limits RVFV Propagation and Is Regulated by Alternative Splicing. *Viruses* **13**, (2021).
188. Z. Zhang, S. Urban, New insights into HDV persistence: The role of interferon response and implications for upcoming novel therapies. *J Hepatol* **74**, 686-699 (2021).
189. P. Farci, G. A. Niro, Clinical features of hepatitis D. *Semin Liver Dis* **32**, 228-236 (2012).
190. G. Fattovich *et al.*, Influence of hepatitis delta virus infection on progression to cirrhosis in chronic hepatitis type B. *J Infect Dis* **155**, 931-935 (1987).
191. H. Yan *et al.*, Sodium taurocholate cotransporting polypeptide is a functional receptor for human hepatitis B and D virus. *Elife* **3**, (2012).

192. Z. Zhang *et al.*, Hepatitis D virus replication is sensed by MDA5 and induces IFN-beta/lambda responses in hepatocytes. *J Hepatol* **69**, 25-35 (2018).
193. E. V. Koonin *et al.*, Computer-assisted assignment of functional domains in the nonstructural polyprotein of hepatitis E virus: delineation of an additional group of positive-strand RNA plant and animal viruses. *Proc Natl Acad Sci U S A* **89**, 8259-8263 (1992).
194. S. Tyagi, H. Korkaya, M. Zafrullah, S. Jameel, S. K. Lal, The phosphorylated form of the ORF3 protein of hepatitis E virus interacts with its non-glycosylated form of the major capsid protein, ORF2. *J Biol Chem* **277**, 22759-22767 (2002).
195. I. Ahmad, R. P. Holla, S. Jameel, Molecular virology of hepatitis E virus. *Virus Res* **161**, 47-58 (2011).
196. D. Cao, X. J. Meng, Molecular biology and replication of hepatitis E virus. *Emerg Microbes Infect* **1**, e17 (2012).
197. A. W. Tam *et al.*, Hepatitis E virus (HEV): molecular cloning and sequencing of the full-length viral genome. *Virology* **185**, 120-131 (1991).
198. M. Surjit, S. Jameel, S. K. Lal, The ORF2 protein of hepatitis E virus binds the 5' region of viral RNA. *J Virol* **78**, 320-328 (2004).
199. S. U. Emerson *et al.*, Release of genotype 1 hepatitis E virus from cultured hepatoma and polarized intestinal cells depends on open reading frame 3 protein and requires an intact PXXP motif. *J Virol* **84**, 9059-9069 (2010).
200. W. Wang *et al.*, The RNA genome of hepatitis E virus robustly triggers an antiviral interferon response. *Hepatology* **67**, 2096-2112 (2018).
201. P. B. Devhare, S. N. Chatterjee, V. A. Arankalle, K. S. Lole, Analysis of antiviral response in human epithelial cells infected with hepatitis E virus. *PLoS One* **8**, e63793 (2013).
202. Y. Nan *et al.*, Hepatitis E virus inhibits type I interferon induction by ORF1 products. *J Virol* **88**, 11924-11932 (2014).
203. J. Myoung, J. Y. Lee, K. S. Min, Methyltransferase of a cell culture-adapted hepatitis E inhibits the MDA5 receptor signaling pathway. *J Microbiol* **57**, 1126-1131 (2019).
204. S. Hingane, N. Joshi, M. Surjit, C. T. Ranjith-Kumar, Hepatitis E Virus ORF2 Inhibits RIG-I Mediated Interferon Response. *Front Microbiol* **11**, 656 (2020).
205. M. He *et al.*, The ORF3 Protein of Genotype 1 Hepatitis E Virus Suppresses TLR3-induced NF-kappaB Signaling via TRADD and RIP1. *Sci Rep* **6**, 27597 (2016).
206. J. Dubuisson, F. L. Cosset, Virology and cell biology of the hepatitis C virus life cycle: an update. *J Hepatol* **61**, S3-S13 (2014).
207. N. Kato, Genome of human hepatitis C virus (HCV): gene organization, sequence diversity, and variation. *Microb Comp Genomics* **5**, 129-151 (2000).
208. H. Barth *et al.*, Cellular binding of hepatitis C virus envelope glycoprotein E2 requires cell surface heparan sulfate. *J Biol Chem* **278**, 41003-41012 (2003).
209. V. Lohmann, Hepatitis C virus RNA replication. *Curr Top Microbiol Immunol* **369**, 167-198 (2013).
210. C. I. Popescu *et al.*, NS2 protein of hepatitis C virus interacts with structural and non-structural proteins towards virus assembly. *PLoS Pathog* **7**, e1001278 (2011).
211. T. Phan, A. Kohlway, P. Dimberu, A. M. Pyle, B. D. Lindenbach, The acidic domain of hepatitis C virus NS4A contributes to RNA replication and virus particle assembly. *J Virol* **85**, 1193-1204 (2011).
212. L. Corless, C. M. Crump, S. D. Griffin, M. Harris, Vps4 and the ESCRT-III complex are required for the release of infectious hepatitis C virus particles. *J Gen Virol* **91**, 362-372 (2010).
213. A. Kell *et al.*, Pathogen-Associated Molecular Pattern Recognition of Hepatitis C Virus Transmitted/Founder Variants by RIG-I Is Dependent on U-Core Length. *J Virol* **89**, 11056-11068 (2015).
214. X. Cao *et al.*, MDA5 plays a critical role in interferon response during hepatitis C virus infection. *J Hepatol* **62**, 771-778 (2015).

215. N. Wang *et al.*, Toll-like receptor 3 mediates establishment of an antiviral state against hepatitis C virus in hepatoma cells. *J Virol* **83**, 9824-9834 (2009).
216. Q. Ding *et al.*, Hepatitis C virus NS4B blocks the interaction of STING and TBK1 to evade host innate immunity. *J Hepatol* **59**, 52-58 (2013).
217. O. Grunvogel *et al.*, Secretion of Hepatitis C Virus Replication Intermediates Reduces Activation of Toll-Like Receptor 3 in Hepatocytes. *Gastroenterology* **154**, 2237-2251 e2216 (2018).
218. B. Hu, H. Guo, P. Zhou, Z. L. Shi, Characteristics of SARS-CoV-2 and COVID-19. *Nat Rev Microbiol* **19**, 141-154 (2021).
219. Y. Chen, Q. Liu, D. Guo, Emerging coronaviruses: Genome structure, replication, and pathogenesis. *J Med Virol* **92**, 418-423 (2020).
220. H. Yang, Z. Rao, Structural biology of SARS-CoV-2 and implications for therapeutic development. *Nat Rev Microbiol* **19**, 685-700 (2021).
221. A. G. Harrison, T. Lin, P. Wang, Mechanisms of SARS-CoV-2 Transmission and Pathogenesis. *Trends Immunol* **41**, 1100-1115 (2020).
222. X. Yin *et al.*, MDA5 Governs the Innate Immune Response to SARS-CoV-2 in Lung Epithelial Cells. *Cell Rep* **34**, 108628 (2021).
223. L. G. Thorne *et al.*, SARS-CoV-2 sensing by RIG-I and MDA5 links epithelial infection to macrophage inflammation. *EMBO J* **40**, e107826 (2021).
224. J. M. Minkoff, B. tenOever, Innate immune evasion strategies of SARS-CoV-2. *Nat Rev Microbiol* **21**, 178-194 (2023).
225. M. Sironi *et al.*, TLR3 Mutations in Adult Patients With Herpes Simplex Virus and Varicella-Zoster Virus Encephalitis. *J Infect Dis* **215**, 1430-1434 (2017).
226. N. Mork *et al.*, Mutations in the TLR3 signaling pathway and beyond in adult patients with herpes simplex encephalitis. *Genes Immun* **16**, 552-566 (2015).
227. H. K. Lim *et al.*, TLR3 deficiency in herpes simplex encephalitis: high allelic heterogeneity and recurrence risk. *Neurology* **83**, 1888-1897 (2014).
228. F. Hidaka *et al.*, A missense mutation of the Toll-like receptor 3 gene in a patient with influenza-associated encephalopathy. *Clin Immunol* **119**, 188-194 (2006).
229. C. N. O. Santos *et al.*, Association Between Zika Virus Microcephaly in Newborns With the rs3775291 Variant in Toll-Like Receptor 3 and rs1799964 Variant at Tumor Necrosis Factor-alpha Gene. *J Infect Dis* **220**, 1797-1801 (2019).
230. A. Nahum, H. Dadi, A. Bates, C. M. Roifman, The L412F variant of Toll-like receptor 3 (TLR3) is associated with cutaneous candidiasis, increased susceptibility to cytomegalovirus, and autoimmunity. *J Allergy Clin Immunol* **127**, 528-531 (2011).
231. S. Biyani *et al.*, Toll-like receptor-3 gene polymorphism in patients with Japanese encephalitis. *J Neuroimmunol* **286**, 71-76 (2015).
232. S. Croci *et al.*, The polymorphism L412F in TLR3 inhibits autophagy and is a marker of severe COVID-19 in males. *Autophagy* **18**, 1662-1672 (2022).
233. R. M. Talaat, S. S. Elsayed, N. E. Abdel-Hakem, S. Z. El-Shenawy, Genetic Polymorphism in Toll-Like Receptor 3 and Interferon Regulatory Factor 3 in Hepatitis C Virus-Infected Patients: Correlation with Liver Cirrhosis. *Viral Immunol* **35**, 609-615 (2022).
234. C. A. Yang *et al.*, Association of TLR3-hyporesponsiveness and functional TLR3 L412F polymorphism with recurrent herpes labialis. *Hum Immunol* **73**, 844-851 (2012).
235. H. K. Lim *et al.*, Severe influenza pneumonitis in children with inherited TLR3 deficiency. *J Exp Med* **216**, 2038-2056 (2019).
236. Y. M. Mosaad, S. S. Metwally, R. E. Farag, Z. F. Lotfy, H. E. AbdelTwab, Association between Toll-Like Receptor 3 (TLR3) rs3775290, TLR7 rs179008, TLR9 rs352140 and Chronic HCV. *Immunol Invest* **48**, 321-332 (2019).
237. Q. Zhang *et al.*, Inborn errors of type I IFN immunity in patients with life-threatening COVID-19. *Science* **370**, (2020).

238. H. H. Hoffmann *et al.*, TMEM41B Is a Pan-flavivirus Host Factor. *Cell* **184**, 133-148 e120 (2021).
239. J. Han *et al.*, Genome-wide CRISPR/Cas9 Screen Identifies Host Factors Essential for Influenza Virus Replication. *Cell Rep* **23**, 596-607 (2018).
240. R. Fang, Q. Jiang, X. Jia, Z. Jiang, ARMH3-mediated recruitment of PI4KB directs Golgi-to-endosome trafficking and activation of the antiviral effector STING. *Immunity* **56**, 500-515 e506 (2023).
241. R. Zhang *et al.*, The Endoplasmic Reticulum ATP13A1 is Essential for MAVS-Mediated Antiviral Innate Immunity. *Adv Sci (Weinh)* **9**, e2203831 (2022).
242. B. Wiedenheft, S. H. Sternberg, J. A. Doudna, RNA-guided genetic silencing systems in bacteria and archaea. *Nature* **482**, 331-338 (2012).
243. R. Barrangou *et al.*, Genomic impact of CRISPR immunization against bacteriophages. *Biochem Soc Trans* **41**, 1383-1391 (2013).
244. E. Deltcheva *et al.*, CRISPR RNA maturation by trans-encoded small RNA and host factor RNase III. *Nature* **471**, 602-607 (2011).
245. M. Jinek *et al.*, A programmable dual-RNA-guided DNA endonuclease in adaptive bacterial immunity. *Science* **337**, 816-821 (2012).
246. R. Barrangou *et al.*, CRISPR provides acquired resistance against viruses in prokaryotes. *Science* **315**, 1709-1712 (2007).
247. J. D. Sander, J. K. Joung, CRISPR-Cas systems for editing, regulating and targeting genomes. *Nat Biotechnol* **32**, 347-355 (2014).
248. M. R. Lieber, Y. Ma, U. Pannicke, K. Schwarz, Mechanism and regulation of human non-homologous DNA end-joining. *Nat Rev Mol Cell Biol* **4**, 712-720 (2003).
249. G. A. Cromie, J. C. Connelly, D. R. Leach, Recombination at double-strand breaks and DNA ends: conserved mechanisms from phage to humans. *Mol Cell* **8**, 1163-1174 (2001).
250. .
251. E. Semenova *et al.*, Interference by clustered regularly interspaced short palindromic repeat (CRISPR) RNA is governed by a seed sequence. *Proc Natl Acad Sci U S A* **108**, 10098-10103 (2011).
252. M. Ikeda *et al.*, Human hepatocyte clonal cell lines that support persistent replication of hepatitis C virus. *Virus Res* **56**, 157-167 (1998).
253. K. J. Blight, J. A. McKeating, C. M. Rice, Highly permissive cell lines for subgenomic and genomic hepatitis C virus RNA replication. *J Virol* **76**, 13001-13014 (2002).
254. M. D. Esposti, The roles of Bid. *Apoptosis* **7**, 433-440 (2002).
255. S. J. Korsmeyer *et al.*, Pro-apoptotic cascade activates BID, which oligomerizes BAK or BAX into pores that result in the release of cytochrome c. *Cell Death Differ* **7**, 1166-1173 (2000).
256. R. Field, S. Campion, C. Warren, C. Murray, C. Cunningham, Systemic challenge with the TLR3 agonist poly I:C induces amplified IFNalpha/beta and IL-1beta responses in the diseased brain and exacerbates chronic neurodegeneration. *Brain Behav Immun* **24**, 996-1007 (2010).
257. N. Dauletbaev, M. Cammisano, K. Herscovitch, L. C. Lands, Stimulation of the RIG-I/MAVS Pathway by Polyinosinic:Polycytidylic Acid Upregulates IFN-beta in Airway Epithelial Cells with Minimal Costimulation of IL-8. *J Immunol* **195**, 2829-2841 (2015).
258. K. Kamieniarz-Gdula *et al.*, Selective Roles of Vertebrate PCF11 in Premature and Full-Length Transcript Termination. *Mol Cell* **74**, 158-172 e159 (2019).
259. A. Ogorodnikov *et al.*, Transcriptome 3'end organization by PCF11 links alternative polyadenylation to formation and neuronal differentiation of neuroblastoma. *Nat Commun* **9**, 5331 (2018).
260. Q. You, H. Shen, Development of multivariable risk signature based on four immune-related RNA-binding proteins to predict survival and immune status in lung adenocarcinoma. *Transl Cancer Res* **11**, 2591-2606 (2022).
261. X. Zhang *et al.*, Identification of STAT3 as a substrate of receptor protein tyrosine phosphatase T. *Proc Natl Acad Sci U S A* **104**, 4060-4064 (2007).

262. Y. Zhao *et al.*, Identification and functional characterization of paxillin as a target of protein tyrosine phosphatase receptor T. *Proc Natl Acad Sci U S A* **107**, 2592-2597 (2010).
263. S. H. Lim *et al.*, Synapse formation regulated by protein tyrosine phosphatase receptor T through interaction with cell adhesion molecules and Fyn. *Embo j* **28**, 3564-3578 (2009).
264. Z. Cheng *et al.*, A molecular threading mechanism underlies Jumonji lysine demethylase KDM2A regulation of methylated H3K36. *Genes Dev* **28**, 1758-1771 (2014).
265. K. W. Wagner *et al.*, KDM2A promotes lung tumorigenesis by epigenetically enhancing ERK1/2 signaling. *J Clin Invest* **123**, 5231-5246 (2013).
266. L. Lu *et al.*, Kdm2a/b Lysine Demethylases Regulate Canonical Wnt Signaling by Modulating the Stability of Nuclear beta-Catenin. *Dev Cell* **33**, 660-674 (2015).
267. C. Chen *et al.*, Targeting KDM2A Enhances T-cell Infiltration in NSD1-Deficient Head and Neck Squamous Cell Carcinoma. *Cancer Res* **83**, 2645-2655 (2023).
268. H. Imai, E. K. Chan, K. Kiyosawa, X. D. Fu, E. M. Tan, Novel nuclear autoantigen with splicing factor motifs identified with antibody from hepatocellular carcinoma. *J Clin Invest* **92**, 2419-2426 (1993).
269. I. Mercier *et al.*, CAPER, a novel regulator of human breast cancer progression. *Cell Cycle* **13**, 1256-1264 (2014).
270. Y. Chai *et al.*, Overexpression of HCC1/CAPERalpha may play a role in lung cancer carcinogenesis. *Tumour Biol* **35**, 6311-6317 (2014).
271. A. H. Sillars-Hardebol *et al.*, CSE1L, DIDO1 and RBM39 in colorectal adenoma to carcinoma progression. *Cell Oncol (Dordr)* **35**, 293-300 (2012).
272. G. A. Stepanyuk *et al.*, UHM-ULM interactions in the RBM39-U2AF65 splicing-factor complex. *Acta Crystallogr D Struct Biol* **72**, 497-511 (2016).
273. P. A. Sharp, Split genes and RNA splicing. *Cell* **77**, 805-815 (1994).
274. P. A. Sharp, RNA splicing and genes. *JAMA* **260**, 3035-3041 (1988).
275. S. Lykke-Andersen, T. H. Jensen, Nonsense-mediated mRNA decay: an intricate machinery that shapes transcriptomes. *Nat Rev Mol Cell Biol* **16**, 665-677 (2015).
276. C. J. Wright, C. W. J. Smith, C. D. Jiggins, Alternative splicing as a source of phenotypic diversity. *Nat Rev Genet* **23**, 697-710 (2022).
277. J. Xiao, S. Jin, X. Wang, J. Huang, H. Zou, CELF1 Selectively Regulates Alternative Splicing of DNA Repair Genes Associated With Cataract in Human Lens Cell Line. *Biochem Genet* **61**, 1319-1333 (2023).
278. A. Ergun *et al.*, Differential splicing across immune system lineages. *Proc Natl Acad Sci U S A* **110**, 14324-14329 (2013).
279. E. Wang *et al.*, Targeting an RNA-Binding Protein Network in Acute Myeloid Leukemia. *Cancer Cell* **35**, 369-384 e367 (2019).
280. P. K. Puvvula *et al.*, Inhibiting an RBM39/MLL1 epigenomic regulatory complex with dominant-negative peptides disrupts cancer cell transcription and proliferation. *Cell Rep* **35**, 109156 (2021).
281. J. E. Melnyk *et al.*, The splicing modulator sulfonamide indisulam reduces AR-V7 in prostate cancer cells. *Bioorg Med Chem* **28**, 115712 (2020).
282. S. Singh *et al.*, Targeting the spliceosome through RBM39 degradation results in exceptional responses in high-risk neuroblastoma models. *Sci Adv* **7**, eabj5405 (2021).
283. D. E. Bussiere *et al.*, Structural basis of indisulam-mediated RBM39 recruitment to DCAF15 E3 ligase complex. *Nat Chem Biol* **16**, 15-23 (2020).
284. T. B. Faust *et al.*, Structural complementarity facilitates E7820-mediated degradation of RBM39 by DCAF15. *Nat Chem Biol* **16**, 7-14 (2020).
285. D. J. Jung, S. Y. Na, D. S. Na, J. W. Lee, Molecular cloning and characterization of CAPER, a novel coactivator of activating protein-1 and estrogen receptors. *J Biol Chem* **277**, 1229-1234 (2002).

286. J. Dutta, G. Fan, C. Gelinas, CAPERalpha is a novel Rel-TAD-interacting factor that inhibits lymphocyte transformation by the potent Rel/NF-kappaB oncoprotein v-Rel. *J Virol* **82**, 10792-10802 (2008).
287. Y. K. Kang *et al.*, CAPER is vital for energy and redox homeostasis by integrating glucose-induced mitochondrial functions via ERR-alpha-Gabpa and stress-induced adaptive responses via NF-kappaB-cMYC. *PLoS Genet* **11**, e1005116 (2015).
288. S. X. Lu *et al.*, Pharmacologic modulation of RNA splicing enhances anti-tumor immunity. *Cell* **184**, 4032-4047 e4031 (2021).
289. Z. Wang *et al.*, Mutational analysis of the tyrosine phosphatome in colorectal cancers. *Science* **304**, 1164-1166 (2004).
290. D. Ladinovic, J. Novotna, S. Jaksova, I. Raska, T. Vacik, A demethylation deficient isoform of the lysine demethylase KDM2A interacts with pericentromeric heterochromatin in an HP1a-dependent manner. *Nucleus* **8**, 563-572 (2017).
291. D. A. Feigelstock, K. B. Mihalik, G. Kaplan, S. M. Feinstone, Increased susceptibility of Huh7 cells to HCV replication does not require mutations in RIG-I. *Virol J* **7**, 44 (2010).
292. C. D. Sadik, M. Bachmann, J. Pfeilschifter, H. Muhl, Activation of interferon regulatory factor-3 via toll-like receptor 3 and immunomodulatory functions detected in A549 lung epithelial cells exposed to misplaced U1-snRNA. *Nucleic Acids Res* **37**, 5041-5056 (2009).
293. Y. C. Lu, W. C. Yeh, P. S. Ohashi, LPS/TLR4 signal transduction pathway. *Cytokine* **42**, 145-151 (2008).
294. M. S. Diamond, M. Farzan, The broad-spectrum antiviral functions of IFIT and IFITM proteins. *Nat Rev Immunol* **13**, 46-57 (2013).
295. M. E. Ermler *et al.*, RNA helicase signaling is critical for type i interferon production and protection against Rift Valley fever virus during mucosal challenge. *J Virol* **87**, 4846-4860 (2013).
296. S. Ramasamy, S. Subbian, Critical Determinants of Cytokine Storm and Type I Interferon Response in COVID-19 Pathogenesis. *Clin Microbiol Rev* **34**, (2021).
297. L. Dalskov *et al.*, Characterization of distinct molecular interactions responsible for IRF3 and IRF7 phosphorylation and subsequent dimerization. *Nucleic Acids Res* **48**, 11421-11433 (2020).
298. H. G. Xu, W. Ren, C. Lu, G. P. Zhou, Characterization of the human IRF-3 promoter and its regulation by the transcription factor E2F1. *Mol Biol Rep* **37**, 3073-3080 (2010).
299. V. S. Ivanova, D. Zimonjic, N. Popescu, W. M. Bonner, Chromosomal localization of the human histone H2A.X gene to 11q23.2-q23.3 by fluorescence in situ hybridization. *Hum Genet* **94**, 303-306 (1994).
300. J. L. Mazzola, M. A. Sirover, Subcellular localization of human glyceraldehyde-3-phosphate dehydrogenase is independent of its glycolytic function. *Biochim Biophys Acta* **1622**, 50-56 (2003).
301. X. Zhang, M. H. Hamblin, K. J. Yin, The long noncoding RNA Malat1: Its physiological and pathophysiological functions. *RNA Biol* **14**, 1705-1714 (2017).
302. T. Han *et al.*, Anticancer sulfonamides target splicing by inducing RBM39 degradation via recruitment to DCAF15. *Science* **356**, (2017).
303. C. Li, L. Ma, X. Chen, Interferon regulatory factor 3-CL, an isoform of IRF3, antagonizes activity of IRF3. *Cell Mol Immunol* **8**, 67-74 (2011).
304. M. Matsumoto, H. Oshiumi, T. Seya, Antiviral responses induced by the TLR3 pathway. *Rev Med Virol* **21**, 67-77 (2011).
305. Y. Guo *et al.*, Herpes simplex virus encephalitis in a patient with complete TLR3 deficiency: TLR3 is otherwise redundant in protective immunity. *J Exp Med* **208**, 2083-2098 (2011).
306. N. O. Pryimenko *et al.*, Genetic polymorphism ARG753GLN of TLR-2, LEU412PHE of TLR-3, ASP299GLY of TLR-4 in patients with influenza and influenza-associated pneumonia. *Wiad Lek* **72**, 2324-2328 (2019).

307. S. O. Lee, R. A. Brown, R. R. Razonable, Association between a functional polymorphism in Toll-like receptor 3 and chronic hepatitis C in liver transplant recipients. *Transpl Infect Dis* **15**, 111-119 (2013).
308. M. Studzinska *et al.*, Association of TLR3 L412F Polymorphism with Cytomegalovirus Infection in Children. *PLoS One* **12**, e0169420 (2017).
309. I. Sghaier *et al.*, TLR3 and TLR4 SNP variants in the liver disease resulting from hepatitis B virus and hepatitis C virus infection. *Br J Biomed Sci* **76**, 35-41 (2019).
310. T. Partanen *et al.*, Heterozygous TLR3 Mutation in Patients with Hantavirus Encephalitis. *J Clin Immunol* **40**, 1156-1162 (2020).
311. O. Parnas *et al.*, A Genome-wide CRISPR Screen in Primary Immune Cells to Dissect Regulatory Networks. *Cell* **162**, 675-686 (2015).
312. A. J. Chui *et al.*, N-terminal degradation activates the NLRP1B inflammasome. *Science* **364**, 82-85 (2019).
313. Y. Song *et al.*, RBM39 Alters Phosphorylation of c-Jun and Binds to Viral RNA to Promote PRRSV Proliferation. *Front Immunol* **12**, 664417 (2021).
314. A. Birmingham *et al.*, 3′ UTR seed matches, but not overall identity, are associated with RNAi off-targets. *Nature Methods* **3**, 199-204 (2006).
315. A. Reynolds *et al.*, Induction of the interferon response by siRNA is cell type- and duplex length-dependent. *RNA* **12**, 988-993 (2006).
316. A. A. Khan *et al.*, Transfection of small RNAs globally perturbs gene regulation by endogenous microRNAs. *Nat Biotechnol* **27**, 549-555 (2009).
317. A. Helwak, G. Kudla, T. Dudnakova, D. Tollervey, Mapping the human miRNA interactome by CLASH reveals frequent noncanonical binding. *Cell* **153**, 654-665 (2013).
318. J. Lu *et al.*, Proximity Labeling, Quantitative Proteomics, and Biochemical Studies Revealed the Molecular Mechanism for the Inhibitory Effect of Indisulam on the Proliferation of Gastric Cancer Cells. *J Proteome Res* **20**, 4462-4474 (2021).
319. N. Ohtani, K. Yamakoshi, A. Takahashi, E. Hara, The p16INK4a-RB pathway: molecular link between cellular senescence and tumor suppression. *J Med Invest* **51**, 146-153 (2004).
320. J. Tissari, J. Siren, S. Meri, I. Julkunen, S. Matikainen, IFN-alpha enhances TLR3-mediated antiviral cytokine expression in human endothelial and epithelial cells by up-regulating TLR3 expression. *J Immunol* **174**, 4289-4294 (2005).
321. G. Gatti *et al.*, Direct effect of dsRNA mimetics on cancer cells induces endogenous IFN-beta production capable of improving dendritic cell function. *Eur J Immunol* **43**, 1849-1861 (2013).
322. D. J. Giard *et al.*, In vitro cultivation of human tumors: establishment of cell lines derived from a series of solid tumors. *J Natl Cancer Inst* **51**, 1417-1423 (1973).
323. K. Schroder, P. J. Hertzog, T. Ravasi, D. A. Hume, Interferon-gamma: an overview of signals, mechanisms and functions. *J Leukoc Biol* **75**, 163-189 (2004).
324. C. R. Bolen, S. Ding, M. D. Robek, S. H. Kleinstein, Dynamic expression profiling of type I and type III interferon-stimulated hepatocytes reveals a stable hierarchy of gene expression. *Hepatology* **59**, 1262-1272 (2014).
325. J. Major *et al.*, Type I and III interferons disrupt lung epithelial repair during recovery from viral infection. *Science* **369**, 712-717 (2020).
326. C. A. Jefferies, Regulating IRFs in IFN Driven Disease. *Front Immunol* **10**, 325 (2019).
327. B. V. Mistry *et al.*, Expression profiling of WD40 family genes including DDB1- and CUL4-associated factor (DCAF) genes in mice and human suggests important regulatory roles in testicular development and spermatogenesis. *BMC Genomics* **21**, 602 (2020).
328. D. C. Fitzgerald *et al.*, Interferon regulatory factor (IRF) 3 is critical for the development of experimental autoimmune encephalomyelitis. *J Neuroinflammation* **11**, 130 (2014).
329. T. M. Petro, IFN Regulatory Factor 3 in Health and Disease. *J Immunol* **205**, 1981-1989 (2020).
330. M. Bekes, D. R. Langley, C. M. Crews, PROTAC targeted protein degraders: the past is prologue. *Nat Rev Drug Discov* **21**, 181-200 (2022).

331. D. Todt *et al.*, Antiviral Activities of Different Interferon Types and Subtypes against Hepatitis E Virus Replication. *Antimicrob Agents Chemother* **60**, 2132-2139 (2016).
332. C. Huang *et al.*, Clinical features of patients infected with 2019 novel coronavirus in Wuhan, China. *Lancet* **395**, 497-506 (2020).
333. K. P. Kumar, K. M. McBride, B. K. Weaver, C. Dingwall, N. C. Reich, Regulated nuclear-cytoplasmic localization of interferon regulatory factor 3, a subunit of double-stranded RNA-activated factor 1. *Mol Cell Biol* **20**, 4159-4168 (2000).
334. S. Marozin *et al.*, Inhibition of the IFN-beta response in hepatocellular carcinoma by alternative spliced isoform of IFN regulatory factor-3. *Mol Ther* **16**, 1789-1797 (2008).
335. A. Y. Karpova, L. V. Ronco, P. M. Howley, Functional characterization of interferon regulatory factor 3a (IRF-3a), an alternative splice isoform of IRF-3. *Mol Cell Biol* **21**, 4169-4176 (2001).
336. S. Mai *et al.*, Global regulation of alternative RNA splicing by the SR-rich protein RBM39. *Biochim Biophys Acta* **1859**, 1014-1024 (2016).
337. K. L. Schey, A. C. Grey, J. J. Nicklay, Mass spectrometry of membrane proteins: a focus on aquaporins. *Biochemistry* **52**, 3807-3817 (2013).
338. B. C. Carlyle *et al.*, Isoform-Level Interpretation of High-Throughput Proteomics Data Enabled by Deep Integration with RNA-seq. *J Proteome Res* **17**, 3431-3444 (2018).
339. C. Peggion *et al.*, Absolute quantification of myosin heavy chain isoforms by selected reaction monitoring can underscore skeletal muscle changes in a mouse model of amyotrophic lateral sclerosis. *Anal Bioanal Chem* **409**, 2143-2153 (2017).
340. S. Mai *et al.*, Functional interaction between nonreceptor tyrosine kinase c-Abl and SR-Rich protein RBM39. *Biochem Biophys Res Commun* **473**, 355-360 (2016).
341. J. Choe, M. S. Kelker, I. A. Wilson, Crystal structure of human toll-like receptor 3 (TLR3) ectodomain. *Science* **309**, 581-585 (2005).
342. Y. Wang, L. Liu, D. R. Davies, D. M. Segal, Dimerization of Toll-like receptor 3 (TLR3) is required for ligand binding. *J Biol Chem* **285**, 36836-36841 (2010).